A dissertation submitted to the

FACULTY OF BIOLOGY, CHEMISTRY AND GEOSCIENCES
UNIVERSITY OF BAYREUTH

to attain the academic degree of
DR. RER. NAT.

Site-specific modelling of turbulent fluxes on the Tibetan Plateau

WOLFGANG BABEL
M.Sc. Global Change Ecology

born 3 November, 1974
in Pfronten, Germany

Bayreuth, March 2013

supervised by PROF. DR. THOMAS FOKEN

Site-specific modelling of turbulent fluxes on the Tibetan Plateau

supervised by Prof. Dr. Thomas Foken

Die vorliegende Arbeit wurde in der Zeit von April 2009 bis März 2013 in Bayreuth an der Abteilung Mikrometeorologie unter Betreuung von Herrn Prof. Dr. Thomas Foken angefertigt.

Vollständiger Abdruck der von der Fakultät für Biologie, Chemie und Geowissenschaften der Universität Bayreuth genehmigten Dissertation zur Erlangung des akademischen Grades eines Doktor der Naturwissenschaften (Dr. rer. nat.).

Dissertation eingereicht am: 6. März 2013
Zulassung durch die Prüfungskommission: 13. März 2013
Wissenschaftliches Kolloquium: 15. Mai 2013

Amtierende Dekanin:
Prof. Dr. Beate Lohnert

Prüfungsausschuss:
Prof. Dr. Thomas Foken (Erstgutachter)
Dr. habil. Eva Falge (Zweitgutachter)
Prof. Dr. Andreas Held (Vorsitz)
Prof. Dr. Michael Hauhs
Prof. Dr. Bernd Huwe

Contents

List of manuscripts

This dissertation is presented in a cumulative form. It is based on three peer-reviewed publications and two submitted manuscripts as listed below.

Peer-reviewed publications

Biermann, T., Babel, W., Ma, W., Chen, X., Thiem, E., Ma, Y., and Foken, T.: Turbulent flux observations and modelling over a shallow lake and a wet grassland in the Nam Co basin, Tibetan Plateau, Theor. Appl. Climatol., accepted

Gerken, T., Babel, W., Hoffmann, A., Biermann, T., Herzog, M., Friend, A. D., Li, M., Ma, Y., Foken, T., and Graf, H.-F.: Turbulent flux modelling with a simple 2-layer soil model and extrapolated surface temperature applied at Nam Co Lake basin on the Tibetan Plateau, Hydrol. Earth Syst. Sci., 16, 1095–1110, doi:10.5194/hess-16-1095-2012, 2012.

Li, M., Babel, W., Tanaka, K., and Foken, T.: Note on the application of planar-fit rotation for non-omnidirectional sonic anemometers, Atmos. Meas. Tech., 6, 221–229, doi:10.5194/amt-6-221-2013, 2013.

Manuscripts submitted

Babel, W., Chen, Y., Biermann, T., Yang, K., Ma, Y., and Foken, T.: Adaptation of a land surface scheme for modeling turbulent fluxes on the Tibetan Plateau under different soil moisture conditions, submitted to J. Geophys. Res.

Charuchittipan, D., Babel, W., Mauder, M., Leps, J.-P., and Foken, T.: Extension of the averaging time of the eddy-covariance measurement and its effect on the energy balance closure, submitted to Bound.-Lay. Meteorol.

List of additional publications

The following list summarises other publications of mine which are not included in the dissertation. They were split up in two parts: Publications which have reference to the thesis and other publications. The first part includes two master theses as well, with reference to the dissertation, initiated and supervised by myself.

Publications with reference to this thesis

Peer-reviewed publications

Zhou, D., Eigenmann, R., Babel, W., Foken, T., and Ma, Y.: The study of near-ground free convection conditions at Nam Co station on the Tibetan Plateau, Theor. Appl. Climatol., 105, 217–228, doi:10.1007/s00704-010-0393-5, 2011.

Non peer-reviewed publications

Babel, W., Eigenmann, R., Ma, Y., and Foken, T.: Analysis of turbulent fluxes and their representativeness for the interaction between the atmospheric boundary layer and the underlying surface on Tibetan Plateau, CEOP-AEGIS Deliverable report De1.2, Ed. University of Strasbourg, France, ISSN 2118-7843: 35 p., 2011a.

Babel, W., Li, M., Sun, F., Ma, W., Chen, X., Colin, J., Ma, Y., and Foken, T.: Aerodynamic and thermodynamic variables for four stations on Tibetan Plateau – Introduction on the CEOP-AEGIS database in NetCDF, CEOP-AEGIS Deliverable report De1.3, Ed. University of Strasbourg, France, ISSN 2118-7843: 90 p., 2011b.

Babel, W.: An R routine for the simplified usage of TERRAFEX (Characterisation of a complex measuring site for flux measurements), Work Report University of Bayreuth, Dept. of Micrometeorology, ISSN 1614-8916, in preparation

Biermann, T., Babel, W., Olesch, J., and Foken, T.: Documentation of the Micrometeorological Experiment, Nam Tso, Tibet, 25th of June – 8th of August 2009, Work Report University of Bayreuth, Dept. of Micrometeorology, ISSN 1614-8916, 41, 38 pp., URL http://opus.ub.uni-bayreuth.de/opus4-ubbayreuth/frontdoor/index/index/docId/626, 2009.

Foken, T. and Babel, W.: Auf dem "Dach der Welt" – Die Rolle Tibets bei der Wasserversorgung Südostasiens, in: Spektrum-Magazin der Universität Bayreuth, Ausgabe 1/2012, 46–48, 2012

Gerken, T., Babel, W., Hoffmann, A., Biermann, T., Herzog, M., Friend, A. D., Li, M., Ma, Y., Foken, T., and Graf, H.-F.: Turbulent flux modelling with a simple 2-layer soil model and extrapolated surface temperature applied at Nam Co Lake basin on the Tibetan Plateau, Hydrol. Earth Syst. Sci. Discuss., 8, 10 275–10 309, doi:10.5194/hessd-8-10275-2011, 2011.

Gerken, T., Fuchs, K., and Babel, W.: Documentation of the Atmospheric Boundary Layer Experiment, Nam Tso, Tibet, 08^{th} of July – 08^{th} of August 2012, Work Report University of Bayreuth, Dept. of Micrometeorology, ISSN 1614-8916, 53, 48pp., 2013

Li, M., Babel, W., Tanaka, K., and Foken, T.: Note on the application of planar-fit rotation for non-omnidirectional sonic anemometers, Atmos. Meas. Tech. Discuss., 5, 7323–7340, doi:10.5194/amtd-5-7323-2012, 2012.

Master theses supervised by myself

Baumer, M.: Vergleich zweier Lagrange'scher Modelle zur Bestimmung des Footprints über heterogenem Gelände, Master thesis, University of Bayreuth, 66pp., 2012.

Thiem, E.: Modelling of the energy exchange above lake and land surfaces, Master thesis, University of Bayreuth, 73pp., 2011.

Other publications not included in this thesis

Irl, S. D. H., Steinbauer, M. J., Babel, W., Beierkuhnlein, C., Blume-Werry, G., Messinger, J., Palomares Martínez, Á., Strohmeier, S., and Jentsch, A.: An 11- yr exclosure experiment in a high-elevation island ecosystem: introduced herbivore impact on shrub species richness, seedling recruitment and population dynamics, J. Veg. Sci., 23, 1114–1125, doi:10.1111/j.1654-1103.2012.01425.x, 2012.

Babel, W., Huneke, S., and Foken, T.: A framework to utilize turbulent flux measurements for mesoscale models and remote sensing applications, Hydrol. Earth Syst. Sci. Discuss., 8, 5165–5225, doi:10.5194/hessd-8-5165-2011, 2011.

Babel, W. and Foken, T.: Preliminary footprint analysis of LAS (Large aperture scintillometer) measurements at Qomolangma station, Tibetan Plateau, CEOP-AEGIS technical report, 2009, available at the CEOP-AEGIS project office, but not published yet

Acknowledgements

Many persons supported me in the development and completion of this thesis in many ways. I would like to thank all of them, in particular:

- Prof. Thomas Foken for his guidance through all stages of this work, for many fruitful discussions about scientific and other questions, and for liberally sharing his vast experience on micrometeorological issues
- Tobias Biermann for many days of common experiment preparation and realisation, data processing and manuscript writing; furthermore for his support, discussions, reviewing manuscripts, and valuable comments through all our time
- All Co-authors for their contributions to the manuscript and discussions, in particular Tobias Gerken, Chen Yingying and Prof. Yang Kun (Institute of Tibetan Plateau Research, Chinese Academy of Sciences, Beijing), Elisabeth Thiem, Charuchittipan Doojdao and Li Maoshan (Cold and Arid Regions Environmental and Engineering Research Institute, Chinese Academy of Sciences, Lanzhou)
- Heinz-Theo Mengelkamp for providing the source code of SEWAB
- All other current and former staff members of the Department of Micrometeorology for their support, helpful programs and scripts, discussions and comments, in particular Rafael Eigenmann, Tiina Markkanen, Mathias Göckede, Stefan Metzger, Lukas Siebicke, Jörg Hübner, and Jo Olesch
- Sun Fanglin, Ma Weiqiang (Cold and Arid Regions Environmental and Engineering Research Institute, Chinese Academy of Sciences, Lanzhou), Chen Xuelong (Faculty of Geo-Information Science and Earth Observation, University of Twente, Enschede, Netherlands), and the staff members of the ITP Nam Co Monitoring and Research Station for their work on the Tibetan Plateau and help during the field trips, and Prof. Ma Yaoming (Institute of Tibetan Plateau Research, Chinese Academy of Sciences, Beijing) as project partner and leader of the Chinese working group
- My family for supporting me all the time

This work has been financed by CEOP-AEGIS, a Collaborative Project/Small or medium-scale focused research project – Specific International Co-operation Action coordinated by the University of Strasbourg, France and funded by the European Commission under FP7 topic ENV.2007.4.1.4.2 “Improving observing systems for water resource management” and by the German Research Foundation (DFG), Priority Programme 1372 “Tibetan Plateau: Formation, Climate, Ecosystems” (TiP).

Summary

The Tibetan Plateau attracts attention in recent decades due to its influence on the East-Asian Monsoon and regional hydrology. Therefore estimates of the regional energy and water balance have come into the focus, utilising remote sensing and regional model approaches, but such attempts require surface-specific flux data of high quality for validation. Eddy-covariance measurements are qualified for this task, but these are scarce on the Tibetan Plateau, incomplete due to quality filtering and potentially biased due to the well-known closure gap of the observed energy balance as well as small-scale heterogeneity. This thesis is related to the infrastructural EU project CEOP-AEGIS, aiming at a standardised processing of eddy-covariance data – including correction of the energy balance closure and gap-filling – on the Tibetan Plateau.

In a pre-analysis step, particular issues about data quality of turbulent fluxes (sensible heat flux and latent heat flux/evapotranspiration) at Tibetan Plateau sites have been addressed. One of them is the degradation of data quality due to the frequent occurrence of near-ground free convective conditions. Another issue arises from coordinate rotation for non-omnidirectional sonic anemometer, which requires a careful handling. In consequence, a sector-wise planar-fit is recommended, disregarding the sector influenced by the anemometer's mounting structure. This can reduce occurrences of invalid momentum flux data, whilst no effect on scalar fluxes can be seen.

As a main topic, this thesis investigates the application of process-based modelling to estimate turbulent flux exchange between the surface and the atmosphere for typical surface types on the Tibetan Plateau. Therefore a case study has been carried out at Nam Co, Tibetan Plateau. Turbulent flux measurements over dry and wet grassland as well as over a shallow lake have been conducted during the summer monsoon season of 2009, and modelled with the land surface scheme SEWAB and a hydrodynamic multilayer model for the lake. Adaptations were implemented to the land surface scheme with regard to the special conditions on the Tibetan Plateau, such as extreme diurnal variation of surface temperature and variation in soil moisture, further called TP version. The analysis includes a consequent model comparison with eddy-covariance data, using model parameters derived independently rather than applying optimisation strategies. Specific attention has been devoted to the impact of observed energy balance closure and its correction, establishing a new correction method according to the Buoyancy flux.

The land surface model reasonably represented the dry and the wet grassland site by only setting the site-specific model parameters, and the TP version performed overall better than the original version, while laboratory measurements of soil parameters failed to improve model performance in comparison to standard parameter values. Soil temperature and moisture measurements as well as field based knowledge of the soil type have been identified as minimum requirements for model parameter acquisition. Lake surface fluxes have been modelled reliably, the lake depth has been taken into account. These results can be transferred to any lake on the Tibetan Plateau given the

required forcing data including a representative lake surface temperature.

The choice of the surface model and the selection of the energy balance closure correction method are inter-related problems. The correction partitions the balance residual to the sensible and latent heat flux. This can be typically done according to the Bowen ratio, or according to the presented new method which attributes a larger fraction to the sensible heat flux. Testing both methods leads to partly ambiguous model performance, especially with respect to the used parameter sets. It clearly leads to shifts in model bias, while the R^2 metric suggests higher model compatibility to the Bowen ratio correction. The latter agrees with previous findings with respect to SEWAB modelling, but is in contradiction with recent experimental findings, attributing the closure gap to secondary circulations, driven by buoyancy. Future research on model structure should account for such processes.

As expected, the flux measurements showed distinct differences between the investigated land use types in magnitude and dynamics. The used models were able to resolve these differences in general with contrasts between surface types exceeding model errors. This must be considered when validating regional flux estimates with eddy-covariance data from the dry Nam Co station. The findings from this thesis provide the basis to process eddy-covariance data on the required level as described above.

Zusammenfassung

Durch seine Höhe und Ausdehnung hat das Hochland von Tibet erheblichen Einfluss auf den ostasiatischen Monsun und den Wasserhaushalt in Ostasien. Daher sind regionale Wasser- und Energiebilanzen schon länger im Blickpunkt der Forschung. Übliche Ansätze der regionalen Modellierung stützen sich auf Fernerkundungsdaten, die wiederum durch hochwertige Flussmessungen über repräsentativen Unterlagen validiert werden. Messungen mit Eddy-Kovarianz bieten zwar die benötigte Genauigkeit, bringen aber typische Nachteile mit sich, wie z.B. Datenlücken oder systematische Abweichungen aufgrund der ungeschlossenen Energiebilanz oder Heterogenität des Messgebiets. Innerhalb des EU Projekts CEOP-AEGIS soll eine einheitliche Bearbeitung von tibetischen Eddy-Kovarianz-Daten festgelegt werden, die sowohl eine Flusskorrektur aufgrund der ungeschlossenen Energiebilanz vorsieht als auch das Füllen von Datenlücken.

In der Dissertation werden zunächst zwei Aspekte der Datenqualität turbulenter Flüsse (fühlbare Wärme und latente Wärme/Verdunstung) auf dem tibetischen Hochland näher untersucht. Zum einen kann in den Messungen häufig bodennahe freie Konvektion nachgewiesen werden, was die Datenqualität beeinträchtigt. Zum anderen konnte gezeigt werden, dass gestörte Windsektoren, wie sie bei manchen Ultraschallanemometern vorkommen, von der Koordinatenrotation mit Planar-fit ausgeschlossen werden sollten. Anderenfalls treten vermehrt unrealistische Messungen des Impulsflusses auf, ein Einfluss auf Skalare wie fühlbare Wärme konnte jedoch nicht bestätigt werden.

Der zentrale Punkt dieser Dissertation ist die prozessorientierte Modellierung turbulenter Flüsse über typischen Unterlagen auf dem tibetischen Hochland. In einer Fallstudie am Nam Co wurden im Sommer 2009 Energiebilanzmessungen über trockener alpiner Steppe und etwas feuchterem Grasland sowie über einem flachen See durchgeführt. Die turbulenten Flüsse über Land wurden anschließend mit dem Energie- und Wasserbilanzmodell SEWAB simuliert, für den See kam ein hydrodynamisches Mehrschichtenmodell zum Einsatz. Die außergewöhnliche Höhenlage erzeugt besondere Bedingungen, vor allem auf trockenen Böden treten extrem hohe Oberflächentemperaturen auf. Deshalb war eine Anpassung von SEWAB an diese Bedingungen notwendig (TP Version). Ein Modellvergleich mit den Eddy-Kovarianz-Daten wurde unter Beachtung der Energiebilanzschließungslücke, wie sie bei Messungen typischerweise auftritt, durchgeführt.

SEWAB konnte die Flüsse auf beiden Graslandflächen konsistent simulieren, d.h. die Unterschiede zwischen der feuchten und der trockenen Fläche wurden nur durch Benutzung der standortspezifischen Modellparameter zufriedenstellend erreicht. Die Modellanpassung (TP Version) kann als Verbesserung angesehen werden. Dies trifft nicht zu für Labormessungen der Modellparameter. Standardparameter für den jeweiligen Vegetations- und Bodentyp lieferten eher bessere Ergebnisse, eine herkömmliche Bodenansprache direkt am Messfeld sowie Messungen der Bodentemperatur und

Feuchte sind jedoch Voraussetzung für den Erfolg. Auch mit dem Seemodell konnten gute Ergebnisse erzielt werden. Durch die Berücksichtigung der Seetiefe kann das Modell auf andere Seen übertragen werden, solange die meteorologischen Antriebsdaten sowie eine repräsentative Wasseroberflächentemperatur gegeben sind.

Erwartungsgemäß beeinflusst die ausgewählte Korrektur zur Energiebilanzschließung auch die Modellanpassung an die "Mess-"Daten. Die Korrektur verteilt das Residuum der Energiebilanz auf die turbulenten Flüsse. Neben der bekannten Methode der Verteilung nach dem Bowenverhältnis wurde auch eine neue Korrektur eingeführt, die das Residuum gemäß der prozentualen Anteile der turbulenten Flüsse am Auftriebsstrom verteilt, was im Vergleich zur vorigen Methode höhere fühlbare Wärmeströme erzeugt. Dadurch wird der Modell-Bias natürlich verändert, was die Ergebnisse teilweise uneindeutig macht. Nach dem Bestimmtheitsmaß zu urteilen, scheint die Aufteilung der Energieflüsse in SEWAB eher zu den Messungen zu passen, die durch das Bowenverhältnis korrigiert wurden. Dies bestätigt Ergebnisse aus der Literatur in Bezug auf Modellierung mit SEWAB, widerspricht aber neueren Erkenntnissen aus experimenteller Sicht, die sekundäre Zirkulationen als Ursache für die Schließungslücke sehen und die Korrektur nach dem Auftriebsstrom favorisieren.

Die verschiedenen Unterlagen am Nam Co unterscheiden sich erwartungsgemäß deutlich, wie die Messungen belegen und die Simulationen auch adäquat abbilden. Diese Heterogenität muss berücksichtigt werden, wenn die Nam Co-Station zur Validierung mesoskaliger Anwendungen herangezogen wird. Aufgrund der Ergebnisse dieser Arbeit kann die oben genannte Datenbearbeitung erfolgreich durchgeführt werden.

1. Introduction

1.1. Motivation: Regional estimates of turbulent fluxes on the Tibetan Plateau

The Tibetan Plateau (TP) has become a topic of strong scientific interest due to its role in the global water cycle and its reaction to climate change (e.g. Immerzeel et al., 2010; Ni, 2011). It is noticed as the largest and highest plateau on earth with an altitude of more than 4000 m a.s.l. on average. The TP is the offspring area of major rivers in South East Asia. Furthermore, it acts as an important heat source in the general circulation with an influence on the East-Asian monsoon (e.g. Yanai et al., 1992; Ye and Wu, 1998; Hsu and Liu, 2003; Duan and Wu, 2005; Kang et al., 2010). Therefore regional flux estimates of sensible and latent heat are important variables to link the energy cycle and the hydrological cycle at the surface on the TP.

Such regional models, driven by remote sensing data, require high quality ground truth of turbulent fluxes for validation. Efforts have been undertaken to understand the role of the TP in the global heat and water budget in intensive observation periods GAME/Tibet from 1996 to 2000 and CAMP/Tibet from 2001 to 2006 (Ma et al., 2005), leading to the Tibetan Observation and Research Platform (TORP Ma et al., 2009b). Despite these efforts direct measurements of sensible and latent heat flux remain sparsely distributed on the TP due to its size and remoteness (Kang et al., 2010; Maussion et al., 2011). Special characteristics are observed on the TP, which are summarised by Ma et al. (2009b). Due to its elevation, the incoming short wave radiation is very high with a very small fraction of diffuse radiation. Likewise, a huge daily variation of surface temperature exists over grassland and bare soil surfaces. Its range strongly depends on soil moisture and can exceed 60 K under dry conditions (Yang et al., 2009). On the other hand, large areas in Central Tibet are formed as heterogeneous landscapes of dry grasslands (*Kobresia* pastures, alpine steppe) together with wetlands or grasslands characterised by shallow groundwater and therefore exhibit strong spatial and temporal variation of soil moisture (Su et al., 2011). Under these conditions the preparation of representative flux measurements is a challenging task.

Some attempts have already been undertaken to up-scale observations of energy fluxes to regional estimates on the TP, but validation has been done yet with standard meteorological measurements using bulk approaches (e.g. Ma et al., 2011), or using eddy-covariance data from a single site (Ma et al., 2009a). As eddy-covariance is the only direct method to measure sensible and latent heat flux, its role in the validation

Table 1.1. Permanent measurement sites on the Tibetan Plateau as selected for the CEOP-AEGIS project

Site	Coordinates	Altitude	Land cover
Naqu (BJ)	31°22′7″N 91°53′55″E	4502 m	Alpine steppe
Nam Co	30°46′22″N 90°57′47″E	4745 m	Alpine steppe
Linzhi	29°45′56″N 94°44′18″E	3327 m	Alpine grassland
Qomolangma	28°21′29″N 86°56′47″E	4293 m	Gravel

of such regional flux maps should be strengthened , but an adequate processing and quality control, as summarised by Rebmann et al. (2012), Foken et al. (2012) and demonstrated on the TP e.g. by Metzger et al. (2006), is a prerequisite.

1.2. My contribution to the project objectives

My work of the last years is mainly related to the project: "**C**oordinated Asia-**E**uropean long-term **O**bserving system of Qinghai–Tibet **P**lateau hydrometeorological processes and the **A**sian-monsoon syst**E**m with **G**round satellite **I**mage data and numerical **S**imulations (CEOP-AEGIS)". It is a collaborative project / Small or medium-scale focused research project – Specific International Co-operation Action financed by the European Commission under FP7 topic ENV.2007.4.1.4.2 "Improving observing systems for water resource management", and is coordinated by the University of Strasbourg, France (www.ceop-aegis.org). Amongst other goals it aims at constructing an observing system to monitor the plateau's water yield by a combination of ground measurements and satellite based observations. This is of immediate interest for water resources management in South-East Asia. The anticipated outcome is providing infrastructure, i.e. an interactive data portal will be delivered, featuring a three-year data set with observations of the water balance terms. Together with higher level products and distributed hydrological modelling a prototype monitoring system is formed including early warning on floods and droughts which is intended to remain in operation beyond project completion.

Within this infrastructural project I was responsible for delivering quality checked ground based observations of surface energy fluxes. The data set incorporates fluxes over three years at four stations on the Tibetan Plateau (see Table 1.1), the turbulent fluxes (sensible heat and latent heat/evapotranspiration) were derived by the eddy-covariance method. Based on previous studies about quality assurance of eddy-covariance measurements in the community and especially in the Department of Micrometeorology, University of Bayreuth, I myself compiled a work flow for the processing of eddy-covariance data in three levels. These are:

Level I Turbulent fluxes, being checked for data quality, footprint, and potential obstacles in the vicinity of the sensor.

Level II Level I data, corrected with respect to the energy balance closure.

Level III Gap-filled level II data.

In the course of this I adapted respective tools for footprint analysis developed by Mathias Göckede (Göckede et al., 2005, 2006, 2008) and merged them into a single, user-optimised R routine (Work report in prep.). The scheme and its implementation up to the creation of NetCDF data sets is described in CEOP-AEGIS technical reports (Babel et al., 2011a,b). As it was not possible to get access to the Chinese original data, I introduced Chinese colleagues to the methods and supervised the processing at all stages.

In general, the presented workload could be straightforwardly handled consulting the relevant literature and executing the necessary steps. Nevertheless, the special conditions on the Tibetan Plateau mentioned in Sect. 1.1 raise the need for investigations beyond existing studies. Gap-filling of turbulent fluxes for Level III aims at representing the system dynamics adequately for this unique environment rather than delivering correct annual sums of evapotranspiration. This cannot be achieved with empirical or statistical approaches as presented by Falge et al. (2001a,b), but with Soil - Vegetation - Atmosphere - Transfer (SVAT) models. Therefore own turbulent flux measurements over different types of surfaces have been conducted in order to derive the essential input parameters as well as turbulent flux observations for validation (Biermann et al., 2009; Gerken et al., in prep.). This was necessary, because the access to Chinese data gathered on the Tibetan Plateau was very limited. The measurements, however, show a significant non-closure of the energy balance, which is distinctive of such heterogeneous environments (Foken, 2008a). Different options exist to close this gap (e.g. Foken et al., 2011) and their application clearly has an impact on the outcome of model validation.

The aim of these efforts is to provide surface model solutions for significant land surface types on the Tibetan Plateau, which serve as a high-standard gap-filling tool and estimation of representativeness of the permanent flux stations within CEOP-AEGIS. Furthermore, inconsistencies in the turbulence measurements caused by specific sensor types had to be investigated in order to assess the effect of such problems on sensible and latent heat flux measurements. From these problems I defined my research tasks further described in the next section.

1.3. Objectives of the thesis

The main focus of this thesis is the application of process based modelling to estimate surface sensible heat fluxes and latent heat fluxes (evapotranspiration) in the specific environment of the Tibetan Plateau. Although several surface model studies already exist on the Tibetan Plateau (see Sect. 2.2), a thorough analysis including eddy-covariance measurements of turbulent fluxes is still missing. Moreover, there is a lack of evaporation measurements above lake surfaces. To my best knowledge, Tobias Biermann and me conducted the first eddy-covariance measurements over a lake surface on the Tibetan Plateau. This made it possible to validate a lake surface model. Based on these preconditions the following research questions have been elaborated.

- Land surface modelling under the specific conditions of the Tibetan Plateau using the land surface scheme SEWAB (Mengelkamp et al., 1999) and validation with eddy-covariance measurements.
- Elaboration of the necessary model parameters: required efforts and impact on model performance.
- Investigation of different methods to correct for the energy balance closure gap and their influence on model performance assessment.
- Potential application of the elaborated model version.
- Specific problems of eddy-covariance data quality on the Tibetan Plateau and mitigation of specific measurement problems occurring with some sonic anemometers.

The publications and manuscripts listed on page v contribute to these research questions as follows: Babel et al. (2013, Appendix C) present an adaptation of the land surface scheme SEWAB (Mengelkamp et al., 1999) to the Tibetan Plateau. The adaptation is designed to consider specific issues of land surface modelling as mentioned in Sect. 2.2. The model performance with respect to turbulent fluxes is investigated by using eddy-covariance measurements above alpine steppe from two nearby sites at Nam Co lake. Parameter sets originating from both standard values and laboratory and in situ measurements are tested in this manuscript. Special emphasis is put on the energy balance closure of turbulent flux measurements and its correction. Besides of using the well known method of distributing the residual according to the Bowen ratio (Twine et al., 2000), a new correction method, suggested by Charuchittipan et al. (2013, Appendix E), has been applied: The residual is distributed according to the relative contribution of the turbulent fluxes to the buoyancy flux. Charuchittipan et al. (2013, Appendix E) analyse a comprehensive data set from the LITFASS-2003 campaign, Lindenberg, Germany. The influence of the averaging time for eddy-covariance fluxes is intensely studied utilising Ogive analysis, block ensemble averaging, wavelet and quadrant analysis. The manuscript suggests secondary circulations to be responsible for the gap in energy balance closure and attributes a dominant role to the sensible heat flux. The proposed new closure correction method is based on these experimental findings. As a novel approach, both two correction methods have been applied to the data and the consequences on model performance evaluation is discussed by Babel et al. (2013, Appendix C).

The SEWAB model successfully simulates turbulent fluxes on the Tibetan Plateau, creating several benefits: It can be as a reference for a more simplistic parametrisations as done by Gerken et al. (2012, Appendix B). Therein the simplistic land surface scheme Hybrid is updated with a new soil model, aiming to eliminate a delayed surface response to atmospheric forcing in the original version. SEWAB is successfully utilised for comparisons in example daily cycles. As SEWAB showed no delay in surface response, its simulations have been used to evaluate Hybrid's responsiveness with cross correlation (Gerken et al., 2012, Appendix B).

Another application is the usage of the simulated timeseries in order to assess landscape heterogeneity at Nam Co (Biermann et al., 2013, Appendix D). The gappy observations of a wet alpine steppe and a shallow lake could be effectively described by modelled timeseries of SEWAB and a hydrodynamic multilayer model (Foken, 1984) with an extension to shallow water exchange (Panin and Foken, 2005). Turbulent fluxes for both surface types are then compared with the SEWAB simulations of the "standard" land surface at Nam Co, dry alpine steppe. It could be shown that the differences among land surface types likely exceed the model uncertainty, so the differences are considerable. The effect of this heterogeneity is discussed in terms of using the eddy-covariance data as ground truth for remote sensing.

In order to use eddy-covariance data for model evaluation some issues about data quality should be clarified in advance. Although not included in the thesis Zhou et al. (2011)[1] provide a basis for further usage of eddy-covariance data at the Nam Co Monitoring and Research Station for Multisphere Interactions: In addition to standard evaluation of footprint and data quality the occurrence of near-ground free convection events is investigated. It is shown that such events can be created on the Tibetan Plateau already due to changing cloudiness, and their influence on data quality is assessed. Furthermore, at one of the CEOP-AEGIS sites the sonic anemometer DAT 600 TR61A probe from Kaijo-Denki is in use. The sensor is not omnidirectional, i.e. in a certain sector the wind field is disturbed by the sensor structure and irregular friction velocities occur as a consequence. The study by Li et al. (2013, Appendix F) highlights this problem and investigates its influence on scalar fluxes and whether such problems occur also with the commonly used CSAT3, Campbell Scientific Ltd. A sector-wise planar-fit is suggested as an appropriate coordinate rotation to mitigate

[1] Together with Rafael Eigenmann I introduced Zhou Degang into the post-processing of the turbulence data, including the usage of TK2 and footprint analysis tools, and into the investigation and relevance of near ground free convection conditions at Nam Co station. I personally supported him in the usage and interpretation of the data quality tools.

such problems.

2. Background

2.1. Observed energy balance and closure

The eddy-covariance method is the only direct method to measure turbulent exchange of heat and scalars between the atmosphere and the underlying surface and is therefore preferred in the community to quantify long-term fluxes of water vapour and carbon dioxide (Foken and Wichura, 1996; Baldocchi et al., 2001). Despite the general trust placed in this method, it became apparent that the energy balance cannot be closed at most experimental sites (e.g. Foken, 2008a). The surface energy balance at the surface is given by

$$-R_{\mathrm{net}} = Q_{\mathrm{H}} + Q_{\mathrm{E}} + Q_{\mathrm{G}} + \Delta Q_{\mathrm{S}} \tag{2.1}$$

with the net radiation R_{net}, the sensible heat flux Q_{H}, the latent heat flux Q_{E}, the ground heat flux Q_{G}, and the change in energy storage ΔQ_{S}. The signs follow the convention that fluxes directed towards the surface are negative and vice versa. Although this theoretical balance should be reproduced with measurements as well, according to Foken (2008a) most studies report that the sum of turbulent energy (Q_{H} and Q_{E}) only yields 70%–100% of the available energy ($-R_{\mathrm{net}} - Q_{\mathrm{G}} - \Delta Q_{\mathrm{S}}$). This residual is typically larger in complex landscapes (e.g. Aubinet et al., 2000; Wilson et al., 2002), while in homogeneous areas or deserts the energy balance can be closed (e.g. Heusinkveld et al., 2004; Mauder et al., 2007).

It is recognized that in the measured energy balance turbulent energy is missing rather than available energy being overestimated so long as the energy storage and the ground heat flux has been addressed adequately (Twine et al., 2000; Foken, 2008a; Foken et al., 2011; Leuning et al., 2012). Especially when comparing eddy-covariance derived turbulent fluxes with those land surface model simulations, which are actually constrained by the energy balance equation, a systematic mismatch can be expected as pointed out by Falge et al. (2005). Therefore a correction of the turbulent fluxes should be considered. A widely used correction method proposed by Twine et al. (2000) distributes the residual according to the Bowen ratio, assuming scalar similarity between latent and sensible heat with respect to the missing flux. In contrast some studies indicate that the missing energy stems from sensible heat only (Mauder and Foken, 2006; Ingwersen et al., 2011). The recent discussion hypothesizes an influence of secondary circulations in complex landscapes, triggering near-ground advective and low-frequency flux components (Steinfeld et al., 2007; Foken et al., 2010, 2011; Stoy et al., 2013; Brötz et al., 2013). Such circulation systems are mainly driven by buoyancy suggesting the buoyancy flux to play a dominant role for the energy balance closure.

2.2. Land surface modelling on the Tibetan Plateau

Due to its remoteness, regional flux estimation on the Tibetan Plateau does not have a long history, see also Babel et al. (2013, Appendix C). First multi-year estimates across a variety of sites on the Tibetan Plateau have been presented by Xu and Haginoya (2001), calculating fluxes from standard meteorological measurements. Within the GEWEX Asian Monsoon Experiment 1998 Takayabu et al. (2001) utilized four land surface models for a comparison study, reported large differences in turbulent flux partitioning, but could not validate the models due to a lack of soil moisture and flux measurements. Only very few studies exist using eddy-covariance flux measurements for validation (e.g. Yang et al., 2009; Hong and Kim, 2010).

These studies find an overestimation of the sensible heat flux as a typical feature of land surface modelling on the Tibetan Plateau. They blame too high turbulent diffusion coefficients for this problem an draw a relationship to the special conditions on the Tibetan Plateau (see Sect. 1.1), in particular the strong diurnal cycle of surface temperature over dry and sparsely vegetated surfaces. Indeed, Yang et al. (2003) and Ma et al. (2002) observed a diurnal variation of the sublayer-Stanton number B, describing the logarithm of the ratio between aerodynamic and thermal roughness lengths $\kappa B^{-1} = \ln(\frac{z_{0\mathrm{m}}}{z_{0\mathrm{h}}})$. Formulations of κB^{-1} as a fixed fraction, or depending on the friction velocity (Zilitinkevich, 1995) cannot resolve this diurnal variation. Therefore (Yang et al., 2008) propose a new formulation with an additional dependence on the temperature scale T_* and empirical adaptation to Tibetan Plateau observations (see Sect. 3.2.1). Leading to the determination of a variable thermal roughness length in land surface models, this parametrisation has been successfully rated in some recent studies in Asian arid regions Yang et al. (2008); Chen et al. (2010, 2011); Liu et al. (2012); Zhang (2012).

Other developments include the influence of soil vertical heterogeneity which is found to be significant in case of remarkable stratification (Yang et al., 2005; van der Velde et al., 2009). For the soil heat flux on the Tibetan Plateau Yang et al. (2005) adapted a parametrisation for the soil thermal conductivity, proposed by Johansen (1975) and recommended by Peters-Lidard et al. (1998). In this form it can be easily transferred to any conditions when dry and saturated thermal conductivities are known. Furthermore, latent heat fluxes can be observed on the Tibetan Plateau even if soil moisture drops below wilting point, a typical feature in deserts or arid landscapes (Agam et al., 2004; Balsamo et al., 2011; Wallace et al., 1991). Different parametrisations of bare soil evaporation in dependence on soil moisture are compared by Mihailović et al. (1995), but these are not tested on the Tibetan Plateau yet.

Another challenge on the Tibetan Plateau is a small-scale heterogeneity of soil moisture (Su et al., 2011). Cold semiarid conditions characterise the landscape consisting of dry grasslands (*Kobresia* pastures, alpine steppe, partly non-vegetated) and wetlands or grasslands with shallow groundwater. The role of the soil moisture interacting with climate is highlighted in a review by Seneviratne et al. (2010). The land–atmosphere coupling strength (influence of soil moisture on precipitation) on the Tibetan Plateau, however, is rated low by Koster et al. (2004), but the local patterns of soil moisture and precipitation cannot be resolved by such studies using ensembles of global circulation models. Land surface models are in principle able to take small-scale heterogeneity of soil moisture into account, but this has to be tested.

Obtaining flux measurements in such a remote environment as the Tibetan Plateau is challenging (Ma et al., 2009b) and land surface modelling can support land surface flux estimation on local and regional scale. A wide range of land surface schemes being suitable for such a task have been evolved in the last decades: Starting with simple schemes (e.g. Manabe, 1969), second-generation land surface models evolved, adding e.g. detailed resistance schemes for evapotranspiration and more complexity into the description of soil processes (Pitman, 2003). More recent developments for third-generation models mainly include a dynamic vegetation, the "greening" of land surface models (Pitman, 2003).

In the context of land surface modelling this thesis lays the focus on how the model description of the special Tibetan Plateau conditions affect land surface fluxes (see Sect. 1.1). Thereby a crucial feature is the comparison with site-specific eddy-covariance measurements. As feedback mechanisms of the land surface to the atmosphere are out-of-scope, the most suitable approach is an offline forced land surface model with prescribed, site-specific state of vegetation and soil properties. The used model SEWAB is a representative of the second-generation land surface models and participated in the Project for Intercomparison of Land-surface Parametrization Schemes (PILPS: Henderson-Sellers et al., 1996; Chen et al., 1997). From this experience it has been improved regarding the description of soil and surface processes (Mengelkamp et al., 1999, 2001; Warrach et al., 2001) and is therefore adequately structured for the intended purpose. Initially developed for humid conditions SEWAB's performance under dry conditions has to be tested yet.

2.3. Lake surface modelling on the Tibetan Plateau

Lake surfaces should be taken into account for regional flux estimation on the Tibetan Plateau as approximately 45 000 km^2 is covered by lakes (Xu et al., 2009). The importance of lake surfaces for the regional energy balance and water cycle has been pointed out by Rouse et al. (2005) and Nordbo et al. (2011). Some evaporation estimates already exist for lake surfaces, modelled with simple bulk approaches based on daily or monthly forcing data from remote sensing or surface observations (Haginoya et al., 2009; Xu et al., 2009; Krause et al., 2010; Yu et al., 2011), in some cases validated with pan evaporation measurements. To my best knowledge no studies are reported yet, utilising or conducting eddy-covariance measurements above lake surfaces on the Tibetan Plateau.

There is a huge amount of lakes on the Tibetan Plateau ($\approx$1090 lakes larger than 10 km^2, Yu et al., 2011), therefore a variety of lake extent and depth can be expected to occur. These factors greatly influence surface temperature (and thereby atmospheric stability) and surface roughness (Rouse et al., 2005; Panin et al., 2006a; Nordbo et al., 2011). These variables in turn typically exhibit a diurnal variation on the one hand and their relationship to the surface fluxes is non-linear. Therefore the processes can only be represented by resolving the diurnal cycle, which is not possible with the methods mentioned above.

For such a purpose a hydrodynamic multilayer (HM) model (Foken, 1979, 1984) is a suitable candidate. It is originally designed for energy exchange above the ocean. Shallow water conditions, however, increase the wave height, depending on wind velocity, and therefore enhance the turbulent exchange (Panin and Foken, 2005). The HM model and the shallow water approach has been validated with eddy-covariance data from a lake in Germany and the impact on exchange over the Caspian Sea has been discussed (Panin et al., 2006b,a). Nevertheless, it has to be tested whether these parametrisations work under the conditions of the Tibetan Plateau as well.

3. Methods

3.1. The Nam Co 2009 experiment

As pointed out in Sect. 1.2 own experiments were inevitable to derive necessary data for input, parametrisation and validation of surface models. The Nam Co site (see description in the following) has been chosen, as it is an area where typical land surfaces of the Tibetan Plateau (dry alpine steppe, more wet and dense grassland, and lakes) occur closely together. Located at the intersection of the Westerlies with the Asian Monsoon circulation systems the Nam Co basin has been considered as a key area of interest (Haginoya et al., 2009; Keil et al., 2010).

3.1.1. Site description

The Nam Co 2009 experiment was carried out from 26 June to 8 August within the 2009 summer monsoon season. The site is located 220 km north of Lhasa in the Nam Co Basin, Tibetan Plateau, with its lake surface at an elevation of 4730 km a.s.l. The basin is dominated by the lake itself and the Nyainqentanglha mountain range, stretched along its SE side and reaching up to 7270 m a.s.l. with an average height of 5230 m (Liu et al., 2010). The Institute of Tibetan Plateau Research (ITP), Chinese Academy of Sciences is operating the Nam Co Monitoring and Research Station for Multisphere Interactions near a small lake in 1 km distance SE to the Nam Co Lake (see Figure 3.1). The vegetation around Nam Co reflects the prevailing arid, high-altitude climate with alpine meadows and steppe grasses (Mügler et al., 2010). Near the Nam Co Station the vegetation coverage and composition are highly variable according to the soil moisture conditions determined by topographic features: Grass genera typical for Alpine steppe (*Stipa, Carex, Helictotrichon, Elymus, Festuca, Kobresia, Poa*, see Biermann et al., 2009; Miehe et al., 2011) have been observed on the hillocks, with a total vegetation coverage of 60 % or less (grass$^-$), while more wet areas are densely covered (>90 %) with alpine meadows dominated by *Kobresia* species (grass$^+$, see Figure 3.1).

3.1.2. Measurements

Turbulent fluxes were obtained by two energy balance systems. One set-up is located directly at the Nam Co station over dry alpine steppe (grass$^-$), further called NamITP, operated by the Institute of Tibetan Plateau Research. The NamITP complex is settled

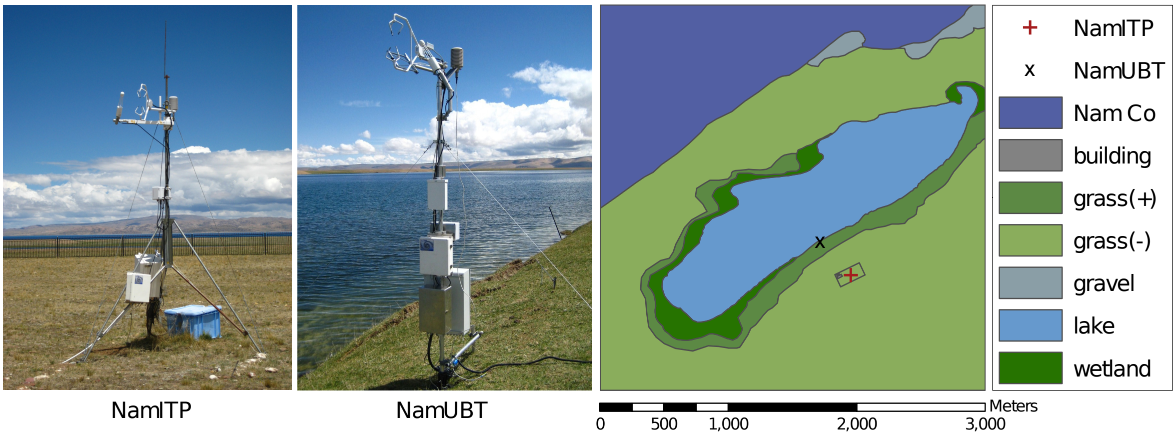

Figure 3.1. Flux measurements at Nam Co 2009, map from Gerken et al. (2012, Appendix B), photos from W. Babel.

on almost flat terrain, but starts to decline smoothly toward the small lake at a distance of 90m NNE. The second station has been set up for this experiment by the University of Bayreuth directly at the shoreline of the small lake (NamUBT). The measured turbulent fluxes correspond to a more wet alpine meadow (grass^{+}), a terraced land surface with a gentle average slope of $\leq 8°$, or to the lake surface, depending on wind direction. Both stations recorded the components needed to obtain the surface energy balance as well as standard meteorological variables. Table 3.1 gives an overview of the used instruments, for further details the reader is referred to Zhou et al. (2011) and Biermann et al. (2009).

3.1.3. Data post-processing

Half hourly fluxes were processed from turbulent raw data using the internationally compared software TK2/3 (Mauder and Foken, 2004, 2011). All post-processing steps and flux corrections recommended by Rebmann et al. (2012) and Foken et al. (2012) are applied within this software package. As NamUBT was located between a gentle sloping land surface and a level lake surface, a sector-wise planar-fit rotation was necessary in order to minimise the mean vertical wind velocity effectively (Biermann et al., 2013, Appendix D).

The data sets have been analysed for the period from July 1 to August 8, 2009. Quality filtering has been applied following Foken et al. (2012). If not otherwise specified, only data with best quality (Flag 1–3 out of 9 classes according to Foken et al., 2004) have been accepted for model performance evaluation and scatterplots, while figures of time series and diurnal cycles include intermediate data quality as well (Flag 1–6).

Furthermore, a footprint analysis and site-specific characterisation approach (Göckede et al., 2004, 2008) was conducted, utilizing a Lagrangian forward stochastic model by

Table 3.1. List of sensors used for retrieving the measured surface energy balance and additional sensors for standard meteorological variables

Type	Instrument	NamUBT	NamITP
Ultrasonic anemometer	CSAT3, Campbell Scientific Ltd.	3.0 m	3.1 m
Gas analyser	Li-7500 IRGA, LiCOR Biosciences	3.0 m	3.1 m
Air temperature and humidity	HMP 45, Vaisala	3.0 m	3.1 m
Net radiometer	CM3/CG3, Kipp & Zonen	-	1.5 m
Net radiometer	CNR1, Kipp & Zonen	2.0 m	-
Rain gauge	tipping bucket	1.0 m	1.0 m
Soil moisture	IMKO-TDR	$-10, -30, -50$ cm	$-10, -20, -40, -80, -160$ cm
Soil temperature	PT100	$-2.5, -5, -10, -15, -20, -30, -50$ cm	$-20, -40, -80, -160$ cm
Soil heat flux	Rimco HP3 heat flux plate	-15 cm	-
Water temperature	PT100	-30 cm	-
Logger	Campbell Scientific Ltd.	CR3000	CR5000

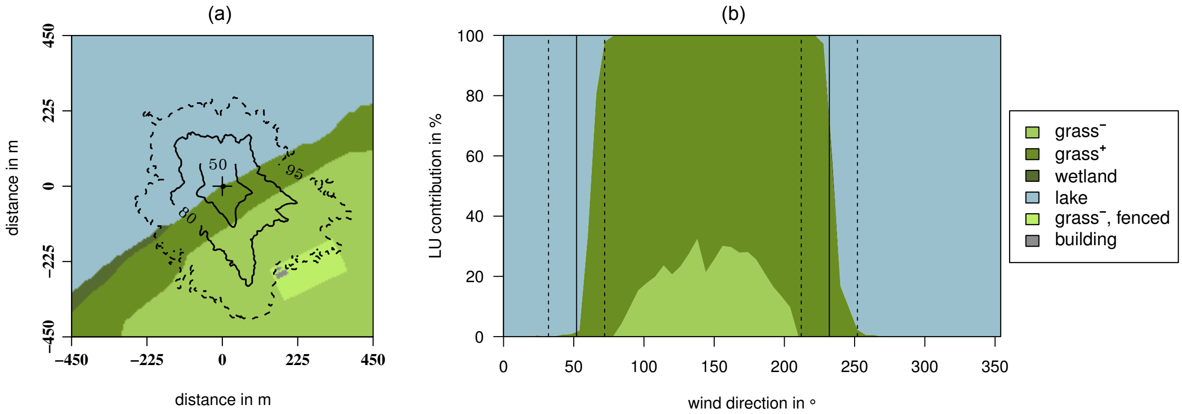

Figure 3.2. Footprint analysis for the 2009 measurement period at NamUBT station, **(a)**: footprint climatology, all stratifications, **(b)**: average land-use contribution in dependence on wind direction for unstable and neutral stratification. Modified from Biermann et al. (2013, Appendix D)

Rannik et al. (2000). The results show a sufficient contribution from the land use of interest, which is grass$^-$ in case of NamITP for all wind sectors. Details about data quality and footprint are given for this station with a data set from 2007 by Zhou et al. (2011). Measurements from NamUBT proved to be representative for the shallow lake in a wind sector of 252°–32° (Fig. 3.2). For the wind sector of 72°–212° the measurements represent grass$^+$ fairly well for unstable and neutral stratification (Fig. 3.2b). Major contributions from grass$^-$ only occur under stable stratification, where the flux differences between both surface types can be neglected.

3.1.4. Energy balance closure and correction

For both land surfaces grass$^-$ and grass$^+$ the components of the measured energy balance according to equation 2.1 has been determined (ΔQ_S can be neglected for short grassland). The ground heat flux for NamUBT has been calculated using the heat flux plate measurements and accounting for the heat storage in the layer above (Liebethal et al., 2005). For NamITP, a gradient method by Yang and Wang (2008) was applied. Both methods showed good agreement with a reference data set. The energy balance for the lake surface could not be determined, because the required measurements were missing to estimate the storage of the lake and the flux into the sediment.

The energy balance closure ratio obtained from the regression slope of turbulent fluxes versus available energy was found to be 81 % and 73 % for grass$^-$ and grass$^+$, respectively. Specific problems compromise the accuracy of the energy balance observed at NamITP (grass$^-$). These are deficiencies in temperature measurements of the uppermost soil layer (Table 3.1) and possibly not representative upwelling radiation measurements influenced by an unproportional large fraction of gravel in the respective footprint, see Babel et al. (2013, Appendix C). Nevertheless, the values observed for the closure ratio are typical for grassland in heterogeneous landscapes (Foken, 2008a).

The turbulent fluxes have been corrected according to the residual of the energy balance before comparing with model simulations. Two methods have been applied, (i) the well known correction after Twine et al. (2000) preserving the Bowen ratio (EBC-Bo), and (ii) a new correction method according to the buoyancy flux (EBC-HB). The latter is motivated by the hypothesis of secondary circulations causing the closure gap (see Sect. 2.1). It distributes the residual according to the relative contribution of sensible and latent heat to the buoyancy flux, described in the outlook of Charuchittipan et al. (2013, Appendix E) as follows: The buoyancy flux Q_{HB} is defined by analogy to the sensible heat flux, but driven by the virtual temperature T_{v},

$$Q_{\mathrm{HB}} = \rho c_{\mathrm{p}} \overline{w' T_{\mathrm{v}}'} \qquad \text{with } T_{\mathrm{v}} = T(1 + 0.61q) \tag{3.1}$$

with the air density ρ, the specific heat capacity c_{p}, the air temperature T and the specific humidity q. The virtual temperature is nearly equal to the sonic temperature (Kaimal and Gaynor, 1991). Thus the relation between sensible heat flux and buoyancy flux can be derived in a similar way as done by Schotanus et al. (1983), applying Reynolds's decomposition for T and q, leading to

$$Q_{\mathrm{HB}} = \rho c_{\mathrm{p}} \overline{w' T_{\mathrm{v}}'} \;\simeq\; \rho c_{\mathrm{p}} \left(\overline{w' T'} + 0.61 \overline{T}\, \overline{w' q'} \right) = Q_{\mathrm{H}} \left(1 + 0.61 \overline{T} \frac{c_{\mathrm{p}}}{\lambda \cdot Bo} \right) \tag{3.2}$$

with the Bowen ratio $Bo = \frac{Q_{\mathrm{H}}}{Q_{\mathrm{E}}}$ and λ is the heat of evaporation. This relationship is utilised in the EBC-HB correction to distribute the residual Res to the turbulent fluxes

$$Q_{\mathrm{H}}^{\mathrm{EBC-HB}} = Q_{\mathrm{H}} + f_{\mathrm{HB}} \cdot Res \tag{3.3}$$

$$Q_{\mathrm{E}}^{\mathrm{EBC-HB}} = Q_{\mathrm{E}} + (1 - f_{\mathrm{HB}}) \cdot Res \tag{3.4}$$

with

$$f_{\mathrm{HB}} = \frac{Q_{\mathrm{H}}}{Q_{\mathrm{HB}}} = \left(1 + 0.61 \overline{T} \frac{c_{\mathrm{p}}}{\lambda \cdot Bo} \right)^{-1} \tag{3.5}$$

The EBC-HB method does not preserve the Bowen ratio, therefore Eqns. 3.3-3.5 have to be calculated iteratively until Bo converges. Both methods can be compared with respect to their dependence on the Bowen ratio (Fig 3.3). As anticipated the EBC-HB method distributes more of the residual to the sensible heat flux. This difference is most pronounced for low Bowen ratios and becomes negligible for very high Bowen ratios.

The assumptions inherent in both correction methods are meaningless for night-time data, therefore the corrections were only applied, when both sensible and latent heat flux exceed a threshold of $10\,\mathrm{W\,m^{-2}}$ and the Bowen ratio is positive. Furthermore, instantaneous residuals $> 150\,\mathrm{W\,m^{-2}}$ may introduce huge errors in the correction, and respective flux observations have been excluded from model evaluation.

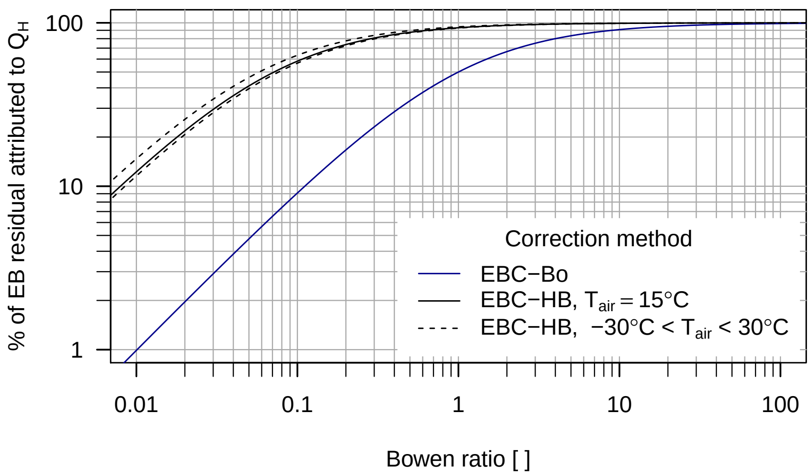

Figure 3.3. General effect of the energy balance correction methods according to the Bowen ratio (EBC-Bo) and according to the buoyancy flux (EBC-HB); the percentage of the residual attributed to Q_{H} is shown in dependence on Bo; EBC-HB weakly depends on air temperature T_{air} and the dashed lines indicate the range of the relationship at $-30°C < T_{\mathrm{air}} < 30°C$; modified from Charuchittipan et al. (2013, Appendix E)

3.2. Land surface modelling for Nam Co 2009

For this thesis a land surface model called SEWAB is used, developed by Mengelkamp et al. (1997) in the former GKSS Research Centre, Geesthacht, Germany. It is a standalone 1D soil-vegetation-atmosphere transfer model, developed for humid conditions in Central Europe and well suited for the purpose of this study (see Sect. 2.2). Model equations are described in detail by Mengelkamp et al. (1999, 2001); Warrach et al. (2001). Nevertheless a summary of the most important features is given in Table 3.2. For this study the energy balance closure of SEWAB is of major interest. SEWAB is constrained by the energy budget equation, and all individual components are computed iteratively solving for the surface temperature. Therefore all fluxes parametrised with the surface temperature are interlinked, which are sensible heat flux, the ground heat flux and the longwave upwelling radiation, but also the latent heat flux via the temperature dependent specific humidity of saturation.

3.2.1. Model versions

In this study the model has been run as described above (original version) and in a version adapted to the conditions of the Tibetan Plateau (TP version). The following set-up has been chosen for both versions:

- 7 soil layers reaching a total depth of 2 m and 5 layers within the first 50 cm.

Table 3.2. Parametrisation of energy balance components in SEWAB and their connection to the surface temperature T_g

Variable	Equation
Net radiation	$R_{net} = -R_{swd}(1-a) - R_{lwd} + \varepsilon\sigma T_g^4$, R_{swd} and R_{lwd} prescribed in forcing data set
Ground heat flux	$Q_G = \lambda_s\,(T_g - T_{S1})\,\Delta z_{S1}^{-1}$, $S1$: uppermost soil layer
Sensible heat flux	$Q_H = C_H \rho c_p u(z)(T_g - T(z))$
Latent heat flux	Evaporation from bare soil E_s, wet foliage E_f and plant transpiration E_{tr} (Noilhan and Planton, 1989) $E_s = C_E \rho u(z)(\alpha q_s(T_g) - q(z))$ $E_f = C_E \rho u(z)(q_s(T_g) - q(z))$ $E_{tr} = (R_a + R_s)^{-1} \rho (q_s(T_g) - q(z))$
Stability dependence	C_H after Louis (1979), $C_E = C_H$
Soil temperature	Distribution solved by the diffusion equation
Soil moisture	Movement solved by the Richards' equation Characteristics from Clapp and Hornberger (1978)

a	albedo [-]	u	wind velocity [m s^{-1}]
C_E	Dalton number [-]	u_*	friction velocity [m s^{-1}]
C_H	Stanton number [-]	z	measurement height [m]
c_p	air heat capacity [J kg^{-1} K^{-1}]		
q	specific humidity [-]	α	dependence factor of soil air humidity to soil water content [-]
q_s	saturation specific humidity [-]		
R_a	turbulent atmospheric resistance [s m^{-1}]	ε	emissivity [-]
R_{lwd}	long wave downward radiation [W m^{-2}]	λ_s	soil thermal conductivity [W m^{-1} K^{-1}]
R_{swd}	short wave downward radiation [W m^{-2}]	ρ	air density [kg m^{-3}]
T	temperature [K]	σ	Stefan Boltzmann constant [W m^{-2}K^{-4}]

- hydrological modules containing tunable parameters, which cannot be determined, are disabled (ponding, variable infiltration capacity, ARNO concept for subsurface runoff and baseflow, depth dependency parametrisation of saturated hydraulic conductivity, see Mengelkamp et al., 1999, 2001)
- offline forcing with measured precipitation, air temperature, wind velocity, air pressure, relative humidity, downwelling short-wave and long-wave radiation using the same data for both grass$^+$ and grass$^-$.
- internal model time step of 10 min, interpolation of 30-min forcing data and aggregation of output to 30 min.
- initialisation of soil moisture and soil temperature profiles with a 3-year forcing data set extracted from the ITPCAS (Institute of Tibetan Plateau Research, Chinese Academy of Sciences) gridded forcing data set (Chen et al., 2011). Test simulations showed reasonable simulations of soil moisture for the grass$^-$ surface, but could not be used for the grass$^+$ surface, as the shallow ground water table at NamUBT could not be reproduced with a single column realisation.
- initialisation of soil moisture and soil temperature profiles with observed profiles. This initialisation showed good agreement with the 3-year spin-up at grass$^-$, therefore it has been solely used for all analysis for both surface types.

The adaptation to the Tibetan Plateau (TP version) aims at addressing the issues mentioned in Sect. 2.2. The changes include:

1. A new calculation of the soil thermal conductivity λ_s following Yang et al. (2005)
$$\lambda_s(\Theta) = \lambda_{dry} + (\lambda_{sat} - \lambda_{dry}) \exp\left[0.36 \cdot (1 - \Theta_{sat}/\Theta)\right] \tag{3.6}$$
with the volumetric soil water content Θ and Θ_{sat} as the porosity. The dry and saturated thermal conductivity limits were estimated from field observations as $\lambda_{dry} = 0.15\,\mathrm{W\,m^{-1}\,K^{-1}}$ and $\lambda_{sat} = 0.8$ and $1.3\,\mathrm{W\,m^{-1}\,K^{-1}}$ for grass$^+$ and grass$^-$, respectively. This parametrisation replaced the original formulation featuring a weighted sum of individual thermal conductivities of dry clay/sand, water, ice and air according to the actual state.

2. To account for diurnal and seasonal variations of the thermal roughness length observed on the Tibetan Plateau (Yang et al., 2003), a formulation according to Yang et al. (2008) has been implemented
$$z_{0h} = \frac{70\nu}{u_*} \exp\left(-\beta u_*^{0.5} |T_*|^{0.25}\right) \tag{3.7}$$
with the kinematic viscosity of air ν, the friction velocity u_*, the dynamic temperature scale $T_* = -\overline{w'T'}/u_*$ and an empirical constant $\beta = 7.2\,\mathrm{s^{0.5}\,m^{-0.5}\,K^{-0.25}}$. As

T_* depends on $z_{0\mathrm{h}}$, the equation has to be solved iteratively (Yang et al., 2010). The original formulation estimates $z_{0\mathrm{h}}$ as a fixed fraction of the aerodynamic roughness length $z_{0\mathrm{h}} = 0.1 z_{0\mathrm{m}}$.

3. Like observed in desert landscapes (Agam et al., 2004; Balsamo et al., 2011; Wallace et al., 1991), latent heat fluxes occur on the Tibetan Plateau even when soil moisture drops below wilting point. The soil air humidity controlling bare soil evaporation is adjusted in SEWAB with a soil moisture dependent factor α (see Table 3.2). To account for dry conditions a formulation by Mihailović et al. (1993) has been implemented

$$\alpha = \begin{cases} 1 - \left(1 - \dfrac{\Theta}{\Theta_{\mathrm{FC}}}\right)^n, & \Theta \leq \Theta_{\mathrm{FC}} \\ 1, & \Theta > \Theta_{\mathrm{FC}} \end{cases} \tag{3.8}$$

with the volumetric water content at field capacity Θ_{FC}, the actual water content of the topsoil Θ and using $n = 2$ as exponent. The original parametrisation $\alpha = 0.5\left[1 - \cos\left(\frac{\Theta}{\Theta_{\mathrm{FC}}}\pi\right)\right]$ for $\Theta \leq \Theta_{\mathrm{FC}}$ (Noilhan and Planton, 1989) is very prohibitive for low Θ as pointed out by Mihailović et al. (1995).

3.2.2. Model parameters

In order to focus on the impact of the model versions on the performance, no optimisation algorithms were applied to constrain the parameter space. Instead, two ways of deriving "reasonable" parameter sets were explored, defining a "measured" parameter set and a "default" parameter set. While the latter can be obtained with a standard knowledge of the surface and soil types involved, the measured parameters represent detailed in situ and laboratory observations of the relevant site-specific properties. A summary of the most important parameters gives Table 3.3. The leaf area index, emissivity, minimum stomatal resistance and maximum stomatal resistance were not measured and therefore uniformly taken for both surface types and parameter sets (Hu et al., 2009; Yang et al., 2009; Alapaty et al., 1997).

Default parameters differ most considerably between both surfaces in the description of the soil. The soil texture was classified as "sand" and "sandy loam", USDA textural classes, for grass$^-$ and grass$^+$, respectively. The corresponding parameters have been collected for SEWAB by Mengelkamp et al. (1997), originating from Clapp and Hornberger (1978) in case of the hydraulic properties. As both land use types are classified as short grassland, the surface parameters differ solely in the fraction of vegetated area and therefore in the over-all albedo (albedo for grassland and dry bare soil from Foken, 2008b).

Measured parameters use meteorological observations for albedo and roughness length for momentum, fraction of vegetated area, canopy height and rooting depth were

Table 3.3. Most important parameters for the model simulations: albedo a, emissivity ε, fraction of vegetated area f_{veg}, leaf area index of vegetated area $\mathrm{LAI}_{\mathrm{veg}}$, canopy height h_{c}, rooting depth z_{r}, roughness length $z_{0\mathrm{m}}$, minimum stomatal resistance $R_{s,\mathrm{min}}$, maximum stomatal resistance $R_{s,\mathrm{max}}$, thermal diffusivity ν_{T}, soil heat capacity $C_{\mathrm{G}} \cdot \varrho_{\mathrm{G}}$, porosity Θ_{sat}, matrix potential at saturation Ψ_{sat}, saturated hydraulic conductivity K_{sat}, volumetric water content at field capacity Θ_{FC}, volumetric water content at wilting point Θ_{WP}, and exponent b for relationships after Clapp and Hornberger (1978).

		Default parameter		Measured parameter	
Parameter	Unit	NamITP	NamUBT	NamITP	NamUBT
Surface and vegetation parameter					
a	-	0.22	0.205	0.196	0.196
ε	-	0.97	0.97	0.97	0.97
f_{veg}	-	0.6	0.9	0.6	0.9
$\mathrm{LAI}_{\mathrm{veg}}$	-	1.0	1.0	1.0	1.0
h_{c}	m	0.15	0.15	0.15	0.07
z_{r}	m	0.3	0.3	0.3	0.5
$z_{0\mathrm{m}}$	m	0.005	0.005	0.005	0.005
$R_{s,\mathrm{min}}$	$\mathrm{s\,m^{-1}}$	60.0	60.0	60.0	60.0
$R_{s,\mathrm{max}}$	$\mathrm{s\,m^{-1}}$	2500	2500	2500	2500
Soil parameter					
ν_{T}	$\mathrm{m^2\,s^{-1}}$	$0.84 \cdot 10^{-6}$	$0.84 \cdot 10^{-6}$	$1.5 \cdot 10^{-7}$	$2.5 \cdot 10^{-7}$
$C_{\mathrm{G}} \cdot \varrho_{\mathrm{G}}$	$\mathrm{J\,m^{-3}\,K^{-1}}$	$2.10 \cdot 10^{6}$	$2.10 \cdot 10^{6}$	$2.10 \cdot 10^{6}$	$2.10 \cdot 10^{6}$
Θ_{sat}	$\mathrm{m^3\,m^{-3}}$	0.395	0.435	0.396	0.63
Ψ_{sat}	m	-0.121	-0.218	-0.51	-0.14
K_{sat}	$\mathrm{m\,s^{-1}}$	$1.76 \cdot 10^{-4}$	$3.47 \cdot 10^{-5}$	$2.018 \cdot 10^{-5}$	$1.38 \cdot 10^{-5}$
Θ_{FC}	$\mathrm{m^3\,m^{-3}}$	0.135	0.150	0.21	0.38
Θ_{WP}	$\mathrm{m^3\,m^{-3}}$	0.068	0.114	0.06	0.19
b	-	4.05	4.90	3.61	6.79

estimated in the field. Soil physical parameters were deduced from laboratory investigation of soil samples taken nearby the measurement set-up (Chen et al., 2012) assuming the samples to be representative on the scale of the EC footprint. Directly measured are soil texture, thermal conductivity, hydraulic conductivity at saturation and the soil water retention curve, providing matrix potential at saturation and exponent b (Clapp and Hornberger, 1978). Backward calculation of the last two yield the volumetric water content at field capacity (pF=2.5 assumed) and at wilting point (pF=4.5 assumed). The latter pF value differs from the standard 4.2, a reasonable assumption for mesophytic grass species (Larcher, 2001, p208).

3.3. Lake surface modelling for Nam Co 2009

Turbulent fluxes over the shallow lake surface near Nam Co were modelled with a hydrodynamic multilayer model (HM) (Foken, 1979, 1984). As the governing principle, surface – atmosphere exchange is parametrised based on a bulk approach, but resolving the molecular boundary layer, the viscous buffer layer and turbulent layer by an integrated profile coefficient Γ. It accounts for stratification by using Monin-Obukhov similarity theory.

The model is forced by measurements, using the same data set as utilised for SEWAB (see Sect. 3.2.1). Lake surface temperature is approximated by the measured lake temperature, hence there is no need for radiation measurements and energy balance closure within the model. The lake surface temperature probe was shielded against direct radiation, a radiation error due to diffuse radiation in the water body has been estimated as approximately 0.2 K, see Biermann et al. (2013, Appendix D). Wendisch and Foken (1989) investigated which forcing variables are most influential to the model error and identified water temperature (50 %) and wind velocity, air temperature and air humidity (10 % to 20 % each).

The HM model is designed for turbulent exchange over the ocean. Shallow water, however, induces larger waves leading to higher roughness and an enhanced exchange depending on wind velocity and lake depth H (Panin et al., 2006b). Therefore the shallow water correction proposed by Panin and Foken (2005) has been implemented in the HM code within a master thesis (Thiem, 2011)

$$Q_{\mathrm{H,E}}^{\mathrm{SW}} = Q_{\mathrm{H,E}}^{\mathrm{ocean}} \left(1 + k_{\mathrm{H,E}}^{\mathrm{SW}} \cdot h \cdot H^{-1}\right) \tag{3.9}$$

with the coefficient $k_{\mathrm{H,E}}^{\mathrm{SW}} \approx 2$. As postulated by the theoretical consideration, the shallow water turbulent fluxes $Q_{\mathrm{H,E}}^{\mathrm{SW}}$ are always larger than the corresponding deep water fluxes $Q_{\mathrm{H,E}}^{\mathrm{ocean}}$. The mean square wave height is parametrised with the empirical expression $h \approx 0.07 u_{10\mathrm{m}}^2 \cdot g^{-1} \left(gHu_{10\mathrm{m}}^{-2}\right)^{0.6}$, formulated by Davidan et al. (1985).

Therefore the influencial parameters for the shallow water extension are wind velocity and lake depth, their impact on the relative increase in fluxes is displayed in Fig. 3.4.

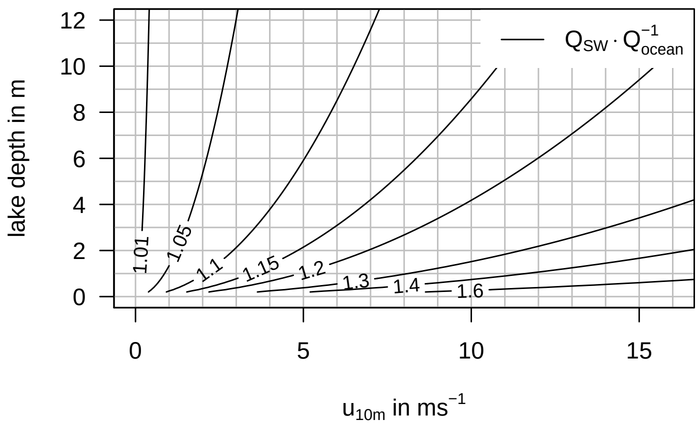

Figure 3.4. Sensitivity of the shallow water term on lake depth H and wind velocity in 10 m height $u_{10\mathrm{m}}$: Isolines show the relative increase of deep water fluxes $Q_{\mathrm{SW}} \cdot Q_{\mathrm{ocean}}^{-1}$ depending on $u_{10\mathrm{m}}$ and H

From the equations local sensitivities can be derived. Using the mean wind velocity of $4\,\mathrm{m\,s^{-1}}$ and a water depth of 1.5 m and assuming corresponding typical errors of $0.3\,\mathrm{m\,s^{-1}}$ and 1 m would lead to flux uncertainties of 1 % and 4 %, respectively.

4. Results

4.1. Data quality on the Tibetan Plateau

The quality of turbulent fluxes from eddy-covariance data has been analysed on four stations on the Tibetan Plateau (Table 1.1) with respect to fulfilment of eddy-covariance requirements, energy balance closure, footprint, as well as obstacles in the vicinity of the sensor and potentially resulting internal boundary layers (Babel et al., 2011a,b). Despite some site-specific sources of disturbance not discussed here, two, more general features can be highlighted.

For one thing near-ground free convective conditions have been found very frequently at Nam Co due to changes in the diurnal land-lake circulation system and due to changing cloud cover inducing sharp contrasts in the surface energy budget especially on the Tibetan Plateau (Zhou et al., 2011). This comes along with a degradation of data quality caused by both instationarity and mismatch to theoretical integral turbulence characteristics. Zhou et al. (2011) argue that data from these situations should not be routinely rejected, as they describe a typical daytime phenomenon within a convective boundary layer.

Secondly, irregular friction velocities have been frequently found in the data from the BJ site (now Naqu station), related to the used sonic anemometer DAT 600 TR61A probe from Kaijo-Denki. Irregular friction means that momentum flux has been frequently observed with the wrong direction, rating the surface erroneously as a source of momentum rather than a sink. The DAT 600 is a non-omnidirectional sensor with a relatively small open sector of 120°. It is shown by Li et al. (2013, Appendix F) that the problem can be reduced for data of the undisturbed (open) sector by applying a sector-wise planar-fit. Basically such partitions in disturbed and undisturbed sectors are relevant to all non-omnidirectional sensors, therefore the impact of using a sector-wise planar-fit is investigated for the CSAT3, Campbell Scientific Ltd. as well. The friction velocity of the sector-wise planar-fit deviates up to 10 % (DAT 600) from the "usual" planar-fit applied for the whole sector of all wind directions. Due to its large open sector of 340° no such differences could be found for CSAT3, but irregular friction could be slightly reduced, especially when the front sector (i.e. the disturbing probe elements occur straight behind the measuring path) is rotated separately. This discrepancy between CSAT3 and DAT 600 is reflected by systematic differences found between the friction velocities derived by both instruments when applying the planar-fit in the usual way. In contrast, for sector-wise planar-fit no differences between both

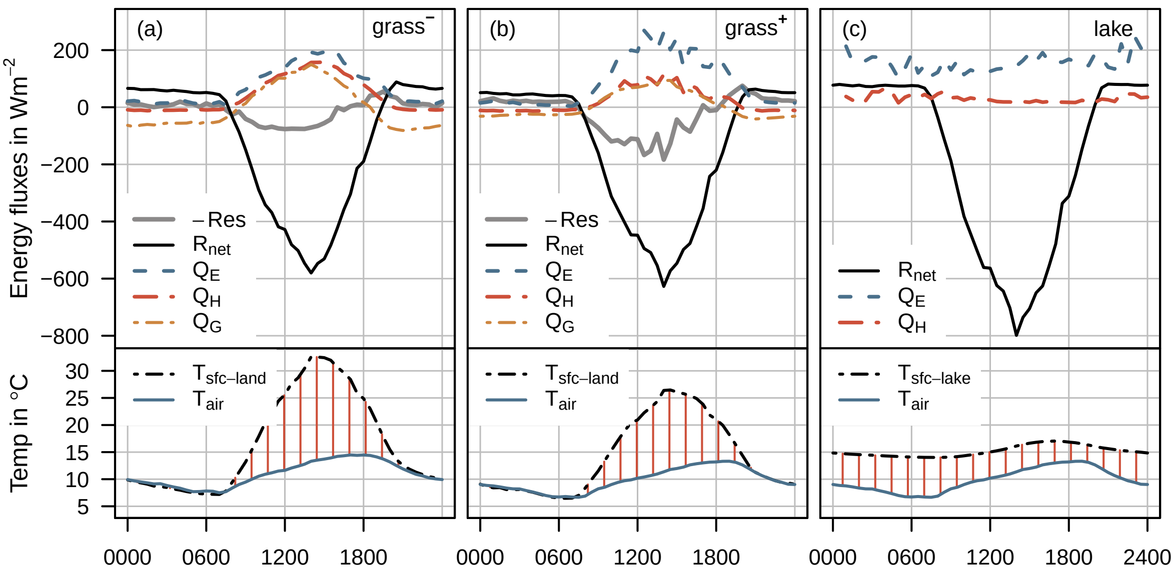

Figure 4.1. Mean diurnal energy fluxes for the whole measurement period, separated for land (**a**: grass^{-} at NamITP, **b**: grass^{+} at NamUBT) and lake (**c**: NamUBT); all components are measured for land fluxes (**a**, **b**); for lake fluxes, the net radiation is calculated from measured downwelling radiation and using an albedo of 0.06 and the lake surface temperature with an emissivity of 0.96; the lower panel shows diurnal surface and air temperature. The time axis is displayed in Beijing standard time (CST), mean local solar noon during the observation period is at 1400 CST. From Biermann et al. (2013, Appendix D)

instruments can be seen. It is also important to mention that scalar fluxes were not affected by the different planar-fit rotations.

4.2. Flux measurements at Nam Co

During the monsoon season, the measured energy fluxes at Nam Co exhibit a distinct spatial heterogeneity corresponding to different surface types, see Babel et al. (2013, Appendix C) and Biermann et al. (2013, Appendix D). Mean diurnal energy fluxes for a dry (grass^{-}) and a wet (grass^{+}) alpine steppe and a shallow lake surface can be seen in Fig. 4.1. The measurements at NamUBT correspond to either grass^{+} or lake surface, depending on wind direction (Fig. 3.2). The land surface fluxes (Fig. 4.1a, b) show a similar diurnal cycle in general, with latent heat fluxes dominating over sensible heat fluxes, a typical feature for the monsoon season on the Tibetan Plateau (e.g. Gu et al., 2005; Ma and Ma, 2006). Nevertheless, evaporation is higher at grass^{+} on average due to soil moisture availability. While grass^{+} is constantly supplied by a shallow ground water table, water availability is highly variable at NamITP with volumetric soil moistures below 5 % most of the time, but with saturated soils shortly after rain events. In such short periods, latent and sensible heat fluxes are approximately equal, some example days are shown by Babel et al. (2013, Appendix C). The NamITP site exhibits the typical features for dry surfaces on the TP with a huge diurnal cycle of the surface temperature (peaks reach up to 50 °C on dry days), and only moderate heat fluxes are not able to redistribute this surface heat content effectively (Yang et al., 2009). The premature change of the sign of the ground heat flux in the early afternoon indicates a strongly heated shallow soil layer, thermally decoupled from the deeper soil and supplying energy to the surface well before surface temperatures drop to the same magnitude as air temperature.

Over the lake surface, the turbulent energy does not show a diurnal cycle, but were constant over the day (Biermann et al., 2013, Appendix D). The lake body is able to release energy at any time, so evaporation is mainly limited by wind velocity and vapour pressure deficit. The shallow lake in particular shows comparably large evaporation due to high wind velocities of $4\,\mathrm{m\,s^{-1}}$ on average and enhanced turbulent exchange caused by unstable stratification even during daytime (Fig. 4.1c). In contrast, stable stratification typically prevails over lakes in daytime (e.g. Beyrich et al., 2006; Nordbo et al., 2011).

4.3. Land surface modelling at Nam Co

In order to assess model performance, model runs for grass$^-$ and grass$^+$ were conducted for measured and default parameters, using both the original version and the adaptation to the Tibetan Plateau (TP version). The simulations were compared with energy balance corrected observations using both correction methods according to the Bowen ratio (EBC-Bo, Twine et al., 2000) and according to the Buoyancy flux (EBC-HB), see Sect. 3.1.4 and Babel et al. (2013, Appendix C).

In general observed patterns (EBC-Bo corrected) were adequately reproduced showing correlation coefficients of 0.9 for both sites, parameter sets and model versions (Babel et al., 2013, Appendix C). This is a notable feature as no optimisation algorithm has been applied so far. Differences between model runs, however, can be found in model bias $B = \overline{\xi_{\mathrm{sim}}} - \overline{\xi_{\mathrm{obs}}}$ and the Nash-Sutcliffe coefficient $NS = 1 - \frac{\sum^N (\xi_{\mathrm{sim}} - \xi_{\mathrm{obs}})^2}{\sum^N (\xi_{\mathrm{obs}} - \overline{\xi_{\mathrm{obs}}})^2}$ (Nash and Sutcliffe, 1970), which can be interpreted similarly to the common coefficient of determination R^2, but is sensitive to bias as well. A large and positive bias for turbulent fluxes is found at grass$^-$, which is not apparent at grass$^+$ (Fig. 4.2a). This is in parts connected to the estimation of the ground heat flux and a high sensitivity of the new thermal conductivity formulation to changes in soil moisture in the dry range (Babel et al., 2013, Appendix C). Nevertheless, bias in ground heat flux could be reduced at grass$^-$ compared to the original version. The TP version reduces the sensible heat flux via the new implementation of thermal roughness and therefore its bias as

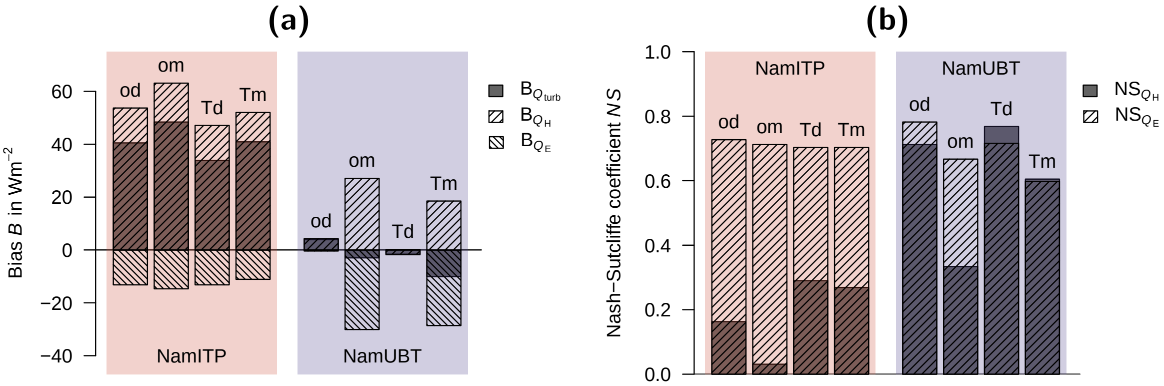

Figure 4.2. Bias (**a**) and Nash-Sutcliffe coefficient NS (**b**) of turbulent fluxes (simulated vs. EBC-Bo corrected observations), NamITP corresponds to grass$^-$, NamUBT to grass$^+$; the individual blocks show **od**: **o**riginal SEWAB version, **d**efault parameters; **om**: **o**riginal SEWAB version, **m**easured parameters; **Td**: **T**P version, **d**efault parameters; **Tm**: **T**P version, **m**easured parameters. Modified from Babel et al. (2013, Appendix C)

well, the bias of latent heat is also slightly reduced. This reduction in bias for the TP version induces a better performance with the NS coefficient (Fig. 4.2b). Simulations with default parameters yield predictions closer to the EBC-Bo corrected observations. This can be mainly attributed to larger field capacities and wilting points in the measured parameter set (Table 3.3), suppressing evapotranspiration on both sites. The new formulation for bare soil evaporation partly compensates this effect at NamITP, at NamUBT bare soil evaporation takes no effect as the fractional area of bare soil is too low.

As expected, the simulations perform better for grass$^+$ than for grass$^-$ in general, as SEWAB formulations have not been validated for such dry conditions before, for example the stomatal resistance by Noilhan and Planton (1989). For the grass$^-$ site the TP version shows better performance without substantially compromising latent heat fluxes. Similar results are found for the grass$^+$ side. Therefore this study not only agrees with previous work over dry surfaces (Yang et al., 2008, 2009; Chen et al., 2010), but shows that the implemented scheme to calculate thermal roughness is not limited to dry surfaces. Furthermore, the new TP version seems to be less sensitive to soil parameters as its performance shows smaller differences between parameter sets than the original version.

The results have been cross-checked with the ground heat flux and important state variables as soil moisture and surface temperature. It could be shown that the new TP version predicts the surface temperature more accurately and is able to reduce bias for the ground heat flux, even if the scatter has been increased. The soil moisture is reasonably resembled for grass$^-$ with both parameter set. For details see Babel et al. (2013, Appendix C).

As SEWAB performed well in general when being forced with measured data, it has been deployed as a reference time series to evaluate a new soil model incorporated in a simplistic land surface model called "Hybrid" (Gerken et al., 2012, Appendix B). The new soil model has been invented to enhance the responsiveness of the surface in hybrid showing a distinct time lag to the observations in its old version. As SEWAB did not show such a time lag, its simulations were ideally suited for a cross correlation analysis with hybrid, where the large gaps in the observed data complicate the interpretation of the results, see Gerken et al. (2012, Appendix B) for detail.

4.4. Influence of the energy balance correction method

In the previous section model evaluations were carried out with EBC-Bo corrected observations only. In order to highlight the role of the energy balance closure for the evaluation of land surface models the new correction method according to the buoyancy flux (EBC-HB) has been considered as well. Table 4.1 summarises the change in performance with respect to (a) model parameters, (b) model version, and (c) method of energy balance closure correction.

Table 4.1a and b confirm the results given in the previous section for EBC-Bo corrected observations. In contrast, EBC-HB corrected observations indicate that measured parameters perform now substantially better at the grass$^+$ site. The same happens there, to a less extent, with respect to model version in case of sensible heat although the positive effect of the TP version prevails in general. The reason for this behaviour is a shift in bias for both turbulent fluxes, as EBC-HB attributes a larger fraction of the residual to the sensible heat flux. Therefore the choice for the method to close the energy balance has a strong influence on the decision on the "right" model parameter set or version. It should be noted that a large bias remains for the sum of turbulent fluxes (Fig. 4.2) which is in fact independent of the method for energy balance correction and must be attributed to other reasons.

Switching between correction methods (Table 4.1c) yields ambiguous results in bias and NS with respect to model version and parameters, but shows advantage for EBC-Bo at grass$^+$ and for EBC-HB at grass$^-$. The pattern statisitics, however, offer another perspective: EBC-Bo yields substantially higher R^2 for the sensible heat flux in any case and lower R^2 for the latent heat flux at grass$^+$. Therefore the SEWAB model is more compatible with EBC-Bo, as exemplarily shown in Fig. 4.3. The simulations of sensible heat flux show more scatter with the EBC-HB corrected observations than for EBC-Bo. This might be caused by an intrinsic model incompatibility to EBC-HB or by problems in estimation of the energy balance closure, incorporating additional uncertainty into the turbulent fluxes. On the other hand, uncorrected observations do not lead to higher R^2 for sensible heat than EBC-Bo corrected (not shown). The red

Table 4.1. Differences in the performance measures Δp, with p as R^2, bias B [$\mathrm{W\,m^{-2}}$] and NS coefficient, with respect to **(a)** model parameters, **(b)** model version, and **(c)** EBC correction method ($\Delta p = p_1 - p_2$, p_i: performance of simulation i). Only absolute values for the bias have been used, i.e. $\Delta B < 0$ always refers to a bias reduction while $\Delta B > 0$ indicates an increase in bias irrespective of the direction of the bias. Changes larger than 0.1 in R^2, $10\,\mathrm{W\,m^{-2}}$ in bias and 0.1 in NS are regarded to be substantial (underlined) and discriminated, whether p_1 is better than p_2 (bold and underlined) or p_2 has advantage over p_1 (underlined only).

Station	Parameter	Version	EBC	Sensible heat flux			Latent heat flux		
				$\Delta\mathrm{R}^2$	ΔB	ΔNS	$\Delta\mathrm{R}^2$	ΔB	ΔNS
(a) Δp with respect to parameter, p_1: measured parameters, p_2: default parameters									
ITP	$p_1 - p_2$	original	Bo	0.02	9.4	$\underline{-0.13}$	−0.03	1.5	−0.02
ITP	$p_1 - p_2$	TP	Bo	0.02	4.9	−0.02	−0.03	−2.1	0.00
UBT	$p_1 - p_2$	original	Bo	0.01	$\underline{22.8}$	$\underline{-0.38}$	−0.01	$\underline{29.7}$	$\underline{-0.12}$
UBT	$p_1 - p_2$	TP	Bo	0.01	$\underline{16.7}$	$\underline{-0.16}$	−0.02	$\underline{28.4}$	$\underline{-0.12}$
ITP	$p_1 - p_2$	original	HB	0.05	9.2	−0.04	−0.02	1.0	0.02
ITP	$p_1 - p_2$	TP	HB	0.03	4.5	0.03	−0.02	−2.7	0.02
UBT	$p_1 - p_2$	original	HB	−0.04	$\underline{\mathbf{-23.2}}$	$\underline{\mathbf{0.25}}$	0.00	$\underline{\mathbf{-31.2}}$	$\underline{\mathbf{0.21}}$
UBT	$p_1 - p_2$	TP	HB	−0.05	$\underline{\mathbf{-20.4}}$	$\underline{\mathbf{0.31}}$	−0.02	$\underline{\mathbf{-30.1}}$	$\underline{\mathbf{0.17}}$
(b) Δp with respect to model version, p_1: TP version, p_2: original version									
ITP	default	$p_1 - p_2$	Bo	−0.02	−6.6	$\underline{\mathbf{0.13}}$	−0.02	0.0	−0.02
ITP	measured	$p_1 - p_2$	Bo	−0.02	$\underline{\mathbf{-11.1}}$	$\underline{\mathbf{0.24}}$	−0.01	−3.6	−0.01
UBT	default	$p_1 - p_2$	Bo	−0.01	−2.5	0.06	−0.07	−0.2	−0.07
UBT	measured	$p_1 - p_2$	Bo	−0.01	−8.6	$\underline{\mathbf{0.27}}$	−0.08	−1.5	−0.07
ITP	default	$p_1 - p_2$	HB	−0.03	−7.4	0.07	0.01	1.2	0.01
ITP	measured	$p_1 - p_2$	HB	−0.05	$\underline{\mathbf{-12.1}}$	$\underline{\mathbf{0.13}}$	0.01	−2.5	0.01
UBT	default	$p_1 - p_2$	HB	−0.06	8.5	$\underline{-0.24}$	0.02	−1.4	0.05
UBT	measured	$p_1 - p_2$	HB	−0.07	$\underline{11.3}$	$\underline{-0.18}$	0.01	−0.3	0.01
(c) Δp with respect to energy balance closure correction method, p_1: EBC-Bo, p_2: EBC-HB									
ITP	default	original	$p_1 - p_2$	$\underline{\mathbf{0.18}}$	$\underline{12.5}$	$\underline{-0.10}$	0.03	$\underline{11.3}$	0.08
ITP	measured	original	$p_1 - p_2$	$\underline{\mathbf{0.15}}$	$\underline{12.7}$	$\underline{-0.20}$	0.02	$\underline{11.8}$	0.04
ITP	default	TP	$p_1 - p_2$	$\underline{\mathbf{0.19}}$	$\underline{13.3}$	−0.04	0.00	$\underline{10.1}$	0.05
ITP	measured	TP	$p_1 - p_2$	$\underline{\mathbf{0.18}}$	$\underline{13.7}$	−0.09	0.00	$\underline{10.7}$	0.03
UBT	default	original	$p_1 - p_2$	$\underline{\mathbf{0.15}}$	$\underline{\mathbf{-32.0}}$	$\underline{\mathbf{0.41}}$	−0.04	$\underline{\mathbf{-32.8}}$	$\underline{\mathbf{0.19}}$
UBT	measured	original	$p_1 - p_2$	$\underline{\mathbf{0.20}}$	$\underline{14.0}$	$\underline{-0.22}$	−0.04	$\underline{28.1}$	$\underline{-0.14}$
UBT	default	TP	$p_1 - p_2$	$\underline{\mathbf{0.21}}$	$\underline{\mathbf{-43.0}}$	$\underline{\mathbf{0.71}}$	$\underline{-0.12}$	$\underline{\mathbf{-31.6}}$	0.07
UBT	measured	TP	$p_1 - p_2$	$\underline{\mathbf{0.26}}$	−5.9	$\underline{\mathbf{0.23}}$	$\underline{-0.13}$	$\underline{26.9}$	$\underline{-0.22}$

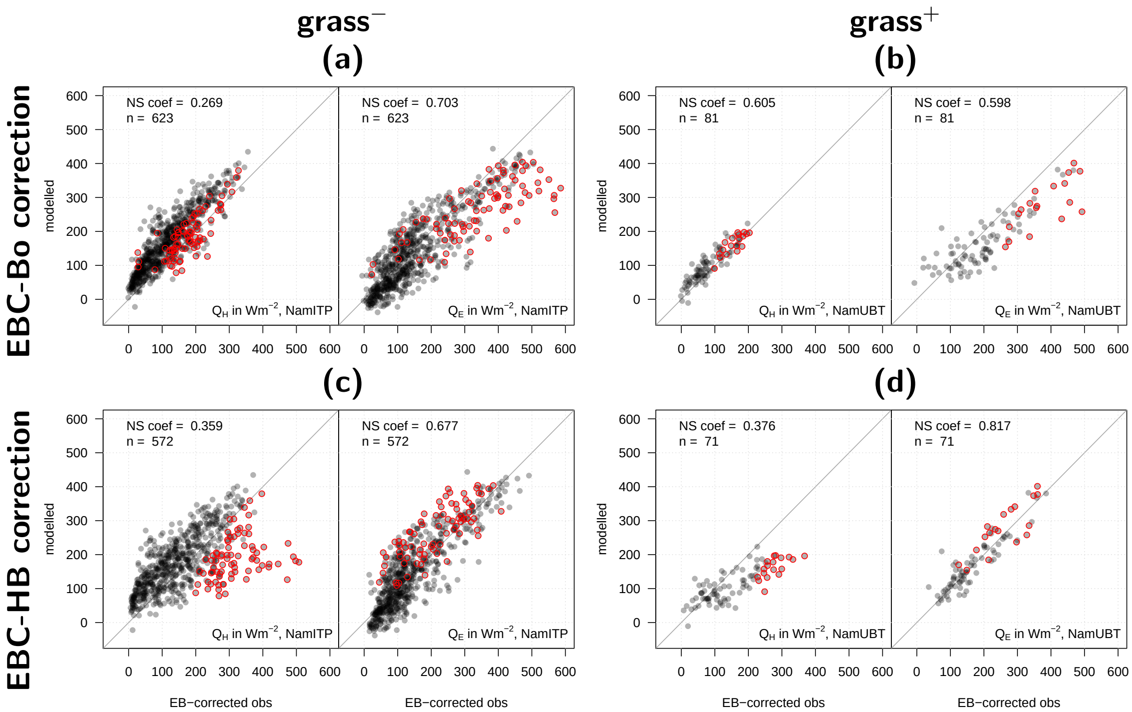

Figure 4.3. Turbulent flux observations versus model simulations, **measured** parameters, TP version, for grass$^-$ (**a**, **c**) and grass$^+$ (**b**, **d**); Observations are displayed using the EBC-Bo correction (**a**, **b**) and the EBC-HB correction (**c**, **d**). The red points indicate data with $-Res > 150\,\mathrm{W\,m^{-2}}$ (not included in the analysis). From Babel et al. (2013, Appendix C).

points indicate values with residuals $-Res > 150\,\mathrm{W\,m^{-2}}$, which were excluded from the analysis. Obviously, these points were most strongly affected by the choice of the correction method. This is especially true for this study as large residuals occur nearly exclusively for low Bowen ratios (not shown). This is no surprise for NamUBT, where only wet conditions occur, but somehow unexpected for NamITP. This effect might be related to uncertainty in the ground heat flux calculation affecting the storage term as described by Leuning et al. (2012).

It can be concluded from this study that SEWAB is more compatible to the common EBC-Bo correction. This can be confirmed with a study over cropland in a temperate humid climate (Kracher et al., 2009). The study shows that the models TERRA (part of the "Lokalmodell" LM, Steppeler et al., 2003) and REMO (Jacob and Podzun, 1997) yield higher Bowen ratios than SEWAB, and therefore might be more compatible with the new EBC-HB correction. However, these models are not constrained with the energy balance, the ground heat fluxes can be regarded as their balance residual. Some other land surface models solve this step similar to SEWAB, such as, for example, the common land model CLM (Dai et al., 2003), or the simple biosphere model SiB2 (Sellers et al., 1996).

4.5. Lake surface modelling at Nam Co

Lake surface modelling has been conducted for the shallow lake at Nam Co station where eddy-covariance measurements exist (Fig. 4.1). For simulations the hydrodynamic multilayer (HM) model (Foken, 1979, 1984) with shallow water extension (Panin and Foken, 2005) is used as described in Sect. 3.3. The performance is demonstrated in a scatterplot of observed eddy-covariance data, selected at NamUBT for lake surface according to the footprint vs. model simulations (Fig. 4.4). The lake depth was estimated as 1.5 m within the average footprint area, and the shallow lake parametrisation for latent heat performs well there (Figure 4.4b). One should take into account that no more parameters exist besides the lake depth that could be used for tuning the results. Changing the lake depth by ±0.5 m exhibits only small influence on the fluxes (Figure 4.4a, c), as already suggested by the sensitivity analysis in Sect. 3.3. Therefore the simulations are assumed to be robust within the uncertainty of eddy-covariance flux measurements. On the other hand the difference is substantial to the assumption of a deep lake, i.e. without shallow water term (Figure 4.4d). This obviously suggests a different flux regime over the large Nam Co lake being present with apparently lower latent heat fluxes. It should be noted, however, that lake depth affects the lake surface temperature as well, especially its diurnal and seasonal cycle. Therefore the example of Figure 4.4d is a hypothetical one, but with knowledge of reliable surface water temperatures, it could be transferred to fluxes above the large Nam Co lake.

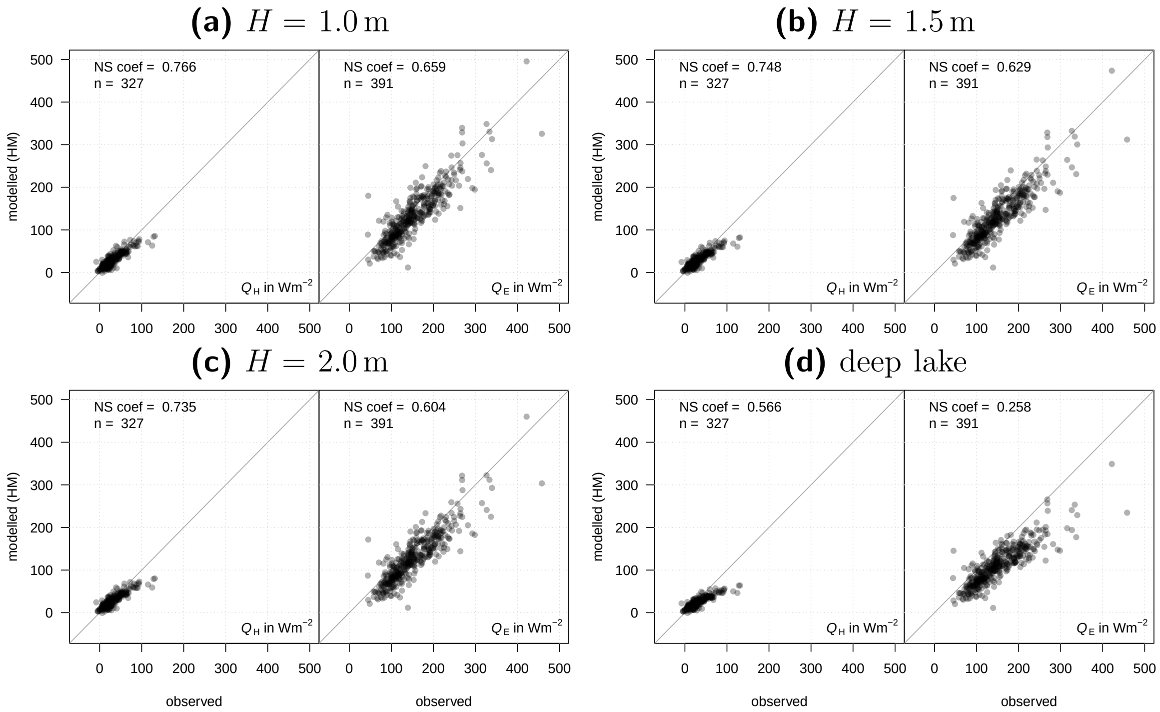

Figure 4.4. Turbulent flux observations above the shallow lake versus HM model simulations for different assumptions of lake depth H within the eddy-covariance footprint; flux simulations in panel **d** are computed without shallow water extension.

4.6. Flux heterogeneity at Nam Co

Previous sections demonstrate the ability of the land surface model SEWAB and the HM model to simulate turbulent fluxes at Nam Co for land and lake surface, respectively. The footprint concept allows for linking the simulations with observations, even if more than one land use type contribute to the measurements. Based on this idea, a spatial integration technique has been applied by Biermann et al. (2013, Appendix D): Simulations of grass$^+$ and lake have been integrated for each time step with a tile approach according to their relative contribution to the fluxes measured at NamUBT. These footprint integrated simulations are now directly comparable to the observations as shown for three example days in Fig. 4.5. The days represent different conditions as they are for 17 July: changing conditions under moderate wind velocities; for 5 August: day with typical land – lake circulation pattern and moderate winds of about $2\,\mathrm{m\,s^{-1}}$ to $6\,\mathrm{m\,s^{-1}}$; and for 6 August: situation with larger than average wind speeds of about $6\,\mathrm{m\,s^{-1}}$. The examples strikingly demonstrate the ability of the footprint concept to link the observations with their sources and with the land-use specific model runs. Also measurements with contributions from both surfaces are reasonably well reflected by the spatial integrated simulation suggesting the tile approach to be valid in this case study. This can be confirmed for the whole measuring period (Biermann et al., 2013, Appendix D), even though situations with miscellaneous footprint did not occur very often and did not show very high fluxes.

Nevertheless, Fig. 4.5 shows that instantaneous turbulent fluxes may differ up to $200\,\mathrm{W\,m^{-2}}$ between land use types. This should obviously affect the landscape scale flux. The observations clearly indicate the differences not only in magnitude but also in the dynamics (Fig. 4.1), which is also reflected in the simulations (Fig. 4.6). As shown in Sect. 4.3 the simulations perform well despite an overestimation of sensible heat fluxes for grass$^-$ and, to a less extent, for grass$^+$.

Nevertheless, the differences between the simulated timeseries can be regarded as significant. It is shown by Biermann et al. (2013, Appendix D) that mean absolute errors between observations and simulations are smaller than mean absolute differences between simulations of different surface types using the same data subset as done for computing the respective mean absolute error. This suggests that the differences in fluxes between land use types exceed the uncertainty with respect to model simulation.

Therefore the flux differences can be adequately represented without data gaps by the modelled time series of each land use type. This is important as eddy-covariance derived fluxes typically have too much gaps to be directly used for such a quantitative assessment, especially for the case of NamUBT, where two land use types are measured with only one set-up. The results for mean fluxes for the whole period is displayed in Fig. 4.7. As expected from the land surface temperatures (Fig. 4.1) the two land surface types already differ in the longwave radiation balance, and the mean latent heat flux becomes more dominant with increasing soil moisture for the land surfaces. The evaporation over the small lake is even higher, due to its shallow water table resulting

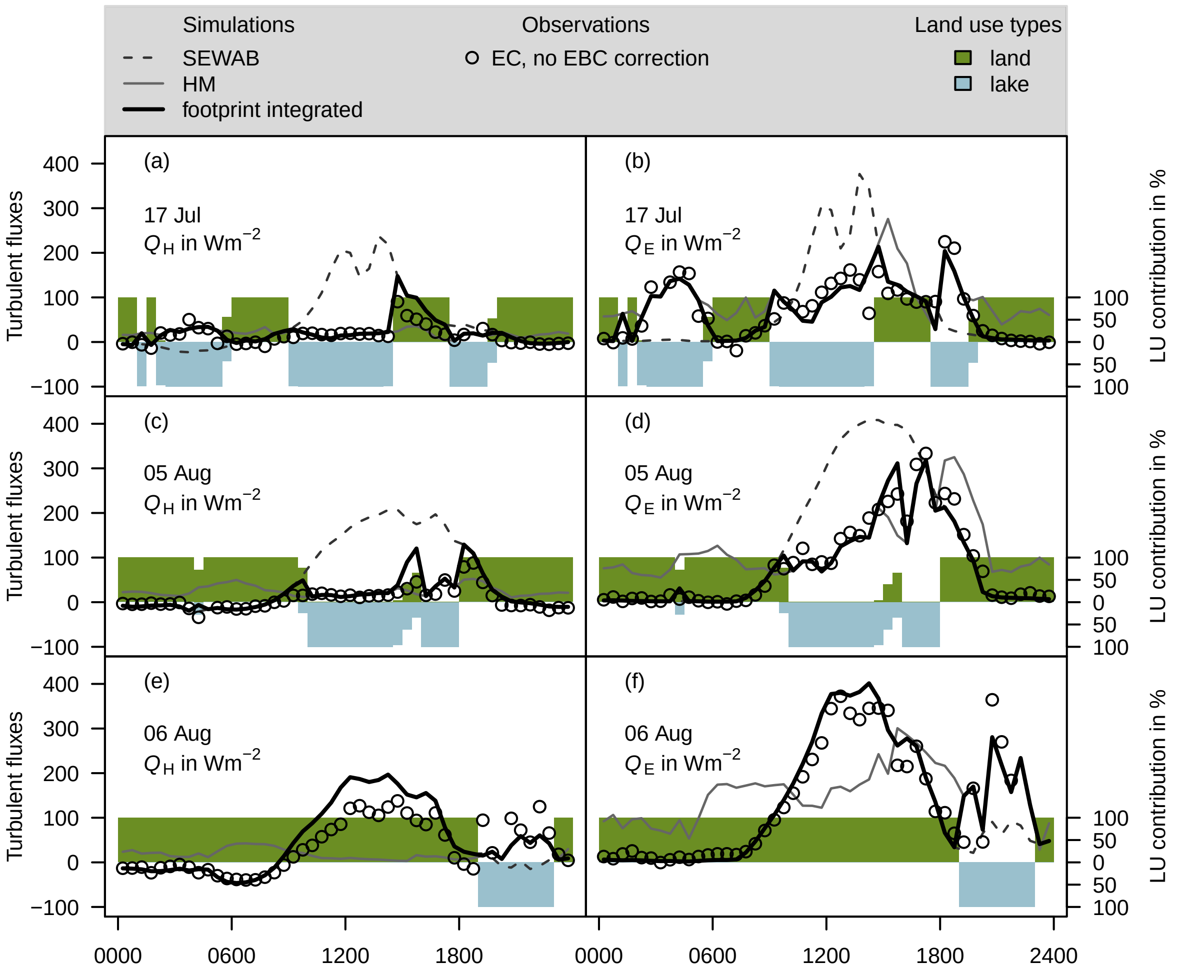

Figure 4.5. Timeseries of observed and simulated fluxes at NamUBT on 17 July, 5 August, and 6 August 2009. Open circles denote the observations without energy balance correction, the solid and the dashed grey line represent simulations for land and lake, respectively. SEWAB simulations are carried out in the TP version using the measured parameters. The thick black line shows the footprint integrated simulations according to the relative contribution of land and lake surface to the observations as denoted in green and blue bars, respectively. From Biermann et al. (2013, Appendix D).

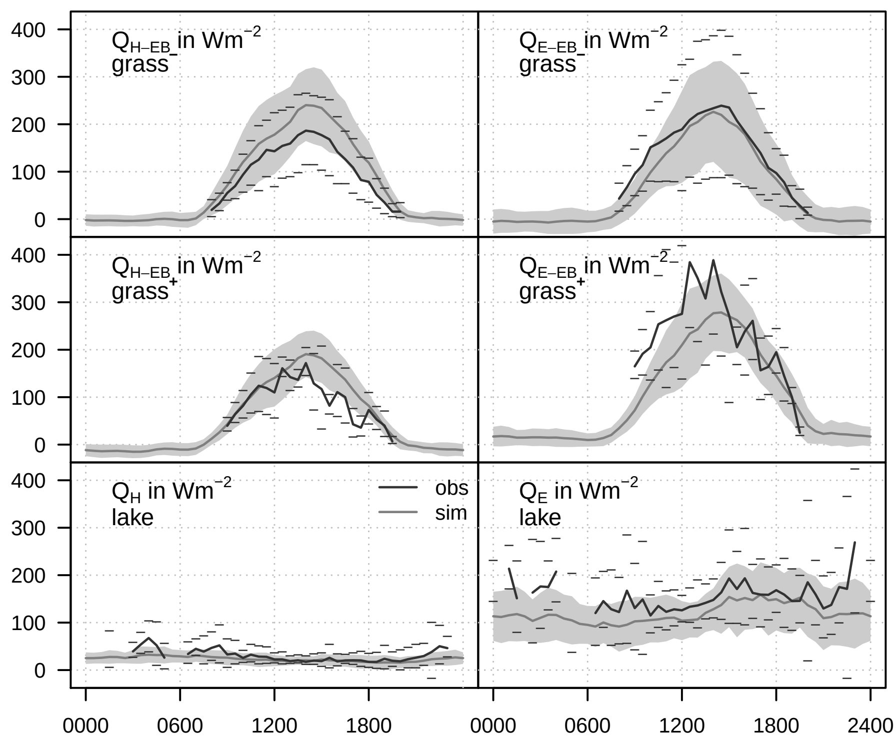

Figure 4.6. Diurnal cycle of observations and simulations at Nam Co 2009. Land surface observations have been corrected according to the Bowen ratio (EBC-Bo), respective simulations have been run in the TP version using the measured parameters. Solid lines represent mean fluxes while horizontal bars and grey shaded areas denote respective standard deviations for observations and simulations. From Biermann et al. (2013, Appendix D).

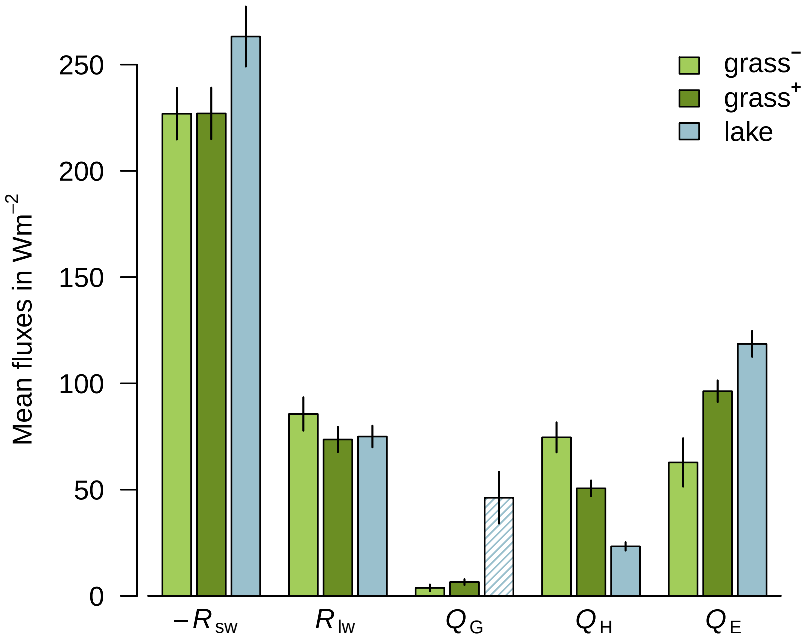

Figure 4.7. Mean fluxes from the whole period for the three surface types from observation-based model runs as used in Figs. 4.5 and 4.6. Net shortwave radiation (R_{sw}) and net longwave radiation (R_{lw}) are parametrised as explained in Fig. 4.1. For the land surface types, Q_{G} represents the ground heat flux. In case of lake surface, Q_{G} denotes the residual of the energy balance, shown as a hatched bar, including the energy fluxes not accounted for, e.g. storage change in the water body and flux into the sediment. Error bars indicate 1.96 times the standard error of the mean, corresponding to the 95 % confidence interval. From Biermann et al. (2013, Appendix D).

in comparatively high surface temperatures. Mean differences of sensible and latent heat flux between grass+ and grass- are $24.0\,\mathrm{W\,m^{-2}}$ and $-33.5\,\mathrm{W\,m^{-2}}$, respectively, and between grass+ and lake are $-27.3\,\mathrm{W\,m^{-2}}$ and $22.3\,\mathrm{W\,m^{-2}}$, respectively.

5. Conclusions

The overarching goal of this thesis is to progress the estimation of turbulent fluxes over typical surface types on the Tibetan Plateau. Achievements have been made related to eddy-covariance observations on the Tibetan Plateau and site-specific land surface modelling. An eddy-covariance data processing scheme has been developed (Babel et al., 2011a,b), major features have been already applied on data of the Tibetan Plateau (Zhou et al., 2011; Biermann et al., 2013, Appendix D). Specific sensor problems with the Kaijo-Denki DAT600 TR61A probe, installed at one of the sites on the Tibetan Plateau, have been encountered with a sector-wise planar-fit rotation (Li et al., 2013, Appendix F). Furthermore, the land surface scheme SEWAB has been successfully adapted to a dry and a wet grassland site for the monsoon season at Nam Co, Tibetan Plateau (Babel et al., 2013, Appendix C). First eddy-covariance measurements over a lake surface have been gathered and a hydrodynamical multilayer model could resemble these observations even resolving the diurnal cycle (Biermann et al., 2013, Appendix D). From these achievements the following conclusions can be drawn:

- Coordinate rotation for non-omnidirectional sonic anemometer need a careful handling, which applies to the Kaijo Denki DAT 600 TR61A probe in particular and, to a less extent, to the CSAT3 (Campbell Scientific Ltd.). Both instrument show frequent occurrences of physical implausible upward momentum fluxes, caused by sensor distortion. It is recommended to apply the planar-fit rotation for only the undisturbed wind sector, and discard momentum fluxes measured in other wind sectors. This can mitigate such problems, and the friction velocity may deviate up to 10 % from those derived by a conventional planar-fit, likely explaining the differences between DAT 600 and CSAT3 found in previous studies as well (Hong et al., 2004). In contrast, no influence of this problem on scalar fluxes could be shown.

- The adaptation of SEWAB to the Tibetan Plateau (TP version) shows a slight, but overall better performance than the original version. The TP version leads to bias reduction especially for sensible heat on the dry surface, which even holds when using energy balance corrected observations according to the buoyancy flux. It performs reasonable also for wet surfaces although the results are ambiguous with respect to the used method to correct the observation for the energy balance closure gap. Nevertheless this demonstrates that the implemented modifications, including the z_{0h}-scheme by Yang et al. (2008) are not limited to dry or bare soil surfaces and the small scale heterogeneity in soil moisture, anticipated by Su et al. (2011), can be resolved with this SEWAB version.

- When comparing simulations with eddy-covariance derived turbulent fluxes, the performance is strongly affected by the measured energy balance closure gap. Thus the selection of the surface model and the choice of the EBC correction method are inter-related problems, which should never be overlooked when validating a model with eddy-covariance data. Kracher et al. (2009) could show, that SEWAB reproduces the observed Bowen ratio quite well. This dissertation supports their findings with data from a total different environment. On the other hand, the EBC-Bo correction may not be appropriate due to poor scalar similarity between sensible and latent heat flux for low frequency contributions, as pointed out by Ruppert et al. (2006). This is confirmed by Charuchittipan et al. (2013, Appendix E), and the new correction according to the buoyancy flux, EBC-HB, is proposed in agreement with findings by e.g. Mauder and Foken (2006); Foken (2008a); Foken et al. (2011); Ingwersen et al. (2011). Therefore future model development of turbulent flux parametrisation should recognize advective fluxes supplying secondary circulations as recent hypotheses concerning the energy balance closure rather than trying to get the best fit to the uncorrected eddy-covariance data. This is a challenging task, and a meaningful future study of model structure at least requires an individual parametrisation of all energy flux components and no item should simply serve as residual of the energy balance.

- The integration of the energy balance closure and its correction demands a high quality measurements of all energy flux components. This may not always be given or, in case of the lake surface, only possible with large efforts. Especially the ground heat flux estimation (observed and simulated) is prone to uncertainties. In the particular case of the grass$^-$ site at Nam Co problems arise due to a large gravel content in the soil. More general, under dry conditions on the Tibetan Plateau, a shallow dry upper soil layer might thermally decouple from the deeper soil. Such a feature is usually not considered in heat flux parametrisations.

- Site-specific land surface model simulations based on eddy-covariance observations has been rarely conducted on the Tibetan Plateau. From this study follows that some field investigations (additional to turbulent flux measurements and forcing data) are inevitable to derive a high quality parameter set (measured or default parameters), which are at least soil moisture measurements, soil temperature measurements and field based knowledge of the soil type, derived at least by a conventional pedological description. The land surface model SEWAB, constrained by such a data set, is reliable enough to be used for validating more simplistic models as done by Gerken et al. (2012, Appendix B).

- Turbulent flux observations and simulations with the HM model pose a unique data set on the Tibetan Plateau, as only studies conducting bulk approaches on daily or monthly basis were reported up to now. However, high quality estimates are necessary since the Tibetan Plateau is covered with a significant lake fraction of various sizes and therefore different characteristics. The HM model with the shallow water term proved its suitability to estimate lake evaporation on a high standard even resolving the diurnal course. Appropriate forcing can be achieved with land derived standard meteorological measurements, a representative surface temperature is the only measurement required directly from the lake. Given these requirements, the model can be transferred to lakes with different size and depth, for example the large Nam Co lake, although more efforts have to be put in estimating a representative surface temperature.

- At the lake shore site (NamUBT) the simulations for land and lake have been integrated by their relative contribution to the measured flux according to the footprint of each time step. Thus measurements and simulations become comparable even under conditions with mixed footprints. It could be shown, that the performance does not deteriorate in such situations and the tile approach is valid in this terrain for spatial integration. Therefore representative flux simulations on a grid cell with edge lengths of 1 km to 5 km can be given for each time step in order to compare with remote sensing data. The simulations of turbulent fluxes for grass$^-$, grass$^+$ and lake differ in mean values and temporal characteristics beyond model uncertainty, with deviations occasionally exceeding 200 W m^{-2} on daytime. In contrast, the measurements over dry grassland at the Nam Co Monitoring and Research Station for Multisphere Interactions (grass$^-$) are considered to be a reference for the land surface exchange in the Nam Co region. This study shows, that the land use distribution within the respective remote sensing pixel or grid cell for mesoscale modelling has to be carefully determined before validating with the dry grassland station. A potential representation error can be reduced by integrating the simulated fluxes of adjacent land use types according to their contribution to the respective grid cell.

The essential findings in this thesis concerning modelling under the conditions of the Tibetan Plateau, energy balance closure and footprint applications provide the basis to process the eddy-covariance data in three levels as described in Sect. 1.2. This is exemplarily shown with the sensible heat flux from Nam Co station in 2009 (Fig. 5.1). Due to data quality filtering, the levels I and II cannot provide complete diurnal cycles. SEWAB simulations from grass$^-$ fill most of the gaps in level II data with high reliability concerning magnitude and dynamics (Fig. 5.1c). Whenever forcing data is missing for simulations, some gaps are still left. In order to obtain no more than seasonal or annual averages, remaining gaps can be eliminated with methods listed by Falge et al. (2001a,b).

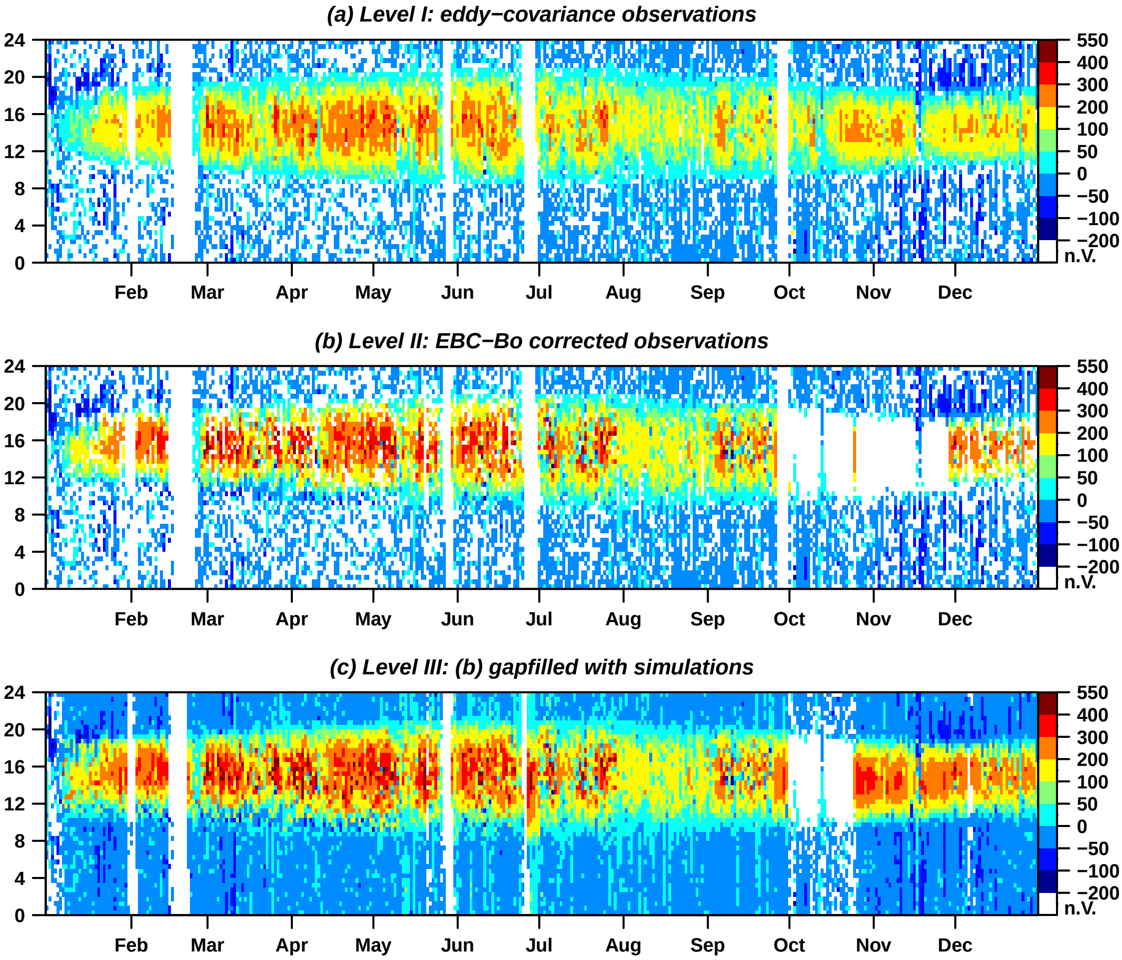

Figure 5.1. Data example: Sensible heat flux at Nam Co, 2009, on different levels of processing as defined for the CEOP-AEGIS project (Sect. 1.2); **(a)**, level I: quality checked eddy-covariance data; **(b)**, level II: energy balance closure corrected observations according to the Bowen ratio, for nighttime values, when EBC correction is not applicable (see Sect. 3.1.4), level I data is accepted unchanged; note that daytime level II data cannot be provided whenever an observed energy balance component is missing **(c)**, level III: data from level II, gap-filled with SEWAB simulations for grass^{-}. Remaining gaps indicate missing forcing data.

References

Agam, N., Berliner, P. R., Zangvil, A., and Ben-Dor, E.: Soil water evaporation during the dry season in an arid zone, J. Geophys. Res., 109, D16 103–, doi: 10.1029/2004JD004802, 2004.

Alapaty, K., Pleim, J. E., Raman, S., Niyogi, D. S., and Byun, D. W.: Simulation of Atmospheric Boundary Layer Processes Using Local- and Nonlocal-Closure Schemes, J. Appl. Meteorol., 36, 214–233, doi:10.1175/1520-0450(1997)036⟨0214:SOABLP⟩2.0.CO;2, 1997.

Aubinet, M., Grelle, A., Ibrom, A., Rannik, U., Moncrieff, J., Foken, T., Kowalski, A., Martin, P., Berbigier, P., Bernhofer, C., Clement, R., Elbers, J., Granier, A., Grünwald, T., Morgenstern, K., Pilegaard, K., Rebmann, C., Snijders, W., Valentini, R., and Vesala, T.: Estimates of the Annual Net Carbon and Water Exchange of Forests: The EUROFLUX Methodology, Adv. Ecol. Res., 30, 113–175, doi:10.1016/S0065-2504(08)60018-5, 2000.

Babel, W., Eigenmann, R., Ma, Y., and Foken, T.: Analysis of turbulent fluxes and their representativeness for the interaction between the atmospheric boundary layer and the underlying surface on Tibetan Plateau, CEOP-AEGIS Deliverable report De1.2, Ed. University of Strasbourg, France, ISSN 2118-7843: 35 p., 2011a.

Babel, W., Li, M., Sun, F., Ma, W., Chen, X., Colin, J., Ma, Y., and Foken, T.: Aerodynamic and thermodynamic variables for four stations on Tibetan Plateau – Introduction on the CEOP-AEGIS database in NetCDF, CEOP-AEGIS Deliverable report De1.3, Ed. University of Strasbourg, France, ISSN 2118-7843: 90 p., 2011b.

Babel, W., Chen, Y., Biermann, T., Yang, K., Ma, Y., and Foken, T.: Adaptation of a land surface scheme for modeling turbulent fluxes on the Tibetan Plateau under different soil moisture conditions, submitted to J. Geophys. Res., see Appendix C, 2013.

Baldocchi, D., Falge, E., Gu, L., Olson, R., Hollinger, D., Running, S., Anthoni, P., Bernhofer, C., Davis, K., Evans, R., Fuentes, J., Goldstein, A., Katul, G., Law, B., Lee, X., Malhi, Y., Meyers, T., Munger, W., Oechel, W., Paw, K. T., Pilegaard, K., Schmid, H. P., Valentini, R., Verma, S., Vesala, T., Wilson, K., and Wofsy, S.:

FLUXNET: A New Tool to Study the Temporal and Spatial Variability of Ecosystem-Scale Carbon Dioxide, Water Vapor, and Energy Flux Densities, B. Am. Meteorol. Soc., 82, 2415–2434, doi:10.1175/1520-0477(2001)082⟨2415:FANTTS⟩2.3.CO;2, 2001.

Balsamo, G., Boussetta, S., Dutra, E., Beljaars, A., Viterbo, P., and van den Hurk, B.: Evolution of land surface processes in the IFS, ECMWF Newslett., 127, 17–22, 2011.

Beyrich, F., Leps, J.-P., Mauder, M., Bange, J., Foken, T., Huneke, S., Lohse, H., Lüdi, A., Meijninger, W., Mironov, D., Weisensee, U., and Zittel, P.: Area-Averaged Surface Fluxes Over the Litfass Region Based on Eddy-Covariance Measurements, Bound.-Lay. Meteorol., 121, 33–65, doi:10.1007/s10546-006-9052-x, 10.1007/s10546-006-9052-x, 2006.

Biermann, T., Babel, W., Olesch, J., and Foken, T.: Documentation of the Micrometeorological Experiment, Nam Tso, Tibet, 25th of June – 8th of August 2009, Work Report University of Bayreuth, Dept. of Micrometeorology, ISSN 1614-8916, 41, 38 pp., URL `http://opus.ub.uni-bayreuth.de/opus4-ubbayreuth/frontdoor/index/index/docId/626`, 2009.

Biermann, T., Babel, W., Ma, W., Chen, X., Thiem, E., Ma, Y., and Foken, T.: Turbulent flux observations and modelling over a shallow lake and a wet grassland in the Nam Co basin, Tibetan Plateau, Theor. Appl. Climatol., accepted, see Appendix D, 2013.

Brötz, B., Eigenmann, R., Dörnbrack, A., Foken, T., and Wirth, V.: Early-morning flow transition in a valley in low-mountain terrain, submitted to Bound.-Lay. Meteorol., 2013.

Charuchittipan, D., Babel, W., Mauder, M., Leps, J.-P., and Foken, T.: Extension of the averaging time of the eddy-covariance measurement and its effect on the energy balance closure, submitted to Bound.-Lay. Meteorol., see Appendix E, 2013.

Chen, T. H., Henderson-Sellers, A., Milly, P. C. D., Pitman, A. J., Beljaars, A. C. M., Polcher, J., Abramopoulos, F., Boone, A., Chang, S., Chen, F., Dai, Y., Desborough, C. E., Dickinson, R. E., Dümenil, L., Ek, M., Garratt, J. R., Gedney, N., Gusev, Y. M., Kim, J., Koster, R., Kowalczyk, E. A., Laval, K., Lean, J., Lettenmaier, D., Liang, X., Mahfouf, J.-F., Mengelkamp, H.-T., Mitchell, K., Nasonova, O. N., Noilhan, J., Robock, A., Rosenzweig, C., Schaake, J., Schlosser, C. A., Schulz, J.-P., Shao, Y., Shmakin, A. B., Verseghy, D. L., Wetzel, P., Wood, E. F., Xue, Y., Yang, Z.-L., and Zeng, Q.: Cabauw Experimental Results from the Project for Intercomparison of Land-Surface Parameterization Schemes, J. Climate, 10, 1194–1215, doi:10.1175/1520-0442(1997)010⟨1194:CERFTP⟩2.0.CO;2, 1997.

Chen, Y., Yang, K., Zhou, D., Qin, J., and Guo, X.: Improving the Noah Land Surface Model in Arid Regions with an Appropriate Parameterization of the Thermal Roughness Length, J. Hydrometeorol., 11, 995–1006, doi:10.1175/2010JHM1185.1, 2010.

Chen, Y., Yang, K., He, J., Qin, J., Shi, J., Du, J., and He, Q.: Improving land surface temperature modeling for dry land of China, J. Geophys. Res., 116, D20 104–, doi:10.1029/2011JD015921, 2011.

Chen, Y., Yang, K., Tang, W., Qin, J., and Zhao, L.: Parameterizing soil organic carbon's impacts on soil porosity and thermal parameters for Eastern Tibet grasslands, Sci. China Earth Sci., 55, 1001–1011, doi:10.1007/s11430-012-4433-0, 2012.

Clapp, R. B. and Hornberger, G. M.: Empirical Equations for some Soil Hydraulic Properties, Water Resour. Res., 14, 601–604, 1978.

Dai, Y., Zeng, X., Dickinson, R. E., Baker, I., Bonan, G. B., Bosilovich, M. G., Denning, A. S., Dirmeyer, P. A., Houser, P. R., Niu, G., Oleson, K. W., Schlosser, C. A., and Yang, Z.-L.: The Common Land Model, B. Am. Meteorol. Soc., 84, 1013–1023, doi:10.1175/BAMS-84-8-1013, 2003.

Davidan, I., Lopatuhin, L., and Rogkov, V.: Volny v okeane (waves in the ocean), Gidrometeoizdat, Leningrad, 256pp., 1985.

Duan, A. and Wu, G.: Role of the Tibetan Plateau thermal forcing in the summer climate patterns over subtropical Asia, Clim. Dynam., 24, 793–807, doi:10.1007/s00382-004-0488-8, 2005.

Falge, E., Baldocchi, D., Olson, R., Anthoni, P., Aubinet, M., Bernhofer, C., Burba, G., Ceulemans, R., Clement, R., Dolman, H., Granier, A., Gross, P., Grünwald, T., Hollinger, D., Jensen, N.-O., Katul, G., Keronen, P., Kowalski, A., Lai, C. T., Law, B. E., Meyers, T., Moncrieff, J., Moors, E., Munger, J. W., Pilegaard, K., Rannik, U., Rebmann, C., Suyker, A., Tenhunen, J., Tu, K., Verma, S., Vesala, T., Wilson, K., and Wofsy, S.: Gap filling strategies for defensible annual sums of net ecosystem exchange, Agr. Forest Meteorol., 107, 43–69, doi:10.1016/S0168-1923(00)00225-2, 2001a.

Falge, E., Baldocchi, D., Olson, R., Anthoni, P., Aubinet, M., Bernhofer, C., Burba, G., Ceulemans, R., Clement, R., Dolman, H., Granier, A., Gross, P., Grünwald, T., Hollinger, D., Jensen, N.-O., Katul, G., Keronen, P., Kowalski, A., Lai, C. T., Law, B. E., Meyers, T., Moncrieff, J., Moors, E., Munger, J. W., Pilegaard, K., Rannik, U., Rebmann, C., Suyker, A., Tenhunen, J., Tu, K., Verma, S., Vesala, T., Wilson, K., and Wofsy, S.: Gap filling strategies for long term energy flux data sets, Agr. Forest Meteorol., 107, 71–77, doi:10.1016/S0168-1923(00)00235-5, 2001b.

Falge, E., Reth, S., Brüggemann, N., Butterbach-Bahl, K., Goldberg, V., Oltchev, A., Schaaf, S., Spindler, G., Stiller, B., Queck, R., Köstner, B., and Bernhofer, C.: Comparison of surface energy exchange models with eddy flux data in forest and grassland ecosystems of Germany, Ecol. Model., 188, 174–216, doi:10.1016/j.ecolmodel.2005.01.057, 2005.

Foken, T.: Vorschlag eines verbesserten Energieaustauschmodells mit Berücksichtigung der molekularen Grenzschicht der Atmosphäre, Z. Meteorol., 29, 32–39, 1979.

Foken, T.: The parameterisation of the energy exchange across the air-sea interface, Dynam. Atmos. Oceans., 8, 297–305, doi:10.1016/0377-0265(84)90014-9, 1984.

Foken, T.: The energy balance closure problem: An overview, Ecol. Appl., 18, 1351–1367, URL `http://www.jstor.org/stable/40062260`, 2008a.

Foken, T.: Micrometeorology, Springer, Berlin, Heidelberg, 308 pp., 2008b.

Foken, T. and Wichura, B.: Tools for quality assessment of surface-based flux measurements, Agr. Forest Meteorol., 78, 83–105, 1996.

Foken, T., Göckede, M., Mauder, M., Mahrt, L., Amiro, B., and Munger, J.: Post-field data quality control, in: Handbook of micrometeorology: A guide for surface flux measurement and analysis, edited by Lee, X., Massman, W., and Law, B., pp. 181–208, Kluwer, Dordrecht, 2004.

Foken, T., Mauder, M., Liebethal, C., Wimmer, F., Beyrich, F., Leps, J.-P., Raasch, S., DeBruin, H., Meijninger, W., and Bange, J.: Energy balance closure for the LITFASS-2003 experiment, Theor. Appl. Climatol., 101, 149–160, doi:10.1007/s00704-009-0216-8, 2010.

Foken, T., Aubinet, M., Finnigan, J. J., Leclerc, M. Y., Mauder, M., and Paw U, K. T.: Results Of A Panel Discussion About The Energy Balance Closure Correction For Trace Gases, B. Am. Meteorol. Soc., 92, ES13–ES18, doi:10.1175/2011BAMS3130.1, 2011.

Foken, T., Leuning, R., Oncley, S. R., Mauder, M., and Aubinet, M.: Corrections and Data Quality Control, in: Eddy Covariance: A Practical Guide to Measurement and Data Analysis, edited by Aubinet, M., Vesala, T., and Papale, D., Springer Atmospheric Sciences, pp. 85–131, Springer Netherlands, doi:10.1007/978-94-007-2351-1_4, 2012.

Gerken, T., Babel, W., Hoffmann, A., Biermann, T., Herzog, M., Friend, A. D., Li, M., Ma, Y., Foken, T., and Graf, H.-F.: Turbulent flux modelling with a simple 2-layer soil model and extrapolated surface temperature applied at Nam Co Lake basin on the Tibetan Plateau, Hydrol. Earth Syst. Sci., 16, 1095–1110, doi:10.5194/hess-16-1095-2012, see Appendix B, 2012.

Gerken, T., Fuchs, K., and Babel, W.: Documentation of the Atmospheric Boundary Layer Experiment, Nam Tso, Tibet, 08th of July – 08th of August 2012, Work Report University of Bayreuth, Dept. of Micrometeorology, ISSN 1614-8916, 53, in prep.

Göckede, M., Rebmann, C., and Foken, T.: A combination of quality assessment tools for eddy covariance measurements with footprint modelling for the characterisation of complex sites, Agr. Forest Meteorol., 127, 175–188, doi:10.1016/j.agrformet.2004.07.012, 2004.

Göckede, M., Markkanen, T., Mauder, M., Arnold, K., Leps, J. P., and Foken, T.: Validation of footprint models using natural tracer measurements from a field experiment, Agr. Forest Meteorol., 135, 314–325, doi:10.1016/j.agrformet.2005.12.008, 2005.

Göckede, M., Markkanen, T., Hasager, C. B., and Foken, T.: Update of a footprint-based approach for the characterisation of complex measurement sites, Bound.-Lay. Meteorol., 118, 635–655, doi:10.1007/s10546-005-6435-3, 2006.

Göckede, M., Foken, T., Aubinet, M., Aurela, M., Banza, J., Bernhofer, C., Bonnefond, J. M., Brunet, Y., Carrara, A., Clement, R., Dellwik, E., Elbers, J., Eugster, W., Fuhrer, J., Granier, A., Grunwald, T., Heinesch, B., Janssens, I. A., Knohl, A., Koeble, R., Laurila, T., Longdoz, B., Manca, G., Marek, M., Markkanen, T., Mateus, J., Matteucci, G., Mauder, M., Migliavacca, M., Minerbi, S., Moncrieff, J., Montagnani, L., Moors, E., Ourcival, J. M., Papale, D., Pereira, J., Pilegaard, K., Pita, G., Rambal, S., Rebmann, C., Rodrigues, A., Rotenberg, E., Sanz, M. J., Sedlak, P., Seufert, G., Siebicke, L., Soussana, J. F., Valentini, R., Vesala, T., Verbeeck, H., and Yakir, D.: Quality control of CarboEurope flux data – Part 1: Coupling footprint analyses with flux data quality assessment to evaluate sites in forest ecosystems, Biogeosciences, 5, 433–450, doi:10.5194/bg-5-433-2008, 2008.

Gu, S., Tang, Y., Cui, X., Kato, T., Du, M., Li, Y., and Zhao, X.: Energy exchange between the atmosphere and a meadow ecosystem on the Qinghai–Tibetan Plateau, Agr. Forest Meteorol., 129, 175–185, doi:10.1016/j.agrformet.2004.12.002, 2005.

Haginoya, S., Fujii, H., Kuwagata, T., Xu, J., Ishigooka, Y., Kang, S., and Zhang, Y.: Air-Lake Interaction Features Found in Heat and Water Exchanges over Nam Co on the Tibetan Plateau, Sola, 5, 172–175, doi:10.2151/sola.2009-044, 2009.

Henderson-Sellers, A., McGuffie, K., and Pitman, A. J.: The Project for Intercomparison of Land-surface Parametrization Schemes (PILPS): 1992 to 1995, Clim. Dynam., 12, 849–859, doi:10.1007/s003820050147, 1996.

Heusinkveld, B., Jacobs, A., Holtslag, A., and Berkowicz, S.: Surface energy balance closure in an arid region: role of soil heat flux, Agr. Forest Meteorol., 122, 21–37, doi:10.1016/j.agrformet.2003.09.005, 2004.

Hong, J. and Kim, J.: Numerical study of surface energy partitioning on the Tibetan Plateau: comparative analysis of two biosphere models, Biogeosciences, 7, 557–568, doi:10.5194/bg-7-557-2010, 2010.

Hong, J., Choi, T., Ishikawa, H., and Kim, J.: Turbulence structures in the near-neutral surface layer on the Tibetan Plateau, Geophys. Res. Lett., 31, L15 106–, doi:10.1029/2004GL019935, 2004.

Hsu, H.-H. and Liu, X.: Relationship between the Tibetan Plateau heating and East Asian summer monsoon rainfall, Geophys. Res. Lett., 30, 2066, doi:10.1029/2003GL017909, 2003.

Hu, Z., Yu, G., Zhou, Y., Sun, X., Li, Y., Shi, P., Wang, Y., Song, X., Zheng, Z., Zhang, L., and Li, S.: Partitioning of evapotranspiration and its controls in four grassland ecosystems: Application of a two-source model, Agr. Forest Meteorol., 149, 1410–1420, doi:10.1016/j.agrformet.2009.03.014, 2009.

Immerzeel, W. W., van Beek, L. P. H., and Bierkens, M. F. P.: Climate Change Will Affect the Asian Water Towers, Science, 328, 1382–1385, doi:10.1126/science.1183188, 2010.

Ingwersen, J., Steffens, K., Högy, P., Warrach-Sagi, K., Zhunusbayeva, D., Poltoradnev, M., Gäbler, R., Wizemann, H.-D., Fangmeier, A., Wulfmeyer, V., and Streck, T.: Comparison of Noah simulations with eddy covariance and soil water measurements at a winter wheat stand, Agr. Forest Meteorol., 151, 345–355, doi:10.1016/j.agrformet.2010.11.010, 2011.

Jacob, D. and Podzun, R.: Sensitivity Studies with the regional climate model REMO, Meteorol. Atmos. Phys., 63, 119–129, 1997.

Johansen, O.: Thermal conductivity of soils, Ph.D. thesis, University of Trondheim, 236 pp., 1975.

Kaimal, J. and Gaynor, J.: Another look at sonic thermometry, Bound.-Lay. Meteorol., 56, 401–410, doi:10.1007/BF00119215, 1991.

Kang, S., Xu, Y., You, Q., Flügel, W.-A., Pepin, N., and Yao, T.: Review of climate and cryospheric change in the Tibetan Plateau, Environ. Res. Lett., 5, 015 101, doi:10.1088/1748-9326/5/1/015101, 2010.

Keil, A., Berking, J., Mügler, I., Schütt, B., Schwalb, A., and Steeb, P.: Hydrological and geomorphological basin and catchment characteristics of Lake Nam Co, South-Central Tibet, Quatern. Int., 218, 118–130, doi:10.1016/j.quaint.2009.02.022, 2010.

Koster, R. D., Dirmeyer, P. A., Guo, Z., Bonan, G., Chan, E., Cox, P., Gordon, C. T., Kanae, S., Kowalczyk, E., Lawrence, D., Liu, P., Lu, C.-H., Malyshev, S., McAvaney, B., Mitchell, K., Mocko, D., Oki, T., Oleson, K., Pitman, A., Sud, Y. C., Taylor, C. M., Verseghy, D., Vasic, R., Xue, Y., and Yamada, T.: Regions of Strong Coupling Between Soil Moisture and Precipitation, Science, 305, 1138–1140, doi:10.1126/science.1100217, 2004.

Kracher, D., Mengelkamp, H. T., and Foken, T.: The residual of the energy balance closure and its influence on the results of three SVAT models, Meteorol. Z., 18, 1–15, doi:10.1127/0941-2948/2009/0412, 2009.

Krause, P., Biskop, S., Helmschrot, J., Flügel, W.-A., Kang, S., and Gao, T.: Hydrological system analysis and modelling of the Nam Co basin in Tibet, Adv. Geosci., 27, 29–36, doi:10.5194/adgeo-27-29-2010, 2010.

Larcher, W.: Ökophysiologie der Pflanzen: Leben, Leistung und Streßbewältigung der Pflanzen in ihrer Umwelt, Verlag Eugen Ulmer Stuttgart, 6th edn., 2001.

Leuning, R., van Gorsel, E., Massman, W. J., and Isaac, P. R.: Reflections on the surface energy imbalance problem, Agr. Forest Meteorol., 156, 65–74, doi:10.1016/j.agrformet.2011.12.002, 2012.

Li, M., Babel, W., Tanaka, K., and Foken, T.: Note on the application of planar-fit rotation for non-omnidirectional sonic anemometers, Atmos. Meas. Tech., 6, 221–229, doi:10.5194/amt-6-221-2013, see Appendix F, 2013.

Liebethal, C., Huwe, B., and Foken, T.: Sensitivity analysis for two ground heat flux calculation approaches, Agr. Forest Meteorol., 132, 253–262, doi:10.1016/j.agrformet.2005.08.001, 2005.

Liu, J., Kang, S., Gong, T., and Lu, A.: Growth of a high-elevation large inland lake, associated with climate change and permafrost degradation in Tibet, Hydrol. Earth Syst. Sci., 14, 481–489, doi:10.5194/hess-14-481-2010, 2010.

Liu, Y., He, Q., Zhang, H., and Mamtimin, A.: Improving the CoLM in Taklimakan Desert Hinterland with Accurate Key Parameters and an Appropriate Parameterization Scheme, Adv. Atmos. Sci., 29, 381–390, doi:10.1007/s00376-011-1068-6, 2012.

Louis, J.: A parametric model of vertical eddy fluxes in the atmosphere, Bound.-Lay. Meteorol., 17, 187–202, doi:10.1007/BF00117978, 1979.

Ma, W. and Ma, Y.: The annual variations on land surface energy in the northern Tibetan Plateau, Environ. Geol., 50, 645–650, doi:10.1007/s00254-006-0238-9, 2006.

Ma, W., Ma, Y., Li, M., Hu, Z., Zhong, L., Su, Z., Ishikawa, H., and Wang, J.: Estimating surface fluxes over the north Tibetan Plateau area with ASTER imagery, Hydrol. Earth Syst. Sci., 13, 57–67, doi:10.5194/hess-13-57-2009, 2009a.

Ma, Y., Tsukamoto, O., Wang, J., Ishikawa, H., and Tamagawa, I.: Analysis of aerodynamic and thermodynamic parameters on the grassy marshland surface of Tibetan Plateau, Prog. Nat. Sci., 12, 36–40, 2002.

Ma, Y., Fan, S., Ishikawa, H., Tsukamoto, O., Yao, T., Koike, T., Zuo, H., Hu, Z., and Su, Z.: Diurnal and inter-monthly variation of land surface heat fluxes over the central Tibetan Plateau area, Theor. Appl. Climatol., 80, 259–273, doi:10.1007/s00704-004-0104-1, 2005.

Ma, Y., Wang, Y., Wu, R., Hu, Z., Yang, K., Li, M., Ma, W., Zhong, L., Sun, F., Chen, X., Zhu, Z., Wang, S., and Ishikawa, H.: Recent advances on the study of atmosphere-land interaction observations on the Tibetan Plateau, Hydrol. Earth Syst. Sci., 13, 1103–1111, doi:10.5194/hess-13-1103-2009, 2009b.

Ma, Y., Zhong, L., Wang, B., Ma, W., Chen, X., and Li, M.: Determination of land surface heat fluxes over heterogeneous landscape of the Tibetan Plateau by using the MODIS and in situ data, Atmos. Chem. Phys., 11, 10 461–10 469, doi:10.5194/acp-11-10461-2011, 2011.

Manabe, S.: Climate And The Ocean Circulation 1: The Atmospheric Circulation And The Hydrology Of The Earth's Surface, Mon. Weather Rev., 97, 739–774, doi:10.1175/1520-0493(1969)097⟨0739:CATOC⟩2.3.CO;2, 1969.

Mauder, M. and Foken, T.: Documentation and instruction manual of the eddy covariance software package TK2, Work Report University of Bayreuth, Dept. of Micrometeorology, ISSN 1614-8916, 26, 42 pp., URL http://opus.ub.uni-bayreuth.de/opus4-ubbayreuth/frontdoor/index/index/docId/639, 2004.

Mauder, M. and Foken, T.: Impact of post-field data processing on eddy covariance flux estimates and energy balance closure, Meteorol. Z., 15, 597–609, doi:10.1127/0941-2948/2006/0167, 2006.

Mauder, M. and Foken, T.: Documentation and Instruction Manual of the Eddy-Covariance Software Package TK3, Work Report University of Bayreuth, Dept. of Micrometeorology, ISSN 1614-8916, 46, 58 pp., URL http://opus.ub.uni-bayreuth.de/opus4-ubbayreuth/frontdoor/index/index/docId/681, 2011.

Mauder, M., Jegede, O. O., Okogbue, E. C., Wimmer, F., and Foken, T.: Surface energy balance measurements at a tropical site in West Africa during the transition from dry to wet season, Theor. Appl. Climatol., 89, 171–183, doi:10.1007/s00704-006-0252-6, 2007.

Maussion, F., Scherer, D., Finkelnburg, R., Richters, J., Yang, W., and Yao, T.: WRF simulation of a precipitation event over the Tibetan Plateau, China – an assessment using remote sensing and ground observations, Hydrol. Earth Syst. Sci., 15, 1795–1817, doi:10.5194/hess-15-1795-2011, 2011.

Mengelkamp, H. T., Warrach, K., and Raschke, E.: A land surface scheme for atmospheric and hydrologic models: SEWAB (Surface Energy and Water Balance), GKSS Report 97/E/69, 40pp., GKSS Geesthacht, 1997.

Mengelkamp, H. T., Warrach, K., and Raschke, E.: SEWAB - a parameterization of the Surface Energy and Water Balance for atmospheric and hydrologic models, Adv. Water Resour., 23, 165–175, doi:10.1016/S0309-1708(99)00020-2, 1999.

Mengelkamp, H. T., Kiely, G., and Warrach, K.: Evaluation of the hydrological components added to an atmospheric land-surface scheme, Theor. Appl. Climatol., 69, 199–212, doi:10.1007/s007040170025, 2001.

Metzger, S., Ma, Y., Markkanen, T., Göckede, M., Li, M., and Foken, T.: Quality assessment of Tibetan Plateau Eddy Covariance measurements utilizing Footprint modeling, Adv. Earth Sci., 21, 1260–1267, 2006.

Miehe, G., Bach, K., Miehe, S., Kluge, J., Yongping, Y., Duo, L., Co, S., and Wesche, K.: Alpine steppe plant communities of the Tibetan highlands, Appl. Veg. Sci., 14, 547–560, doi:10.1111/j.1654-109X.2011.01147.x, 2011.

Mihailović, D. T., Pielke, R. A., Rajković, B., Lee, T. J., and Jeftić, M.: A Resistance Representation of Schemes for Evaporation from Bare and Partly Plant-covered Surfaces for Use in Atmospheric Models, J. Appl. Meteorol., 32, 1038–1054, doi:10.1175/1520-0450(1993)032⟨1038:ARROSF⟩2.0.CO;2, 1993.

Mihailović, D. T., Rajković, B., Lalić, B., and Dekić, L.: Schemes for Parameterizing Evaporation from a Non-Plant-Covered Surface and Their Impact on Partitioning the Surface Energy in Land-Air Exchange Parameterization, J. Appl. Meteorol., 34, 2462–2475, doi:10.1175/1520-0450(1995)034⟨2462:SFPEFA⟩2.0.CO;2, 1995.

Mügler, I., Gleixner, G., Günther, F., Mäusbacher, R., Daut, G., Schütt, B., Berking, J., Schwalb, A., Schwark, L., Xu, B., Yao, T., Zhu, L., and Yi, C.: A multi-proxy approach to reconstruct hydrological changes and Holocene climate development of Nam Co, Central Tibet, J. Paleolimnol., 43, 625–648, doi:10.1007/s10933-009-9357-0, 2010.

Nash, J. E. and Sutcliffe, J. V.: River flow forecasting through conceptual models part I – A discussion of principles, J. Hydrol., 10, 282–290, doi:10.1016/0022-1694(70)90255-6, 1970.

Ni, J.: Impacts of climate change on Chinese ecosystems: key vulnerable regions and potential thresholds, Reg. Environ. Change, 11, 49–64, doi:10.1007/s10113-010-0170-0, 2011.

Noilhan, J. and Planton, S.: A Simple Parameterization of Land Surface Processes for Meteorological Models, Mon. Weather Rev., 117, 536–549, doi:10.1175/1520-0493(1989)117⟨0536:ASPOLS⟩2.0.CO;2, 1989.

Nordbo, A., Launiainen, S., Mammarella, I., Leppäranta, M., Huotari, J., Ojala, A., and Vesala, T.: Long-term energy flux measurements and energy balance over a small boreal lake using eddy covariance technique, J. Geophys. Res., 116, D02 119, doi:10.1029/2010JD014542, 2011.

Panin, G., Nasonov, A., and Foken, T.: Evaporation and heat exchange of a body of water with the atmosphere in a shallow zone, Izv. Atmos. Ocean. Phys., 42, 337–352, 2006a.

Panin, G. N. and Foken, T.: Air–sea interaction including a shallow and coastal zone, J. Atmos. Ocean Sci., 10, 289–305, doi:10.1080/17417530600787227, 2005.

Panin, G. N., Nasonov, A. E., Foken, T., and Lohse, H.: On the parameterisation of evaporation and sensible heat exchange for shallow lakes, Theor. Appl. Climatol., 85, 123–129, doi:10.1007/s00704-005-0185-5, 2006b.

Peters-Lidard, C. D., Blackburn, E., Liang, X., and Wood, E. F.: The Effect of Soil Thermal Conductivity Parameterization on Surface Energy Fluxes and Temperatures, J. Atmos. Sci., 55, 1209–1224, doi:10.1175/1520-0469(1998)055⟨1209:TEOSTC⟩2.0.CO;2, 1998.

Pitman, A. J.: The evolution of, and revolution in, land surface schemes designed for climate models, Int. J. Climatol., 23, 479–510, doi:10.1002/joc.893, 2003.

Rannik, U., Aubinet, M., Kurbanmuradov, O., Sabelfeld, K. K., Markkanen, T., and Vesala, T.: Footprint analysis for measurements over a heterogeneous forest, Bound.-Lay. Meteorol., 97, 137–166, doi:10.1023/A:1002702810929, 2000.

Rebmann, C., Kolle, O., Heinesch, B., Queck, R., Ibrom, A., and Aubinet, M.: Data Acquisition and Flux Calculations, in: Eddy Covariance: A Practical Guide to Measurement and Data Analysis, edited by Aubinet, M., Vesala, T., and Papale, D., Springer Atmospheric Sciences, pp. 59–83, Springer Netherlands, doi:10.1007/978-94-007-2351-1_3, 2012.

Rouse, W. R., Oswald, C. J., Binyamin, J., Spence, C., Schertzer, W. M., Blanken, P. D., Bussières, N., and Duguay, C. R.: The Role of Northern Lakes in a Regional Energy Balance, J. Hydrometeorol., 6, 291–305, doi:doi:10.1175/JHM421.1, 2005.

Ruppert, J., Thomas, C., and Foken, T.: Scalar Similarity for Relaxed Eddy Accumulation Methods, Bound.-Lay. Meteorol., 120, 39–63, doi:10.1007/s10546-005-9043-3, 2006.

Schotanus, P., Nieuwstadt, F., and De Bruin, H.: Temperature measurement with a sonic anemometer and its application to heat and moisture fluxes, Bound.-Lay. Meteorol., 26, 81–93, doi:10.1007/BF00164332, 1983.

Sellers, P., Randall, D., Collatz, G., Berry, J., Field, C., Dazlich, D., Zhang, C., Collelo, G., and Bounoua, L.: A Revised Land Surface Parameterization (SiB2) for Atmospheric GCMs. Part I: Model Formulation, J. Climate, 9, 676–705, doi: 10.1175/1520-0442(1996)009⟨0676:ARLSPF⟩2.0.CO;2, 1996.

Seneviratne, S. I., Corti, T., Davin, E. L., Hirschi, M., Jaeger, E. B., Lehner, I., Orlowsky, B., and Teuling, A. J.: Investigating soil moisture–climate interactions in a changing climate: A review, Earth-sci. Rev., 99, 125–161, doi:10.1016/j.earscirev.2010.02.004, 2010.

Steinfeld, G., Letzel, M., Raasch, S., Kanda, M., and Inagaki, A.: Spatial representativeness of single tower measurements and the imbalance problem with eddy-covariance fluxes: results of a large-eddy simulation study, Bound.-Lay. Meteorol., 123, 77–98, doi:10.1007/s10546-006-9133-x, 2007.

Steppeler, J., Doms, G., Schattler, U., Bitzer, H. W., Gassmann, A., Damrath, U., and Gregoric, G.: Meso-gamma scale forecasts using the nonhydrostatic model LM, Meteorol. Atmos. Phys., 82, 75–96, 2003.

Stoy, P. C., Mauder, M., Foken, T., Marcolla, B., Boegh, E., Ibrom, A., Arain, M. A., Arneth, A., Aurela, M., Bernhofer, C., Cescatti, A., Dellwik, E., Duce, P., Gianelle, D., van Gorsel, E., Kiely, G., Knohl, A., Margolis, H., McCaughey, H., Merbold, L., Montagnani, L., Papale, D., Reichstein, M., Saunders, M., Serrano-Ortiz, P., Sottocornola, M., Spano, D., Vaccari, F., and Varlagin, A.: A data-driven analysis of energy balance closure across FLUXNET research sites: The role of landscape scale heterogeneity, Agr. Forest Meteorol., 171–172, 137–152, doi: 10.1016/j.agrformet.2012.11.004, 2013.

Su, Z., Wen, J., Dente, L., van der Velde, R., Wang, L., Ma, Y., Yang, K., and Hu, Z.: The Tibetan Plateau observatory of plateau scale soil moisture and soil temperature (Tibet-Obs) for quantifying uncertainties in coarse resolution satellite and model products, Hydrol. Earth Syst. Sci., 15, 2303–2316, doi:10.5194/hess-15-2303-2011, 2011.

Takayabu, I., Takata, K., Yamazaki, T., Ueno, K., Yabuki, H., and Haginoya, S.: Comparison of the Four Land Surface Models Driven by a Common Forcing Data Prepared from GAME/Tibet POP'97 Products – Snow Accumulation and Soil Freezing Processes –, J. Meteorol. Soc. Jpn., 79, 535–554, doi:10.2151/jmsj.79.535, 2001.

Thiem, E.: Modeling of the energy exchange above lake and land surfaces, Master thesis, University of Bayreuth, 73pp., 2011.

Twine, T. E., Kustas, W. P., Norman, J. M., Cook, D. R., Houser, P. R., Meyers, T. P., Prueger, J. H., Starks, P. J., and Wesely, M. L.: Correcting eddy-covariance flux underestimates over a grassland, Agr. Forest Meteorol., 103, 279–300, doi:10.1016/S0168-1923(00)00123-4, 2000.

van der Velde, R., Su, Z., Ek, M., Rodell, M., and Ma, Y.: Influence of thermodynamic soil and vegetation parameterizations on the simulation of soil temperature states and surface fluxes by the Noah LSM over a Tibetan Plateau site, Hydrol. Earth Syst. Sci., 13, 759–777, doi:10.5194/hess-13-759-2009, 2009.

Wallace, J., Wright, I., Stewart, J., and Holwill, C.: The Sahelian Energy Balance Experiment (SEBEX): Ground based measurements and their potential for spatial extrapolation using satellite data, Adv. Space Res., 11, 131–141, doi:10.1016/0273-1177(91)90413-E, 1991.

Warrach, K., Mengelkamp, H.-T., and Raschke, E.: Treatment of frozen soil and snow cover in the land surface model SEWAB, Theor. Appl. Climatol., 69, 23–37, doi:10.1007/s007040170033, 2001.

Wendisch, M. and Foken, T.: Sensitivity test of a multilayer energy exchange model, Z. Meteorol., 39, 36–39, 1989.

Wilson, K., Goldstein, A., Falge, E., Aubinet, M., Baldocchi, D., Berbigier, P., Bernhofer, C., Ceulemans, R., Dolman, H., Field, C., Grelle, A., Ibrom, A., Law, B. E., Kowalski, A., Meyers, T., Moncrieff, J., Monson, R., Oechel, W., Tenhunen, J., Valentini, R., and Verma, S.: Energy balance closure at FLUXNET sites, Agr. Forest Meteorol., 113, 223–243, 2002.

Xu, J. and Haginoya, S.: An Estimation of Heat and Water Balances in the Tibetan Plateau, J. Meteorol. Soc. Jpn., 79, 485–504, doi:10.2151/jmsj.79.485, 2001.

Xu, J., Yu, S., Liu, J., Haginoya, S., Ishigooka, Y., Kuwagata, T., Hara, M., and Yasunari, T.: The Implication of Heat and Water Balance Changes in a Lake Basin on the Tibetan Plateau, Hydrol. Res. Lett., 3, 1–5, doi:10.3178/hrl.3.1, 2009.

Yanai, M. H., Li, C. F., and Song, Z. S.: Seasonal Heating of the Tibetan Plateau and its Effects on the Evolution of the Asian Summer Monsoon, J. Meteorol. Soc. Jpn., 70, 319–351, 1992.

Yang, K. and Wang, J.: A temperature prediction-correction method for estimating surface soil heat flux from soil temperature and moisture data, Sci. China Ser. D, 51, 721–729, doi:10.1007/s11430-008-0036-1, 2008.

Yang, K., Koike, T., and Yang, D.: Surface flux parameterization in the Tibetan Plateau, Bound.-Lay. Meteorol., 116, 245–262, doi:10.1023/A:1021152407334, 2003.

Yang, K., Koike, T., Ye, B., and Bastidas, L.: Inverse analysis of the role of soil vertical heterogeneity in controlling surface soil state and energy partition, J. Geophys. Res., 110, D08101, doi:10.1029/2004JD005500, 2005.

Yang, K., Koike, T., Ishikawa, H., Kim, J., Li, X., Liu, H., Wang, J., Liu, S., and Ma, Y.: Turbulent Flux Transfer over Bare-Soil Surfaces: Characteristics and Parameterization, J. Appl. Meteorol. Clim., 47, 276–290, doi:10.1175/2007JAMC1547.1, 2008.

Yang, K., Chen, Y.-Y., and Qin, J.: Some practical notes on the land surface modeling in the Tibetan Plateau, Hydrol. Earth Syst. Sci., 13, 687–701, doi: 10.5194/hess-13-687-2009, 2009.

Yang, K., Guo, X., and Wu, B.: Recent trends in surface sensible heat flux on the Tibetan Plateau, SCIENCE CHINA Earth Sciences, pp. 1–10, doi:10.1007/s11430-010-4036-6, 2010.

Ye, D.-Z. and Wu, G.-X.: The role of the heat source of the Tibetan Plateau in the general circulation, Meteorol. Atmos. Phys., 67, 181–198, doi:10.1007/BF01277509, 1998.

Yu, S., Liu, J., Xu, J., and Wang, H.: Evaporation and energy balance estimates over a large inland lake in the Tibet-Himalaya, Environ. Earth Sci., 64, 1169–1176, doi:10.1007/s12665-011-0933-z, 2011.

Zhang, X.: Improvement of a soil-atmosphere-transfer model for the simulation of bare soil surface energy balances in semiarid areas, Asia Pac. J. Atmos. Sci., 48, 97–105, doi:10.1007/s13143-012-0009-3, 2012.

Zhou, D., Eigenmann, R., Babel, W., Foken, T., and Ma, Y.: The study of near-ground free convection conditions at Nam Co station on the Tibetan Plateau, Theor. Appl. Climatol., 105, 217–228, doi:10.1007/s00704-010-0393-5, 2011.

Zilitinkevich, S. S.: Non-local turbulent transport: Pollution dispersion aspects of coherent structure of convective flows, in: Air Pollution – Volume I. Air Pollution Theory and Simulation, edited by Power, H., Moussiopoulos, N., and Brebbia, C. A., pp. 53–60, Computational Mechanics Publications, 1995.

A. Individual contributions to the joint publications

This cumulative thesis consists of publications and manuscripts listed hereafter. Other authors contributed to these papers as well. Therefore my own contribution to the individual manuscripts is specified in this section.

Nam Co experiment 2009 and data preparation

Some of the following publications is based on the Nam Co experiment in 2009, further described in section 3.1. Together with Tobias Biermann I was responsible for the realisation of the experiment. The setup and design was planned and prepared together with Tobias Biermann in equal shares. We both assembled the measurement complex at the site, while Tobias Biermann alone was responsible for data collection and maintenance during the whole campaign.

The data from the Nam Co experiment (NamUBT) as well as data provided from the permanent station of the ITP (NamITP) have been post-processed as follows: Tobias Biermann did quality checks on low frequency data and turbulent flux processing with the TK2/TK3 software package, including sector-wise planar-fit for NamUBT. I myself elaborated the actual land use distribution and contributed with the footprint analysis as well as the calculation of the ground heat flux and energy balance, including the EBC correction methods.

Appendix B

Gerken, T., Babel, W., Hoffmann, A., Biermann, T., Herzog, M., Friend, A. D., Li, M., Ma, Y., Foken, T., and Graf, H.-F.: Turbulent flux modelling with a simple 2-layer soil model and extrapolated surface temperature applied at Nam Co Lake basin on the Tibetan Plateau, Hydrol. Earth Syst. Sci., 16, 1095–1110, doi:10.5194/hess-16-1095-2012, 2012.

- Tobias Gerken developed the idea of the manuscript and coordinated individual contributions. He conducted the Hybrid modelling and the analysis. He wrote the whole publication and acted as corresponding author.

- I provided the NamUBT data from the Nam Co experiment together with Tobias Biermann (see p. 54). I myself conducted SEWAB simulations for ITP and UBT land surface and gathered respective model parameters.

- Alex Hoffmann contributed to the Hybrid model development relevant to this paper.

- Michael Herzog contributed with technical advice on the manuscript.

- Andrew Friend is the original author of Hybrid. The provided assistance with the handling of Hybrid.

- Li Maoshan and Ma Yaoming provided data from the ITP station and supported the field trip.

- Thomas Foken and Hans-F. Graf contributed to the manuscript at various stages with fruitful discussions.

Appendix C

Babel, W., Chen, Y., Biermann, T., Yang, K., Ma, Y., and Foken, T.: Adaptation of a land surface scheme for modeling turbulent fluxes on the Tibetan Plateau under different soil moisture conditions, submitted to J. Geophys. Res.

- I myself developed the idea of this manuscript. It was me who adapted the SEWAB code, gathered the model parameters and calculated all simulations. Together with Tobias Biermann I provided the NamUBT data from the Nam Co experiment (p. 54). I alone conducted the whole statistical analysis and wrote the manuscript. Finally I act as corresponding author for the submitted manuscript.

- Chen Yingying provided source code for the roughness length parametrisation of the TP version and for the ground heat flux calculation at NamITP station. He conducted laboratory measurements of soil samples he took over various places on the TP, which I used to derive the measured parameters.

- Yang Kun was the developer of the new roughness length parametrisation and the new soil thermal conductivity calculation. Together with him I had fruitful discussions about model simulation results.

- Ma Yaoming provided data from the ITP station and gave support during the field trip.

- As my supervisor Thomas Foken contributed with scientific discussions throughout all stages of analysis and manuscript preparation

Appendix D

Biermann, T., Babel, W., Ma, W., Chen, X., Thiem, E., Ma, Y., and Foken, T.: Turbulent flux observations and modelling over a shallow lake and a wet grassland in the Nam Co basin, Tibetan Plateau, Theor. Appl. Climatol., accepted

- The idea of this manuscript was developed in equal parts by Tobias Biermann and me. We both realised the Nam Co experiment and data preparation (p. 54) and wrote the text in equal shares. While Tobias Biermann focused more on literature and scope of the manuscript as well as the experimental part, I put my emphasis on data analysis and the modelling parts. Tobias Biermann acts as corresponding author for the submitted manuscript.
- Ma Yaoming, Chen Xuelong and Ma Weiqiang supported us during the field trip in 2009 and gave access to data from the ITP station
- Elisabeth Thiem contributed to the manuscript's workload within a master thesis under the supervision of me and Thomas Foken. Thereby she filled gaps in the model forcing data, implemented the shallow water term into the lake model HM, and conducted a preliminary sensitivity analysis for the lake model.
- Thomas Foken acted as supervisor and liberally shared his experience in encouraging and fruitful discussions.

Appendix E

Charuchittipan, D., Babel, W., Mauder, M., Leps, J.-P., and Foken, T.: Extension of the averaging time of the eddy-covariance measurement and its effect on the energy balance closure, submitted to Bound.-Lay. Meteorol.

- Doojdao Charuchittipan conducted the whole data analysis and wrote the text of the manuscript. She acts as corresponding author for the submitted manuscript.
- I developed the proposed new energy balance closure correction algorithm together with DC and realised the respective part in the conclusions.
- Matthias Mauder initiated the use of wavelets to analyse the long-term fluctuations.
- Jens-Peter Leps provided data from several LITFASS-2003 stations and generated land-use classified data.
- Thomas Foken encouraged the structure of the manuscript and contributed with many scientific discussions. Furthermore, he initiated the project related to the manuscript.

Appendix F

Li, M., Babel, W., Tanaka, K., and Foken, T.: Note on the application of planar-fit rotation for non-omnidirectional sonic anemometers, Atmos. Meas. Tech., 6, 221–229, doi:10.5194/amt-6-221-2013, 2013.

- Li Maoshan was in charge of the data used in this publication. He did the data preparation and analysis according to my instructions. Furthermore he wrote the description of BJ station.
- I myself coordinated the analysis and wrote the main text passages. Finally I acted as the corresponding author.
- Kenji Tanaka conducted first investigations of irregular friction occurring for the Kaijo Denki DAT 600 at BJ site. He did this work in Bayreuth during a sabbatical, his results are not published yet.
- Due to his experience with the Kaijo Denki DAT 600 over decades, Thomas Foken initiated the investigation on this topic and contributes to its progress with several scientific discussions.

B. Gerken et al. (2012)

Gerken, T., Babel, W., Hoffmann, A., Biermann, T., Herzog, M., Friend, A. D., Li, M., Ma, Y., Foken, T., and Graf, H.-F.: Turbulent flux modelling with a simple 2-layer soil model and extrapolated surface temperature applied at Nam Co Lake basin on the Tibetan Plateau, Hydrol. Earth Syst. Sci., 16, 1095–1110, doi:10.5194/hess-16-1095-2012, 2012.

Hydrol. Earth Syst. Sci., 16, 1095–1110, 2012
www.hydrol-earth-syst-sci.net/16/1095/2012/
doi:10.5194/hess-16-1095-2012

Hydrology and Earth System Sciences

Turbulent flux modelling with a simple 2-layer soil model and extrapolated surface temperature applied at Nam Co Lake basin on the Tibetan Plateau

T. Gerken[1,2], W. Babel[2], A. Hoffmann[1], T. Biermann[2], M. Herzog[1], A. D. Friend[3], M. Li[4], Y. Ma[5], T. Foken[2,6], and H.-F. Graf[1]

[1]Centre for Atmospheric Science, Department of Geography, University of Cambridge, UK
[2]Department of Micrometeorology, University of Bayreuth, Germany
[3]Department of Geography, University of Cambridge, UK
[4]Cold and Arid Region Environmental and Engineering Research Institute, Chinese Academy of Sciences, Lanzhou, China
[5]Institute of Tibetan Plateau Research, Chinese Academy of Sciences, Beijing, China
[6]Member of Bayreuth Center of Ecology and Environmental Research (BayCEER), University of Bayreuth, Germany

Correspondence to: T. Gerken (tobias.gerken@uni-bayreuth.de)

Received: 19 October 2011 – Published in Hydrol. Earth Syst. Sci. Discuss.: 21 November 2011
Revised: 8 March 2012 – Accepted: 27 March 2012 – Published: 3 April 2012

Abstract. This paper introduces a surface model with two soil-layers for use in a high-resolution circulation model that has been modified with an extrapolated surface temperature, to be used for the calculation of turbulent fluxes. A quadratic temperature profile based on the layer mean and base temperature is assumed in each layer and extended to the surface. The model is tested at two sites on the Tibetan Plateau near Nam Co Lake during four days during the 2009 Monsoon season. In comparison to a two-layer model without explicit surface temperature estimate, there is a greatly reduced delay in diurnal flux cycles and the modelled surface temperature is much closer to observations. Comparison with a SVAT model and eddy covariance measurements shows an overall reasonable model performance based on RMSD and cross correlation comparisons between the modified and original model. A potential limitation of the model is the need for careful initialisation of the initial soil temperature profile, that requires field measurements. We show that the modified model is capable of reproducing fluxes of similar magnitudes and dynamics when compared to more complex methods chosen as a reference.

1 Introduction

Turbulent fluxes of momentum, latent heat (Q_E) and sensible heat (Q_H) are some of the most important interactions between land surface and atmosphere. These fluxes are responsible for the development or modification of mesoscale circulations and the generation of clouds feed back on surface fluxes through the modification of solar radiation. The effects of vegetation influencing boundary layer structure and moisture are widely acknowledged (i.e. Freedman et al., 2001; van Heerwaarden et al., 2009), while the feedback from short-lived clouds is less understood, but important. Shallow cumulus-surface interactions were shown in an LES (large eddy simulation) study to impact surface temperature and fluxes on very short time scales (Lohou and Patton, 2011). For improved process understanding, it is necessary to use: (1) atmospheric models with sufficiently high resolution ($\mathcal{O}(100\,\mathrm{m})$) to resolve boundary layer processes as well as clouds and (2) surface models capable of reproducing the system's surface flux dynamics.

Our research focuses on surface-atmosphere interactions on the Tibetan Plateau (TP) in the Nam Co Lake region. With more than 4700 m a.s.l., a semi-arid climate and with a highly adapted *Kobresia pygmea* alpine steppe (Miehe et al., 2011), the TP proves to be a difficult environment for surface models (Yang et al., 2003, 2009). Specific problems

Published by Copernicus Publications on behalf of the European Geosciences Union.

include large temporal and spatial variability in soil moisture (Su et al., 2011), large diurnal variations of surface temperature from surface freezing before sunrise to more than 30 °C at noon. Ma et al. (2009) give an overview about the TP surface-atmosphere processes. On the TP, the fraction of diffuse solar radiation is very small, making cloud feedbacks especially important for the surface-atmosphere system. The model studies with a regional model of Cui et al. (2007) imply that some of the precipitation events on the TP are predominantly local and therefore not captured by coarser resolution models.

In this paper we present results of a rather simple flux algorithm based on a modified two-layer soil model that is part of a vegetation dynamics and biosphere model Hybrid (Friend et al., 1997; Friend and Kiang, 2005; Friend, 2010). The original model produces a substantial delay in the diurnal turbulent flux cycle due to the low responsiveness of the model's upper soil layer to changes in atmospheric forcing and fails to capture important dynamics. We therefore introduce an extrapolated surface temperature and show that this new approach is capable of reproducing diurnal flux dynamics for two vegetation covered surfaces near Nam Co Lake. These sites are representative for the basin, but show very different dynamics. In our future studies, the same surface-model version will also be coupled to the spatially and temporally high resolution atmospheric model ATHAM (Active Tracer High-resolution Atmospheric Model, Oberhuber et al., 1998; Herzog et al., 1998) including radiation, cloud microphysics and active tracer transport. As simulations of the high-resolution model will be run for approximately 24 h we tested the surface model in column mode forced with standard atmospheric measurements for the same period of time with initialisation at 00:00 h Beijing Standard Time (BST). We acknowledge that this approach is different from most surface model studies that are run for longer periods, but it is necessary for the planned study of the coupled surface-atmosphere system. Such a surface flux algorithm is generally suitable for high-resolution atmospheric modelling studies of different ecosystems as it does not have built in assumptions about horizontal scales.

It is our objective to test the suitability of a simple two-layer soil model with an improved surface or "skin" temperature estimated from the mean temperature of the uppermost layer that shall subsequently be used for driving an atmospheric circulation model for the Nam Co region on the TP. Therefore, fluxes derived from the surface flux algorithm with and without a specific formulation for "skin" temperature are compared to fluxes measured by eddy-covariance technique and to fluxes derived by a more complex Surface-Vegetation-Atmosphere Transfer (SVAT) Model, with five soil layers.

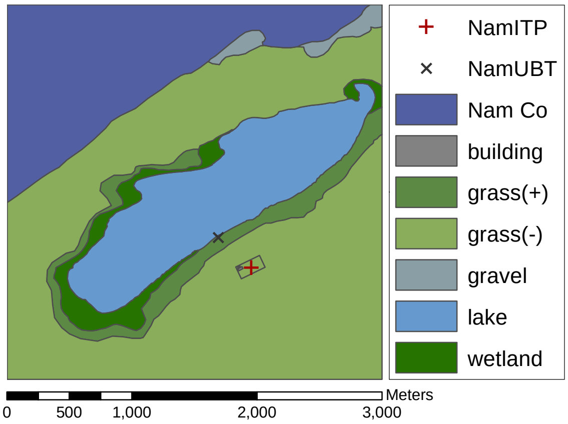

Fig. 1. Landcover map of study area: the black cross indicates the station identified as UBT, close to the small lake with denser surface cover [grass (+)], the red cross shows the station location ITP with sparse surface cover [grass (-)].

2 Site description and model forcing data

From 27 June to 8 August by the University of Bayreuth (UBT) and the Institute of Tibetan Plateau Research, Chinese Academy of Sciences (ITP) conducted a joint field campaign at Nam Co Lake.

2.1 Site description

Nam Co Lake is located on the Tibetan Plateau at approximately 4730 m a.s.l., circa 150 km north of Lhasa. Data from two locations in the vicinity of the lake are used (Fig. 1). Site 1, referred to and operated by UBT, is an eddy-covariance setup on the south shore of a small lake that itself is situated approximately 500 m south of Nam Co lake. UBT has a fairly constant soil moisture below circa 60 cm depth due to the influence of ground water. Additionally, the atmospheric measurements are influenced by a land-lake breeze that originates from Nam Co Lake. Site 2 (operated by and referred to as ITP) is at the Nam Co Station for Multisphere Observation and Research (Li et al., 2009; Cong et al., 2009), approximately 300 m south from both UBT and the direct influence of the small lake with a sandy soil and a very low field capacity (FC = 5 %) compared to overall pore volume (39 %). The vegetation at both sites is grassland (Metzger et al., 2006) with UBT having a small bare soil fraction (0.1) compared to 0.4 at ITP). Small FC and the generally low volumetric top soil water contents (θ_v) at ITP, lead to large sensible energy fluxes compared to latent heat fluxes ($Q_H \gg Q_E$). After rain events however, θ_v may exceed FC by a factor of up to 3 leading to a similar flux regime at the two stations with $Q_E > Q_H$. Due to the generally drier conditions, reducing soil total heat capacity and the smaller influence of the lake on the temperature cycle at ITP surface temperature

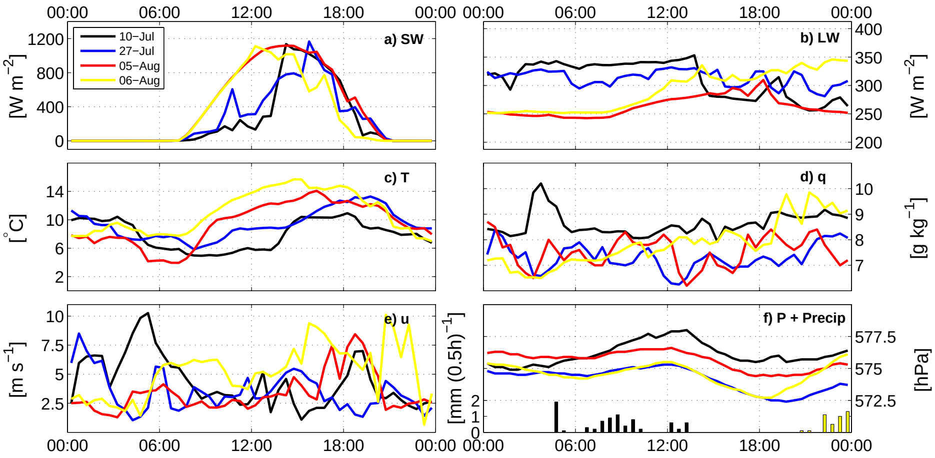

Fig. 2. Forcing data measured at UBT used for model runs: **(a)** downward shortwave radiation (SW [W m^{-2}]); b) downward longwave radiation (LW [W m^{-2}]); **(c)** air temperature (T [°C]); **(d)** water vapour mixing ratio (q [g kg^{-1}]); **(e)** wind speed (U [m s^{-1}]); **(f)** surface pressure (P [hPa]) and precipitation [mm (0.5h)$^{-1}$]) Height c–e is 3 m.

frequently drops below 0 °C in the early morning hours. At UBT there were soil temperature sensors installed at 2.5, 5, 10, 20, 30 and 50 cm depths. At ITP no soil temperatures were available at depths above 20 cm, with data measured at 20, 40, 80 and 160 cm below ground. Comprehensive information of ITP and UBT surface and soil properties, measurement setup and data availability is found in (Biermann et al., 2009) and an overview over the parameters used in the model is presented in Table 1.

2.2 Model forcing data

The data used in the modelling study was selected according to the data quality of turbulence data (Foken et al., 2004) and the wind direction. Finally, we selected four days with high data quality over the whole day encompassing different weather situation. The 24-h model runs are initialised with the soil temperature profile and soil moisture at 00:00 BST (∼22:00 in local solar time). 10 July was a complex day with rain in the morning and sunshine in the afternoon. 27 July was a cloudy day without rain. 5 August was a radiation day after a period of rain leading to moist conditions and large Q_E at ITP. 6 August was similar to the previous day, but with some of the water drained from the soil at ITP and developing clouds in the afternoon. During 10 July and 5 August, the station close to the lake (UBT) came under the influence of a lake breeze during which the forcing data (except for radiation measurements) correspond rather to the nearby lake than the land surface. Due to the overcast sky on 27 July the lake breeze and thus the influence of the lake surface was severely weakened as described in Zhou et al. (2011), so that there was only limited influence of the lake surface onto the atmospheric measurements.

The model is forced with measured atmospheric data from UBT (Fig. 2) and ITP (Fig. 3) providing air temperature, water vapour mixing ratio, wind speed, air pressure, precipitation and downwelling long and shortwave radiation. In general 30-min mean values were linearly interpolated to the surface model time step that was the same as a typical time step of an atmospheric model ($\Delta t = 2.5$ s). The only selected day with precipitation during day-time was 10 July 2009. However, there was also rain recorded at UBT from about 22:00 BST on 6 August 2009, while no precipitation data was available at ITP. Half hourly precipitation was scaled down to the model time step assuming a constant precipitation rate per 30-min interval. There was little difference between the data measured at ITP and UBT, as expected due to the proximity of the sites. However there was an offset of approx. 5 hPa between the recorded pressures, that was not corrected for as this is likely within the uncertainty of the sensors and the model should not be too sensitive to such a pressure difference. Unlike UBT where rain 30-min precipitation was available, there were only daily sums recorded for ITP, which had to be downscaled to 30-min values by scaling them linearly with UBT observations.

3 Modelling approach

The surface model Hybrid (Friend et al., 1997; Friend and Kiang, 2005) is currently coupled to the high-resolution Active Tracer High-resolution Atmospheric Model (ATHAM) by Oberhuber et al. (1998) and Herzog et al. (1998) for the investigation of feedbacks between atmospheric processes and surface fluxes.

Table 1. Description of the two sites (UBT and ITP) near Nam Co lake and the parameters used the model setup (Biermann et al., 2009).

Parameter	UBT	ITP
Coordinates	30°46.50′ N 90°57.61′ E	30°46.44′ N 90°57.72′ E
Soil	sandy-loamy	sandy
Porosity	0.63	0.393
Field capacity [$m^3\,m^{-3}$]	0.184	0.05
Wilting point [$m^3\,m^{-3}$]	0.115	0.02
Heat capacity of dry soil (c_{p_d}) [$J\,m^{-3}\,K^{-1}$]	2.5×10^6	2.2×10^6
Thermal conductivity [$W\,m^{-1}\,K^{-1}$]	0.53	0.20
Surface albedo (α)	0.20	0.20
Surface emissivity (ϵ)	0.97	0.97
Vegetated fraction	0.9	0.6
LAI [$m^2\,m^{-2}$] (estim. from: Hu et al., 2009)	0.9	0.6
Vegetation height [m]	0.07	0.15

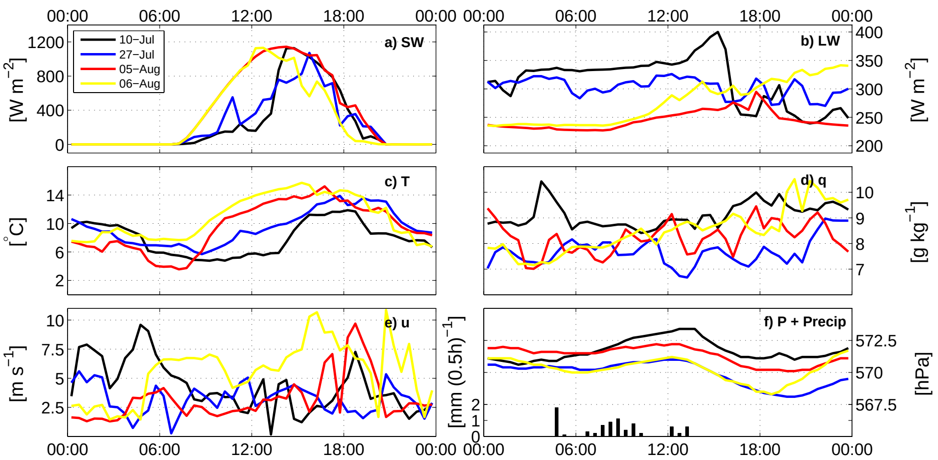

Fig. 3. Same as Fig. 2, but with forcing data measured at ITP. Precipitation at ITP was measured daily and for the purpose of this study distributed to 30 minute intervals according to the recorded rain fall at UBT.

Our high-resolution modelling approach aims at a spatial and temporal resolution in the order of 500 m and 2.5 s, respectively. As our focus is on diurnal surface-atmosphere interactions, the surface model must capture the magnitude of the fluxes and must be able to react quickly to changes in atmospheric forcing. Therefore, a surface model that is capable of reproducing realistic turbulent energy and water vapour fluxes at a sufficiently high temporal resolution and at reasonable computational costs is needed. We decided against a model with more than two soil-layers due to higher computational cost and instead modified the original Hybrid model to meet these requirements.

3.1 The surface model

The modified version of Hybrid which is a process based terrestrial ecosystem and surface model, incorporates a simple two-layer representation of the soil and uses the turbulent transfer parameterisations taken from the GISS model II (Hansen et al., 1983). The transfer equations in Hybrid are described in Friend and Kiang (2005). Bare soil parameterisation follows the approach of SSiB (Xue et al., 1996) that is based on Camillo and Gurney (1986) and Sellers et al. (1986). Turbulent fluxes are calculated using a bulk approach for the sensible heat flux:

$$Q_H = c_p\, \rho\, C_H\, u(z)\; (T_0 - T(z)) \tag{1}$$

with air specific heat capacity (c_p [$J\,kg^{-1}\,K^{-1}$]), the Stanton number (C_H) which is calculated as a function of roughness length (z_0) and Bulk Richardson Number, air density (ρ [kg m^{-3}]), measured wind speed ($u(z)$ [m s^{-1}]), air temperature ($T(z)$) at measurement height (z [m]) and surface temperature (T_0). All temperatures used are in K. The latent heat flux is derived in a more complex manner from bulk soil evaporation (EV) and a canopy resistance approach estimating plant transpiration (TR), with $Q_E = \mathrm{EV} + \mathrm{TR}$:

$$\mathrm{EV} = \left(\rho \frac{f_\mathrm{h} q_\mathrm{s} - q_\mathrm{a}}{r_\mathrm{s} + r_\mathrm{a}}\right) \times \exp(-0.7\mathrm{LAI}) \tag{2}$$

$$\mathrm{TR} = \frac{\rho \Delta q_\mathrm{a}}{r_\mathrm{c} + r_\mathrm{a}}, \tag{3}$$

with the relative humidity of soil air (f_h), saturation water mixing ratio at surface temperature (q_s), atmospheric water vapour mixing ratio (q_a), soil and aerodynamic resistance (r_s, r_a), leaf area index (LAI) and canopy resistance (r_c) calculated by the vegetation model component. Transfer coefficients are modified from Deardorff (1968). Plant physiology and stomatal conductance are included via generalised plant types (GPT). As an ecosystem model Hybrid is designed to work on hourly to climate scales (Friend, 2010) and and should therefore be capable of reproducing diurnal flux cycles as well as ecosystem changes on climate scales. It was originally developed as a biosphere-surface component for the GISS GCM. A "thin" upper layer of 10 cm thickness follows the daily cycle of surface temperatures, whereas a lower layer with 4 m thickness acts as the memory for the annual cycle in both model versions. However, an upper layer of such thickness imposes a substantial dampening on the diurnal temperature cycle and will effectively act as a low-pass filter for events of short durations such as cloud shading that, especially under the conditions found at the TP, has a substantial immediate impact on surface temperatures and on fluxes as well. This can be seen in Fig. 12 of Hansen et al. (1983), where a time delay of approximately 2 h is visible for surface temperature in the diurnal cycle. A similar behaviour of the original Hybrid is discussed in Sect. 5.4. Shortcomings with the representation of diurnal cycles may also impact on longer term studies as the model drifts away from a realistic state. As we plan to apply the coupled model for high-resolution simulations with a time step in the order of seconds, we focus in this work on the accuracy of the diurnal flux cycles that can be achieved with such a model.

3.2 The modified soil model in Hybrid

In order to improve the delay in diurnal flux evolution and the weak responsiveness of sudden short-term changes in atmospheric forcing, new simulation approaches for surface temperature and heat diffusion were introduced in Hybrid.

3.2.1 Diagnostic surface temperature

An extrapolated surface temperature (T_0) is being introduced that is then subsequently used for the calculation of atmospheric stability through the Bulk Richardson number as well as for Q_H and Q_E. This approach is somewhat similar to the "force-restore method" (Blackadar, 1979) that also aims at providing a realistic surface temperature imitating the behaviour of real soils. However, while "force-restore" uses an oscillating heat source as forcing term and a heat flux into the ground as restoring term (Yee, 1988), our method is not dependent on a periodic heating function and uses the concept of layer heat storage. T_0 is derived from a set of assumptions that were already included in Hybrid going back to Hansen et al. (1983). For both layers denoted with the subscripts 1 and 2 from the model top, we assume a quadratic temperature profile ($T(z)$) (Fig. 4):

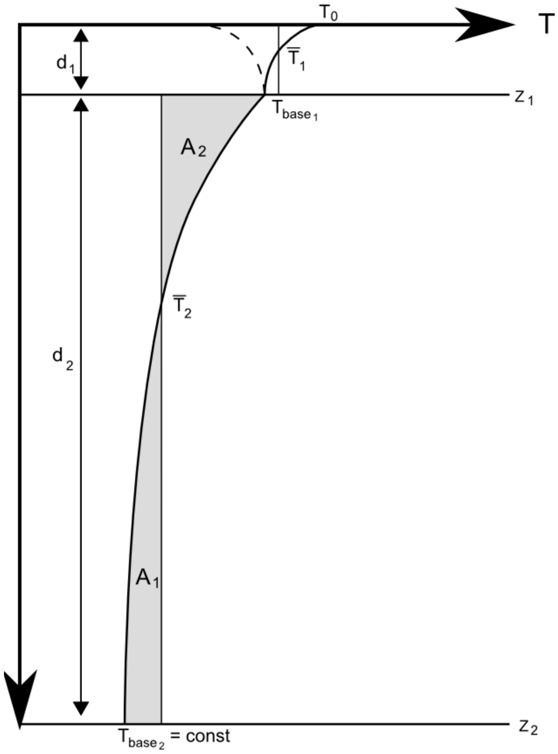

Fig. 4. Conceptional drawing of the assumed quadratic subgrid soil temperature profile and the associated parameters. In order to derive $\bar{T}_1$ and $\bar{T}_2$ geometrically the areas A_1 and A_2 must be equal.

$$T_{1,2}(z_\mathrm{rel}) = a_{1,2}\,\left(z_\mathrm{rel} - d_{1,2}\right)^2 + T_{\mathrm{base}_{1,2}} \tag{4}$$

with a constant (a [K m^{-2}]), the depth below the top of the layer (z_{rel} [m]), the layer thickness (d [m]) and the temperature at the lower boundary of the respective layer (T_base). There is assumed to be no transfer of heat through the lower model boundary i.e. T_{base_2} is constant and equal to the annual mean temperature of 0 °C (You et al., 2006, recited from Keil et al., 2010). We are aware of this being a simplification.

However, the annual temperature cycle at 4 m is expected to be small and the rate of change as well as the diurnal temperature cycle is too small to have an impact on the day scale. For future research the seasonal mean temperature could be used in order to remove this potential source of error. The relationship between layer heat content E [J] and temperature profile is given by:

$$E = c_{\mathrm{p_s}} \int_{z_\mathrm{L}}^{z_\mathrm{U}} T(z)\,\mathrm{d}z \tag{5}$$

where z_L and z_U are the lower and upper boundaries of the layer and $c_{\mathrm{p_s}}$ [$\mathrm{J\,m^{-3}\,K^{-1}}$] is the total soil heat capacity. Hence, with a known heat content for each layer it is possible to solve for

$$a_2 = \frac{\frac{E_2}{c_{\mathrm{p_s},2}} - d_2 T_{\mathrm{base}_2}}{\frac{{d_2}^3}{3}}, \tag{6}$$

by integrating Eq. (5) with Eq. (4) from $z_L = 0$ to $z_U = d_2$ and solving for a_2. The base temperature of the first layer is related to T_{base_2} through

$$T_{\mathrm{base}_1} = T_{\mathrm{base}_2} + a_2 {d_2}^2. \tag{7}$$

In a similar fashion a_1 and T_0 can be approximated:

$$a_1 = \frac{\frac{E_1}{c_{\mathrm{p_s},1}} - d_1 T_{\mathrm{base}_1}}{\frac{-{z_1}^3}{3}} \tag{8}$$

and

$$T_0 = T_{\mathrm{base}_1} + a_1 {d_1}^2. \tag{9}$$

As T_{base_1} is a parameter of both Eqs. (7) and (9) and $a_{1,2}$ are of crucial importance to the initialisation of $E_{1,2}$, special care has to be taken, when assigning initial conditions (see discussion in Sect. 3.3).

3.2.2 Heat diffusion estimation

The soil heat flux is derived from the residual of the surface energy balance. In the original heat diffusion algorithm of Hybrid (Hansen et al., 1983), the heat flux from the first to the second soil layer $F(z)$ is dependent on the difference between mean surface layer temperatures ($\bar{T}$), the soil heat flux calculated as residual of turbulent and radiation fluxes ($F(0)$), layer thickness and thermal resistances r,

$$F(z) = \frac{3\bar{T}_1 - 3\bar{T}_2 - 0.5F(0)r_1}{r_1 + r_2} \times \Delta\mathrm{t}, \tag{10}$$

where Δt is model time-step. This leads to unrealistic modelled heat fluxes $F(z)$ as $F(z)$ is largely dominated by $F(0)$, which is positive during nighttime and negative during daytime, thus leading to a net transfer of heat from a cold to a warm layer. With the assumption of a subgrid temperature profile the heat flux between the two layers Eq. (10) was modified with a heat diffusion approach and integration of

$$\frac{\partial T}{\partial t} = D\frac{\partial^2 T}{\partial z^2} \approx D\Delta\mathrm{t}\frac{T(z_1+\Delta z) - 2T(z_1) + T(z_1 - \Delta z)}{2\Delta z} \tag{11}$$

with D being a soil moisture dependent diffusion constant for heat. We assume ∂z to be approximated by the diffusion length $L = 2\sqrt{\Delta \mathrm{t} D} = \Delta z$ and the temperatures are taken from the assumed profile. As the model is run with the short time-step of the atmospheric model, such a formulation becomes valid. A rough calculation for L with $D = 10^{-6}\,\mathrm{m^2\,s^{-1}}$, which is close to the determined value, and $\Delta\mathrm{t} = 30$ min gives $L = 0.08$ m, which is close to d_1, posing an upper limit on Δt for this method.

3.3 Surface temperature profile initialisation

Due to the quadratic nature of the soil layer temperature profiles and their potential kink at the layer interface (see Fig. 4), the modified model depends on careful initialisation that fulfills two requirements: (1) a realistic estimate of surface temperature and (2) an appropriate estimate of ground heat storage (E) allowing the upper layer to react in a realistic way. In this study soil temperature measurements at several depths were used in order to accomplish both requirements. Surface temperature was estimated from upwelling longwave radiation according to the Stefan-Boltzmann law with a longwave emissivity of $\epsilon = 0.97$. We initialised E_2 by setting T_{base_1} to the measured 10 cm temperature and then subsequently fitted the temperature curve for the first model layer by minimising the squared mean error with regard to measured soil temperatures. Due to the lacking 10 cm temperature at ITP, this temperature had to be estimated from the 20 cm measurement and T_0 was approximated in order to estimate the initial E_1. It should be noted that the assumed quadratic temperature profile in the lower soil layer clearly underestimated the vertical temperature gradient in the soil as estimated UBT temperatures at 50 cm were always higher than measured temperatures. This difference is reduced from July to August as the summer warming reaches lower layers. This is a limitation due to fixed layer depths.

Table 2 shows the initial temperatures for each day. From the span of layer temperatures $\bar{T}_1$ and $\bar{T}_2$, the theoretical parameter space of T_0 for a constant T_{base_2} (Fig. 5) can be derived. While Fig. 5a and b show the individual dependence of temperature variables on each other as expressed in the respective Eqs. (7) and (9), Fig. 5c shows the combined effect of parameter variation. A random combination of the initial temperatures given in Table 2 would yield T_0 in the rage of -10 to 30 °C. In contrast, the actual model layer temperatures, indicated by the crosses in Fig. 5c, occupy a much smaller area and are, with the exception of one day, clustered closely. This highlights the importance of a careful initialisation of the soil temperature profile requiring knowledge

Table 2. Initial soil temperatures used in this study ($\bar{T_2}$ and $\bar{T_1}$ are estimated from the respective base and top temperatures of the layer according to a quadratic temperature profile), change of layer 1 mean temperature ($\Delta\bar{T_1}$) over the modified Hybrid run, soil moisture content of layer 1 at beginning of the modified model run ($\theta_{1_{obs}}$) and at the end of the simulation ($\theta_{1_{end}}$). The values in parenthesis are expressed as θ_1/FC [-].

Site	Date	$\bar{T_2}$ [°C]	$T_{1,\mathrm{base}}$ [°C]	$\bar{T_1}$ [°C]	T_0 [°C]	$\Delta\bar{T_1}$ [°C]	$\theta_{1_{obs}}$ [%]	$\theta_{1_{end}}$ [%]
UBT	10 July	3.9	11.8	10.9	9.3	−1.6	26.9 (1.47)	41.1(2.24)
	27 July	4.5	13.4	12.5	10.6	−1.6	20.8 (1.14)	17.0 (0.92)
	5 August	4.8	14.4	13.4	11.2	−3.0	26.9 (1.47)	19.1 (1.04)
	6 August	4.75	14.3	12.8	9.8	−1.4	25.4 (1.39)	34.0 (1.85)
ITP	10 July	5.4	16.2	13.2	7.2	−1.2	6.0 (1.1)	25.1 (5.02)
	27 July	7.2	21.6	17.8	10.2	−1.7	3.0 (0.6)	1.6 (0.32)
	5 August	5.7	17.1	11.1	−0.8	0.2	11.0 (2.2)	4.3 (0.86)
	6 August	5.6	16.8	11.6	1.1	1.9	9.0 (1.8)	3.7 (0.73)

about subsurface temperatures that are difficult to estimate without field measurements.

4 Flux comparison

Surface fluxes derived with any method contain inaccuracies such as measurement errors or theoretical limitations. Therefore we are not comparing our modelling results to the absolute truth, but to two flux references.

4.1 EC and SEWAB reference fluxes

Fluxes estimated by both versions of Hybrid are compared with observed fluxes derived by eddy covariance (EC) method and fluxes modelled by the SVAT model SEWAB (Surface Energy and Water Balance model – Mengelkamp et al., 1999), which has been configured for the two sites for gap-filling and up-scaling of flux measurements. Both flux references yield fluxes averaged over 30-min intervals. Unlike many SVAT models that derive the soil heat flux from the flux residual, SEWAB is solving the surface energy balance equation ($Q_\mathrm{E}+Q_\mathrm{H}+Q_\mathrm{Rad}+Q_\mathrm{Soil}=0$) iteratively for T_0 by Brent's method (Mengelkamp et al., 1999), hence closing the energy balance locally (Kracher et al., 2009). In contrast, the surface energy balance closure derived by EC is only in the order of 0.7 at Nam Co Lake (Zhou et al., 2011). Consequently, 30 % of the net radiation is not captured by surface flux measurements. However, energy balance closure must not be used as a quality measure for flux measurements (Aubinet et al., 1999) as surface heterogeneity leads to organised low frequency structures and mesoscale circulations (Panin et al., 1998; Kanda et al., 2004) that are mainly responsible for the lack of closure (Foken, 2008). The energy balance problem for eddy-covariance measurements is summarized in Foken et al. (2011). Additionally, in sea (lake) breeze systems a significant portion of the energy fluxes is transported horizontally (Kuwagata et al., 1994). Therefore, SEWAB (and Hybrid) fluxes are comparatively larger than the measured ones. When the energy balance is closed artificially by redistributing the residual to fluxes according to the Bowen ratio (Twine et al., 2000), the resulting fluxes are in much better agreement with SEWAB (not shown). Therefore energy balance corrected fluxes are used whenever possible ($Q_{\mathrm{E_{EC,EBC}}}$ and $Q_{\mathrm{H_{EC,EBC}}}$). Artificial energy balance closure is only possible, when the Bowen ratio can be determined from flux measurements and when data about the available energy is measured. EC data were collected at 3 m height and calculated using the TK3 package (Mauder et al., 2008; Mauder and Foken, 2011). Quality checks were performed according to Foken et al. (2004). A detailed description of the instrumentation can be found in Biermann et al. (2009). The rain event of 10 July leads to the exclusion of fluxes due to quality concerns. Both Hybrid and SEWAB produce fluxes during rain, but their quality is unknown as they cannot be compared to measurements.

Measuring in close proximity to the lake also means that depending on wind direction the fluxes measured at UBT are originating from land, water or a mixture of both as the footprint of the EC system and thus also of the forcing data is located upwind of the site. This leads to problems in the energy balance closure and the integration of fluxes. The development of a lake breeze system at Nam Co means that during most days there are no flux measurements available from the late morning or early afternoon until the lake breeze ceases. The days of 27 July and 6 August are the only days during which the field campaign provides data that do not have a full lake breeze influence at UBT. Therefore it is beneficial to compare not only to measured fluxes, but also to SEWAB ($Q_{\mathrm{E_{SEWAB}}}$ and $Q_{\mathrm{H_{SEWAB}}}$).

For completeness, fluxes over the lake calculated by the TOGA-COARE algorithm (Fairall et al., 1996a,b) that is also part of the coupled surface-atmosphere model are given during lake breeze events.

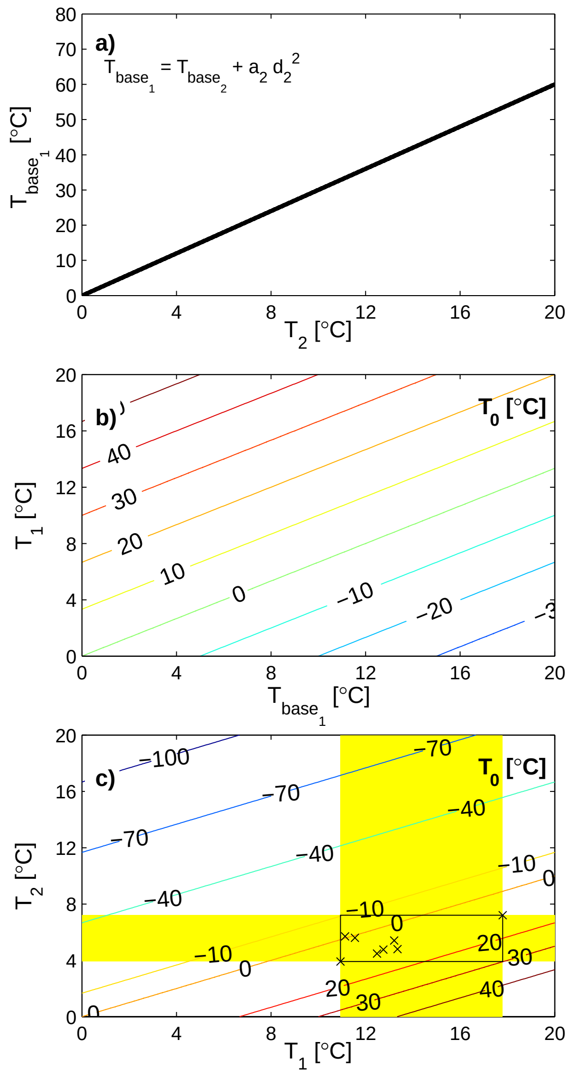

Fig. 5. Dependency of soil temperature parameters: **(a)** relationship between mean temperature of layer 2 ($\bar{T}_2$) and bottom temperature of layer 1 [T_{base_1}, Eq. (7)] – a_2 is calculated according to Eq. (6); **(b)** surface temperature (T_0) contour plot as function of T_{base_1} and layer 1 mean temperature ($\bar{T}_1$) and **(c)** contours of (T_0) as function of $\bar{T}_2$ and $\bar{T}_1$. The black rectangle at the intersection of the layer temperature ranges (yellow) indicates the theoretical parameter space given by the temperature values used in this study and the black crosses mark the actual configurations.

4.2 Statistical evaluation measures

Model quality was assessed by Root Mean Square Deviation (RMSD)

$$\mathrm{RMSD} = \sqrt{\frac{1}{N}\sum_{i=1}^{N}(P_\mathrm{p} - P_\mathrm{r})_i^2} \tag{12}$$

and Cross Correlation according to the coefficient of determination (R^2):

$$R^2(j) = \left(\frac{\mathrm{cov}\left(P_\mathrm{p}(1+j:N), P_\mathrm{r}(1:N-j)\right)}{\sigma_{P_\mathrm{p}(1+j:N)}\sigma_{P_\mathrm{r}(1:N-j)}}\right)^2 \tag{13}$$

with $R^2(j)$ being the coefficients of determination for the predicted (P_p) and reference (P_r) flux time series shifted by j elements, the total number of elements in each time series (N) and σ as their respective standard deviations. Both SEWAB and EC measurements produce 30-min flux averages, whereas Hybrid was set to 10-min averaged fluxes. Therefore the reference fluxes were linearly interpolated to Hybrid's output times before statistical evaluation. Periods when no energy balance corrected EC measurements were available (see Figs. 6 and 7 for details) were excluded from the calculation of the statistical measures.

5 Results and discussion

The following section presents and discusses the improvements that are achieved for a simple two-layer model when a new algorithm for the surface temperature was implemented.

The original two-layer model Hybrid fails to reproduce the diurnal dynamics observed at UBT (Figs. 6 and 7) due to the thermal inertia of the top-layer. The delayed response in surface temperature leads to a shift in the resulting turbulent surface fluxes. This causes an underestimation of Q_E and Q_H until ∼18:00 BST and later to an overestimation due to delayed surface cooling. The improvement of the modified Hybrid over the original formulation is discussed in more detail in Sects. 5.1 and 5.4.

The latent (Fig. 6 – left column) and sensible heat fluxes (right column) estimated with the modified Hybrid model are generally in good agreement with the reference fluxes derived by EC and SEWAB. The diagnostic surface temperature (right column) also shows a close agreement. In some instances there remains a small shift in fluxes compared to the reference values, but this has been greatly improved compared to the original Hybrid. The surface temperatures are also in good agreement after sunrise, despite the fact that during the clear sky days in August excessive night-time surface cooling is simulated. This is less of an issue during the overcast nights.

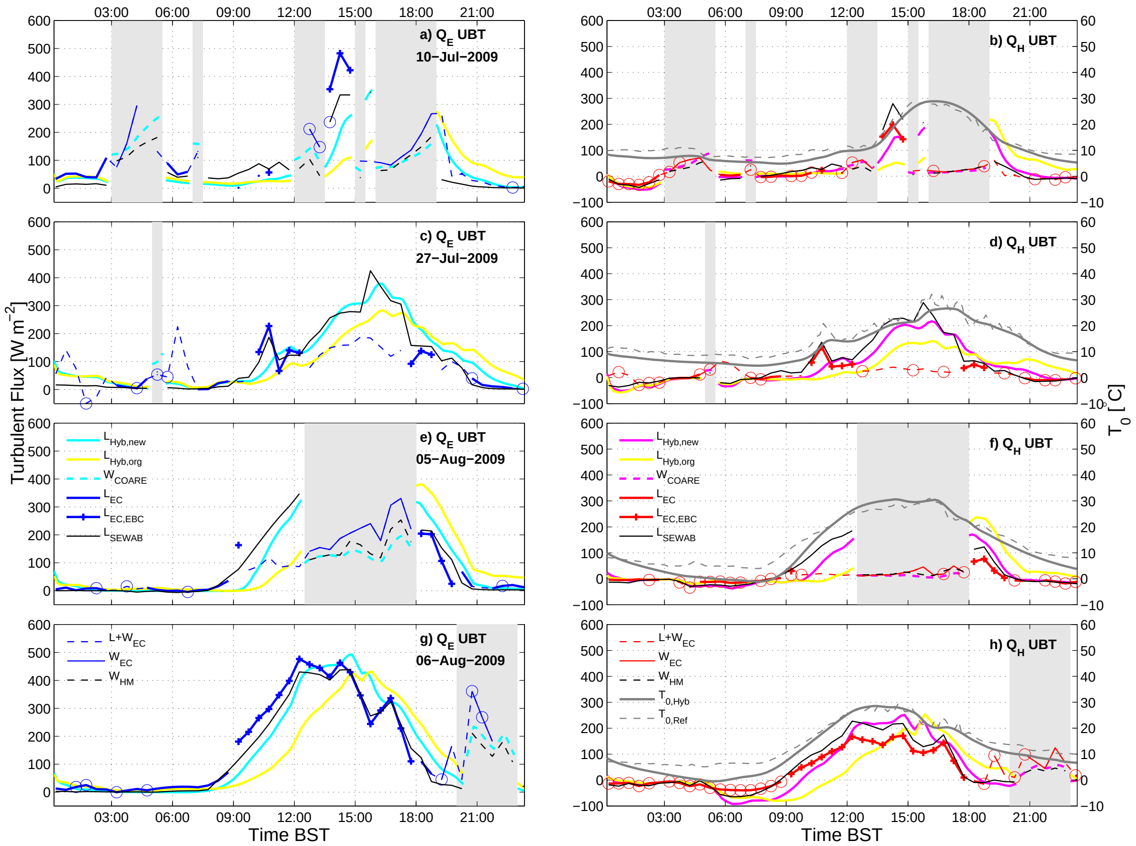

Fig. 6. Model results for the modified Hybrid at UBT for 10 July 2009 **(a–b)**, 27 July 2009 **(c–d)**, 5 August 2009 **(e–f)** and 6 August 2009 **(g–h)**. Left column: latent heat flux (Q_E); right column: sensible heat flux (Q_H) and surface temperature T_0 [°C]. *L* and *W* refer to "land" and "water" as origin of the fluxes. *L+W* is the complete available time series. The subscripts *Hyb,mod* and *Hyb,org* refer to fluxes from the modified and original Hybrid and *COARE* are fluxes from the lake derived by TOGA-COARE whereas *SEWAB* is a SVAT model and *HM* refers to a hydrodynamic multi-layer lake model after Foken (1984) and Panin et al. (2006). *EC* and *EC,EBC* refer to measurements by eddy covariance method where in the latter the energy balance has been closed by distributing the residual according to Bowen-ratio (this requires good data quality and fluxes and can only be done for fluxes that are attributed to land). The circles indicate poor data quality of the EC system according to Foken et al. (2004). Gray shading indicates times where the flux footprint of UBT was over the lake.

The situation at ITP is quite similar to UBT. The modified model agrees well with the EC and SEWAB reference data. On 5 August the turbulent flux dynamics, but not the magnitude of the fluxes, match the EC measurements closely (Fig. 7), while the original Hybrid showed a strong delay in the flux response as the soil remained frozen during the morning. While the magnitude of the latent heat flux is close to EC measurements, Q_H produced by Hybrid are of a similar magnitude as Q_H from SEWAB. These are considerably larger than the fluxes measured by EC and corrected for energy balance closure. For 6 August the modelled maximum of Q_E is larger than the maximum $Q_{\mathrm{E}_\mathrm{EC,EBC}}$ and much greater throughout most of the day compared to SEWAB. Q_H in contrast shows similar diurnal dynamics as $Q_{\mathrm{H}_\mathrm{EC,EBC}}$, but with its magnitude between the sensible heat flux derived by SEWAB and $Q_{\mathrm{H}_\mathrm{EC,EBC}}$. Around 18:00 h the Q_H-fluxes from the different methods become more similar. A large negative Q_H-flux in the morning hours is apparent but greatly improved compared to the unmodified Hybrid version. Figure 6a and b also highlights some limitations of ecosystem research as a large portion of the data had to be rejected due to limitations described in Sect. 4.1.

During lake breeze events the surface fluxes over water derived from TOGA-COARE are displayed. Sensible heat fluxes are in close agreement with EC data and fluxes derived by a hydrodynamic multi-layer lake model (Foken, 1984; Panin et al., 2006). Latent heat fluxes show a similar behaviour and are of similar magnitude on 10 July

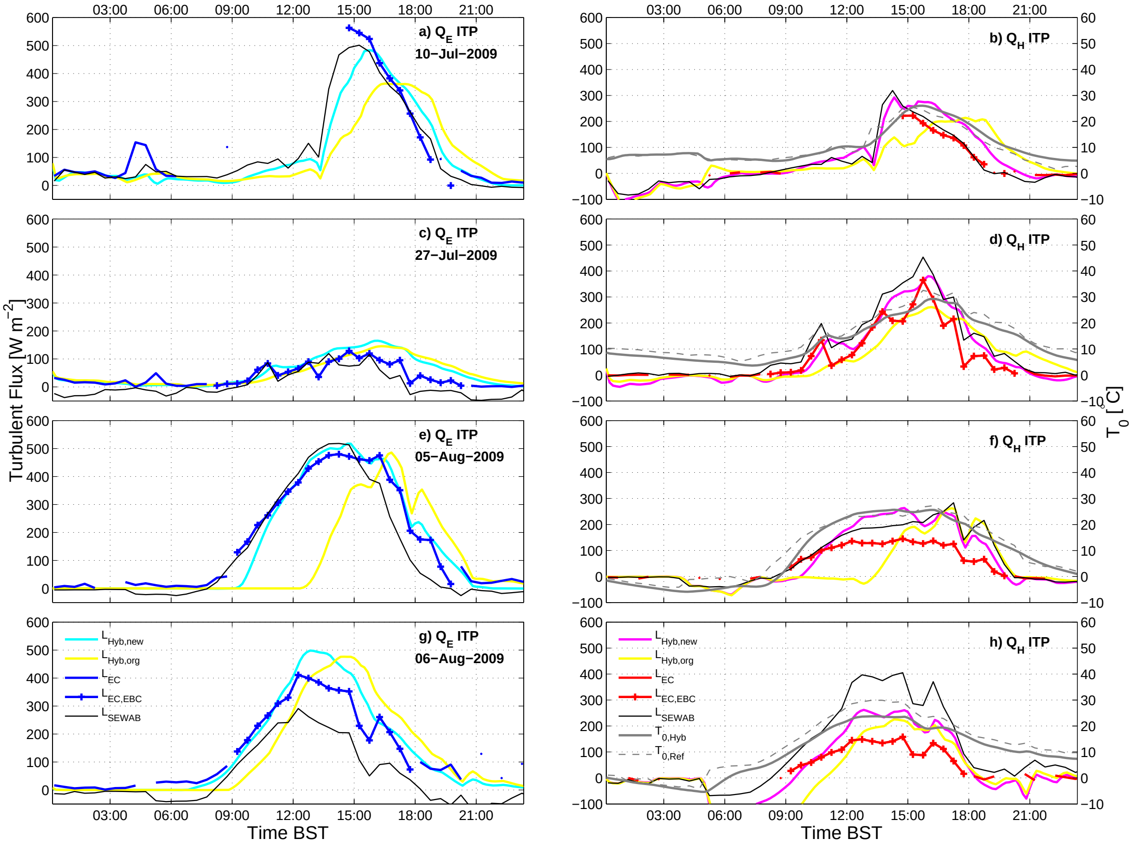

Fig. 7. Same as Fig. 6, but for ITP. There are no contributions from the lake.

and 6 August. On 5 August there is at least a qualitative agreement between COARE and EC measurements.

5.1 Discussion of turbulent fluxes

The original two layer model reacts only slowly to the atmospheric forcing, delaying the fluxes' response. Such a time lag leads to a shift in the diurnal cycle and is problematic for the coupling to atmospheric models since surface fluxes are one of the main drivers of regional and local circulation as well as cloud development. These will certainly be affected by erroneous surface flux dynamics. In our specific case, the dampening of the diurnal temperature cycle and the delay in surface fluxes may reduce the intensity of the land-lake breeze or may delay its development through a reduction of differential heating between land and lake surface. However, there is still a minor delay visible in the modified Hybrid as the surface temperature is purely diagnostic and dependent on $\bar{T}_1$. This is discussed in more detail in Sect. 5.4.

Table 3 shows the results of the RMSD between the modelled results and the reference quantities. With the modified Hybrid model there is a 40–60 % improvement in the RMSDs compared to the original Hybrid, when both are compared against SEWAB. The only notable exception for this is 6 August at ITP, where a strong deviation of turbulent fluxes derived by SEWAB and measured fluxes was encountered. This is due to an underestimation of soil water content by SEWAB as 6 August falls into a dry interval between rainy periods, where SEWAB underestimates the soil water content. The picture is more diverse for the comparison between the energy balance corrected EC fluxes and Hybrid. There is a reduction in the error for all cases, except Q_H on 6 August at ITP, but the reductions cover a much larger range from less than 1 to 80 %. Due to data quality concerns the number of comparable elements is much lower (N given in Table 3) and probably too small for meaningful statistics in case of UBT. This is especially true as the daytime lake breeze influence coincides with the times with periods of usually higher quality of EC fluxes. As flux qualities are usually lower during conditions with limited vertical exchange (stable stratification), EC fluxes at ITP mainly reflect the daytime model performance whereas the comparison with SEWAB also takes

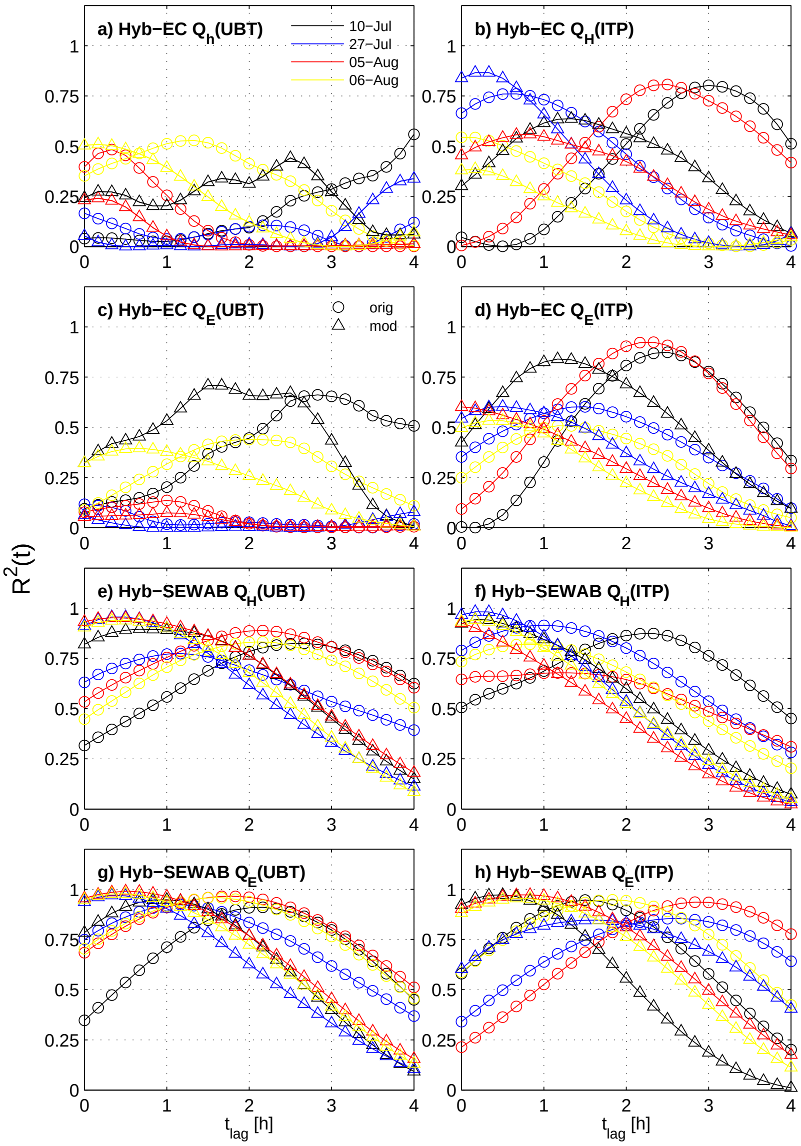

Fig. 8. Cross correlation $R^2(t)$ of simulated fluxes against flux reference shifted by t_{lag} as multiples of 10 minutes for each of the four days simulated with the original and modyfied Hybrid. The maximum number of elements used in the calculation of R^2 for each curve can be taken from Table 3.

into account the night-time, where fluxes and therefore absolute differences are smaller. The small improvement of RMSD of Q_{H} and $Q_{\mathrm{H_{EC,EBC}}}$ at ITP can be explained by the fact that the modified Hybrid follows the dynamics of EC, but flux estimates are larger and of the same magnitude as fluxes calculated by SEWAB. Mauder et al. (2006) have estimated the error or EC measurements to be 5 % or <10 W m^2 for Q_{H} and 15 % or <30 W m^{-2} for Q_{E}. Additional uncertainty is added to the measured fluxes by the lack in energy balance closure. When this is taken into account there is a significant difference between the $Q_{\mathrm{H_{Hybrid}}}$ and $Q_{\mathrm{H_{EC,EBC}}}$ for ITP on 6 August. On 5 August (ITP) and 6 August (UBT) the deviation of fluxes may still be explained by measurement errors and by shortcomings in the energy balance closure scheme. Indeed, there is no indication to assume scalar similarity between temperature and moisture transport (Ruppert et al.,

Table 3. Root mean square deviation (RMSD) between the modelled quantities of the original and modified Hybrid and reference values. The reference quantities used are either measured by EC and corrected for energy balance closure (EC,EBC) or modelled with SEWAB for fluxes or taken from longwave outgoing radiation for T_0. The values in parenthesis (N) correspond to the number of elements used for calculation of RMSD and $R^2(l=0)$ in Fig. 8.

			RMSD				
Site	Date	Run	Q_E EC,EBC	Q_H [W m^{-2}]	Q_E SEWAB	Q_H [W m^{-2}]	T_0 [°C]
UBT	10 July	orig	318	117 (8)	94	74 (94)	4.3 (139)
	27 July		97	58 (19)	60	59 (139)	4.5 (143)
	5 August		168	139 (11)	90	64 (110)	4.3 (143)
	6 August		159	84 (52)	87	71 (128)	3.7 (143)
ITP	10 July	orig	182	93 (25)	97	69 (143)	3.7 (143)
	27 July		43	64 (72)	58	75 (143)	3.8 (143)
	5 August		224	103 (64)	179	68 (143)	8.3 (143)
	6 August		118	80 (52)	130	119 (143)	5.1 (143)
UBT	10 July	mod	214	43 (8)	51	36 (94)	2.3 (139)
	27 July		79	44 (19)	32	28 (139)	2.9 (143)
	5 August		93	62 (11)	36	26 (110)	3.4 (143)
	6 August		78	57 (52)	39	32 (128)	3.2 (143)
ITP	10 July	mod	74	73 (25)	42	32 (143)	1.6 (143)
	27 July		42	58 (72)	55	36 (143)	2.6 (143)
	5 August		44	80 (64)	64	30 (143)	2.6 (143)
	6 August		68	82 (52)	113	77 (143)	3.5 (143)
UBT	all	orig	170	92 (90)	83	67 (471)	4.2 (568)
		mod	100	54 (90)	39	31 (471)	3.0 (568)
ITP	all	orig	152	84 (213)	125	86 (572)	5.6 (572)
		mod	54	73 (213)	74	48 (572)	2.7 (572)

2006; Mauder et al., 2007). Therefore, additional research, such as high-resolution atmospheric modelling studies, need to be carried out in order to determine the contributions of Q_H and Q_E to the "missing" energy. It should be noted that all modelled fluxes and measurements have errors, so that there is no absolute way of knowing which method produces the best flux estimates. The incorporation of surface fluxes into a regional circulation model may give some insight into whether modelled surface atmosphere interactions lead to realistic atmospheric flow patterns.

The large negative and potentially unreasonable night-time Q_H-fluxes that are modelled for ITP on 6 August are owed to a frozen soil and strong surface winds that lead to an overestimation of the temperature gradient, delayed reaction of the surface model and resulted in a potential underestimation of modelled surface temperatures and thus surface fluxes.

5.2 Discussion of surface temperature

For surface temperature there is a notable decrease in RMSD for all cases. Additionally, the source of the error changes. In the original model the error in T_0 was mainly due to the time-lag and a general underestimation of daytime maximum surface temperatures. In the new model daytime T_0 matches a lot better with observations except for ITP 6 August, where evaporative cooling due to excessive evapotranspiration contributes to too small warming rates. In return, the cooling during the nighttime is overestimated. This may either be due to errors in soil moisture, surface emissivity (ϵ) or due to the surface temperature extrapolation function used in this work.

5.3 Soil moisture variation and evapotranspiration

After a 24 h run the moisture content of the first model layer (last two columns of Table 2) is smaller than measurements suggest. For UBT, measured soil moisture content does hardly vary on a day to day scale and is kept well above FC due to groundwater influence. This is not reflected by the model as it lacks the capability to include groundwater tables. The true soil moisture at ITP has a much larger variation due to its low FC and comparatively large pore volume. During the dry day of 27 July the upper soil layer loses 1.5 mm of water whereas during the moist days of August there is a total loss from layer one of 6.7 and 5.3 mm d^{-1}, respectively. Comparing $\theta_{1_{end}}$ of 5 August with $\theta_{1_{obs}}$ of the next day shows that the model would perform considerably worse if it were not restarted every day. This is caused by a very limited soil hydrology included in Hybrid. Hu et al. (2008) have estimated the summer evapotranspiration on a central Tibetan grassland site to be in the order of 4–6 mm d^{-1}. An experiment conducted within the framework of TiP has estimated bare soil evaporation and evapotranspiration of a very dry soil at Kema in 2010 (∼150 km northeast of Nam Co Lake) at 2 mm d^{-1} rising to at least 6 mm d^{-1} and possibly more for a vegetated *Kobresia* pasture during an irrigation experiment (H. Coners – University of Göttingen, personal communication, 27 June 2011). Even though the soils are not directly comparable this suggests similar dynamics in Q_E to the ITP site. One factor likely to play a role in the local water cycle that is not included is dew fall in the early morning hours. Direct absorption of atmospheric moisture on bare soil (Agam (Ninari) and Berliner, 2004) and dew fall are often considered a significant moisture input for semi-arid environments (Agam and Berliner, 2006). Heavy dewfall in the vicinity of Nam Co Lake is frequently observed, but has, at least to our knowledge, never been quantified. This additional source of water and the associated local recycling of water may account for a significant fraction of the missing water. In addition to this, the too simplistic representation of soil hydrology is very likely responsible for the remaining water deficit in the upper layer of the soil model.

5.4 Cross correlation of turbulent fluxes

A different way of looking at the model performance is cross correlation of the modelled surface fluxes against EC measurements and SEWAB (Fig. 8). These measures give an insight into the reasons for the delayed response of the surface model and the amount of flux-variance explained, but does not yield information whether the model and the reference fluxes show a true one-to-one correlation. As with RMSD the quality of the analysis is limited by the number of data points that can be correlated, which is comparatively small for the energy balance corrected EC measurements at ITP and even smaller at UBT due to lake breeze influences (Fig. 8a–e). Hence, it is very difficult to interpret the cross correlations for EC. It is probably fair to say that there is a tendency for smaller time lags during the time series with higher number of elements, notably UBT 6 August and all days of ITP and that the total explained variances are at the same level of determination, when comparing the maximum $R^2(j)$. A notable exception is ITP 5 August.

For the comparison with SEWAB (Fig. 8f–h), it becomes notable that for many cases the maximum $R^2(j)$ of the modified Hybrid approach $R^2 \rightarrow 1$ and that their maxima are usually found at lags of 10–30 min ($j = 1-3$). Solar radiation rapidly modifies the skin temperature that is governing turbulent fluxes. As SEWAB has an instantaneous surface temperature solver for each model time step, one would expect a direct response of SEWAB to changes in solar radiation. This may even be faster than in reality, especially for Q_E flux that is not only dependent on the actual skin temperature, but also on the vegetation's response. Including negative values of j into Fig. 8 would show a gradual decrease of correlations with decreasing j, showing that the flux dynamics of Hybrid never precede EC measurements or SEWAB.

5.5 Natural variability of fluxes

Atmospheric quantities and turbulent surface fluxes have a large natural variability that is difficult to measure or to model. The EC approach is dependent on averaging procedures and most standard measurements will yield mean values. In order to use high-frequency measurements for flux estimation, less common techniques such as conditional sampling or wavelet-spectra have to be used. Even if models are capable of reproducing variability on realistic scales it is difficult to supply forcing data with similar resolution. The forcing data used in this study, sampled and averaged 10 or 30 min means, are used for SEWAB. Running Hybrid at time steps comparable to a high-resolution mesoscale model requires interpolation of the forcing data and therefore potentially causes a smoothing of the model's response compared to the actual weather forcing as it would be provided by a coupled model. As surface models share a similar approach to the parameterisation of surface fluxes and close the surface energy balance locally, SEWAB and Hybrid fluxes are more similar to each other than they are to field measurements.

6 Conclusions

The accurate generation of surface fluxes is a necessary prerequisite for studies of surface-atmosphere interactions and local to mesoscale circulations. In order to gain a better process understanding of the interaction between atmospheric circulation, clouds, radiation and surface fluxes, the generated diurnal flux cycles have to be of realistic magnitude and without temporal shift. The original two-layer surface model without a specific formulation for T_0 produced both a considerable time lag and failed to capture the full diurnal dynamics due to its unresponsiveness.

We have demonstrated that the introduction of an extrapolated surface temperature enables even a quite simplistic soil model to realistically simulate skin temperatures and thus to generate more realistic surface fluxes. The delay of fluxes during the daily cycle was greatly reduced, making the model usable for diurnal process studies. The total magnitude of fluxes is also much improved, when few and computationally cheap additional physically based processes are introduced. Comparing SEWAB with Hybrid, the RMSD for both fluxes and surface temperature is decreased by generally 40–60 %. The improvement in quality was somewhat more varied in comparison to EC measurements, as comparison of models and measurements is not straight forward. The improved $R^2(j)$ for smaller values of j shows that temporal shifts of the flux time series have been greatly reduced and the overall correlations are high. As with any natural system it is impossible to obtain complete data sets that capture the full amount of natural variability. However, the modified model has been tested for a larger spectrum of environmental conditions on the TP and produced reasonable results for both dry and moist conditions.

We have shown that a rather simple soil surface model can efficiently calculate turbulent fluxes at a high temporal resolution when driven by realistic atmospheric conditions. Nevertheless, it is quite clear that such an approach with extrapolated surface temperature needs careful model initialisation. The initial soil heat contents and therefore knowledge of soil temperature profiles is necessary. Due to the fact that the surface temperature in this study is a purely diagnostic quantity, there may still be some limitations such as a delayed or smoothed response to atmospheric forcing on very short timescales, such as the feedback between passing boundary-layer clouds and the surface fluxes. The influence of surface fluxes and their dynamics to regional circulation will be investigated in a future study.

Acknowledgements. This research was funded by the German Research Foundation (DFG) Priority Programme 1372 "Tibetan Plateau: Formation, Climate, Ecosystems" as part of the Atmosphere – Ecology – Glaciology Cluster (TiP-AEG). ITP data was provided through CEOP-AEGIS, which is a EU-FP7 Collaborative Project/ Small or medium-scale focused research project – Specific International Co-operation Action coordinated by the University of Strasbourg, France under the call ENV.2007.4.1.4.2: "Improving observing systems for water resource management." The authors would like to thank everyone who has contributed to the collection of field data in one of the world's most remote regions. ADF acknowledges support from the European Community's Seventh Framework Programme (FP7/2007-2013) under grant agreement no. 238366. AH acknowledges funding by the Fonds National de la Recherche (FNR-Luxembourg), under the grant BFR07-089 and support by the Cambridge European Trust (CET-UK).

Edited by: C. de Michele

References

Agam (Ninari), N. and Berliner, P. R.: Diurnal Water Content Changes in the Bare soil of a coastal desert, J. Hydrometeorol., 5, 922–933, doi:10.1175/1525-7541(2004)005<0922:DWCCIT>2.0.CO;2, 2004.

Agam, N. and Berliner, P. R.: Dew formation and water vapor adsorption in semi-arid environments – A review, J. Arid Environ., 65, 572–590, doi:10.1016/j.jaridenv.2005.09.004, 2006.

Aubinet, M., Grelle, A., Ibrom, A., Rannik, U., Moncrieff, J., Foken, T., Kowalski, A., Martin, P., Berbigier, P., Bernhofer, C., Clement, R., Elbers, J., Granier, A., Grünwald, T., Morgenstern, K., Pilegaard, K., Rebmann, C., Snijders, W., Valentini, R., Vesala, T., Fitter, A., and Raffaelli, D.: Estimates of the annual net carbon and water exchange of forests: The EUROFLUX Methodology, Adv. Ecol. Res., 30, 113–175, doi:10.1016/S0065-2504(08)60018-5, 1999.

Biermann, T., Babel, W., Olesch, J., and Foken, T.: Mesoscale circulations and energy and gas exchange over the Tibetan Plateau – Documentation of the micrometeorological experiment, Nam Tso, Tibet – 25 June–8 August 2009, Arbeitsergebnisse 41, University of Bayreuth, ISSN 1614-8616, Bayreuth, 2009.

Blackadar, A.: High resolution models of the planetary boundary layer, in: Advances in Environmental Science and Engineering, edited by: Pfafflin, J. and Ziegler, E., Vol. 1, 50–85, Gordon and Breach, New York, 1979.

Camillo, P. J. and Gurney, R. J.: A resistance parameter for bare-soil evaporation models, Soil Sci., 141, 95–105, 1986.

Cong, Z., Kang, S., Smirnov, A., and Holben, B.: Aerosol optical properties at Nam Co, a remote site in central Tibetan Plateau, Atmos. Res., 92, 42–48, doi:10.1016/j.atmosres.2008.08.005, 2009.

Cui, X., Langmann, B., and Graf, H.: Summer monsoonal rainfall simulation on the Tibetan Plateau with a regional climate model using a one-way double-nesting system, SOLA, 3, 49–52, 2007.

Deardorff, J. W.: Dependence of air-sea transfer coefficients on bulk stability, J. Geoph. Res., 73, 2549–2557, 1968.

Fairall, C. W., Bradley, E. F., Godfrey, J. S., Wick, G. A., Edson, J. B., and Young, G. S.: Cool-skin and warm-layer effects on sea surface temperature, J. Geophys. Res., 101, 1295–1308, 1996a.

Fairall, C. W., Bradley, E. F., Rogers, D. P., Edson, J. B., and Young, G. S.: Bulk parameterization of air-sea fluxes for Tropical Ocean-Global Atmosphere Coupled-Ocean Atmosphere Response Experiment, J. Geophy. Res., 101, 3747–3764, 1996b.

Foken, T.: The parameterisation of the energy exchange across the air-sea interface, Dynam. Atmos. Ocean, 8, 297–305, doi:10.1016/0377-0265(84)90014-9, 1984.

Foken, T.: The energy balance closure problem: An overview, Ecol. Appl., 18, 1351–1367, 2008.

Foken, T., Göckede, M., Mauder, M., Mahrt, L., Amiro, B., and Munger, J.: Post field data quality control, in: Handbook of Micrometeorology: A guide for surface flux measurements and analysis, edited by: Lee, X., Massman, W., and Law, B., 181–208, Kluwer, Dordrecht, 2004.

Foken, T., Aubinet, M., Finnigan, J. J., Leclerc, M. Y., Mauder, M., and Paw U, K. T.: Results Of A Panel Discussion About The Energy Balance Closure Correction For Trace Gases, B. Am. Meteorol. Soc., 92, ES13–ES18, doi:10.1175/2011BAMS3130.1, 2011.

Freedman, J. M., Fitzjarrald, D. R., Moore, K. E., and Sakai, R. K.: Boundary layer clouds and vegetation-atmosphere feedbacks, J. Climate, 14, 180–197, doi:10.1175/1520-0442(2001)013<0180:BLCAVA>2.0.CO;2, 2001.

Friend, A. D.: Terrestrial plant production and climate change, J. Exp. Bot., 61, 1293–1309, doi:10.1093/jxb/erq019, 2010.

Friend, A. D. and Kiang, N. Y.: Land surface model development for the GISS GCM: effects of improved canopy physiology on simulated climate, J. Climate, 18, 2883–2902, 2005.

Friend, A. D., Stevens, A. K., Knox, R. G., and Cannell, M. G. R.: A process-based, terrestrial biosphere model of ecosystem dynamics (Hybrid v3.0), Ecol. Model., 95, 249–287, 1997.

Hansen, J., Russell, G., Rind, D., Stone, P., Lacis, A., Lebedeff, S., Ruedy, R., and Travis, L.: Efficient three-dimensional global models for climate studies: Models I and II, Mon. Weather Rev., 111, 609–662, 1983.

Herzog, M., Graf, H., Textor, C., and Oberhuber, J. M.: The effect of phase changes of water on the development of volcanic plumes, J. Volcanol. Geoth. Res., 87, 55–74, doi:10.1016/S0377-0273(98)00100-0, 1998.

Hu, Z., Yu, G., Fu, Y., Sun, X., Li, Y., Shi, P., Wang, Y., and Zheng, Z.: Effects of vegetation control on ecosystem water use efficiency within and among four grassland ecosystems in China, Glob. Change Biol., 14, 1609–1619, doi:10.1111/j.1365-2486.2008.01582.x, 2008.

Hu, Z., Yu, G., Zhou, Y., Sun, X., Li, Y., Shi, P., Wang, Y., Song, X., Zheng, Z., Zhang, L., and Li, S.: Partitioning of evapotranspiration and its controls in four grassland ecosystems: Application of a two-source model, Agric. For. Meteorol., 149, 1410–1420, doi:10.1016/j.agrformet.2009.03.014, 2009.

Kanda, M., Inagaki, A., Letzel, M. O., Raasch, S., and Watanabe, T.: LES Study of the energy imbalance problem with eddy covariance fluxes, Bound.-Lay. Meteorol., 110, 381–404, doi:10.1023/B:BOUN.0000007225.45548.7a, 2004.

Keil, A., Berking, J., Mügler, I., Schütt, B., Schwalb, A., and Steeb, P.: Hydrological and geomorphological basin and catchment characteristics of Lake Nam Co, South-Central Tibet, Quart. Int., 218, 118–130, 2010.

Kracher, D., Mengelkamp, H., and Foken, T.: The residual of the energy balance closure and its influence on the results of three SVAT models, Meteorologische Z., 18, 647–661, doi:10.1127/0941-2948/2009/0412, 2009.

Kuwagata, T., Kondo, J., and Sumioka, M.: Thermal effect of the sea breeze on the structure of the boundary layer and the heat budget over land, Bound.-Lay. Meteorol., 67, 119–144, doi:10.1007/BF00705510, 1994.

Li, M., Ma, Y., Hu, Z., Ishikawa, H., and Oku, Y.: Snow distribution over the Namco lake area of the Tibetan Plateau, Hydrol. Earth Syst. Sci., 13, 2023–2030, doi:10.5194/hess-13-2023-2009, 2009.

Lohou, F. and Patton, E. G.: Land-surface response to shallow cumulus, EGU General Assembly, Vienna, Austria, 3–8 April 2011, EGU2011-10280-1, 2011.

Ma, Y., Wang, Y., Wu, R., Hu, Z., Yang, K., Li, M., Ma, W., Zhong, L., Sun, F., Chen, X., Zhu, Z., Wang, S., and Ishikawa, H.: Recent advances on the study of atmosphere-land interaction observations on the Tibetan Plateau, Hydrol. Earth Syst. Sci., 13, 1103–1111, doi:10.5194/hess-13-1103-2009, 2009.

Mauder, M. and Foken, T.: Documentation and instruction manual of the eddy covariance software package TK3, Arbeitsergebnisse 46, University of Bayreuth, ISSN 1614-8916, Bayreuth, 2011.

Mauder, M., Oncley, S. P., Vogt, R., Weidinger, T., Ribeiro, L., Bernhofer, C., Foken, T., Kohsiek, W., Bruin, H. A. R., and Liu, H.: The energy balance experiment EBEX-2000. Part II: Intercomparison of eddy-covariance sensors and post-field data processing methods, Bound.-Lay. Meteorol., 123, 29–54, doi:10.1007/s10546-006-9139-4, 2006.

Mauder, M., Desjardins, R. L., and MacPherson, I.: Scale analysis of airborne flux measurements over heterogeneous terrain in a boreal ecosystem, J. Geophys. Res., 112, D13112, doi:10.1029/2006JD008133, 2007.

Mauder, M., Foken, T., Clement, R., Elbers, J. A., Eugster, W., Grünwald, T., Heusinkveld, B., and Kolle, O.: Quality control of CarboEurope flux data – Part 2: Inter-comparison of eddy-covariance software, Biogeosciences, 5, 451–462, doi:10.5194/bg-5-451-2008, 2008.

Mengelkamp, H., Warrach, K., and Raschke, E.: SEWAB – a parameterization of the surface energy and water balance for atmospheric and hydrologic models, Adv. Wat. Resour., 23, 165–175, doi:10.1016/S0309-1708(99)00020-2, 1999.

Metzger, S., Ma, Y., Markkanen, T., Göckede, M., Li, M., and Foken, T.: Quality assessment of Tibetan Plateau Eddy covariance measurements utilizing footprint modeling, Adv. Earth Sci., 21, 1260–1267, 2006.

Miehe, G., Miehe, S., Bach, K., Nölling, J., Hanspach, J., Reudenbach, C., Kaiser, K., Wesche, K., Mosbrugger, V., Yang, Y., and Ma, Y.: Plant communities of central Tibetan pastures in the Alpine Steppe/Kobresia pygmaea ecotone, J. Arid Environ., 75, 711–723, doi:10.1016/j.jaridenv.2011.03.001, 2011.

Oberhuber, J. M., Herzog, M., Graf, H., and Schwanke, K.: Volcanic plume simulation on large scales, J. Volcanol. Geoth. Res., 87, 29–53, doi:10.1016/S0377-0273(98)00099-7, 1998.

Panin, G. N., Tetzlaff, G., and Raabe, A.: Inhomogeneity of the land surface and problems in the parameterization of surface fluxes in natural conditions, Theor. Appl. Climatol., 60, 163–178, doi:10.1007/s007040050041, 1998.

Panin, G. N., Nasonov, A. E., and Foken, T.: Evaporation and heat exchange of a body of water with the atmosphere in a shallow zone, Izvestiya, Atmos. Ocean. Phys., 42, 337–352, doi:10.1134/S0001433806030078, 2006.

Ruppert, J., Thomas, C., and Foken, T.: Scalar similarity for relaxed eddy accumulation methods, Bound.-Lay. Meteorol., 120, 39–63, doi:10.1007/s10546-005-9043-3, 2006.

Sellers, P. J., Mintz, Y., Sud, Y. C., and Dalcher, A.: A Simple Biosphere Model (SIB) for use within general circulation models, J. Atmos. Sci., 43, 505–531, 1986.

Su, Z., Wen, J., Dente, L., van der Velde, R., Wang, L., Ma, Y., Yang, K., and Hu, Z.: The Tibetan Plateau observatory of plateau scale soil moisture and soil temperature (Tibet-Obs) for quantifying uncertainties in coarse resolution satellite and model products, Hydrol. Earth Syst. Sci., 15, 2303–2316, doi:10.5194/hess-15-2303-2011, 2011.

Twine, T. E., Kustas, W. P., Norman, J. M., Cook, D. R., Houser, P. R., Meyers, T. P., Prueger, J. H., Starks, P. J., and Wesely, M. L.: Correcting eddy-covariance flux underestimates over a grassland, Agric. For. Meteorol., 103, 279–300, doi:10.1016/S0168-1923(00)00123-4, 2000.

van Heerwaarden, C. C., de Arellano, J. V., Moene, A. F., and Holtslag, A. A. M.: Interactions between dry-air entrainment, surface evaporation and convective boundary-layer development, Q. J. Roy. Meteorol. Soc., 135, 1277–1291, doi:10.1002/qj.431, 2009.

Xue, Y., Zeng, F. J., and Schlosser, C. A.: SSiB and its sensitivity to soil properties – a case study using HAPEX-Mobilhy data, Glob. Planet. Change, 13, 183–194, doi:10.1016/0921-8181(95)00045-3, 1996.

Yang, K., Koike, T., and Yang, D.: Surface flux parameterization in the Tibetan Plateau, Bound.-Lay. Meteorol., 106, 245–262, doi:10.1023/A:1021152407334, 2003.

Yang, K., Chen, Y.-Y., and Qin, J.: Some practical notes on the land surface modeling in the Tibetan Plateau, Hydrol. Earth Syst. Sci., 13, 687–701, doi:10.5194/hess-13-687-2009, 2009.

Yee, S. Y. K.: The force-restore method revisited, Bound.-Lay. Meteorol., 43, 85–90, doi:10.1007/BF00153970, 1988.

You, Q. L., Kang, S. C., Li, C. L., Li, M. S., and Liu, J. S.: Features of meteorological parameters at Nam Co station, Tibetan Plateau, in: Annual Report of Nam Co Monitoring and Research Station for Multisphere Interactions, edited by: Nam Co Monitoring and Research Station for Multisphere Interaction, 1–8, Chinese Academy of Sciences, Beijing, 2006 (in Chinese with English abstract).

Zhou, D., Eigenmann, R., Babel, W., Foken, T., and Ma, Y.: The study of near-ground free convection conditions at Nam Co station on the Tibetan Plateau, Theor. Appl. Climatol., 105, 217–228, doi:10.1007/s00704-010-0393-5, 2011.

C. Babel et al. (2013)

Babel, W., Chen, Y., Biermann, T., Yang, K., Ma, Y., and Foken, T.: Adaptation of a land surface scheme for modeling turbulent fluxes on the Tibetan Plateau under different soil moisture conditions, submitted to J. Geophys. Res.

JOURNAL OF GEOPHYSICAL RESEARCH, VOL. ???, XXXX, DOI:10.1029/,

Adaptation of a land surface scheme for modeling turbulent fluxes on the Tibetan Plateau under different soil moisture conditions

W. Babel[1], Y. Chen[2], T. Biermann[1], K. Yang[2], Y. Ma[2], and T. Foken[1,3]

Abstract. Surface fluxes over the Tibetan Plateau play a prominent role in the East Asian circulation system. Regional estimates of these fluxes usually do not consider existing small-scale heterogeneities of soil moisture.

In this study the land surface scheme SEWAB is adapted to the typical conditions of the Tibetan Plateau, namely dry conditions over bare soil or very low vegetation. Turbulent fluxes (sensible and latent heat) were simulated for two adjacent sites near the Nam Co lake: a dry alpine steppe site and a wet alpine meadow site. Simulations incorporate the original and the adapted model version, soil properties were described with default parameter sets on the one hand, and parameter derived by laboratory measurements on the other hand. The results have been compared with carefully checked eddy-covariance observations from both sites. The turbulent flux observations have been corrected according to the measured energy balance closure gap and particular attention has been paid to the closure correction method.

The investigation shows that SEWAB is able to represent fluxes for both surfaces reasonably well. The adaptation of the model to Tibetan Plateau conditions increased model performance, while the measured parameters did not appear to be superior to the default parameters. Large variation is attributed to the energy balance closure correction of the observations. This should be taken into account whenever validating model performance with eddy-covariance measurements.

1. Introduction

The Tibetan Plateau plays an important role in the Asian climate system. It acts as an important heat source in the general circulation, influencing the East-Asian monsoon circulation [e.g. *Yanai et al.*, 1992; *Ye and Wu*, 1998; *Hsu and Liu*, 2003; *Duan and Wu*, 2005; *Kang et al.*, 2010]. In order to understand these relationships in more detail, estimates of surface fluxes distributed over the Tibetan Plateau are a prerequisite. Turbulent surface flux measurements, however, are scarce on the plateau. Therefore, process based simulations are needed for regionalization.

Xu and Haginoya [2001] presented inter-annual, seasonal and daily variations of turbulent fluxes over the Tibetan Plateau, calculated from standard meteorological measurements of 14 sites. Furthermore, a model comparison study was conducted on the Tibetan Plateau by *Takayabu et al.* [2001] within the GEWEX Asian Monsoon Experiment 1998. Although successful in modeling soil characteristics, they reported large differences in turbulent flux partitioning among four land surface models , but they lacked data (soil moisture and flux measurements) for validation. Special problems for land surface modeling occur due to a strong diurnal cycle of the surface temperature, which is observed in dry conditions over bare soil or very low vegetation, a typical situation on the Tibetan Plateau: land surface models tend to overestimate surface sensible heat flux [e.g. *Yang et al.*, 2009; *Hong and Kim*, 2010] caused by too high turbulent diffusion coefficients. These coefficients were usually parameterized by a fixed fraction between the roughness length of momentum and heat, also called the sublayer-Stanton number. In contrast, *Yang et al.* [2003] and *Ma et al.* [2002] observed a diurnal variation of the sublayer-Stanton number, leading to a parameterization of the thermal roughness length [*Yang et al.*, 2008] adapted to Tibetan Plateau conditions. This parameterization has been applied successfully in some recent studies in Asian arid and semi-arid regions, e.g. *Chen et al.* [2010, 2011]; *Liu et al.* [2012]; *Zhang* [2012]. Furthermore, *Yang et al.* [2005] examined the influence of soil stratification with a single source model and optimized parameters and found a significant impact, where remarkable vertical heterogeneity exists. Similar results were found by *van der Velde et al.* [2009].

On the other hand, large areas in Central Tibet are characterized by cold semiarid conditions, forming a heterogeneous landscape of dry grasslands (*Kobresia* pastures, alpine steppe) together with wetlands or grasslands characterized by shallow groundwater [*Su et al.*, 2011]. This small-scale heterogeneity of soil moisture obviously produces a heterogeneity in surface fluxes, for which land surface models should account. It is impossible, however, to represent such heterogeneities by routine observations, especially in remote areas like the Tibetan Plateau. Nevertheless, the influence can be estimated by land surface models, which in turn have to be tested as to whether they are able to reproduce these special conditions.

In this study, the land surface scheme SEWAB [*Mengelkamp et al.*, 1999] is used to model turbulent surface fluxes on a wet and a dry grassland surface on the Tibetan Plateau, and the simulations are compared with eddy-covariance (EC) measurements. A field campaign has been

[1]Department of Micrometeorology, University of Bayreuth, Bayreuth, Germany.

[2]Key Laboratory of Tibetan Environment Changes and Land Surface Processes, Institute of Tibetan Plateau Research, Chinese Academy of Sciences, Beijing, China.

[3]Member of Bayreuth Institute of Ecology and Environmental Research (BayCEER)

0148-0227/13/$9.00

conducted to derive the necessary micrometeorological measurements over the wet surface in addition to the dry site nearby. Due to the close proximity, both sites undergo the same meteorological forcing, and the setup enables us to investigate the following questions: (i) Is the SEWAB scheme capable of reproducing turbulent fluxes on the Tibetan Plateau under different soil moisture regimes? (ii) Does a detailed investigation of soil physical properties substantially improve model simulations compared to default parameters according to soil type from a low resolution soil map? Finally, we address the influence of the observed energy balance closure gap on model performance estimation.

2. Material and Methods

2.1. Site Description

The experiment site is located 220 km north of Lhasa in the Nam Co Basin, Tibetan Plateau, at an elevation of 4730 km a.s.l. The Institute of Tibetan Plateau Research (ITP), Chinese Academy of Sciences, is operating the Nam Co Monitoring and Research Station for Multisphere Interactions (30°46.44′ N, 90°59.31′ E) near a small lake located 1 km SE of the Nam Co Lake (see Figure 1). The closed Nam Cobasin is dominated by the lake itself and the Nyainqentanglha mountain range, stretching along its SE side and reaching up to 7270 m a.s.l. with an average height of 5230 m [*Liu et al.*, 2010]. The Nam Co Lake shore is characterized by alpine steppe and desert soils in general, while the southern shore often consists of alpine and sub alpine meadow soils as well as marshland soils, due to the fluvial process and low water table [*Gao*, 1985]. The vegetation around Nam Co reflects the prevailing arid, high-altitude climate with alpine meadows and steppe grasses [*Mügler et al.*, 2010]. Near the Nam Co Station the vegetation coverage and composition are highly variable according to topographic features which determine soil moisture conditions (Figure 1): Grass genera typical for Alpine steppe (*Stipa, Carex, Helictotrichon, Elymus, Festuca, Kobresia, Poa*) have been observed on the hillocks, with a total vegetation coverage of 60 % or less (“grass-”), while more wet areas are densely covered (>90 %) with alpine meadows dominated by *Kobresia* species (“grass+”).

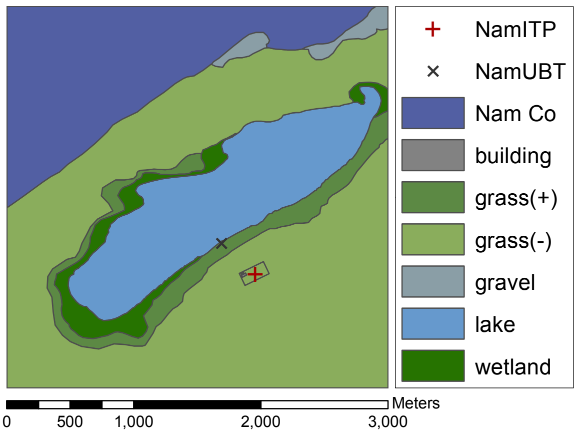

Figure 1. The experiment site at a shallow lake near Nam Co lake: the land use map is based on unsupervised classification of remote sensing images and field observations during the campaign in 2009 [from *Gerken et al.*, 2012].

2.2. Measurements

Turbulent fluxes were obtained by two EC systems, one directly at the Nam Co station over dry alpine steppe (designated NamITP) and another directly at the shoreline of the small lake (NamUBT), measuring over more wet alpine meadow in the respective wind sector. The NamITP complex is set up on almost flat terrain, but this starts to decline smoothly toward the small lake at a distance of 90m NNE. The data collected by the NamUBT complex in a wind sector of 72° – 212° corresponds to a terraced land surface with a gentle average slope of $\leq 8°$. The fluxes were processed and analyzed for the period from 1 July to 8 August 2009. The instruments used to obtain the measured surface energy balance are listed in Table 1.

Soil physical parameters were determined from soil samples of both surfaces by laboratory measurements [*Chen et al.*, 2012]. This information was used in this study to estimate realistic soil parameters for land surface modeling, assuming that the samples obtained are representative on the scale of the EC footprint. The following derived quantities are relevant: hydraulic conductivity at saturation, matrix potential at saturation, exponent b for Clapp & Hornberger relationships [*Clapp and Hornberger*, 1978], thermal conductivity and soil texture. For details about sampling and measuring processes please refer to *Chen et al.* [2012].

2.3. Data Processing

Half-hourly turbulent fluxes of both stations were calculated using the software package TK2/3 [*Mauder and Foken*, 2004, 2011], and state of the art flux corrections were applied following the recommendations by *Foken et al.* [2012]. The planar fit coordinate rotation [*Wilczak et al.*, 2001] was applied for the whole period under investigation, but for NamUBT only within the relevant wind sector of 72° – 212°. In this study, the flux data was filtered, preserving only high quality fluxes, i.e. data with quality flags of 1–3 were maintained, using a scheme ranging from 1 to 9 described by *Foken et al.* [2012]. A footprint analysis and site-specific characterization approach [*Göckede et al.*, 2004, 2008] was conducted, utilizing a Lagrangian forward stochastic model by *Rannik et al.* [2000]. The results show a sufficient contribution of the desired land use type (within the selected wind sector in case of NamUBT) and no significant disturbance within the remaining high quality flux data. More details about data quality at NamITP for another period were given by *Zhou et al.* [2011].

2.4. Energy Balance Closure and Correction

The balance of measured surface energy fluxes typically results in a residual *Res*,

$$-Res = R_{\mathrm{net}} + Q_{\mathrm{G}} + Q_{\mathrm{H}} + Q_{\mathrm{E}} \quad (1)$$

here calculated from the net radiation R_{net} and soil heat flux Q_{G} (available energy), as well as turbulent fluxes of sensible heat Q_{H} and latent heat Q_{E}, where positive signs indicate fluxes away from the surface. The soil heat flux has been determined for NamUBT by the measured flux at 15 cm depth and the storage change in the layer above [*Liebethal et al.*, 2005]. As no reliable heat flux plate measurement was available at NamITP, the soil heat flux was calculated using a gradient method by *Yang and Wang* [2008]. A comparison of both methods with a reference data set showed good agreement.

The relative residuals were determined as the slope from the regression of turbulent fluxes vs. available energy and found to be 81 % and 73 % for NamITP and NamUBT, respectively. These values are well within the range expected

Table 1. List of sensors used for retrieving the measured surface energy balance

Component	Instrument	height/depth
NamITP		
Turbulent fluxes	Campbell CSAT3 sonic anemometer	3.1 m
	Li-7500 IRGA, LiCOR Biosciences	3.1 m
Radiation (4 comp.)	CM3 and CG3, Kipp & Zonen	1.5 m
Soil temperature	PT100	-20, -40, -80, -160 cm
Soil moisture	IMKO-TDR	-10, -20, -40, -80, -160 cm
NamUBT		
Turbulent fluxes	Campbell CSAT3	3.0 m
	Li-7500 IRGA, LiCOR Biosciences	3.0 m
Radiation (4 comp.)	CNR1 Kipp & Zonen	2.0 m
Soil temperature	PT100	-2.5, -5, -10, -15 cm
Soil moisture	IMKO-TDR	-10, -30 cm
Soil heat flux	Rimco HP3 heat flux plate	-15 cm

for grassland in heterogeneous landscapes [*Foken*, 2008a], but they are too large to ignore.

The turbulent fluxes are corrected for the energy balance gap prior to comparing with model simulations. In this study we applied the correction preserving the Bowen ratio by *Twine et al.* [2000], further indicated with "EBC-Bo". The method is only applied when both sensible and latent heat flux exceed a threshold of $10\,\mathrm{W\,m^{-2}}$ and the Bowen ratio is positive. Any values not in line with these requirements were excluded from further analysis. In combination with the quality filtering, less than 40 % of the available data remain for the analysis, while most of the nighttime data is discarded.

Some specific problems at NamITP, however, reduce the accuracy of the observed energy balance: The first reliable soil temperature measurement starts at 20 cm depth, introducing large uncertainty to the soil heat flux calculation. The influence of an erroneous storage term on the observed energy budget has been pointed out by *Leuning et al.* [2012]. We found relatively small soil heat fluxes and especially large residuals after rain events in the late night or early morning, which could be related to the problem mentioned before. Secondly, the footprint of the upwelling radiation measurements is characterized by a large gravel content and low vegetation fraction, which differs to some extent from the EC footprint.

The energy balance closure correction, on the other hand, relies only on hypotheses and can introduce huge uncertainties with large residuals to be closed. Therefore we treat observations with $-Res > 150\,\mathrm{W\,m^{-2}}$ as low quality data and discard them from evaluation. Further, we discuss the influence of the EBC correction on model performance, testing a correction related to buoyancy ("EBC-HB", see Sect. 3.3).

2.5. Land Surface Modeling

2.5.1. Model Description

In this study a Soil–Vegetation–Atmosphere transfer scheme called SEWAB is used, developed by *Mengelkamp et al.* [1999] in the former GKSS Research Center, Geesthacht, Germany. It is a single column model, forced by measured standard meteorological variables. The effective parameters constraining the model correspond to each type of land-use.

Model equations are described in detail by *Mengelkamp et al.* [1999, 2001], nevertheless we highlight here the main features for clarification. Soil temperature distribution is described by the diffusion equation and vertical soil water movement is governed by the Richards' equation. The relationships between soil moisture characteristics from *Clapp and Hornberger* [1978] were used. All energy balance components are given in separate equations, the soil heat flux and turbulent fluxes were parameterized with bulk approaches (Table 2). The EB closure is achieved by an iteration of the surface temperature until the residual disappears. Thus, instead of one flux serving as balance residual, the discrepancy is shared by all fluxes sensitive to surface temperature. Directly affected are the sensible heat flux, the ground heat flux and the long-wave upwelling radiation, but also the latent heat flux via the temperature dependent specific humidity of saturation.

2.5.2. Original Version

The model has been run in this study in a nearly unchanged version as previously reported [*Mengelkamp et al.*, 1999, 2001], which is accordingly designated *original version*. The configuration is chosen as follows: The soil model has been run with 7 soil layers, with 5 layers within the first 50 cm, and reaching 2 m depth in total.

All hydrological extra modules in SEWAB such as ponding, variable infiltration capacity, subsurface runoff and base flow according to the ARNO concept, or depth dependent saturated hydraulic conductivity [*Mengelkamp et al.*, 1999, 2001] are switched off as they all contain parameters for which it is problematic to find realistic values. Furthermore, small technical refinements have been made; amongst others, these are: When water is taken for evapotranspiration from layers below root level, the water is no longer supplied below wilting point. In the case that less water is available than actually transpired for this time step, the overshooting amount of evapotranspiration is transferred to sensible heat. This prevents a model collapse for very dry conditions.

2.5.3. TP Version: Adaptation to the Tibetan Plateau

In order to address the already mentioned issues for land surface modeling on the Tibetan Plateau [*Yang et al.*, 2009; *Hong and Kim*, 2010], an adaptation of the original version (Sect. 2.5.1 and 2.5.2) has been set up and named *TP version*. The changes include (i) the calculation of the soil thermal conductivity, (ii) the determination of the thermal roughness length and (iii) the parameterization of bare soil evaporation.

The soil thermal conductivity λ_s was parameterized in the original code by a weighted sum of individual thermal conductivities of dry clay/sand, water, ice and air according to the actual state. We changed it to a formulation by *Yang et al.* [2005]

$$\lambda_\mathrm{s}(\Theta) = \lambda_\mathrm{dry} + (\lambda_\mathrm{sat} - \lambda_\mathrm{dry})\exp\left[k_\mathrm{T}\left(1 - \Theta_\mathrm{sat}/\Theta\right)\right] \quad (2)$$

with the volumetric soil water content Θ, the porosity Θ_sat and the coefficient k_T, which is set to 0.36 following *Yang et al.* [2005]. The dry and saturated thermal conductivity limits were estimated from field observations (Sect. 2.2) as $\lambda_\mathrm{dry} = 0.15\,\mathrm{W\,m^{-1}\,K^{-1}}$ and $\lambda_\mathrm{sat} = 0.8$ and $1.3\,\mathrm{W\,m^{-1}\,K^{-1}}$ for NamUBT and NamITP, respectively.

The thermal roughness length z_0h has been set to a fixed fraction of the aerodynamic roughness length $z_\mathrm{0h} = 0.1 z_\mathrm{0m}$ in the original code. In contrast, this relation has been observed to show diurnal and seasonal variations [*Yang et al.*, 2003]. Therefore we used a formulation recommended by *Yang et al.* [2008]

$$z_\mathrm{0h} = \frac{70\nu}{u_*}\exp\left(-\beta u_*^{0.5}|T_*|^{0.25}\right) \quad (3)$$

Table 2. Parameterization of energy balance components in SEWAB and their connection to the surface temperature T_g

Variable	Equation
Net radiation	$R_{net} = -R_{swd}(1-a) - R_{lwd} + \varepsilon\sigma T_g^4$, R_{swd} and R_{lwd} in forcing data
Ground heat flux	$Q_G = \lambda_s (T_g - T_{S1}) \Delta z_{S1}^{-1}$, $S1$: uppermost soil layer
Sensible heat flux	$Q_H = C_H \rho c_p u(z)(T_g - T(z))$
Latent heat flux	Evaporation from bare soil E_s, wet foliage E_f and plant transpiration E_{tr} [*Noilhan and Planton*, 1989]
	$E_s = C_E \rho u(z)(\alpha q_s(T_g) - q(z))$
	$E_f = C_E \rho u(z)(q_s(T_g) - q(z))$
	$E_{tr} = (R_a + R_s)^{-1} \rho(q_s(T_g) - q(z))$
	Jarvis-type stomata resistance R_s after *Noilhan and Planton* [1989]
Stability dependence	Stanton number C_H after *Louis* [1979], $C_E = C_H$

a	albedo [-]	u_*	friction velocity [m s^{-1}]
c_p	air heat capacity [J kg^{-1} K^{-1}]	z	measurement height [m]
q	specific humidity [-]		
q_s	saturation specific humidity [-]	α	dependence factor of soil air humidity to soil water content [-]
R_a	turbulent atmospheric resistance [s m^{-1}]		
R_{lwd}	long wave downward radiation [W m^{-2}]	ε	emissivity [-]
R_{swd}	short wave downward radiation [W m^{-2}]	λ_s	soil thermal conductivity [W m^{-1} K^{-1}]
T	temperature [K]	ρ	air density [kg m^{-3}]
u	wind velocity [m s^{-1}]	σ	Stefan Boltzmann constant [W m^{-2}K^{-4}]

with the kinematic viscosity of air ν, the friction velocity u_*, the dynamic temperature scale $T_* = -\overline{w'T'}/u_*$ and an empirical constant $\beta = 7.2\,\mathrm{s}^{0.5}\,\mathrm{m}^{-0.5}\,\mathrm{K}^{-0.25}$. However, in order to provide T_*, z_{0h} has to be known in advance. Equation (3) has therefore been solved iteratively as suggested by *Yang et al.* [2010]. The performance of this formulation has been evaluated positively by *Yang et al.* [2008], and *Chen et al.* [2010] have successfully included the scheme in the Noah land surface model.

The third change is related to bare soil evaporation. Latent heat fluxes can be observed on the Tibetan Plateau even under soil moisture conditions below wilting point. Similar features have been observed in the Negev desert [*Agam et al.*, 2004] or in the Sahel [*Balsamo et al.*, 2011; *Wallace et al.*, 1991]. Bare soil evaporation is calculated as a bulk approach adjusted by an α formulation, see Table 2. That means that the saturation specific humidity at the soil surface is scaled by a soil moisture dependent factor α. The currently used α parameterization by *Noilhan and Planton* [1989], however, is very prohibitive under dry conditions compared to other schemes [*Mihailović et al.*, 1995]. Therefore, we used the expression by *Mihailović et al.* [1993]

$$\alpha = \begin{cases} 1 - \left(1 - \dfrac{\Theta}{\Theta_{FC}}\right)^n, & \Theta \leq \Theta_{FC} \\ 1, & \Theta > \Theta_{FC} \end{cases} \tag{4}$$

with exponent $n = 2$, the volumetric water content at field capacity Θ_{FC} and the actual water content of the topsoil Θ.

In the results we compare the performance of these changes (TP version) with the original version of SEWAB (Sect. 2.5.2).

2.5.4. Model Forcing

The model simulations for both sites were driven by a half-hourly dataset, consisting of precipitation, air temperature, wind velocity, air pressure, relative humidity, downwelling short-wave and long-wave radiation. The model has been run at a time step of 10 min, interpolating the forcing data and aggregating the output again to half-hourly values. The soil moisture and temperature profile was initialized in two ways, (i) using the observed profiles and (ii), spinning up the model by a 3-years forcing data set in order to reach an equilibrium state. For the first case, the forcing set consists solely of measured data, starting 4 days before the beginning of the evaluation period on 1 July 2009. In the latter case, this data set has to be expanded 3 years into the past and the required data was therefore extracted from the ITPCAS gridded forcing data set [*Chen et al.*, 2011]. Test simulations at the NamITP site showed only small differences between both initialization methods. Therefore we used observed profiles for all further investigations, as it is not possible to spin up the shallow ground water table at NamUBT by simulating only a single column.

2.5.5. Model Parameter

In this study, no optimization strategy is conducted to constrain the parameter space. Instead, we chose two parameter sets, a "default" and a "measured" parameter set. The most important parameters were summarized in Table 3.

The measured parameters use observed values for albedo, fraction of vegetated area, canopy height, rooting depth and roughness length. The leaf area index of the vegetated area, emissivity, and minimum and maximum stomatal resistance follow *Hu et al.* [2009]; *Yang et al.* [2009]; *Alapaty et al.* [1997]. The soil hydraulic and thermal properties were deduced from soil samples, which are analyzed in the lab (see Sect. 2.2). The volumetric water content at field capacity (assumed pF=2.5) and at wilting point (assumed pF=4.5) are calculated backward from matrix potential at saturation and Clapp & Hornberger exponent b, derived by the measured soil retention curve. The pF value for wilting point differs from the standard assumption of 4.2, which should be reasonable for mesophytic grass species [*Larcher*, 2001, p208].

The default parameters for NamITP and NamUBT differ most considerably between soil parameters. These were taken for the USDA textural classes "sand" and "sandy loam", respectively, from *Mengelkamp et al.* [1997] (which were from *Clapp and Hornberger* [1978] in the case of the hydraulic properties). In contrast, the surface parameters are assumed to be the same for the default set, differing only in the fraction of vegetated area f_{veg} and, consequently, in albedo a as the latter is deduced from albedo for grassland and dry bare soil [*Foken*, 2008b].

3. Results

We investigate the differences in simulated and observed turbulent fluxes over the dry grassland surface (NamITP) and the wetter grassland surface (NamUBT) near the lake. Model runs have been conducted for both surfaces, with different parameter sets (measured and default parameters), and with different model versions (original SEWAB code and TP – Tibetan Plateau – version). Furthermore, turbulent flux observations have been corrected according to the Bowen ratio (EBC-Bo). We assess model performance for this layout and examine accompanying variables as well. Finally, we compare these outcomes with the results obtained when using an energy balance closure correction according to the buoyancy flux (EBC-HB, for details see Sect. 3.3).

Table 3. Most important parameters for the model simulations: albedo a, emissivity ε, fraction of vegetated area f_{veg}, leaf area index of vegetated area $\mathrm{LAI}_{\mathrm{veg}}$, canopy height h_{c}, rooting depth z_{r}, roughness length $z_{0\mathrm{m}}$, minimum stomatal resistance $R_{s,\mathrm{min}}$, maximum stomatal resistance $R_{s,\mathrm{max}}$, thermal diffusivity ν_{T}, soil heat capacity $C_{\mathrm{G}} \cdot \varrho_{\mathrm{G}}$, porosity Θ_{sat}, matrix potential at saturation Ψ_{sat}, saturated hydraulic conductivity K_{sat}, volumetric water content at field capacity Θ_{FC}, volumetric water content at wilting point Θ_{WP}, and exponent b for relationships after *Clapp and Hornberger* [1978].

		Default parameters		Measured parameters	
Parameter	Unit	NamITP	NamUBT	NamITP	NamUBT
Surface and vegetation parameters					
a	-	0.22	0.205	0.196	0.196
ε	-	0.97	0.97	0.97	0.97
f_{veg}	-	0.6	0.9	0.6	0.9
$\mathrm{LAI}_{\mathrm{veg}}$	-	1.0	1.0	1.0	1.0
h_{c}	m	0.15	0.15	0.15	0.07
z_{r}	m	0.3	0.3	0.3	0.5
$z_{0\mathrm{m}}$	m	0.005	0.005	0.005	0.005
$R_{s,\mathrm{min}}$	$\mathrm{s\,m^{-1}}$	60.0	60.0	60.0	60.0
$R_{s,\mathrm{max}}$	$\mathrm{s\,m^{-1}}$	2500	2500	2500	2500
Soil parameters					
ν_{T}	$\mathrm{m^2\,s^{-1}}$	$0.84 \cdot 10^{-6}$	$0.84 \cdot 10^{-6}$	$1.5 \cdot 10^{-7}$	$2.5 \cdot 10^{-7}$
$C_{\mathrm{G}} \cdot \varrho_{\mathrm{G}}$	$\mathrm{J\,m^{-3}\,K^{-1}}$	$2.10 \cdot 10^{6}$	$2.10 \cdot 10^{6}$	$2.10 \cdot 10^{6}$	$2.10 \cdot 10^{6}$
Θ_{sat}	$\mathrm{m^3\,m^{-3}}$	0.395	0.435	0.396	0.63
Ψ_{sat}	m	-0.121	-0.218	-0.51	-0.14
K_{sat}	$\mathrm{m\,s^{-1}}$	$1.76 \cdot 10^{-4}$	$3.47 \cdot 10^{-5}$	$2.018 \cdot 10^{-5}$	$1.38 \cdot 10^{-5}$
Θ_{FC}	$\mathrm{m^3\,m^{-3}}$	0.135	0.150	0.21	0.38
Θ_{WP}	$\mathrm{m^3\,m^{-3}}$	0.068	0.114	0.06	0.19
b	-	4.05	4.90	3.61	6.79

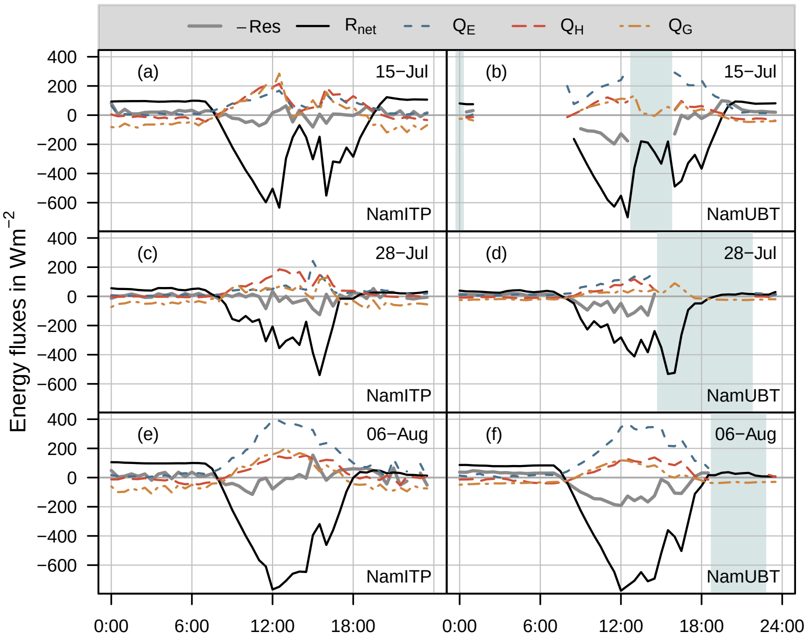

Figure 2. Diurnal cycles of the observed energy fluxes at Nam Co and the balance residual *Res* on 15 July (a,b), 28 July (c,d) and 6 August, 2009 (e,f) at NamITP (a,c,e) and NamUBT (b,d,f); blue shaded areas for NamUBT indicate missing data due to insufficient fetch (wind direction from the lake).

3.1. Observations

The energy balance at NamITP shows a different behavior than NamUBT, being influenced by the soil moisture regime. With volumetric soil moistures below 5 % most of the time during the period, NamITP clearly drops below a threshold to where e.g. *Brilli et al.* [2011] would expect substantial changes in stomatal conductance and therefore evapotranspiration. Three days with varying soil moisture conditions have been selected for illustrating the different behavior at both sites: 15 July, 5 days after the last significant rain event, 28 July, 18 days after the last significant rain event, and 6 August, right after a series of substantial rain events. The diurnal cycles of the observed energy fluxes including the balance residuum *Res* are shown in Figure 2. As expected, on 15 June the latent heat flux is significantly larger at NamUBT with low Bowen ratio, while turbulent fluxes were almost equally partitioned at NamITP (Figure 2a and 2b). Even after a longer drying phase, the Bowen ratio remains lower at NamUBT (2c and 2d), while under wet conditions on 6 August, turbulent flux differences between NamITP and NamUBT become insignificant (2e and

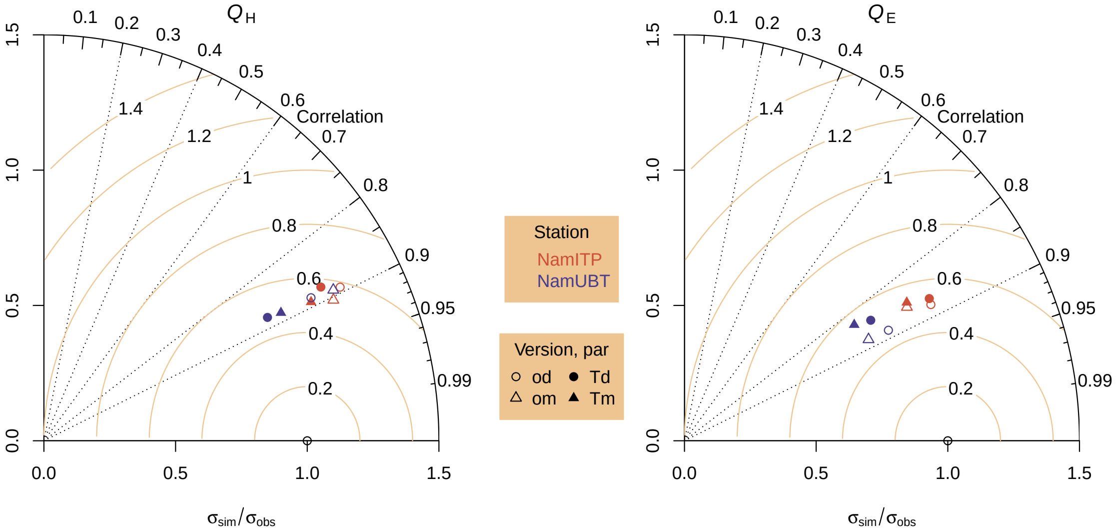

Figure 3. Normalized Taylor diagram [*Taylor*, 2001] for EBC-Bo corrected observations vs. simulated turbulent fluxes, left: sensible heat flux, right: latent heat flux. The symbols indicate: (○) **od**: **o**riginal SEWAB version, **d**efault parameters; (△) **om**: **o**riginal SEWAB version, **m**easured parameters; (●) **Td**: **T**P version, **d**efault parameters; (▲) **Tm**: **T**P version, **m**easured parameters; colors represent the stations with red for NamITP and blue for NamUBT.

2f). NamUBT receives a larger total available energy than NamITP. This can be attributed to smaller surface temperatures at NamUBT, resulting in smaller outgoing long wave radiation and ground heat flux.

3.2. General Model Performance

3.2.1. Statistics for Turbulent Fluxes

Performance of the conducted simulations is given as an overview in a normalized Taylor diagram [*Taylor*, 2001]: In a polar plot, the standard deviation of simulations σ_{sim}, normalized with the standard deviation of observations σ_{obs}, represent the radial coordinate. The Pearson correlation coefficient is defined with the cosine of the angle to the x-axis.

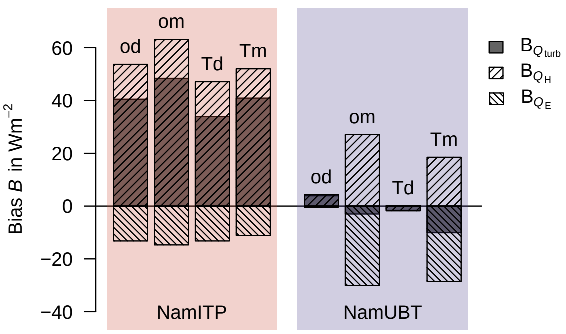

Figure 4. Bias of turbulent fluxes (simulated vs. EBC-Bo corrected observations), left: NamITP, right: NamUBT. Bars with ascending shading lines denote sensible heat flux bias, descending shading lines latent heat flux bias and the sum is the turbulent heat flux bias (grey bars); the individual blocks show **od**: **o**riginal SEWAB version, **d**efault parameters; **om**: **o**riginal SEWAB version, **m**easured parameters; **Td**: **T**P version, **d**efault parameters; **Tm**: **T**P version, **m**easured parameters.

Given this setup, the centered-pattern root-mean-square deviation can be obtained, which is the root-mean-square deviation of two bias-corrected time series (in this case normalized by σ_{obs}). It reads as the distance between the reference point at P(1/0), defined by the observations, and the test points, defined by the simulations.

Figure 3 shows that, in general, simulations reproduce observed pattern well with correlation coefficients around 0.9. Model runs for NamUBT exhibit smaller normalized standard deviations, but perform similarly to simulations for NamITP. They show only small differences with respect to model version and parameter set. The original version performs slightly better than the TP version for latent heat while in the case of sensible heat there is a small advantage for measured parameters at NamITP and for the TP version at NamUBT.

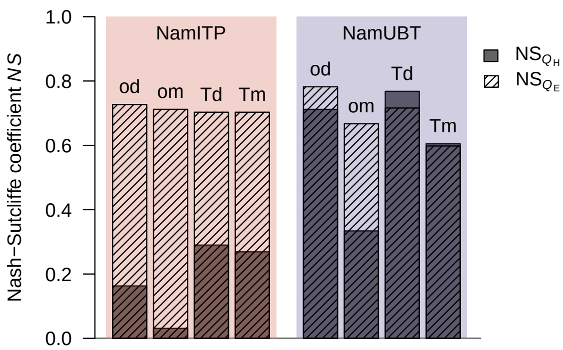

Figure 5. Nash-Sutcliffe coefficient (NS) for turbulent fluxes (simulated vs. EBC-Bo corrected observations), left: NamITP, right: NamUBT. Grey bars denote NS for sensible heat flux and bars with shading lines denote NS for latent heat flux; individual blocks are coded as in Figure 4.

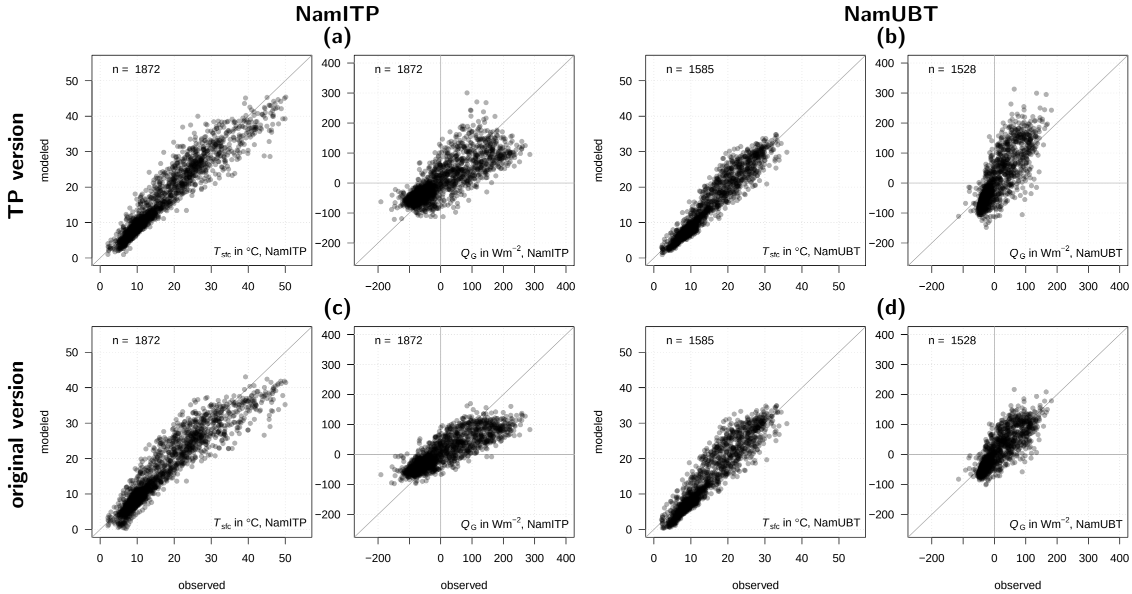

Figure 6. Observations of surface temperature and ground heat flux versus model simulations, **measured** parameters at NamITP (a,c) and NamUBT (b,d); simulations are displayed for TP version (a,b) and original version (c,d).

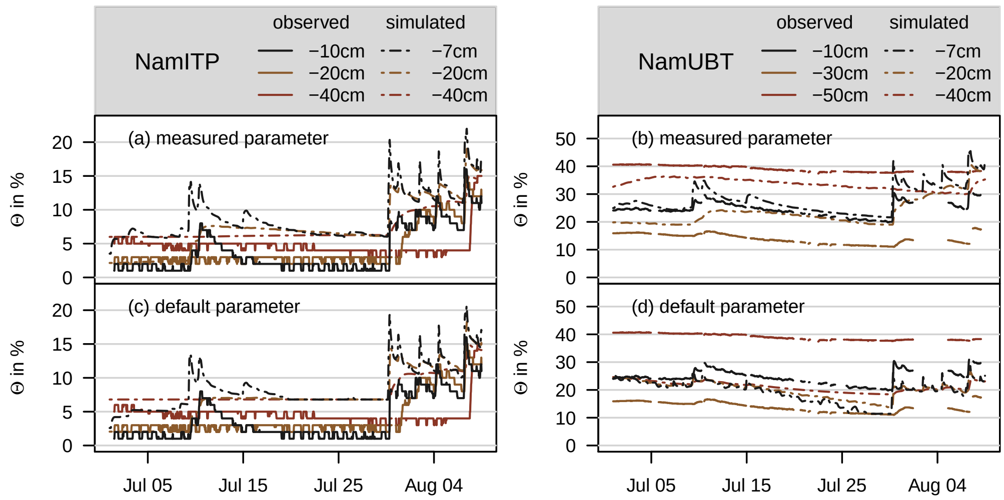

Figure 7. Timeseries of observed and simulated volumetric soil moisture content at various depths, **TP version**, at NamITP (a,c) and NamUBT (b,d); simulations are displayed for measured parameters (a,b) and default parameters (c,d). Note, that simulated soil depths do not match the observed soil depths in case of NamUBT.

The Taylor diagram handles measures of performance which largely ignore model bias. Therefore an overview of the model bias $B = \overline{\xi_{\mathrm{sim}}} - \overline{\xi_{\mathrm{obs}}}$ is given in Figure 4, displaying bias forsensible heat, latent heat and the sum of turbulent fluxes, for the same combinations as in Figure 3. It should be noted that the bias is calculated with EBC-Bo corrected observations, therefore "observed" turbulent fluxes also equal the observed available energy.

The turbulent flux bias is in general large and positive at NamITP, while it is nearly vanishing at NamUBT. This can be attributed to the ground heat flux, which is discussed in the next section. In general the TP version reduces the sensible heat flux and therefore its bias as well as, to a smaller extent, the bias of latent heat. Simulations with default parameters show less bias than those with measured parameters, which is more pronounced at NamUBT than NamITP. This is caused by parameter differences of field capacity and wilting point: The high measured wilting point suppresses evapotranspiration compared to the lower default values at NamUBT. At NamITP, this effect of different field capacity and wilting point can be partly compensated by bare soil evaporation, which is even higher due to the changed parameterization in the TP version.

In Figure 5 the model performance is summed up with theNash-Sutcliffe coefficient [*Nash and Sutcliffe*, 1970], further abbreviated as NS. The NS coefficient can be similarly interpreted as the common coefficient of determination R^2, but in contrast, the NS is sensitive to both correlation and bias. Again, observations are EBC-Bo corrected. In general, model simulations perform better at NamUBT than at NamITP, as a result of smaller bias (Figure 4). This can be attributed to SEWAB formulations which have not been validated for such dry conditions before, such as the scheme to calculate stomatal resistance by *Noilhan and Planton* [1989]. It is further shown for NamITP that the TP version performs considerably better with the sensible heat flux, and negative effects on latent heat are very small and can be neglected. This result agrees with previous studies over dry surfaces [*Yang et al.*, 2008, 2009; *Chen et al.*, 2010]. Furthermore, turbulent fluxes at NamUBT are not compromised by the TP version. Predictions of sensible heat flux even improve, partly at the expense of latent heat flux performance. This suggests that the implemented z_{0h}-scheme is not limited to dry surfaces. The simulations with the default parameters perform significantly better than the ones with the measured parameters, but this difference is larger for the original version than for the TP version. Thus the TP version seems to be less sensitive to soil parameters.

3.2.2. Soil Moisture and Ground Heat Flux

In order to judge if "meaningful" parameters have been set, it is important to also look into accompanying variables. Most prominent are ground heat flux and surface temperature, rendering the budget for turbulent fluxes, and soil moisture, which determines the water availability for evapotranspiration.

Figure 6 compares simulations of soil heat flux and surface temperature (original and TP version, measured parameters) with observations. As expected, the drier NamITP site exhibits higher surface temperatures than NamUBT with maximum temperatures around 50 °C and 35 °C, respectively. In general, simulations reflect these observations reasonably well, except that the maximum surface temperature at NamITP in the TP version (Figure 6a) performs slightly better than the original version (Figure 6c). However, the soil heat flux is moderately or even poorly represented. It clearly explains the observed bias of turbulent fluxes for measured parameters in Figure 4: Underestimation of surface temperature (and therefore long-wave upwelling radiation) as well as underestimation of the soil heat flux lead to an overestimation of available energy at NamITP, while the overestimation of soil heat flux at NamUBT leads to an underestimation of turbulent fluxes. At NamITP, the new parameterization of thermal conductivity (TP version) shows less bias, but more scatter (Figure 6a). This can be attributed to the different model formulations for the thermal conductivity (Figure 8). Within the observed soil moisture rangeat NamITP the TP version shows a much larger sensitivity than the original version, therefore errors in soil moisture produce a larger scatter. Another handicap for ground heat flux simulation at NamITP might be the thermal decoupling of the upper soil layer from deeper layers under very dry conditions. At NamUBT, the TP version predicts the surface temperature accurately, but overestimates the soil heat flux, as a consequence of higher thermal conductivities within the relevant soil moisture range (Figure 8). However, the measured thermal conductivity fits well to calculated values in the TP version, therefore this overestimation is somewhat surprising.

Looking at soil moisture, both measured and default parameters slightly overestimate the observed soil moisture at NamITP (Figure 7). This illustrates the large range of realistic estimates for soil properties: When using a field capacity of 0.05 and wilting point of 0.02, taken from a general soil water retention curve for sandy soil [*Blume et al.*, 2010, p. 228], the model resembles the measured soil moisture much better (not shown). However we stick here to the parameters from the laboratory measurements for consistency. Here soil moisture and temperature was initialized by the measured profile. Additional simulations, using a 3-year spin-up forcing data set, yield similar results for soil moisture at NamITP (not shown). At NamUBT, measured parameters roughly approximate the special moisture profile near the lake. Default parameters, however, show a different profile, despite the better performance for turbulent fluxes. This characteristic profile could not be realized with longer spin-up periods because of the near, but unknown, position of the groundwater table and its seasonal variation. This problem has to be solved when using the model for a longer period at such a location. Furthermore, modeling with detailed parameters for different soil layers may improve the moisture profile, as measured soil parameters differ substantially within the first 50 cm depth.

3.3. Influence of the Method for Energy Balance Closure Correction

Model simulations were compared to observations corrected for energy balance closure according to the Bowen ratio (EBC-Bo). This correction assumes scalar similarity of sensible and latent heat fluxes with respect to the observed residual. Some studies suggest, however, that a large part of the residual should be attributed to the sensible heat flux [*Mauder and Foken*, 2006; *Ingwersen et al.*, 2011]. Recent discussion hypothesizes an influence of secondary circulations on the energy balance closure [*Foken et al.*, 2011, 2010; *Foken*, 2008a].

If secondary circulations in the longwave part of the turbulence spectra – not measured with the eddy-covariance

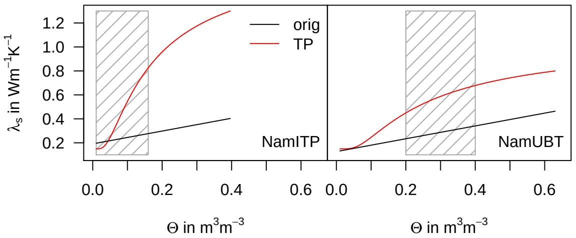

Figure 8. Simulated thermal conductivity λ_s in dependence on soil moisture Θ; grey rectangles indicate the observed range of upper soil moisture for the respective station.

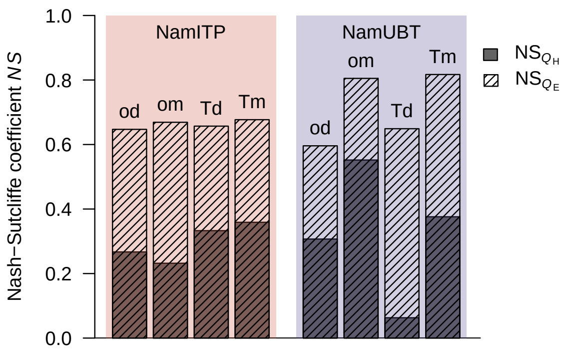

Figure 9. Similar to Figure 5, but for EBC-HB corrected observations.

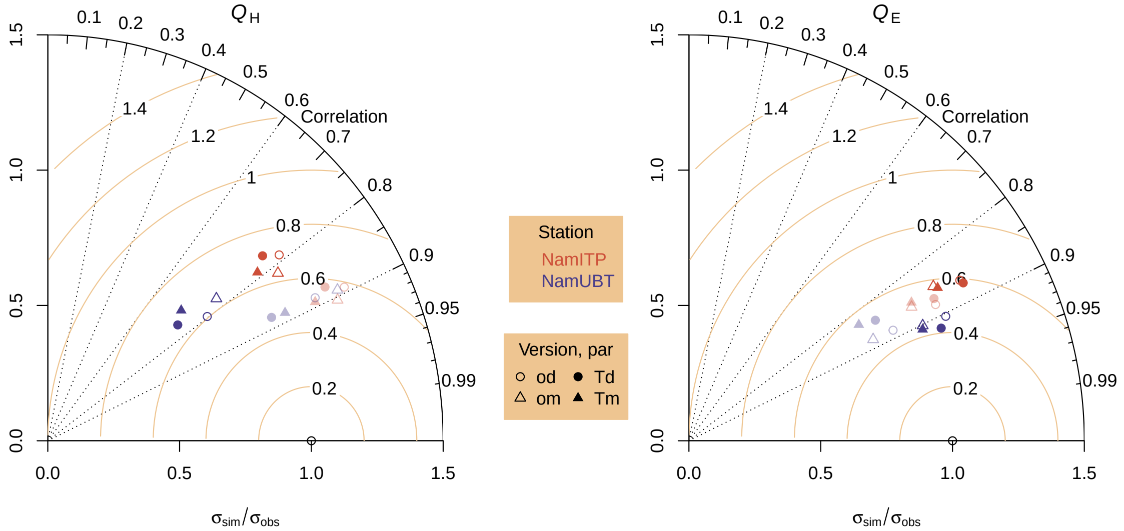

Figure 10. Normalized Taylor diagram similar to Figure 3, but for EBC-HB corrected observations. The results with EBC-Bo corrected observations are displayed in light colors for comparison.

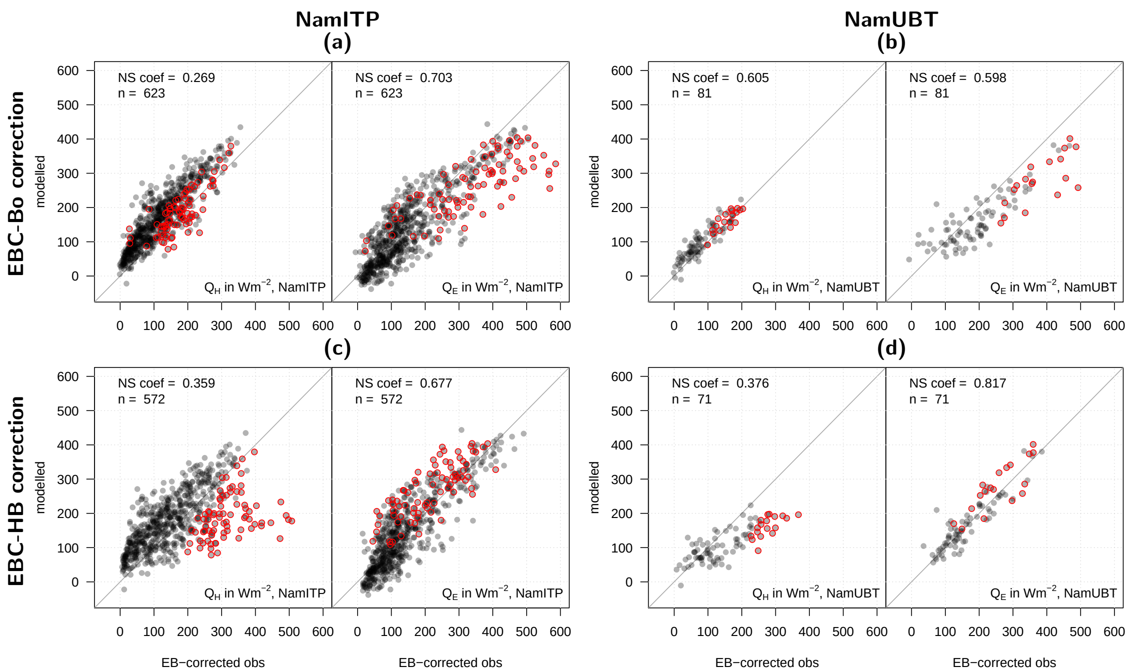

Figure 11. Turbulent flux observations versus model simulations, **measured** parameters, TP version, at NamITP (a,c) and NamUBT (b,d); Observations are displayed using the EBC-Bo correction (a,b) and the EBC-HB correction (c,d). The red points indicate data with $-Res > 150\,\mathrm{W\,m^{-2}}$ (not included in the analysis).

method – due to convection are the reason for the unclosed energy balance, the residual should not simply be added to the sensible heat flux. Because density is also affected by moisture *Charuchittipan et al.* [2013] propose a correction with the buoyancy flux Q_{HB}, further named EBC-HB

$$Q_{\mathrm{H}}^{\mathrm{EBC-HB}} = Q_{\mathrm{H}} + f_{\mathrm{HB}} \cdot Res \tag{5}$$

$$Q_{\mathrm{E}}^{\mathrm{EBC-HB}} = Q_{\mathrm{E}} + (1 - f_{\mathrm{HB}}) \cdot Res, \quad \text{with} \tag{6}$$

$$f_{\mathrm{HB}} = \frac{Q_{\mathrm{H}}}{Q_{\mathrm{HB}}} = \left(1 + 0.61\overline{T}\frac{c_{\mathrm{p}}}{\lambda \cdot Bo}\right)^{-1} \tag{7}$$

where c_{p} is the air heat capacity and λ is the heat of evaporation. There is a weak dependency of EBC-HB to air temperature $\overline{T}$. For $Bo = 1$, more than 90 % of the residual is added to the sensible heat flux, while for $Bo = 0.1$ it is approximately 60 %.

A general effect on model performance in terms of pattern statistics is summarized in a Taylor diagram in Figure 10. The EBC-HB correction correlates less with the simulations than EBC-Bo in the case of sensible heat, but the correlation is similar for latent heat fluxes. The increase of observed sensible heat fluxes due to the EBC-HB correction leads to larger "observed" standard deviations and therefore smaller normalized standard deviations (and, vice versa, the decrease of latent heat fluxes leads to larger normalized standard deviations).

The NS coefficients still attribute better performance to the TP version with respect to the original version (Figure 9). But in contrast, themeasured parameters now show slightly higher NS values for NamITP than the default parameters and significantly better performance for NamUBT, which is the opposite result than is obtained from Figure 5. The EBC-HB correction in general shifts sensible heat flux bias from EBC-Bo corrected observations (Figure 4) in the negative direction and latent heat flux bias in the positive direction. This leads to the pattern change for the NS.

Considering an example in detail, Figure 11 shows observed vs. simulated fluxes (TP version, measured parameters) at both sites and for both correction methods. Looking at the black dots, the simulations of sensible heat flux show more scatter with the EBC-HB corrected observations than for EBC-Bo. This problem is not so pronounced for the latent heat flux; at NamUBT simulations fit even better. The red points indicate values with residuals $-Res > 150\,\mathrm{W\,m^{-2}}$, which were not used in the analysis. Obviously, these points were most strongly affected by the choice of the correction method, particularly because these large residuals occur nearly exclusively for low Bowen ratios (not shown). This is no surprise for NamUBT, where only wet conditions occur, but somehow unexpected for NamITP. The reason might be uncertainty in the ground heat flux calculation affecting the storage term [*Leuning et al.*, 2012], as already mentioned in Sect. 2.4.

Also *Kracher et al.* [2009] show with another data set, that the energy balance implementation in SEWAB roughly preserves the Bowen ratio measured by eddy-covariance. From their calculations it follows that models which determine the fluxes independently, such as TERRA [part of the "Lokalmodell" LM, *Steppeler et al.*, 2003] and REMO [*Jacob and Podzun*, 1997], would follow the proposed algorithm better, but at the expense of the ground heat flux, which is not determined by these models and in fact equals the residual of their energy balance. Other familiar land surface models such as, for example, the common land model CLM [*Dai et al.*, 2003], or the simple biosphere model SiB2 [*Sellers et al.*, 1996] solve this step in a way similar to SEWAB.

4. Discussion and Conclusions

Two data sets of energy fluxes over a wet and a dry grassland site on the Tibetan Plateau were derived for a six-week period in summer 2009. The carefully quality-checked eddy-covariance measurements have been corrected for energy balance closure. Furthermore, the turbulent fluxes have been modeled with the land surface model SEWAB in its original version and a version adapted to Tibetan Plateau conditions (TP version). Both versions have been run with two different parameter sets, a default set and one with soil physical parameters from laboratory investigations of field samples.

Both parameter sets – default and measured –, perform reasonably well, taking into account that no calibration algorithm has been applied. However, measured parameters do not prove to give better results; rather the opposite is true. This might be attributed to the high spatial variability of soil properties in the field, which are not adequately reflected by the taken sample. Another aspect is that a given model structure might require effective parameter values to yield optimal performance, which deviate from measured ones. Nevertheless, some field investigations will be inevitable to derive a high quality parameter set (measured or default parameters), namely soil moisture measurements and field based knowledge of the soil type, derived at least by a conventional pedological description.

SEWAB has been adapted to Tibetan Plateau conditions, modifying formulations for the soil thermal conductivity, bare soil evaporation and $z_{0\mathrm{h}}$. In agreement with previous studies, this version improves predictions of sensible heat flux on the dry surface, although the original model already performs quite well. Interestingly, predictions of fluxes over the wet surface are not (or not substantially) compromised, thus the observed spatial differences in surface fluxes due to small scale heterogeneity in soil moisture could be reproduced with a consistent model version. Therefore this study suggests that the $z_{0\mathrm{h}}$-scheme by *Yang et al.* [2008] is not limited to dry or bare soil surfaces. Moreover, the sensitivity due to soil parameters seems to decrease with the TP version, implying more robust results.

Investigations concerning the energy balance closure correction clearly show that SEWAB is more compatible with the observations corrected by preserving the Bowen ratio. However, there is no proof that this closure method reflects reality. In contrast, the recent discussion of the closure problem tends to attribute the residual more – or in total – to the sensible heat flux as the driver for advective fluxes not resolved by EC systems [*Mauder and Foken*, 2006; *Foken*, 2008a; *Foken et al.*, 2011; *Ingwersen et al.*, 2011; *Charuchittipan et al.*, 2013]. While the TP version outperforms the original version for both correction methods, the ranking between the parameter sets change. In summary, this case study yields huge differences in model performance dependent on the closure method. Thus it follows that the closure issue should not be neglected when models were validated with EC measurements.

Typically for case studies, this work is limited by the amount of data sets and sites enclosed, and in the first instance the results are representative for the Nam Co region. They could be strengthened by extending the investigations over a larger variety of measurement periods and sites to test the robustness of the model performance. Furthermore, the errors of observations are not explicitly taken into account. Beside the usual errors to be expected, there are some difficulties at the NamITP site due to a large gravel content in the soil and the surface as well as missing top soil temperature measurements. Firstly, this compromises quality and representativeness of the measured available energy; secondly, laboratory investigations of soil physical properties become very uncertain and difficult to carry out. Even "realistic" parameters have obviously to be considered within a range due to model and measurement uncertainty as well as soil heterogeneity. Especially for the wet site, soil properties change a lot within the vertical profile, which should be taken into account by land surface models.

This study shows that a successful modeling of turbulent fluxes requires a careful model selection and parameter investigation. However, when comparing simulations with eddy-covariance derived turbulent fluxes, the performance is strongly affected by the measured energy balance closure gap. This is especially important in a sensitive region like the Tibetan Plateau, in which *Kobresia* pastures and alpine vegetation are supposed to be highly susceptible to climate change and livestock grazing [*Miehe et al.*, 2008, 2011]. The selected data sets also imply that surface flux heterogeneity, generated by landscape heterogeneity, could be remarkable in a short distance. This should be taken into account when regarding flux measurements as representative for a larger area. This study prepares the SEWAB model to be usable for such issues.

Acknowledgments. The authors acknowledge the staff members of the ITP Nam Co Monitoring and Research Station for their work on the Tibetan Plateau, and Heinz-Theo Mengelkamp for making SEWAB available. The work described in this publication has been supported by the European Commission (Call FP7-ENV-2007-1 Grant nr. 212921) as part of the CEOP-AEGIS project (http://www.ceop-aegis.org/) coordinated by the University of Strasbourg. Furthermore, this work has been funded by the DFG Priority Programme 1372 "Tibetan Plateau: Formation, Climate, Ecosystems". Dr. Yingying Chen gratefully acknowledges the support of the National Natural Science Foundation of China (Grant No. 41105003).

References

Agam, N., P. R. Berliner, A. Zangvil, and E. Ben-Dor (2004), Soil water evaporation during the dry season in an arid zone, *J. Geophys. Res.*, *109*(D16), D16,103–, doi:10.1029/2004JD004802.

Alapaty, K., J. E. Pleim, S. Raman, D. S. Niyogi, and D. W. Byun (1997), Simulation of atmospheric boundary layer processes using local- and nonlocal-closure schemes, *J. Appl. Meteorol.*, *36*(3), 214–233, doi:10.1175/1520-0450(1997)036⟨0214:SOABLP⟩2.0.CO;2.

Balsamo, G., S. Boussetta, E. Dutra, A. Beljaars, P. Viterbo, and B. van den Hurk (2011), Evolution of land surface processes in the IFS, *ECMWF Newslett.*, *127*, 17–22.

Blume, H.-P., G. W. Brümmer, R. Horn, E. Kandeler, I. Kögel-Knabner, R. Kretzschmar, K. Stahr, and B.-M. Wilke (2010), *Scheffer/Schachtschabel Lehrbuch der Bodenkunde*, 16 ed., 569 pp., Spektrum Akademischer Verlag Heidelberg.

Brilli, F., L. Hörtnagl, A. Hammerle, A. Haslwanter, A. Hansel, F. Loreto, and G. Wohlfahrt (2011), Leaf and ecosystem response to soil water availability in mountain grasslands, *Agr. Forest Meteorol.*, *151*(12), 1731–1740, doi:10.1016/j.agrformet.2011.07.007.

Charuchittipan, D., W. Babel, M. Mauder, J.-P. Leps, and T. Foken (2013), Extension of the averaging time of the eddy-covariance measurement and its effect on the energy balance closure, submitted to *Bound.-Lay. Meteorol.*

Chen, Y., K. Yang, D. Zhou, J. Qin, and X. Guo (2010), Improving the Noah land surface model in arid regions with an appropriate parameterization of the thermal roughness length, *J. Hydrometeorol.*, *11*(4), 995–1006, doi:10.1175/2010JHM1185.1.

Chen, Y., K. Yang, J. He, J. Qin, J. Shi, J. Du, and Q. He (2011), Improving land surface temperature modeling for dry land of china, *J. Geophys. Res.*, *116*(D20), D20,104–, doi:10.1029/2011JD015921.

Chen, Y., K. Yang, W. Tang, J. Qin, and L. Zhao (2012), Parameterizing soil organic carbon's impacts on soil porosity and thermal parameters for eastern tibet grasslands, *Sci. China Earth Sci.*, *55*, 1001–1011, doi:10.1007/s11430-012-4433-0.

Clapp, R. B., and G. M. Hornberger (1978), Empirical equations for some soil hydraulic properties, *Water Resour. Res.*, *14*(4), 601–604.

Dai, Y., et al. (2003), The common land model, *B. Am. Meteorol. Soc.*, *84*(8), 1013–1023, doi:10.1175/BAMS-84-8-1013.

Duan, A., and G. Wu (2005), Role of the tibetan plateau thermal forcing in the summer climate patterns over subtropical asia, *Clim. Dynam.*, *24*, 793–807, doi:10.1007/s00382-004-0488-8.

Foken, T. (2008a), The energy balance closure problem: An overview, *Ecol. Appl.*, *18*(6), 1351–1367.

Foken, T. (2008b), *Micrometeorology*, 308 pp., Springer, Berlin, Heidelberg.

Foken, T., et al. (2010), Energy balance closure for the LITFASS-2003 experiment, *Theor. Appl. Climatol.*, *101*, 149–160, doi:10.1007/s00704-009-0216-8.

Foken, T., M. Aubinet, J. J. Finnigan, M. Y. Leclerc, M. Mauder, and K. T. Paw U (2011), Results of a panel discussion about the energy balance closure correction for trace gases, *B. Am. Meteorol. Soc.*, *92*(4), ES13–ES18, doi:10.1175/2011BAMS3130.1.

Foken, T., R. Leuning, S. R. Oncley, M. Mauder, and M. Aubinet (2012), Corrections and data quality control, in *Eddy Covariance: A Practical Guide to Measurement and Data Analysis*, edited by M. Aubinet, T. Vesala, and D. Papale, Springer Atmospheric Sciences, pp. 85–131, Springer Netherlands, doi:10.1007/978-94-007-2351-1_4.

Gao, Y. X. (1985), *Tibetan soil*, Science Press, Beijing, pp 2–15.

Gerken, T., et al. (2012), Turbulent flux modelling with a simple 2-layer soil model and extrapolated surface temperature applied at nam co lake basin on the tibetan plateau, *Hydrol. Earth Syst. Sci.*, *16*(4), 1095–1110, doi:10.5194/hess-16-1095-2012.

Göckede, M., C. Rebmann, and T. Foken (2004), A combination of quality assessment tools for eddy covariance measurements with footprint modelling for the characterisation of complex sites, *Agr. Forest Meteorol.*, *127*(3-4), 175–188, doi:10.1016/j.agrformet.2004.07.012.

Göckede, M., et al. (2008), Quality control of carboeurope flux data - part 1: Coupling footprint analyses with flux data quality assessment to evaluate sites in forest ecosystems, *Biogeosciences*, *5*(2), 433–450, doi:10.5194/bg-5-433-2008.

Hong, J., and J. Kim (2010), Numerical study of surface energy partitioning on the Tibetan Plateau: comparative analysis of two biosphere models, *Biogeosciences*, *7*(2), 557–568, doi:10.5194/bg-7-557-2010.

Hsu, H.-H., and X. Liu (2003), Relationship between the tibetan plateau heating and east asian summer monsoon rainfall, *Geophys. Res. Lett.*, *30*(20), 2066, doi:10.1029/2003GL017909.

Hu, Z., et al. (2009), Partitioning of evapotranspiration and its controls in four grassland ecosystems: Application of a two-source model, *Agr. Forest Meteorol.*, *149*(9), 1410–1420, doi:10.1016/j.agrformet.2009.03.014.

Ingwersen, J., et al. (2011), Comparison of noah simulations with eddy covariance and soil water measurements at a winter wheat stand, *Agr. Forest Meteorol.*, *151*(3), 345–355, doi:10.1016/j.agrformet.2010.11.010.

Jacob, D., and R. Podzun (1997), Sensitivity studies with the regional climate model REMO, *Meteorol. Atmos. Phys.*, *63*, 119–129.

Kang, S., Y. Xu, Q. You, W.-A. Flügel, N. Pepin, and T. Yao (2010), Review of climate and cryospheric change in the tibetan plateau, *Environ. Res. Lett.*, *5*(1), 015,101, doi:10.1088/1748-9326/5/1/015101.

Kracher, D., H. T. Mengelkamp, and T. Foken (2009), The residual of the energy balance closure and its influence on the results of three svat models, *Meteorol. Z.*, *18*(6), 1–15, doi:10.1127/0941-2948/2009/0412.

Larcher, W. (2001), *Ökophysiologie der Pflanzen: Leben, Leistung und Streßbewältigung der Pflanzen in ihrer Umwelt*, 6th ed., 408 pp., Verlag Eugen Ulmer Stuttgart.

Leuning, R., E. van Gorsel, W. J. Massman, and P. R. Isaac (2012), Reflections on the surface energy imbalance problem, *Agr. Forest Meteorol.*, *156*(0), 65–74, doi:10.1016/j.agrformet.2011.12.002.

Liebethal, C., B. Huwe, and T. Foken (2005), Sensitivity analysis for two ground heat flux calculation approaches, *Agr. Forest Meteorol.*, *132*, 253–262, doi:10.1016/j.agrformet.2005.08.001.

Liu, J., S. Kang, T. Gong, and A. Lu (2010), Growth of a high-elevation large inland lake, associated with climate change and permafrost degradation in tibet, *Hydrol. Earth Syst. Sci.*, *14*(3), 481–489, doi:10.5194/hess-14-481-2010.

Liu, Y., Q. He, H. Zhang, and A. Mamtimin (2012), Improving the colm in taklimakan desert hinterland with accurate key parameters and an appropriate parameterization scheme, *Adv. Atmos. Sci.*, *29*(2), 381–390, doi:10.1007/s00376-011-1068-6.

Louis, J. (1979), A parametric model of vertical eddy fluxes in the atmosphere, *Bound.-Lay. Meteorol.*, *17*, 187–202, doi:10.1007/BF00117978.

Ma, Y., O. Tsukamoto, J. Wang, H. Ishikawa, and I. Tamagawa (2002), Analysis of aerodynamic and thermodynamic parameters on the grassy marshland surface of tibetan plateau, *Prog. Nat. Sci.*, *12*, 36–40.

Mauder, M., and T. Foken (2004), Documentation and instruction manual of the eddy covariance software package TK2, Work Report University of Bayreuth, Dept. of Micrometeorology, ISSN 1614-8916, 26, 42 pp.

Mauder, M., and T. Foken (2006), Impact of post-field data processing on eddy covariance flux estimates and energy balance closure, *Meteorol. Z.*, *15*(13), 597–609, doi:10.1127/0941-2948/2006/0167.

Mauder, M., and T. Foken (2011), Documentation and instruction manual of the eddy-covariance software package TK3, Work Report University of Bayreuth, Dept. of Micrometeorology, ISSN 1614-8916, 46, 58 pp.

Mengelkamp, H. T., K. Warrach, and E. Raschke (1997), A land surface scheme for atmospheric and hydrologic models: SEWAB (Surface Energy and Water Balance), *GKSS Report 97/E/69, 40pp.*, GKSS Geesthacht.

Mengelkamp, H. T., K. Warrach, and E. Raschke (1999), SEWAB - a parameterization of the surface energy and water balance for atmospheric and hydrologic models, *Adv. Water Resour.*, *23*(2), 165–175, doi:10.1016/S0309-1708(99)00020-2.

Mengelkamp, H. T., G. Kiely, and K. Warrach (2001), Evaluation of the hydrological components added to an atmospheric land-surface scheme, *Theor. Appl. Climatol.*, *69*(3-4), 199–212, doi:10.1007/s007040170025.

Miehe, G., S. Miehe, K. Kaiser, L. Jianquan, and X. Zhao (2008), Status and dynamics of the kobresia pygmaea ecosystem on the tibetan plateau, *Ambio*, *37*(4), 272–279, doi:10.1579/0044-7447(2008)37[272:SADOTK]2.0.CO;2.

Miehe, G., K. Bach, S. Miehe, J. Kluge, Y. Yongping, L. Duo, S. Co, and K. Wesche (2011), Alpine steppe plant communities of the tibetan highlands, *Applied Vegetation Science*, *14*(4), 547–560, doi:10.1111/j.1654-109X.2011.01147.x.

Mihailović, D. T., R. A. Pielke, B. Rajković, T. J. Lee, and M. Jeftić (1993), A resistance representation of schemes for evaporation from bare and partly plant-covered surfaces for use in atmospheric models, *J. Appl. Meteorol.*, *32*(6), 1038–1054, doi:10.1175/1520-0450(1993)032⟨1038:ARROSF⟩2.0.CO;2.

Mihailović, D. T., B. Rajković, B. Lalić, and L. Dekić (1995), Schemes for parameterizing evaporation from a non-plant-covered surface and their impact on partitioning the surface energy in land-air exchange parameterization, *J. Appl. Meteorol.*, *34*(11), 2462–2475, doi:10.1175/1520-0450(1995)034⟨2462:SFPEFA⟩2.0.CO;2.

Mügler, I., et al. (2010), A multi-proxy approach to reconstruct hydrological changes and Holocene climate development of Nam Co, Central Tibet, *J. Paleolimnol.*, *43*, 625–648, doi:10.1007/s10933-009-9357-0.

Nash, J. E., and J. V. Sutcliffe (1970), River flow forecasting through conceptual models part I – A discussion of principles, *J. Hydrol.*, *10*(3), 282–290, doi:10.1016/0022-1694(70)90255-6.

Noilhan, J., and S. Planton (1989), A simple parameterization of land surface processes for meteorological models, *Mon. Weather Rev.*, *117*(3), 536–549, doi:10.1175/1520-0493(1989)117⟨0536:ASPOLS⟩2.0.CO;2.

Rannik, U., M. Aubinet, O. Kurbanmuradov, K. K. Sabelfeld, T. Markkanen, and T. Vesala (2000), Footprint analysis for measurements over a heterogeneous forest, *Bound.-Lay. Meteorol.*, *97*(1), 137–166, doi:10.1023/A:1002702810929.

Sellers, P., D. Randall, G. Collatz, J. Berry, C. Field, D. Dazlich, C. Zhang, G. Collelo, and L. Bounoua (1996), A revised land surface parameterization (SiB2) for atmospheric GCMs. part I: Model formulation, *J. Climate*, *9*(4), 676–705, doi:10.1175/1520-0442(1996)009⟨0676:ARLSPF⟩2.0.CO;2.

Steppeler, J., G. Doms, U. Schattler, H. W. Bitzer, A. Gassmann, U. Damrath, and G. Gregoric (2003), Meso-gamma scale forecasts using the nonhydrostatic model LM, *Meteorol. Atmos. Phys.*, *82*, 75–96.

Su, Z., J. Wen, L. Dente, R. van der Velde, L. Wang, Y. Ma, K. Yang, and Z. Hu (2011), The Tibetan Plateau observatory of plateau scale soil moisture and soil temperature (tibet-obs) for quantifying uncertainties in coarse resolution satellite and model products, *Hydrol. Earth Syst. Sci.*, *15*(7), 2303–2316, doi:10.5194/hess-15-2303-2011.

Takayabu, I., K. Takata, T. Yamazaki, K. Ueno, H. Yabuki, and S. Haginoya (2001), Comparison of the four land surface models driven by a common forcing data prepared from GAME/Tibet POP'97 products – snow accumulation and soil freezing processes –, *J. Meteorol. Soc. Jpn.*, *79*(1B), 535–554, doi:10.2151/jmsj.79.535.

Taylor, K. E. (2001), Summarizing multiple aspects of model performance in a single diagram, *J. Geophys. Res.*, *106*(D7), 7183–7192, doi:10.1029/2000JD900719.

Twine, T. E., W. P. Kustas, J. M. Norman, D. R. Cook, P. R. Houser, T. P. Meyers, J. H. Prueger, P. J. Starks, and M. L. Wesely (2000), Correcting eddy-covariance flux underestimates over a grassland, *Agr. Forest Meteorol.*, *103*(3), 279–300, doi:10.1016/S0168-1923(00)00123-4.

van der Velde, R., Z. Su, M. Ek, M. Rodell, and Y. Ma (2009), Influence of thermodynamic soil and vegetation parameterizations on the simulation of soil temperature states and surface fluxes by the Noah LSM over a Tibetan Plateau site, *Hydrol. Earth Syst. Sci.*, *13*(6), 759–777, doi:10.5194/hess-13-759-2009.

Wallace, J., I. Wright, J. Stewart, and C. Holwill (1991), The sahelian energy balance experiment (SEBEX): Ground based measurements and their potential for spatial extrapolation using satellite data, *Adv. Space Res.*, *11*(3), 131–141, doi:10.1016/0273-1177(91)90413-E.

Wilczak, J., S. Oncley, and S. Stage (2001), Sonic anemometer tilt correction algorithms, *Bound.-Lay. Meteorol.*, *99*, 127–150, doi:10.1023/A:1018966204465.

Xu, J., and S. Haginoya (2001), An estimation of heat and water balances in the Tibetan Plateau, *J. Meteorol. Soc. Jpn.*, *79*(1B), 485–504, doi:10.2151/jmsj.79.485.

Yanai, M. H., C. F. Li, and Z. S. Song (1992), Seasonal heating of the Tibetan Plateau and its effects on the evolution of the Asian Summer Monsoon, *J. Meteorol. Soc. Jpn.*, *70*(1B), 319–351.

Yang, K., and J. Wang (2008), A temperature prediction-correction method for estimating surface soil heat flux from soil temperature and moisture data, *Sci. China Ser. D*, *51*, 721–729, doi:10.1007/s11430-008-0036-1.

Yang, K., T. Koike, and D. Yang (2003), Surface flux parameterization in the Tibetan Plateau, *Bound.-Lay. Meteorol.*, *116*, 245–262, doi:10.1023/A:1021152407334.

Yang, K., T. Koike, B. Ye, and L. Bastidas (2005), Inverse analysis of the role of soil vertical heterogeneity in controlling surface soil state and energy partition, *J. Geophys. Res.*, *110*(D8), D08101, doi:10.1029/2004JD005500.

Yang, K., T. Koike, H. Ishikawa, J. Kim, X. Li, H. Liu, J. Wang, S. Liu, and Y. Ma (2008), Turbulent flux transfer over bare-soil surfaces: Characteristics and parameterization, *J. Appl. Meteorol. Clim.*, *47*, 276–290, doi:10.1175/2007JAMC1547.1.

Yang, K., Y.-Y. Chen, and J. Qin (2009), Some practical notes on the land surface modeling in the Tibetan Plateau, *Hydrol. Earth Syst. Sci.*, *13*(5), 687–701, doi:10.5194/hess-13-687-2009.

Yang, K., X. Guo, and B. Wu (2010), Recent trends in surface sensible heat flux on the tibetan plateau, *Sci. China Earth Sci.*, pp. 1–10, doi:10.1007/s11430-010-4036-6.

Ye, D.-Z., and G.-X. Wu (1998), The role of the heat source of the Tibetan Plateau in the general circulation, *Meteorol. Atmos. Phys.*, *67*(1), 181–198, doi:10.1007/BF01277509.

Zhang, X. (2012), Improvement of a soil-atmosphere-transfer model for the simulation of bare soil surface energy balances in semiarid areas, *Asia Pac. J. Atmos. Sci.*, *48*(1), 97–105, doi:10.1007/s13143-012-0009-3.

Zhou, D., R. Eigenmann, W. Babel, T. Foken, and Y. Ma (2011), The study of near-ground free convection conditions at nam co station on the tibetan plateau, *Theor. Appl. Climatol.*, *105*, 217–228, doi:10.1007/s00704-010-0393-5.

W. Babel, Abt. Mikrometeorologie, Universität Bayreuth, 95440 Bayreuth, Germany. (wolfgang.babel@uni-bayreuth.de)

T. Biermann, Abt. Mikrometeorologie, Universität Bayreuth, 95440 Bayreuth, Germany.

Y. Chen, Institute of Tibetan Plateau Research, Chinese Academy of Sciences, 4A Datun Road, Chaoyang District, Beijing 100101, China.

T. Foken, Abt. Mikrometeorologie, Universität Bayreuth, 95440 Bayreuth, Germany.

Y. Ma, Institute of Tibetan Plateau Research, Chinese Academy of Sciences, 4A Datun Road, Chaoyang District, Beijing 100101, China.

K. Yang, Institute of Tibetan Plateau Research, Chinese Academy of Sciences, 4A Datun Road, Chaoyang District, Beijing 100101, China.

D. Biermann et al. (2013)

Biermann, T., Babel, W., Ma, W., Chen, X., Thiem, E., Ma, Y., and Foken, T.: Turbulent flux observations and modelling over a shallow lake and a wet grassland in the Nam Co basin, Tibetan Plateau, Theor. Appl. Climatol., accepted

Turbulent flux observations and modelling over a shallow lake and a wet grassland in the Nam Co basin, Tibetan Plateau

Tobias Biermann[1], Wolfgang Babel[1], Weiqiang Ma[2], Xuelong Chen[3], Elisabeth Thiem[4], Yaoming Ma[5], Thomas Foken[1,6]

[1] Department of Micrometeorology, University of Bayreuth, Bayreuth, Germany

[2] Cold and Arid Regions Environment and Engineering Research Institute, Chinese Academy of Sciences, Lanzhou, China

[3] Faculty of Geo-Information Science and Earth Observation, University of Twente, Enschede, The Netherlands

[4] Department of Geography, Ludwig-Maximilian University, Munich, Germany

[5] Laboratory of Tibetan Environment Changes and Land Surface Processes, Institute of Tibetan Plateau Research, Chinese Academy of Sciences, Beijing, China

[6] Member of Bayreuth Center of Ecology and Ecosystem Research (BayCEER)

Corresponding author address:

Tobias Biermann, Abt. Mikrometeorologie, Universität Bayreuth, Universitätsstr. 30 , 95440 Bayreuth, Germany

Phone: +49 921 552180

Fax: +49 921 552366

E-mail: tobias.biermann@uni-bayreuth.de

Abstract

The Tibetan Plateau plays an important role in the global water cycle and is strongly influenced by climate change. While energy and matter fluxes have been more intensely studied over land surfaces, a large proportion of lakes have been either neglected or parameterised with simple bulk approaches. Therefore turbulent fluxes were measured over wet grassland and a shallow lake with a single eddy-covariance complex at the shoreline in the Nam Co basin in summer 2009. Footprint analysis was used to split observations according to the underlying surface, and two sophisticated surface models were utilised to derive gap-free time series. Results were then compared with observations and simulations from a nearby eddy-covariance station over dry grassland, yielding pronounced differences. Observations and footprint integrated simulations compared well, even for situations with flux contributions including grassland and lake. It is shown that the accessibility problem for EC measurements on lakes can be overcome by combining standard meteorological measurements at the shoreline with model simulations, only requiring representative estimates of lake surface temperature.

Keywords: Eddy-covariance, Lake, Nam Co, Surface modelling, Tibetan Plateau, Turbulent fluxes

1. Introduction

The role of the Tibetan Plateau in the global water cycle and its reaction to climate change has become a topic of strong scientific interest (e.g. Immerzeel et al. 2011, Ni 2011). Representing a unique geological formation, the Tibetan Plateau is considered the largest and highest plateau on earth, with an average elevation greater than 4000 m a.s.l.. Furthermore, the Tibetan Plateau is the source of a large number of major rivers in Asia. Its role in the modulation of the Asian Monsoon and the climate for large parts of Asia, due to its heat budget caused by its elevation in conjunction with the bordering Himalayan mountain range, has been of major research interest (Molnar et al. 2010, Boos and Kuang 2010).
To understand the role of the Tibetan Plateau for the global heat and water budget, much effort has been put into the estimation of energy balance and turbulent flux measurements within international campaigns like GAME/Tibet (GEWEX-Global Energy and Water cycle Experiment Asian Monsoon Experiment) and (CAMP -Coordinated Enhanced Observing Period Asia-Australia Monsoon Project) (Xu and Haginoya 2001; Ma et al. 2003; Ma et al. 2005) and in the framework of the Tibetan Observation and Research Platform, TORP (Ma et al. 2009).
Despite these efforts, observations on the Tibetan Plateau are sparse due to its remote location (Frauenfeld et al. 2005, Kang et al. 2010, Maussion et al. 2011). The importance of evaporation for the hydrological cycle under the influence of climate change has been highlighted by Yang et al. (2011).
Most long-term observation stations focus on the major land cover types such as alpine steppe, *Kobresia* pastures and wetlands (Zhao et al. 2010), however approximately 45.000 km² of the plateau are covered by lakes (Xu et al. 2009). This lake area has been subject to changes in the last decades, the reasons are not well understood due to lack of observational data (Xu et al. 2009). Although Huang et al. (2008) report a general decrease of lake volume in Qinghai-Tibet Plateau, the Nam Co lake area has been increasing (Liu et al. 2010, Wu and Zhu 2008, Zhu et al. 2010). They attribute this change to increasing precipitation as well as thawing permafrost and glacial melt due to rising mean annual temperatures , nevertheless the relative contribution of the balance components, especially the role of evaporation, is discussed controversially. Consequently fluxes over lake surfaces on the Tibetan Plateau should not be neglected, since various studies have shown the contribution of lakes to the regional energy balance and water cycle in different catchments around the world (Rouse et al. 2005, Nordbo et al. 2011). Until now, estimations of evaporation over lake surfaces on the Tibetan Plateau have been modelled using remote sensing or land surface observations as forcing (Xu et al. 2009, Haginoya et al. 2009), whereas no direct measurements of turbulent fluxes over a lake surface have been conducted so far. The installation of a flux station in a lake on the Tibetan Plateau is nearly impossible, due to problems of accessibility, strong winds and waves during the summer, as well as ice cover during winter.
Nevertheless, it is known from model estimations that evaporation over lake surfaces differs from evapotranspiration over land throughout the year due to the heat storage capacity of the lakes, and has a strong effect on convection and thus on local climates (Haginoya et al. 2009). The landscape on the Tibetan Plateau is fairly heterogeneous, including alpine steppe, *Kobresia pygmea* mats, wetlands and open water surfaces in various sizes. Therefore high quality evaporation measurements over water surfaces on the Tibetan Plateau need to be considered

when data based on satellites or estimated with models is validated with ground based flux measurements. It can be expected that lakes differ strongly in their temperature regimes and exchange coefficients due to extent and depth (Rouse et al. 2005, Panin et al. 2006a, Nordbo et al. 2011). Evaporation estimation with simple bulk approaches on daily or monthly timescales (Haginoya et al. 2009, Xu et al. 2009, Krause et al. 2010, Yu et al. 2011) are not appropriate for resolving such differences. These specific characteristics of each lake, such as a diurnal course of atmospheric stratification over the lake surface, can only be captured by eddy measurements and more sophisticated models.

For this study, we selected the area around Nam Co, the largest and deepest lake in the Tibet Autonomous Region (Xu et al. 2009, Liu et al. 2010). The Nam Co basin is considered one of the key areas of interest on the Tibetan Plateau due to its location influenced by the Westerlies, the South West Asian Monsoon and the East Asian Monsoon (Haginoya et al. 2009, Keil et al. 2010).

In order to measure fluxes over lake and land surfaces, we set up an eddy-covariance station at the shoreline of a shallow lake next to Nam Co. Measured fluxes were utilised to validate simulations of two different surface models in order to estimate turbulent fluxes over the lake and adjacent grassland surface. For the lake surface a validated hydrodynamic multilayer model (HM; Foken 1979, 1984) with an extension for shallow lakes (Panin and Foken 2005) and for the land surface a SVAT model (SEWAB; Mengelkamp et al. 1999, 2001) were used to generate a complete time series for each surface. The simulated data set was then used to characterise the exchange for these surfaces and to link the simulations with spatial heterogeneity on footprint scale.

2. Material and methods

2.1. Site description and setup of the EC stations

The experiment was carried out during the 2009 summer monsoon season. The observation site was located in the Nam Co Basin, 220 km north of Lhasa, at 4730 m a.s.l. on the Tibetan Plateau. The basin is dominated by Nam Co Lake and the Nyainqentanglha mountain range which stretches along the lake's SE side at approximately 5-10 km distance and reaches up to 7270 m a.s.l. with an average height of 5230 m (Liu et al. 2010). In the year 2000 the great lake had an area of 1,980 km² (Wu and Zhu 2008).

Atmospheric fluxes were observed with two eddy-covariance and energy balance stations. One station was set up by the University of Bayreuth (NamUBT) at a shallow lake of approximately 1 km² in area located at the SE side of Nam Co Lake. It was installed adjacent to the southern shoreline of the lake to ensure that measurements from the lake and land surface were identifiable according to the instantaneous wind direction. The other station at roughly 300 m distance is the permanently operating eddy-covariance complex (NamITP) within the Nam Co Monitoring and Research Station for Multisphere Interactions, NAMORS (30°46′22″N, 90°57′47″E) operated by the Institute of Tibetan Plateau Research (ITP), Chinese Academy of Sciences (CAS) (Ma et al. 2009). A detailed map of the field site and pictures of the two stations can be seen in Fig. 1.

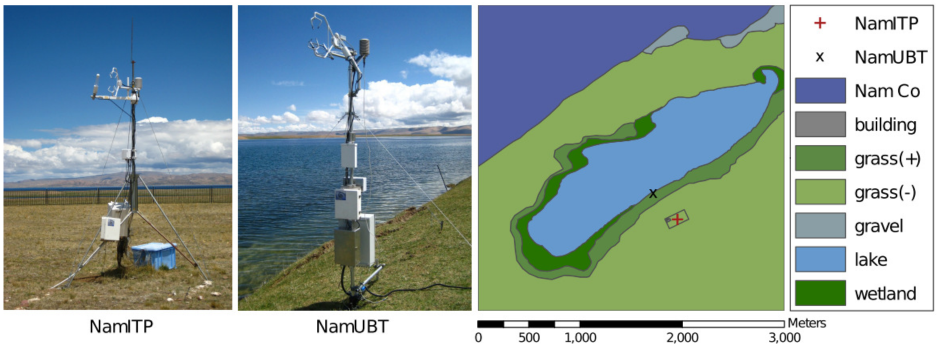

Fig. 1 Measurement site in Nam Co Basin, showing the small lake, the land use, the EC Stations NamITP (left Photo) and NamUBT (right Photo). NamITP is marked with a red + and NamUBT with a black x. Land use is classified as wetland (dark green), moist ($^+$, medium green) and dry ($^-$, light green) grassland, the small lake (light blue) and Nam Co (dark blue). Additionally, at the shore line of Nam Co partly flooded gravel bars are shown in light grey. The Nam Co Station buildings are marked in dark grey (Illustration from Gerken et al. 2012)

Due to the influence of the water table around the small lake, the soil is moister at NamUBT than at NamITP. To account for the effect of higher moisture supply on the vegetation, we have classified the grassland into grass$^+$ for denser and moister vegetation and grass$^-$ for comparatively drier and sparser vegetation. From NamUBT the terrain rises gently in three terraces to the level of NamITP, with an average slope of approximately 8°. The shoreline of the small lake in the vicinity of NamUBT is fairly steep, with the lake starting out quite shallow and reaching a maximum depth of 12 m at the centre. Soils and vegetation around both stations are typical for a semi-arid to semi-humid climate at this altitude. Soil types range from alpine steppe to desert soils and the vegetation is dominated by alpine meadow and steppe grasses including species of *Stipa*, *Carex*, *Kobresia* and *Oxytropis* (Mügler et al. 2010).
Both eddy-covariance stations were equipped with an ultrasonic anemometer and an infrared gas analyser. Standard meteorological measurements are available for both stations and, additionally, all necessary components for the estimation of the energy balance were measured. For specifications of the two stations see Table 1 or Biermann et al. (2009) for NamUBT, and Zhou et al. (2011) for NamITP.

2.2. Analysis of observed data

2.2.1. EC Data processing

The measurements of both eddy-covariance stations were post-processed using the TK2/3 software package, developed at the Department of Micrometeorology, University of Bayreuth (Mauder and Foken 2004, 2011) and evaluated in an international comparison study by Mauder et al. (2008). The software applies all necessary flux corrections and post-processing steps for turbulence measurements as recommended in Foken et al. (2012) and Rebmann et al. (2012).

Further data processing included quality filtering according to Foken and Wichura (1996), using the quality flagging scheme as recommended by Foken et al. (2004).

Table 1: Specifications of the eddy-covariance stations NamUBT and NamITP.

	Instrument	NamUBT	NamITP
Surface		lake, grass$^+$, grass$^-$	grass$^-$
Ultrasonic anemometer	CSAT3 (Campbell Scientific Ltd.)	3.0 m	3.1m
Gas analyser	LI-COR 7500 (LI-COR Biosciences)	2.9 m	3.1m
Temperature-humidity sensor	HMP 45 (Vaisalla)	3.0m	3.1m
Net-radiometer	CNR1 (Kipp&Zonen)	2.0m	-
Net-radiometer	CM3 & CG3 (Kipp&Zonen)	-	1.5m
Rain gauge	tipping bucket	1m	1m
Soil moisture	Imko-TDR	-0.1,-0.3,-0.5	-0.1, -0.2, -0.4, -0.8, -1.60
Soil Temperature	Pt100	-0.025,-0.05,-0.1,-0.15,-0.2, -0.3,-0.5	-0.2, -0.4, -0.8, -1.60
Soil heat flux	HP3	-0.15	-
Water temperature	Pt100	-0.3	-
Logger	(Campbell Scientific Ltd.)	CR3000	CR5000

For displaying diurnal cycles, we used best to intermediate quality flagged data (Flag 1-6 out of 9 classes) and for model performance evaluation, we used best quality flagged data (Flag 1-3).

2.2.2. Coordinate rotation and footprint analysis

In this section we describe the coordinate rotation and footprint analysis which was conducted for both EC stations. We focus mainly on the analysis for NamUBT, since for NamITP detailed studies of footprint and data quality can be found for other data sets in Zhou et al. (2011) and Metzger et al. (2006).

The wind direction exhibits a strong diurnal pattern due to a land – lake circulation system, which can be seen in NamUBT data (Fig. 2).
During midday the wind came predominantly from the direction of the lake while in the morning, evening and night-time hours wind from the land surface dominated. Therefore NamUBT provides flux measurements over the land and water surface only for certain periods of the day, while NamITP always represents fluxes from the land surface.

For the necessary coordinate rotation we chose the planar-fit method according to Wilczak et al. (2001) which rotates the coordinate system into the mean streamlines by fitting a plane to individual half-hourly mean wind velocity components. While the mean vertical wind for the whole period is set to zero by this method, the individual half-hourly values do not vanish completely.

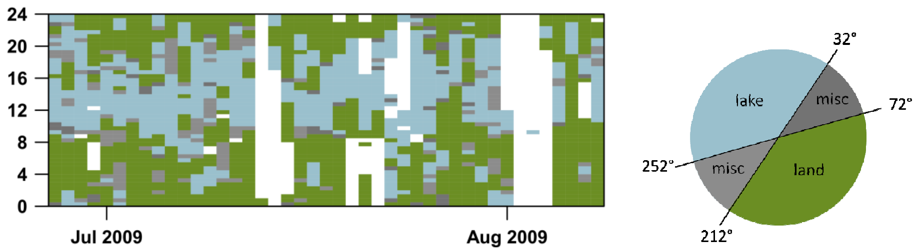

Fig. 2 Temporal distribution of the wind direction for the measuring period 27 June to 8 August and corresponding land use in upwind direction, classified according to the sectors shown on the right

Eddy-covariance measurements require a homogeneous flow field as a prerequisite. In our study this is not the case at NamUBT due to the transition from the plane lake surface to the gently sloping grassland. Paw U et al. (2000) and Finnigan (2003) suggest considering such terrain structures in the rotation procedure of the eddy-covariance data. Therefore the planar-fit rotation was applied for four different sectors according to Fig. 2. This procedure accounts for two planes with different slopes and two transition areas. Most of the vertical wind speed disappears after the rotation; 95% of the vertical wind speed data for the lake and for the land surface remain within ±0.1 ms^{-1} and ±0.07 ms^{-1}, respectively. For wind sectors parallel to the shoreline, 95% of the residual mean vertical wind velocity stays within ±0.12 ms^{-1}. These values stay within acceptable limits, compared to a multi-site quality analysis by Göckede et al. (2008).

The footprint analysis was conducted following Göckede et al. (2004, 2008). The approach is based on a Lagrangian stochastic forward model providing two dimensional contributions of source areas (Rannik et al. 2000). The resulting footprint for NamUBT (Fig. 3) shows that flux contributions from the lake are not found under stable conditions, which are typical for night times, while they can be found during unstable and neutral stratification. These findings match well with the distribution of wind directions mentioned above.

The footprint analysis includes not only the calculation of the footprint, but also the spatial distribution of flux quality according to Göckede et al. (2008), which enables the user to identify spatial patterns such as obstacles or heterogeneities contributing to the quality of the measured fluxes. In our study no such patterns could be identified for either station.

The average land use contribution to the measured signal for unstable and neutral stratification depending on the wind direction is shown in Fig. 4. The differentiation between stability classes were defined by the stability parameter with the measurement height and as the Obukhov length. The contribution from grass^{+} dominates the influence of the land surface in the respective wind sector. Influence of wetland and buildings are close to zero, even for stable conditions (not shown). The influence of grass^{-} is comparatively small. During stable conditions it is larger but these occur mostly at night, when flux differences between grass^{-} and grass^{+} are negligible. Therefore it is reasonable to relate land surface parameters to the wetter grass^{+} surface and we continue with a

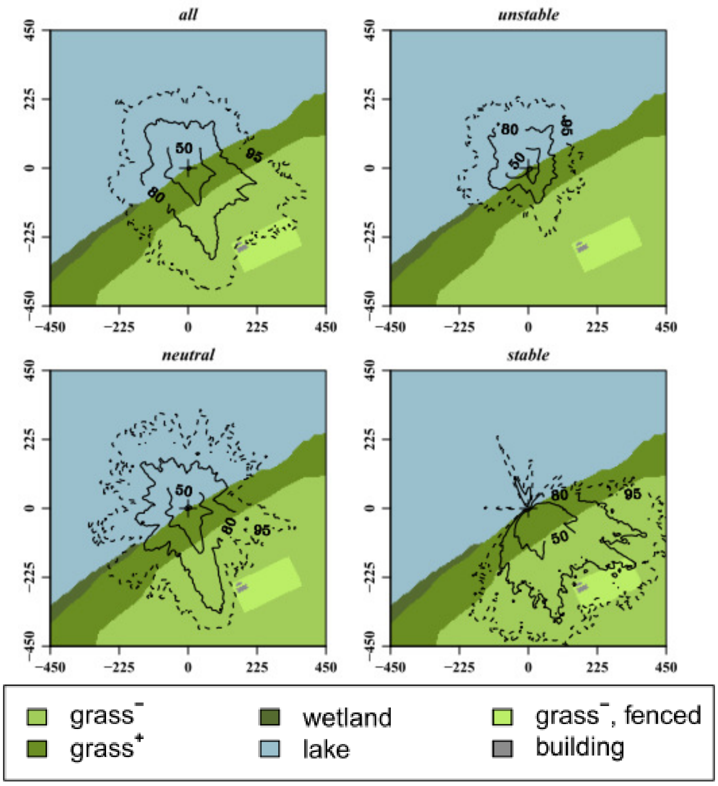

Fig. 3 Footprint climatology of NamUBT for the measuring period 27 June to 8 August. The figures show a combined footprint as well as footprints under unstable ($z\,L^{-1} < -0.0625$), neutral ($-0.0625 \le z\,L^{-1} \le 0.0625$) and stable stratification ($z\,L^{-1} > 0.0625$) of the atmosphere

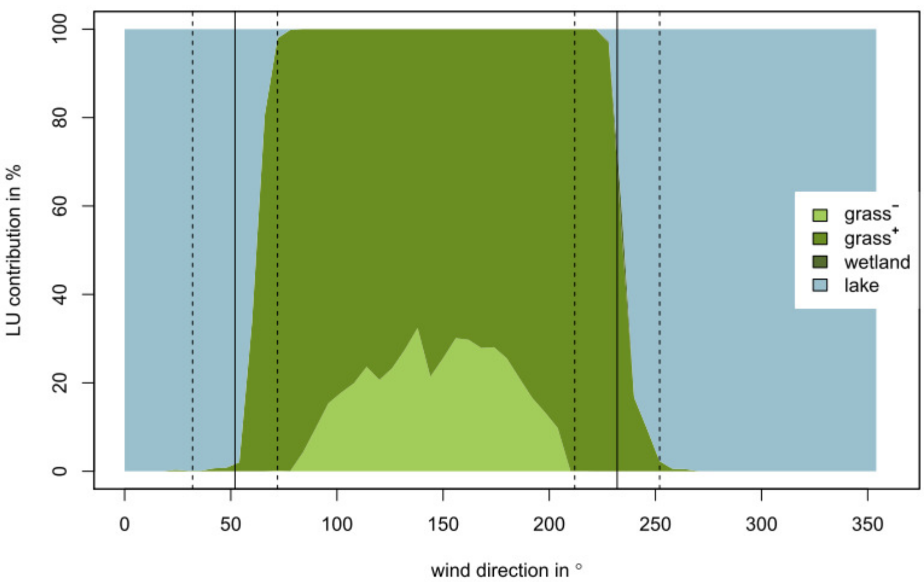

Fig. 4 Average land use contribution of NamUBT under unstable and neutral conditions ($z\,L^{-1} \le 0.0625$) for all wind directions. Solid lines represent the shoreline, dashed lines represent the borders of the sectors classified as land, lake and miscellaneous (misc) in Fig. 2

simplified land use scheme, discriminating only between land (grass^{+}) and lake for NamUBT. The footprint analysis of NamITP confirmed the representativeness of this station for grass^{-}.

2.2.3. Energy balance correction

Investigation of the energy balance closure (Foken 2008) at NamUBT shows that 70% of the energy balance is closed for the measurement period, a typical value for flux stations in heterogeneous landscapes. The energy balance closure correction (EBC) for the land surface fluxes was calculated after Twine et al. (2000), distributing the residual of the energy balance according to the Bowen ratio to the latent and sensible heat flux. We subsequently refer to this correction as EBC-Bo. Since Kracher et al. (2009) show with another data set that the land surface model SEWAB, which is used in this study (see section 2.3.1), roughly preserves the Bowen ratio measured by eddy-covariance, we regard EBC-Bo as a suitable correction for comparing the observations with SEWAB.

Nevertheless, recent studies suggest that a predominant fraction of the residual should be attributed to the sensible heat flux (Mauder and Foken 2006; Ingwersen et al. 2011; Foken et al. 2012). In case the reason for the unclosed energy balance is the existence of secondary circulations due to convection, as hypothesized by Foken et al. (2010, 2011); a physically meaningful correction would be related to buoyancy. The buoyancy flux Q_{HB} is driven by differences in air density and thus can be decomposed into a fraction governed by sensible heat (density differences due to temperature) and a fraction governed by latent heat (density differences due to moisture). The findings mentioned above suggest a correction where the residual of the energy balance is distributed to the sensible and latent heat flux according to their contribution to the buoyancy flux. This fraction depends on the Bowen ratio Bo and (to a small extent) on air temperature, and more than 90% are attributed to the sensible heat flux in the case of $Bo = 1$ and approximately 60% in the case of $Bo = 0.1$. We applied this correction, here named EBC-HB, for comparison with the more common EBC-Bo.

The EBC for the lake surface could not be estimated since only one sensor was used to measure the water temperature and no measurements of the storage flux within the lake or the sediment were conducted.

2.3. Modelling of the turbulent fluxes

Due to the location of NamUBT at the shore line, the wind direction determined whether turbulent fluxes over the land or the lake surface were measured, resulting in gaps of one or the other time series. Therefore a model was applied for each surface type and validated with the existing data. The results then complete the flux time series for the land and lake surface. In addition fluxes for grass^{-} at NamITP were modelled using the same land surface model.

Table 2. Governing equations for the hydrodynamic multilayer (HM) model (Foken 1979, 1984) with shallow water extension (Panin and Foken 2005)

Variable/component	Equation
Sensible heat flux	$Q_H^{ocean} = \Gamma\left(T_{sfc} - T_z\right)$ with $\Gamma = \kappa \cdot u_* \cdot \left[\left(\kappa \cdot \mathrm{Pr} - \frac{1}{6}\right) \cdot \delta_T^+ + 5 + \ln \frac{u_* \cdot z}{30\nu}\right]^{-1}$
Latent heat flux	Analogue to Q_H^{ocean}, assuming $\delta_T^+ \approx \delta_q^+$, $\Delta T^+ \approx \Delta q^+$, and replacing Pr with Sc
Stability dependence	Monin-Obukhov Similarity Theory, universal function after Foken and Skeib (1983)
Shallow water term	$Q_{H,E}^{SW} = Q_{H,E}^{ocean} \cdot \left(1 + k_{H,E}^{SW} \cdot hH^{-1}\right)$ with mean square wave height $h \approx 0.07 u_z^2 \left(gH \cdot (u_z^{-2})\right)^{0.6} \cdot g^{-1}$ (Davidan et al., 1985) and $k_{H,E}^{SW} \approx 2$ (Panin et al. 2006b)
Symbols	g gravity acceleration [ms^{-2}] H lake depth [m] h mean square wave height [m] $k_{H,E}^{SW}$ empirical correction factor [-] Pr Prandtl number [-] $Q_{H,E}^{ocean}$ sensible (H) and latent (L) heat flux without shallow water correction [Wm^{-2}] $Q_{H,E}^{SW}$ sensible (H) and latent (L) heat flux with shallow water correction [Wm^{-2}] q specific humidity [-] Sc Schmid number [-] T temperature [K] T^+ dimensionless temperature [-] u_* friction velocity [ms^{-1}] u_z wind velocity in height z [ms^{-1}] z measurement height [m] Γ profile coefficient [ms^{-1}] δ_T^+ dimensionless thickness of the molecular temperature boundary layer [-] κ von Kármán constant [-] ν kinematic viscosity [m^{2}s^{-1}]

2.3.1. Description of the models used

For the lake surface a hydrodynamic multilayer model (HM) by Foken (1979, 1984) was utilised. In order to account for multiple layers within the surface layer, turbulent fluxes are parameterised in HM using an integrated profile coefficient. As opposed to a single bulk coefficient the integrated profile coefficient resolves the molecular boundary layer, the viscous buffer layer, and the turbulent layer. Therefore near-surface exchange conditions are reflected according to hydrodynamic theory. Originally designed for exchange over the ocean, a correction term for shallow water (Panin and Foken 2005) was added, resulting in increased turbulent fluxes due to an enhanced mixing by higher waves in shallow water. The model has been successfully applied to simulate fluxes above ocean surfaces and lakes with a large fetch as well as over arctic snow fields (Panin et al. 2006b, Foken 1986, Lüers and Bareiss 2010). Details of the governing equations can be found in Table 2.

Turbulent fluxes over the land surface were simulated with the one-dimensional Surface Energy and WAter Balance scheme (SEWAB, Mengelkamp et al. 1999, 2001), a soil-vegetation-atmosphere-transfer model. All energy balance components are given separately. Turbulent fluxes are formulated with bulk approaches, atmospheric stability is considered. The main features are summarized in Table 3. The energy balance is then closed by iteration of the surface temperature. Evapotranspiration from vegetation is calculated with a single leaf concept in a Jarvis-type scheme after Noilhan and Planton (1989). Emphasis is placed on the description of soil processes. Soil temperature distribution and vertical soil water movement are described by the diffusion equation and the Richards equation, respectively. Soil moisture characteristics are inter-related following Clapp and Hornberger (1978).

Both models were forced with standard meteorological in-situ measurements. In order to provide gap-free input data, the small gaps within the forcing data from NamUBT were filled by linear interpolation while larger gaps were filled by linear regression using the data from NAMORS.

2.3.2. Application of the HM model to a shallow lake

The forcing data set for the HM model includes the standard meteorological parameters wind velocity, air temperature, humidity and air pressure. Radiation measurements are not required for the HM model, instead water surface temperature has to be supplied instead. In this study we used the measured water temperature (Table 1) as an estimate for the water surface temperature.

Wendisch and Foken (1989) investigated the relative error contribution of model parameter, amongst others water temperature, air temperature, air humidity and wind velocity, to the model output with a sensitivity analysis (Fourier Amplitude Sensitivity Test by Cukier et al., 1978). Assuming typical measurement errors for the initial parameter distribution they estimated that water temperature contributed up to 50% of the overall error while the influence of wind velocity, air temperature and humidity are comparatively small, each contributing 10-20% to the error. Since the temperature probe was only shielded against direct (downward) radiation, the effect of diffuse radiation on the accuracy of the water temperature measurements was evaluated. The radiation error has been estimated with a graphical analysis of short term temperature perturbations as related to rapid changes in downward shortwave radiation. Caused by the small fraction of diffuse radiation in the low air density of the Tibetan Plateau and sudden cloud cover changes, the shortwave radiation observations occasionally drop from 1000 Wm^{-2} to 150 Wm^{-2} (or increase in reverse) within a few minutes. The corresponding shifts in water temperature suggest a possible radiation error of approximately 0.2 K. Therefore water temperature measurements have been accepted for model forcing without correction.

The shallow water parameterisation included in the current version of the HM model accounts for an enhanced turbulent exchange due to increased wave heights in shallow water. Consequently, the turbulent fluxes increase with the mean square wave height (Table 2). Together with the wave height parameterisation after Davidan et al. (1985), additional parameters influence the model results. These are the wind velocity, lake depth and an empirical coefficient, which was set to 2 in this study following Panin et al. (2006b). In this study the water depth has been estimated as 1.5 m within the average footprint area of the measurement period.

Table 3. Governing equations for SEWAB (Mengelkamp et al. 1999, 2001) and adaptations to the Tibetan Plateau as used in Babel et al. (2013).

Variable/component	Equation
Net radiation	$R_{net} = -R_{swd}(1-a) - R_{lwd} + \epsilon\sigma T_{sfc}^4$ R_{swd} and R_{lwd} in forcing data set
Ground heat flux	$Q_G = \lambda_s\left(T_{sfc} - T_{S1}\right) \cdot \Delta z_{S1}^{-1}$
Sensible heat flux	$Q_H = C_H \rho c_p u(z)\left(T_{sfc} - T(z)\right)$
Latent heat flux	Composed of bare soil E_s, wet foliage E_f and plant transpiration E_{tr} after Noilhan and Planton (1989) $E_s = C_E \rho u(z)\left(\alpha q_s\left(T_{sfc}\right) - q(z)\right)$ $E_f = C_E \rho u(z)\left(q_s\left(T_{sfc}\right) - q(z)\right)$ $E_{tr} = (R_a - R_s)^{-1} \rho\left(q_s\left(T_{sfc}\right) - q(z)\right)$
Stability dependence	C_H after Louis (1979), $C_E = C_H$
Adaptations to TP:	
I) Soil thermal conductivity	$\lambda_s(\Theta) = \lambda_{dry} + \left(\lambda_{sat} - \lambda_{dry}\right) \exp[k_T(1 - \Theta_{sat}/\Theta)]$, k_T=0.36 (Yang et al. 2005)
II) thermal roughness length	$z_{0h} = 70\nu \cdot u_*^{-1} \cdot \exp(-\beta u_*^{0.5} \lvert T_* \rvert^{0.25})$ $\beta = 7.2\ s^{0.5} m^{-0.5} K^{-0.25}$ (Yang et al. 2008)
III) bare soil evaporation	$\alpha = \begin{cases} 1 - \left(1 - \frac{\Theta}{\Theta_{FC}}\right)^2, & \Theta \leq \Theta_{FC} \\ 1, & \Theta > \Theta_{FC} \end{cases}$ (Mihailović et al. 1993)
Symbols	a albedo [-] C_H Stanton number [-] C_E Dalton number [-] c_p air heat capacity [J kg^{-1} K^{-1}] q specific humidity [-] q_s saturation specific humidity [-] R_a turbulent atmospheric resistance [s m^{-1}] R_s stomata resistance [s m^{-1}] R_{lwd} long wave downward radiation [Wm^{-2}] R_{swd} short wave downward radiation [Wm^{-2}] T temperature [K] T_* dynamic temperature scale [K] T_{sfc} surface temperature [K] T_{S1} temperature in first soil layer [K] u_* friction velocity [ms^{-1}] z measurement height [m] Δz_{S1} thickness of first soil layer [m] α dependence factor of soil air humidity to soil water content [-] ϵ emissivity [-] Θ volumetric soil water content [-] Θ_{sat} volumetric soil water content at saturation, porosity [-] Θ_{FC} volumetric soil water content at field capacity [-] λ_s soil thermal conductivity [$Wm^{-1}K^{-1}$] λ_{dry} soil thermal conductivity for dry soil [$Wm^{-1}K^{-1}$] λ_{sat} soil thermal conductivity, soil moisture at saturation [$Wm^{-1}K^{-1}$] ρ air density [kg m^{-3}] σ Stefan Boltzmann constant [$Wm^{-2}K^{-4}$] ν kinematic viscosity [m^2s^{-1}]

The influence of the shallow water term becomes dominant with increasing wind velocity and decreasing water depth. Calculation of the shallow water equations described in Table 2 with the estimated water depth of 1.5 m and the average wind velocity of 4 ms^{-1} yields an increase in turbulent fluxes of 14.5 % compared to deep water conditions. Consideration of small changes in wind velocity and water depth yields local sensitivities of roughly 2.9% of the deep water fluxes per ms^{-1} and -3.9% per m water depth, respectively. For high wind velocities (10 ms^{-1}) the shallow water extension causes an increase of 30.1% with sensitivities of 2.4% per ms^{-1} and -8.0% per m water depth. Assuming a typical error of 0.3 ms^{-1} for wind velocity and variability of the lake depth up to 1 m within the footprint leads to flux uncertainties of 1% and 4%, respectively. These errors, although not negligible, are within the uncertainty range of the EC flux measurements.

2.3.3. Adaptation of SEWAB

On the Tibetan Plateau a strong diurnal cycle of the surface temperature during dry periods over bare soil and short grassland have been observed, which typically leads to an overestimation of surface sensible heat flux (Yang et al. 2009, Hong and Kim 2010). To account for these conditions, SEWAB has been adapted for the Tibetan Plateau by (i) a revised calculation of the soil thermal conductivity as used in Yang et al. (2005), (ii) a different formulation of the thermal roughness length after Yang et al. (2008) and (iii), by changing the parameterisation of bare soil evaporation according to Mihailović et al. (1993). The formulations can be seen in Table 3.
These changes have been implemented using flux data from NamITP station and flux data from NamUBT corresponding to land surface (Babel et al. 2013), who evaluated this adaptation as an improvement compared to the original version.

SEWAB has been run offline, forced by measurements of precipitation, air temperature, wind velocity, air pressure, relative humidity and downwelling shortwave and longwave radiation. The respective parameters for both land surface types were estimated by a combination from the in-situ measurements and laboratory investigation of soil characteristics (Chen et al., 2012). Surface emissivity, leaf area index and minimum stomatal resistence have been derived from various sources (Yang et al. 2009, Hu et al. 2009, Alapaty et al. 1997)

2.4. Statistics

For evaluation of model performance, simple comparisons were carried out using the bias $B = N^{-1} \sum_{i=1}^{N} (P_i - O_i)$ and the mean absolute error $MAE = N^{-1} \sum_{i=1}^{N} |P_i - O_i|$, with O as the observations and P the model predictions.
In equivalence to the *MAE* the differences between two time series of predictions can be quantified and we define the desired measure as

$$\delta_{sim} := N^{-1} \sum_{i=1}^{N} |P_{1,i} - P_{2,i}| \qquad (1)$$

with P_1 and P_2 as predictions from the respective land use types 1 and 2. The Nash-Sutcliffe coefficient NS serves as a goodness of fit measure

$$NS = 1 - \frac{\sum_{i=1}^{N} (P_i - O_i)^2}{\sum_{i=1}^{N} (O_i - \bar{O})^2} \qquad (2)$$

with $\bar{O}$ as the mean of the observations.

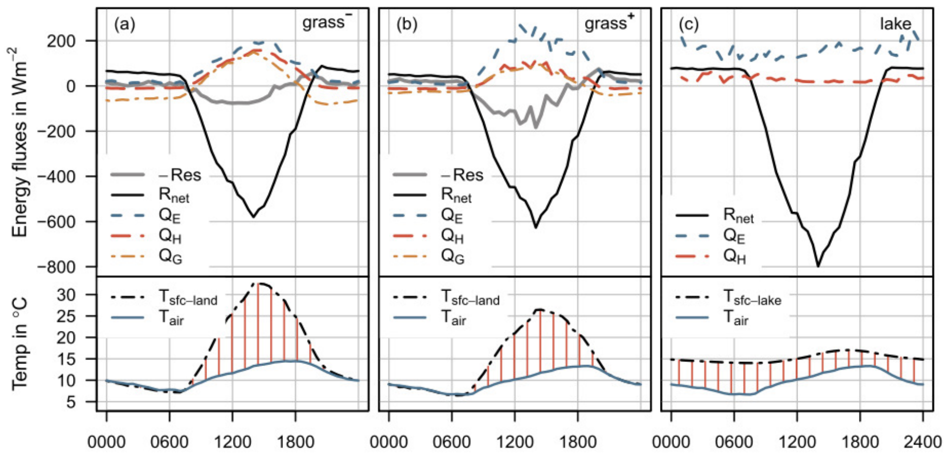

Fig. 5 Mean diurnal energy fluxes for the whole measurement period, separated for (a) grass^{-}, (b) grass^{+} and (c) lake; for land surfaces, all components are measured; lake fluxes: the net radiation is calculated from measured downwelling radiation and using an albedo of 0.06 and the lake surface temperature with an emissivity of 0.96; the lower panel shows diurnal surface and air temperature. The time axis is displayed in Beijing standard time (CST), mean local solar noon during the observation period is at 1400 CST

3. Results

3.1. Flux measurements

The measured energy fluxes over the lake surface and land (grass^{+}) show pronounced differences in their magnitude and dynamics. The daytime net radiation is substantially higher over the lake surface, caused by a lower albedo and decreased upwelling longwave radiation due to damped surface temperatures over the lake (Fig. 5c). However, upward radiation components were only measured over the land surface; for the lake surface they were parameterised using an albedo of 0.06 and the lake surface temperature with an emissivity of 0.96.

As expected for the monsoon season on the Tibetan Plateau, the latent heat flux over the land surface was larger than the sensible heat flux (Fig. 5a,b). This observation is in agreement with e.g. Gu et al. (2005) and Ma and Ma (2006). The mean diurnal cycles of surface and air temperature also show the typical dynamics above land surface, with unstable stratification during daytime but higher surface temperatures are observed over grass^{-}. Ground heat flux and sensible heat flux are in the same order of magnitude for each land surface again with higher values for grass^{-}. In consequence the latent heat flux is lower over this land surface.

The turbulent fluxes over the lake, however, do not show a diurnal cycle, but remain constant over the day. The energy input from radiation is stored in the lake body and is available at any time as indicated by the lake surface temperature in

Table 4: Model performance of turbulent fluxes for the three land use types and two energy balance correction methods for the land observations: n (number of observations), bias, MAE (mean absolute error), offset and slope from linear regression (mean geometric regression) as well as NS (Nash-Sutcliffe coefficient) and R^2.

Flux	Land use	EBC	n	Bias	MAE	Offset	Slope	NS	R²
				[Wm^{-2}]	[Wm^{-2}]	[Wm^{-2}]	[-]	[-]	[-]
Q_H	grass$^-$	Bo	627	52.2	55.5	36.8	1.13	0.26	0.80
		HB	572	38.3	55.5	36.9	1.01	0.36	0.62
	grass$^+$	Bo	81	18.5	23.8	17.2	1.02	0.61	0.78
		HB	71	-24.4	40.5	12.9	0.7	0.38	0.52
	lake	-	327	-2.7	7.6	5.3	0.72	0.75	0.79
Q_E	grass$^-$	Bo	627	-10.8	45.3	-8.6	0.99	0.70	0.73
		HB	572	-0.4	42.0	-14.3	1.1	0.68	0.74
	grass$^+$	Bo	81	-28.6	50.8	13.5	0.77	0.60	0.69
		HB	71	1.7	23.4	5.4	0.98	0.82	0.82
	lake	-	392	-23.3	30.3	-8.5	0.9	0.50	0.64

Fig. 5c. No complete energy balance could be estimated over the lake surface, as no measurements exist for the heat storage in the water body and heat fluxes into the sediment.

Evaporation is comparably high for lake surfaces due to high wind velocities of 4 ms^{-1} on average. In addition, high lake surface temperatures, caused by the shallow water table and the small extent of this lake, lead to unstable stratification even during daytime (Fig. 5c). Therefore turbulent exchange is enhanced compared to stable stratification typically found over lake surfaces during daytime (e.g. Beyrich et al. 2006, Nordbo et al. 2011).

3.2. Model performance

Different measures for model performance are summarised in Table 4. The results from grass$^+$ simulations show reasonable performance, although there are only few observations left after filtering, separation and energy balance closure correction (Fig. 6). In case of EBC-Bo corrected observations, the latent heat flux is slightly underestimated while the simulation of the sensible heat flux resembles the measurements quite well. The opposite is true when using the buoyancy flux method for energy balance closure correction (EBC-HB). The correlation is affected in a similar way. Good R^2 values are achieved for the sensible heat flux corrected using EBC-Bo and latent heat flux corrected using EBC-HB, and they decrease for the other two cases. Lake surface modelling yields reasonable coherence to the EC observations within the footprint of the measurements, with a bias of -23.3 W m^{-2} and -2.7 W m^{-2} for the latent heat flux Q_E and the sensible heat flux Q_H, respectively. For grass$^-$ at NamITP, mean absolute errors for sensible heat flux are larger, mainly caused by the bias, although a good correlation is obtained in the case of EBC-Bo corrected observations. Aside from model deficiencies, the reason for the remaining bias can be attributed to uncertainties in estimation of the observed ground heat flux due to high gravel content in the soil and a lack of temperature measurements in the topmost soil layer.

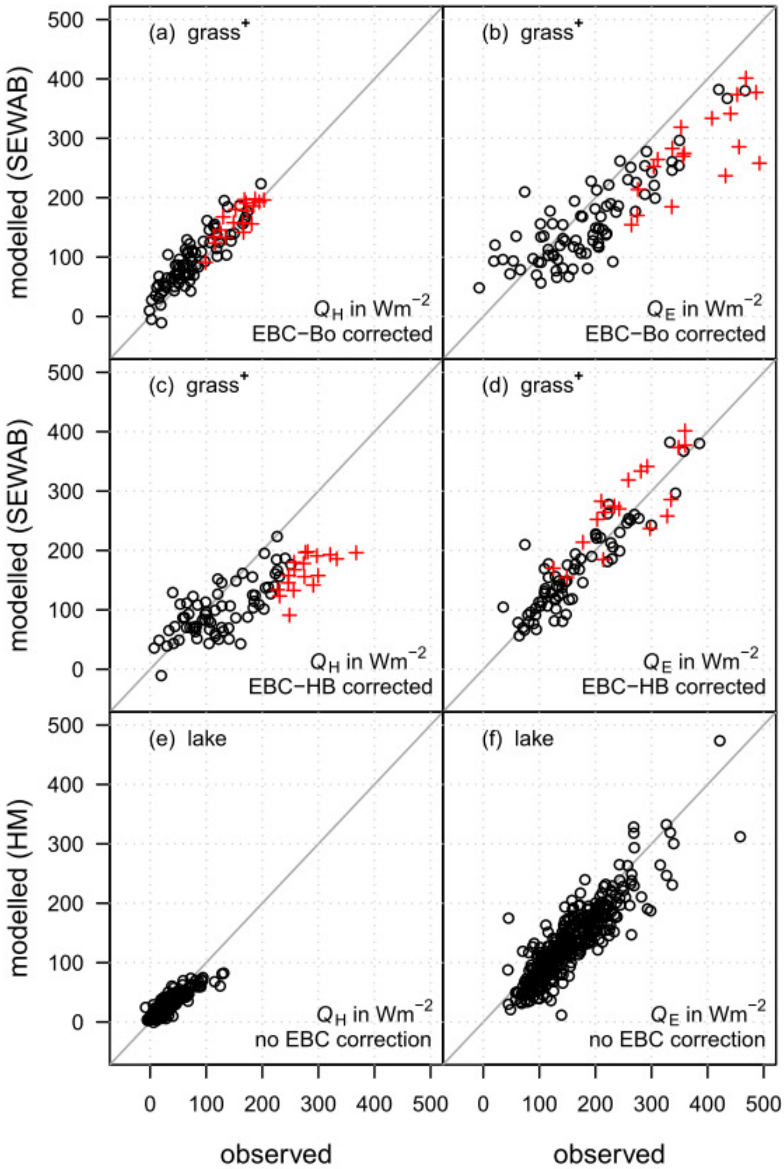

Fig. 6 Scatterplots of modelled and observed turbulent fluxes. For land surface flux observations (grass$^+$) vs. SEWAB model simulations, observations are energy balance corrected with the Bowen ratio method (*a,b*) and with the buoyancy method (*c,d*). Turbulent fluxes without EBC correction over lake vs. HM model runs (*e,f*). Model performance is indicated with the Nash-Sutcliffe coefficient (NS coef), bias and the squared Pearson correlation coefficient. Red crosses indicated data excluded due to residuals $-Res > 150\ Wm^{-2}$

3.3. Footprint and spatial integration

In the previous section we have shown that eddy-covariance measurements, selected according to their footprint as pure fluxes from each surface type, can be represented by SEWAB in case of grassland and by the HM model in case of the lake surface. However, a part of the measurements show contributions from more than one land use type as well. The footprint concept enables us to link the simulations even with such observations. For each time step, the footprint approach provides the relative contribution of all involved surfaces to the measured fluxes. The simulations are then related to the observations by calculating a weighted mean from the output of both models according to the actual land use contribution. This is shown with the footprint integrated simulations for lake and grass^{+} together with the EC observations at NamUBT in Fig. 7 for three different situations: 17 July – changing conditions under moderate wind velocities, 5 August – typical day with land - lake circulation and moderate winds of about 2-6 ms^{-1}, and 6 August – situation with larger than average wind speeds of about 6 ms^{-1}. In all selected situations the eddy-covariance measurements can be closely modelled by the footprint integrated simulation. This also holds for measurements with contributions from both surfaces, seen in some events on 17 July and 5 August. Due to the different exchange of each surface with its atmosphere over the course of the day, instantaneous turbulent fluxes can show differences of up to 200 Wm^{-2}. The performance of the footprint integrated simulation is displayed in Fig. 8 for the whole period. Situations with contributions from both surface types larger than 20% (misc) are highlighted. The simulations for such situations follow the same pattern as simulations for the pure surface types (contribution of a single surface greater than 80%). Miscellaneous footprints, however, did not occur for situations with very high fluxes.

3.4. Flux heterogeneity at Nam Co

It is well known that heterogeneous surfaces affect the landscape scale fluxes. The presented measurements have shown that the fluxes over land and lake surfaces behave differently. To consider the most abundant surfaces near Nam Co station, grass^{-} at NamITP has also been included in addition to the observations and simulations of grass^{+} and lake at NamUBT. Fig. 9 shows the mean diurnal cycles of measured fluxes, corrected with EBC-Bo for land surfaces, and modelled fluxes. The model simulations resemble the observed characteristics of the different surfaces in a reasonable sense. Since simulations overestimated the sensible heat flux for both land surfaces, the differences between land use types were maintained.

The obvious differences in characteristics of the investigated surfaces, especially between land and lake, are also reflected in mean fluxes for the whole period (Fig. 10). The two land surface types already differ in the longwave radiation balance. As expected, the mean latent heat flux became more dominant with increasing soil moisture for the land surfaces. The evaporation over the small lake is even higher, due to its shallow water table resulting in comparatively high surface temperatures. Mean differences of sensible and latent heat flux between grass^{+} and grass^{-} are 24.0 Wm^{-2} and -33.5 Wm^{-2}, respectively, and between grass^{+} and lake are -27.3 Wm^{-2} and 22.3 Wm^{-2}, respectively.

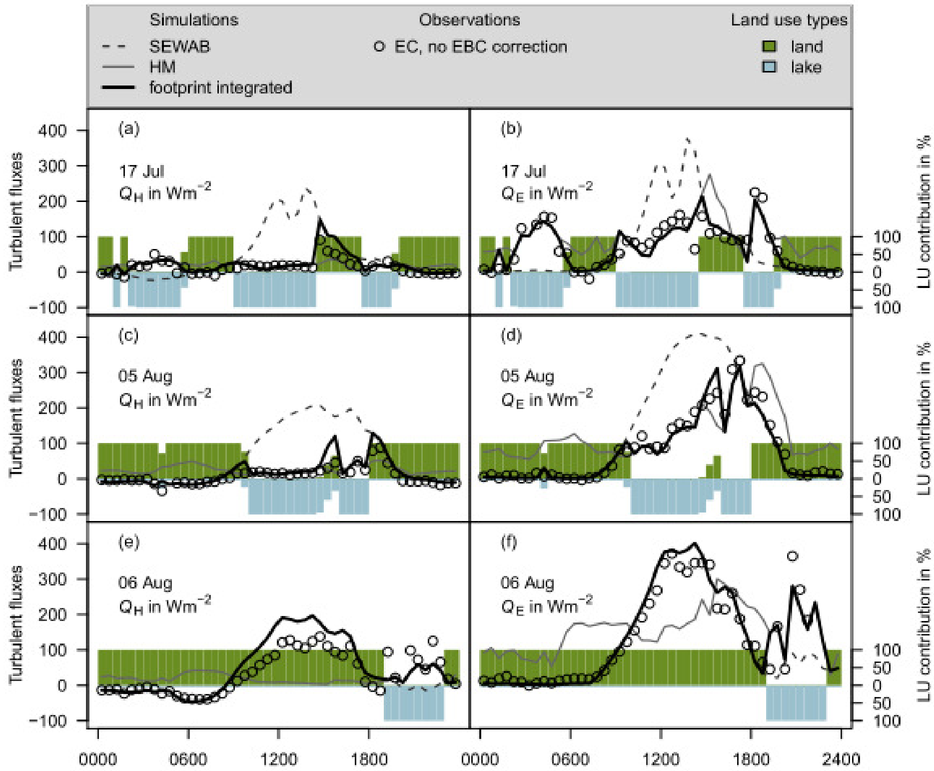

Fig. 7 Source weight integrated modelled fluxes at NamUBT, 17 July (*a,b*), 5 August (*c,d*), 6 August (*e,f*). Displayed are simulated fluxes with SEWAB (dashed line) and HM (solid grey line) and integrated simulations (solid black line) according to contributions of lake or land within the footprint. Observations (not energy balance corrected) are shown as black circles. The land use contribution in % is indicated as bar plot, with upwind situations from the land in green and upwind situations from lake in blue. The time axis is displayed in Beijing standard time (CST), mean local solar noon during the observation period is at 1400 CST

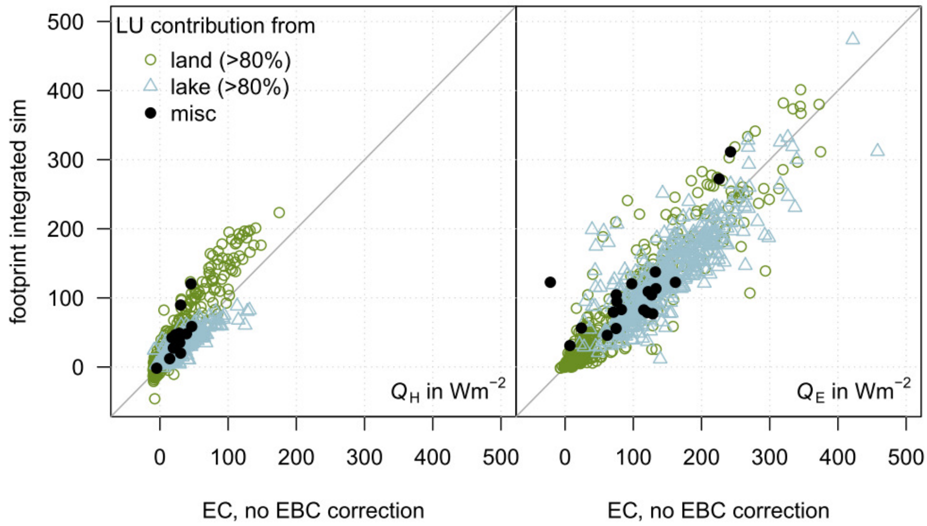

Fig. 8 Observations vs. footprint integrated model simulations at NamUBT. Three classes of data are presented, cases with a greater contribution than 80% of one land use type are considered as representative. The misc cases contain all fluxes with a contribution less than 80% for both land use types. Since no EBC correction could be performed for the lake data, all data is shown without correction for better inter comparison

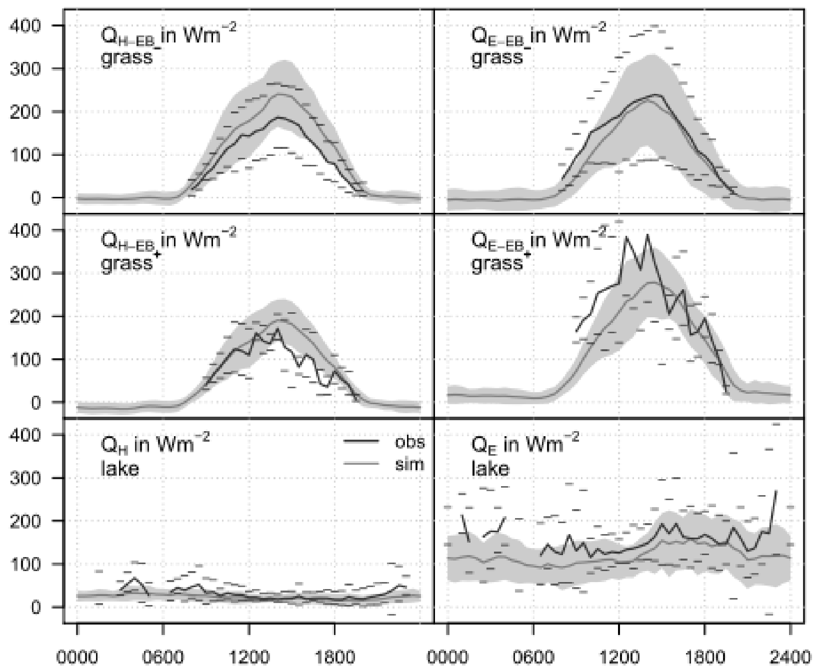

Fig. 9 Mean diurnal cycles for the whole measurement period. Observed fluxes (corrected with EBC-Bo) are denoted by black solid lines, the horizontal bars indicate the respective standard deviation; grey lines show the modelled fluxes with standard deviations given by the grey shaded area. The time axis is displayed in Beijing standard time (CST), mean local solar noon during the observation period is at 1400 CST

Table 5: Mean absolute differences (δ_{sim}) between simulations of grass$^+$ and the other two land use types: grass$^-$ and lake. Numbers in parentheses are the number of data points used, corresponding to the number of observations used to calculate the MAE for grass$^+$ in Table 4.

	Q_H	Q_E
grass$^+$ – grass$^-$	43.3 (81) 45.9 (71)	59.5 (81) 59.1 (71)
grass$^+$ – lake	76.1 (81) 83.5 (71)	68.1 (81) 57.8 (71)

Furthermore, we investigated whether these mean differences were substantial with respect to the performance of the simulation. Table 5 displays the mean absolute differences δ_{sim} between grass$^+$ and the other two surface types. As δ_{sim} is calculated for the data subset used to evaluate the model performance at grass$^+$ (n=81 for EBC-Bo and n=71 for EBC-HB), it can be compared directly to the respective MAE for grass$^+$. When comparing the sensible heat flux of the two land surfaces, mean differences between simulations slightly exceed the respective MAE, and it is substantially higher in the other cases, especially between the lake surface and grass$^+$. Obviously this also holds true when comparing grass$^-$ with lake (not shown). This suggests that the differences in fluxes between land use types exceed the uncertainty with respect to model simulation.

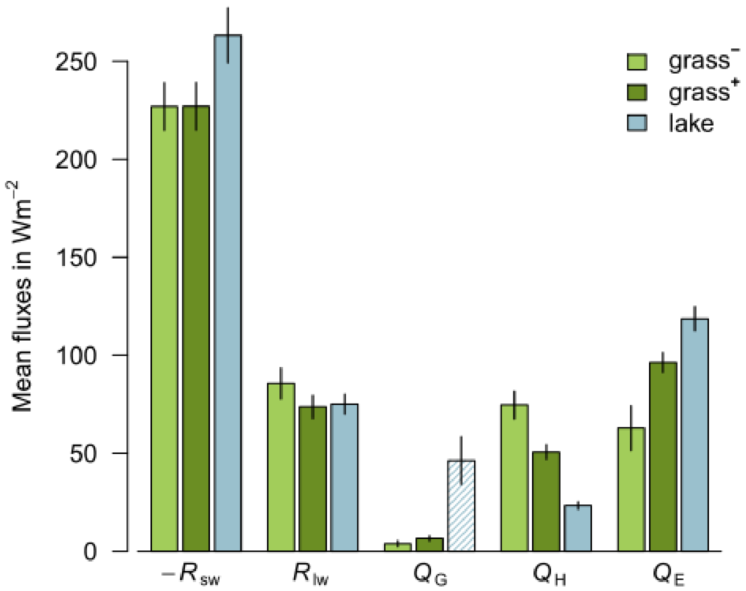

Fig. 10 Mean fluxes for the three surface types (grass$^-$, grass$^+$, lake) from observation-based simulations. Land surfaces fluxes are SEWAB output. Net shortwave radiation (R_{sw}) and net longwave radiation (R_{lw}) for the lake surface are calculated as explained for Fig.5. The residual of the lake energy balance is shown as hatched bar (Q_g); it sums up the energy fluxes not accounted for, e.g. storage change in the water body and flux into the sediment. For land surface fluxes, Q_g represents the ground heat flux. Error bars indicate 1.96 times the standard error of the mean, based on daily mean fluxes; assuming normal distribution and statistical independence of daily mean fluxes the bars would correspond to the 95% confidence interval

4. Conclusions

Turbulent fluxes over wet grassland and a shallow lake were measured with a single eddy-covariance complex at a shallow lake in the Nam Co basin during the monsoon season in 2009. The measurements were split up according to the underlying surface by footprint analysis, and the coordinate rotation for this non-flat terrain has been successfully performed with a sector-wise application of the planar-fit method. Energy balance closure algorithms were deployed, and gap-free time series were derived by surface modelling. We showed that the modelled time series can be linked to the measurements by integration according to the contribution of each surface type. Finally, this data set was compared with observed and modelled fluxes from the nearby ITP station with a target land use of dry grassland. Sharp differences in characteristics of turbulent fluxes from the three dominant land use types found in close vicinity to the lake were revealed.

Both models we used, HM and SEWAB, are able to reproduce the characteristics, magnitude and dynamics reasonably well without deploying optimisation algorithms. There are no parameters which need to be tuned for the HM model except the lake depth. The sensitivity and error analysis for the HM model suggests that expected errors do not exceed the measurement uncertainty of eddy-covariance fluxes. The model parameters for SEWAB have been constrained by measurements. However, a bias remains, in particular at the grass^{-} site. This depends not only on model deficiencies, but on the method applied for the energy balance closure correction as well. As long as the underlying mechanism causing the gap is not specified clearly (Foken et al. 2011), this error cannot be exactly determined. On the other hand, measurements of available energy are prone to errors as well, especially in the estimation of the ground heat flux. Nonetheless, it was shown that the differences among land use types of dry grassland, wet grassland and lake exceed the simulation errors. We therefore assume that the simulated time series are able to resolve the differences between the land use types involved here.

The footprint (source weight) integrated modelled fluxes resemble the observations at NamUBT reasonably well, even for conditions where both lake and grass^{+} contribute to the measured flux. With the tile approach, a grid cell with edge lengths of 1-5 km can be directly linked to the simulation as long as the relative contribution of each land use type is known for this cell. Our finding shows that the tile approach is valid in this terrain for spatial integration. Therefore representative flux simulations can be given for each time step for comparison with remote sensing data.

The measurements over dry grassland at NAMORS are considered to be a reference for the land surface exchange in the Nam Co region. However, in regional estimates the pronounced differences in the fluxes from the three investigated surface types make it obvious that the fluxes above the lake and moist grassland should be taken into account as well. Daytime turbulent fluxes over the lake surface can differ from the land surface fluxes up to 200 Wm^{-2}. Therefore the land use distribution within a remote sensing pixel or grid cell for mesoscale modelling has to be carefully determined before validating with the dry grassland station. This potential representation error can be reduced by integrating the simulated fluxes of adjacent land use types according to their contribution to the respective grid cell.

The conducting of eddy covariance measurements over lake surfaces on the Tibetan Plateau poses a rarely-met challenge. Nevertheless, more accurate flux estimates will be necessary since a significant fraction of the Tibetan Plateau is covered with lakes of various sizes and therefore different characteristics. Based on this study, we can conclude that theoretical requirements for eddy-covariance are not substantially violated by the topography at the shoreline station and that the data can be accepted for the HM model validation. Unfortunately data from the lake surface was only available for unstable and neutral stratification. We showed that the HM model can be used to estimate lake evaporation for these conditions at a high quality standard and a temporal resolution, even resolving the diurnal course. This can be derived from standard land-based meteorological measurements, and a representative surface temperature being the only measurement required directly from the lake. Lake surface exchange under stable conditions, however, could not be validated, but the results from Panin et al. (2006b) indicate reasonable performance also for stable conditions. On the other hand, due to the prevailing high wind velocities, strong stable stratification above lake surfaces on the Tibetan Plateau are unlikely. However, temperature profile measurements at different locations in the lake (and sediment, where indicated) would be a costly but valuable addition to estimate necessary storage terms and thereby the observed energy balance closure. Especially for large lakes like the Nam Co, the estimation of water temperature requires more efforts, since multiple locations within the lake should be sampled.

Acknowledgements: This work was funded by the German Research Foundation (Deutsche Forschungsgemeinschaft; DFG) Priority Programme 1372 “Tibetan Plateau: Formation, Climate, Ecosystems”(TiP) and CEOP-AEGIS, a Collaborative Project/Small or medium-scale focused research project – Specific International Co-operation Action coordinated by the University of Strasbourg, France and funded by the European Commission under FP7 topic ENV.2007.4.1.4.2 “Improving observing systems for water resource management”. The authors would like to thank everybody who participated in the collection of the data on the Tibetan plateau, especially the colleagues from the ITP for logistical support during the field campaign. Furthermore the authors acknowledge H.T. Mengelkamp for providing the source code of SEWAB.

References

Alapaty K, Pleim JE, Raman S, Niyogi DS, Byun DW (1997) Simulation of atmospheric boundary layer processes using local- and nonlocal-closure schemes. J Appl Meteorol 36(3):214–233, DOI 10.1175/1520-0450(1997)036<0214:SOABLP>2.0.CO;2

Babel W, Chen Y, Biermann T, Yang K, Ma Y, Foken T (submitted 2013) Adaptation of a land surface scheme for modeling turbulent fluxes on the Tibetan plateau under different soil moisture conditions, submitted to J. Geophys. Res.

Beyrich F, Leps J, Mauder M, Bange J, Foken T, Huneke S, Lohse H, Lüdi A, Meijninger WML, Mironov D, Weisensee U, Zittel P (2006) Area-Averaged Surface Fluxes Over the Litfass Region Based on Eddy-Covariance Measurements. Boundary-Layer Meteorol 121(1):33–65, DOI 10.1007/s10546-006-9052-x

Biermann T, Babel W, Olesch J, Foken T (2009) Documentation of the micrometeorological experiment, Nam Tso, Tibet, 25 th of June – 8 th of August 2009. Work Report University of Bayreuth, Dept. of Micrometeorology, ISSN 1614-8916, 41, 38 pp., URL http://opus.ub.uni-bayreuth.de/opus4-ubbayreuth/frontdoor/index/index/docId/626

Boos WR, Kuang Z (2010) Dominant control of the South Asian monsoon by orographic insulation versus plateau heating. Nature 463(7278):218–222, DOI 10.1038/nature08707

Chen Y, Yang K, Tang W, Qin J, Zhao L (2012) Parameterizing soil organic carbon's impacts on soil porosity and thermal parameters for Eastern Tibet grasslands. Sci China Earth Sci 55:1001–1011, DOI 10.1007/s11430-012-4433-0

Clapp RB, Hornberger GM (1978) Empirical equations for some soil hydraulic properties. Water Resour Res 14(4):601–604

Cukier R, Levine H, Shuler K (1978) Nonlinear sensitivity analysis of multi-parameter model systems. J Comput Phys 26(1):1–42, DOI 10.1016/0021-9991(78)90097-9

Davidan I, Lopatuhin L, Rogkov V (1985) Volny v okeane (waves in the ocean). Gidrometeoizdat, Leningrad, 256pp.

Finnigan J, Clement R, Malhi Y, Leuning R, Cleugh H (2003) A re-evaluation of long-term flux measurement techniques part i: Averaging and coordinate rotation. Bound-Lay Meteorol 107:1–48, DOI 10.1023/A:1021554900225

Foken T (1979) Vorschlag eines verbesserten Energieaustauschmodells mit Berücksichtigung der molekularen Grenzschicht der Atmosphäre. Z Meteorol 29:32–39

Foken T (1984) The parameterisation of the energy exchange across the air-sea interface. Dynam Atmos Oceans 8(3-4):297–305, DOI 10.1016/0377-0265(84)90014-9

Foken T (1986) An operational model of the energy exchange across the air-sea interface. Z Meteorol 36:354–359

Foken T (2008) The energy balance closure problem: An overview. Ecol Appl 18(6):1351–1367, URL http://www.jstor.org/stable/40062260

Foken T, Skeib G (1983) Profile measurements in the atmospheric near-surface layer and the use of suitable universal functions for the determination of the turbulent energy exchange. Bound-Lay Meteorol 25:55–62, DOI 10.1007/BF00122097

Foken T, Wichura B (1996) Tools for quality assessment of surface-based flux measurements. Agr Forest Meteorol 78(1-2):83–105

Foken T, Göckede M, Mauder M, Mahrt L, Amiro B, Munger W (2004) Post-Field Data Quality Control. In: Lee X, Massman W, Law B (eds) Handbook of Micrometeorology, Kluwer, Dordrecht, pp 181-208

Foken T, Mauder M, Liebethal C, Wimmer F, Beyrich F, Leps JP, Raasch S, DeBruin H, Meijninger W, Bange J (2010) Energy balance closure for the LITFASS-2003 experiment. Theor Appl Climatol 101:149–160 DOI 10.1007/s00704-009-0216-8

Foken T, Aubinet M, Finnigan JJ, Leclerc MY, Mauder M, Paw U KT (2011) Results of a panel discussion about the energy balance closure correction for trace gases. B Am Meteorol Soc 92(4): ES13–ES18 DOI 10.1175/2011BAMS3130.1

Foken T, Leuning R, Oncley SR, Mauder M, Aubinet M (2012) Corrections and data quality control. In: Aubinet M, Vesala T, Papale D (eds) Eddy Covariance: A Practical Guide to Measurement and Data Analysis, Springer Atmospheric Sciences, Dordrecht, pp 85–131, DOI 10.1007/978-94-007-2351-1_4

Frauenfeld OW, Zhang T, Serreze MC (2005) Climate change and variability using European Centre for Medium-Range Weather Forecasts reanalysis (ERA-40) temperatures on the Tibetan Plateau. J. Geophys. Res. 110(D2):D02101, DOI 10.1029/2004JD005230

Gerken T, Babel W, Hoffmann A, Biermann T, Herzog M, Friend AD, Li M, Ma Y, Foken T, Graf HF (2012) Turbulent flux modelling with a simple 2-layer soil model and extrapolated surface temperature applied at Nam Co lake basin on the Tibetan Plateau. Hydrol Earth Syst Sci 16(4):1095–1110, DOI 10.5194/hess-16-1095-2012

Göckede M, Rebmann C, Foken T (2004) A combination of quality assessment tools for eddy covariance measurements with footprint modelling for the characterisation of complex sites. Agr Forest Meteorol 127(3-4):175–188, DOI 10.1016/j.agrformet.2004.07.012

Göckede M, Foken T, Aubinet M, Aurela M, Banza J, Bernhofer C, Bonnefond JM, Brunet Y, Carrara A, Clement R, Dellwik E, Elbers J, Eugster W, Fuhrer J, Granier A, Grunwald T, Heinesch B, Janssens IA, Knohl A, Koeble R, Laurila T, Longdoz B, Manca G, Marek M, Markkanen T, Mateus J, Matteucci G, Mauder M, Migliavacca M, Minerbi S, Moncrieff J, Montagnani L, Moors E, Ourcival JM, Papale D, Pereira J, Pilegaard K, Pita G, Rambal S, Rebmann C, Rodrigues A, Rotenberg E, Sanz MJ, Sedlak P, Seufert G, Siebicke L, Soussana JF, Valentini R, Vesala T, Verbeeck H, Yakir D (2008) Quality control of carboeurope flux data – part 1: Coupling footprint analyses with flux data quality assessment to evaluate sites in forest ecosystems. Biogeosciences 5(2):433–450, DOI 10.5194/bg-5-433-2008

Gu S, Tang Y, Cui X, Kato T, Du M, Li Y, Zhao X (2005) Energy exchange between the atmosphere and a meadow ecosystem on the Qinghai–Tibetan Plateau. Agr and Forest Meteorol 129(3-4):175–185. doi:10.1016/j.agrformet.2004.12.002

Haginoya S, Fujii H, Kuwagata T, Xu J, Ishigooka Y, Kang S, Zhang Y (2009) Air-lake interaction features found in heat and water exchanges over Nam Co on the Tibetan Plateau. Sola 5:172–175, DOI 10.2151/sola.2009-044

Hong J, Kim J (2010) Numerical study of surface energy partitioning on the Tibetan Plateau: comparative analysis of two biosphere models. Biogeosciences 7(2):557–568, DOI 10.5194/bg-7-557-2010

Hu Z, Yu G, Zhou Y, Sun X, Li Y, Shi P, Wang Y, Song X, Zheng Z, Zhang L, Li S (2009) Partitioning of evapotranspiration and its controls in four grassland ecosystems: Application of a two-source model. Agr Forest Meteorol 149(9):1410–1420, DOI 10.1016/j.agrformet.2009.03.014

Huang Z, Xue B, Yao S, Pang Y (2008) Lake evolution and its implication for environmental changes in China during 1950–2000. J. Geogr. Sci. 18(2):131-141. DOI 10.1007/s11442-008-0131-4

Immerzeel WW, van Beek LPH, Bierkens MFP (2010) Climate change will affect the Asian water towers. Science 328(5984):1382–1385, DOI 10.1126/science.1183188

Ingwersen J, Steffens K, Högy P, Warrach-Sagi K, Zhunusbayeva D, Poltoradnev M, Gäbler M, Wizemann HD, Fangmeier A, Wulfmeyer V, Streck T (2011) Comparison of Noah simulations with eddy covariance and soil water measurements at a winter wheat stand. Agr Forest Meteorol 151(3):345–355, DOI 10.1016/j.agrformet.2010.11.010

Kang S, Xu Y, You Q, Flügel W, Pepin N, Yao T (2010) Review of climate and cryospheric change in the Tibetan Plateau. Environmental Research Letters 5(1):15101

Keil A, Berking J, Mügler I, Schütt B, Schwalb A, Steeb P (2010) Hydrological and geomorphological basin and catchment characteristics of Lake Nam Co, South-Central Tibet. Quaternary International 218(1-2):118–130, DOI 10.1016/j.quaint.2009.02.022

Kracher D, Mengelkamp HT, Foken T (2009) The residual of the energy balance closure and its influence on the results of three SVAT models. Meteorol Z 18(6):1–15, DOI 10.1127/0941-2948/2009/0412

Krause P, Biskop S, Helmschrot J, Flügel W, Kang S, Gao T (2010) Hydrological system analysis and modelling of the Nam Co basin in Tibet. Adv Geosci 27:29–36, DOI 10.5194/adgeo-27-29-2010

Liu J, Kang S, Gong T, Lu A (2010) Growth of a high-elevation large inland lake, associated with climate change and permafrost degradation in Tibet. Hydrol Earth Syst Sci 14(3):481–489, DOI 10.5194/hess-14-481-2010

Louis J (1979) A parametric model of vertical eddy fluxes in the atmosphere. Bound-Lay Meteorol 17:187–202, DOI 10.1007/BF00117978

Lüers J, Bareiss J (2010) The effect of misleading surface temperature estimations on the sensible heat fluxes at a high arctic site – the arctic turbulence experiment 2006 on svalbard (ARCTEX-2006). Atmos Chem Phys 10(1):157–168, DOI 10.5194/acp-10-157-2010

Ma W, Ma Y (2006) The annual variations on land surface energy in the northern Tibetan Plateau. Environ Geol 50(5):645–650. doi:10.1007/s00254-006-0238-9

Ma Y, Su Z, Koike T, Yao T, Ishikawa H, Ueno K, Menenti M (2003) On measuring and remote sensing surface energy partitioning over the Tibetan Plateau—from GAME/Tibet to CAMP/Tibet. Applications of Quantitative Remote Sensing to Hydrology 28(1–3):63–74. doi:10.1016/S1474-7065(03)00008-1

Ma Y, Fan S, Ishikawa H, Tsukamoto O, Yao T, Koike T, Zuo H, Hu Z, Su Z (2005) Diurnal and inter-monthly variation of land surface heat fluxes over the central Tibetan Plateau area. Theor Appl Climatol 80(2-4):259–273. doi:10.1007/s00704-004-0104-1

Ma Y, Wang Y, Wu R, Hu Z, Yang K, Li M (2009) Recent advances on the study of atmosphere-land interaction observations on the Tibetan Plateau. Hydrol Earth Syst Sci 13(7):1103–1111

Mauder M, Foken T (2004) Documentation and instruction manual of the eddy covariance software package TK2. Work Report University of Bayreuth, Dept. of Micrometeorology, ISSN 1614-8916, 26, 42 pp., URL http://opus.ub.uni-bayreuth.de/opus4-ubbayreuth/frontdoor/index/index/docId/639

Mauder M, Foken T (2006) Impact of post-field data processing on eddy covariance flux estimates and energy balance closure. Meteorol Z 15(13):597–609, DOI 10.1127/0941-2948/2006/0167

Mauder M, Foken T (2011) Documentation and instruction manual of the eddy-covariance software package TK3. Work Report University of Bayreuth, Dept. of Micrometeorology, ISSN 1614-8916, 46, 58 pp., URL http://opus.ub.uni-bayreuth.de/opus4-ubbayreuth/frontdoor/index/index/docId/681

Mauder M, Foken T, Clement R, Elbers JA, Eugster W, Grünwald T, Heusinkveld B, Kolle O (2008) Quality control of CarboEurope flux data – Part 2: Inter-comparison of eddy-covariance software. Biogeosciences 5(2):451–462. doi:10.5194/bg-5-451-2008

Maussion F, Scherer D, Finkelnburg R, Richters J, Yang W, Yao T (2011) WRF simulation of a precipitation event over the Tibetan Plateau, China – an assessment using remote sensing and ground observations. Hydrol Earth Syst Sci 15(6):1795–1817, DOI 10.5194/hess-15-1795-2011

Mengelkamp HT, Warrach K, Raschke E (1999) SEWAB - a parameterization of the surface energy and water balance for atmospheric and hydrologic models. Adv Water Resour 23(2):165–175, DOI 10.1016/S0309-1708(99)00020-2

Mengelkamp HT, Kiely G, Warrach K (2001) Evaluation of the hydrological components added to an atmospheric land-surface scheme. Theor Appl Climatol 69(3-4):199–212, DOI 10.1007/s007040170025

Metzger S, Ma Y, Markkanen T, Göckede M, Li M, Foken T (2006) Quality Assessment of Tibetan Plateau Eddy Covariance Measurements Utilizing Footprint Modeling. Advances in Earth Sciences 21(12):1260–1267

Mihailović DT, Pielke RA, Rajković B, Lee TJ, Jeftić M (1993) A resistance representation of schemes for evaporation from bare and partly plant-covered surfaces for use in atmospheric models. J Appl Meteorol 32(6):1038–1054, DOI 10.1175/1520-0450(1993)032<1038:ARROSF>2.0.CO;2

Molnar P, Boos WR, Battisti DS (2010) Orographic Controls on Climate and Paleoclimate of Asia: Thermal and Mechanical Roles for the Tibetan Plateau. Annu. Rev. Earth Planet. Sci. 38(1):77–102, DOI 10.1146/annurev-earth-040809-152456

Mügler I, Gleixner G, Günther F, Mäusbacher R, Daut G, Schütt B, Berking J, Schwalb A, Schwark L, Xu B, Yao T, Zhu L, Yi C (2010) A multi-proxy approach to reconstruct hydrological changes and Holocene climate development of Nam Co, Central Tibet. J Paleolimnol 43(4):625–648, DOI 10.1007/s10933-009-9357-0

Ni J (2011) Impacts of climate change on Chinese ecosystems: key vulnerable regions and potential thresholds. Regional Environmental Change 11(1):49-64, DOI 10.1007/s10113-010-0170-0

Noilhan J, Planton S (1989) A simple parameterization of land surface processes for meteorological models. Mon Weather Rev 117(3):536–549, DOI 10.1175/1520-0493(1989)117<0536:ASPOLS>2.0.CO;2

Nordbo A, Launiainen S, Mammarella I, Lepparanta M, Huotari J, Ojala A, Vesala T (2011) Long-term energy flux measurements and energy balance over a small boreal lake using eddy covariance technique. J. Geophys. Res 116(D2):D02119

Panin GN, Foken T (2005) Air–sea interaction including a shallow and coastal zone. Journal of Atmospheric & Ocean Science 10(3):289–305, DOI 10.1080/17417530600787227

Panin GN, Nasonov AE, Foken T (2006a) Evaporation and heat exchange of a body of water with the atmosphere in a shallow zone. Izv. Atmos. Ocean. Phys. 42(3):337–352. doi:10.1134/S0001433806030078

Panin GN, Nasonov AE, Foken T, Lohse H (2006b) On the parameterization of evaporation and sensible heat exchange for shallow lakes. Theor Appl Climatol 85:123–129, DOI 10.1007/s00704-005-0185-5

Paw U K, Baldocchi D, Meyers T, Wilson K (2000) Correction of eddy-covariance measurements incorporating both advective effects and density fluxes. Bound-Lay Meteorol 97:487–511, DOI 10.1023/A:1002786702909

Rannik U, Aubinet M, Kurbanmuradov O, Sabelfeld KK, Markkanen T, Vesala T (2000) Footprint analysis for measurements over a heterogeneous forest. Bound-Lay Meteorol 97(1):137–166, DOI 10.1023/A:1002702810929

Rebmann C, Kolle O, Heinesch B, Queck R, Ibrom A, Aubinet M (2012) Data Acquisition and Flux Calculations. In: Aubinet M, Vesala T, Papale D (eds) Eddy Covariance. Springer Netherlands, pp 59-83

Rouse WR, Oswald CJ, Binyamin J, Spence C, Schertzer WM, Blanken PD, Bussières N, Duguay CR (2005) The Role of Northern Lakes in a Regional Energy Balance. Journal of Hydrometeorology. J. Hydrometeor 6(3):291–305, DOI 10.1175/JHM421.1

Twine TE, Kustas WP, Norman JM, Cook DR, Houser PR, Meyers TP, Prueger JH, Starks PJ, Wesely ML (2000) Correcting eddy-covariance flux underestimates over a grassland. Agr Forest Meteorol 103(3):279–300. doi:10.1016/S0168-1923(00)00123-4

Wendisch M, Foken T (1989) Sensitivity test of a multilayer energy exchange model. Z Meteorol 39:36–39

Wilczak J, Oncley S, Stage S (2001) Sonic anemometer tilt correction algorithms. Bound-Lay Meteorol 99:127–150, DOI 10.1023/A:1018966204465

Wu Y, Zhu L (2008) The response of lake-glacier variations to climate change in Nam Co Catchment, central Tibetan Plateau, during 1970–2000. J. Geogr. Sci. 18(2):177–189, DOI 10.1007/s11442-008-0177-3

Xu J, Haginoya S (2001) An estimation of heat and water balances in the tibetan plateau. J Meteorol Soc Jpn 79(1B):485–504, DOI 10.2151/jmsj.79.485

Xu J, Yu S, Liu J, Haginoya S, Ishigooka Y, Kuwagata T, Hara M, Yasunari T (2009) The Implication of Heat and Water Balance Changes in a Lake Basin on the Tibetan Plateau. Hydrological Research Letters 3:1–5, DOI 10.3178/hrl.3.1

Yang K, Koike T, Ye B, Bastidas L (2005) Inverse analysis of the role of soil vertical heterogeneity in controlling surface soil state and energy partition. J Geophys Res 110(D8):D08101, DOI 10.1029/2004JD005500

Yang K, Chen YY, Qin J (2009) Some practical notes on the land surface modeling in the Tibetan Plateau. Hydrol Earth Syst Sci 13(5):687–701, DOI 10.5194/hess-13-687-2009

Yang K, Koike T, Ishikawa H, Kim J, Li X, Liu H, Wang J, Liu S, Ma Y (2008) Turbulent flux transfer over bare-soil surfaces: Characteristics and parameterization. J Appl Meteorol Clim 47:276–290, DOI 10.1175/2007JAMC1547.1

Yang K, Ye B, Zhou D, Wu B, Foken T, Qin J, Zhou Z (2011) Response of hydrological cycle to recent climate changes in the Tibetan Plateau. Climatic Change 109(3-4):517–534, DOI 10.1007/s10584-011-0099-4

Yu S, Liu J, Xu J, Wang H (2011) Evaporation and energy balance estimates over a large inland lake in the Tibet-Himalaya. Environ Earth Sci 64(4):1169–1176. doi:10.1007/s12665-011-0933-z

Zhao L, Li J, Xu S, Zhou H, Li Y, Gu S, Zhao X (2010) Seasonal variations in carbon dioxide exchange in an alpine wetland meadow on the Qinghai-Tibetan Plateau. Biogeosciences 7(4):1207–1221, DOI 10.5194/bg-7-1207-2010

Zhou D, Eigenmann R, Babel W, Foken T, Ma Y (2011) The study of near-ground free convection conditions at Nam Co station on the Tibetan Plateau. Theor Appl Climatol 105(1-2):217-228, DOI 10.1007/s00704-010-0393-5

Zhu L, Xie M, Wu Y (2010) Quantitative analysis of lake area variations and the influence factors from 1971 to 2004 in the Nam Co basin of the Tibetan Plateau. Chin. Sci. Bull. 55(13):1294–1303. DOI 10.1007/s11434-010-0015-8

E. Charuchittipan et al. (2013)

Charuchittipan, D., Babel, W., Mauder, M., Leps, J.-P., and Foken, T.: Extension of the averaging time of the eddy-covariance measurement and its effect on the energy balance closure, submitted to Bound.-Lay. Meteorol.

Noname manuscript No.
(will be inserted by the editor)

Extension of the averaging time of the eddy-covariance measurement and its effect on the energy balance closure

Doojdao Charuchittipan · Wolfgang Babel · Matthias Mauder · Jens-Peter Leps · Thomas Foken

Received: date / Accepted: date

Abstract In this study, the modified ogive analysis and block ensemble average were employed to investigate the impact of the averaging time extension on the energy balance closure over six different land use types. The modified ogive analysis suggests that the standard averaging time of 30 minutes is still generally enough for the eddy-covariance measurement. The block ensemble average reveals that the averaging time extension over several days can improve energy balance closure for some sites and over some specific time, when secondary circulations exist in the vicinity of the sensor. These near-surface secondary circulations mainly transport sensible heat, and when near-ground warm air is transported upward, the sensible heat flux observed by the block ensemble average will increase at longer averaging times. The close relationship between near-surface secondary circulations and sensible heat flux suggests an alternative energy balance correction for a near-surface eddy-covariance measurement by using the buoyancy flux ratio, which is the larger fraction of the residual attribute to the sensible heat flux.

Keywords Energy balance closure · Ensemble average · LITFASS · Ogive analysis

D. Charuchittipan (☐) · W. Babel · T. Foken
Department of Micrometeorology, University of Bayreuth, D-95440 Bayreuth, Germany
Tel.: +49-921-552176
Fax: +49-921-552366
E-mail: doojdao@uni-bayreuth.de

T. Foken
Member of Bayreuth Center of Ecology and Environmental Research (BayCEER), University of Bayreuth, Germany

M. Mauder
Institute of Meteorology and Climate Research, Karlsruhe Institute of Technology, D-82467 Garmisch-Partenkirchen, Germany

J.-P. Leps
German Meteorological Service, Richard-Aßmann-Observatory, D-15848 Lindenberg, Germany

1 Introduction

The imbalance of the measured fluxes at the earth's surface is known as the energy balance closure problem and micrometeorologists have been aware of it since the late 1980s (Foken, 2008a; Leuning et al., 2012). Many micrometeorological experiments over low vegetation reveal that the available energy, which is the sum of the net radiation and the ground heat flux, is larger than the sum of the sensible and latent heat fluxes. These experiments include the EBEX experiment (Oncley et al., 2007), which was especially designed to study the energy balance at the earth's surface, and the LITFASS-2003 experiment (Beyrich and Mengelkamp, 2006), which aimed to study the effect of surface heterogeneity. To conserve energy, the residual was added to the energy budget equation over low vegetation at the earth's surface,

$$Res = -Q^{*} - (Q_G + Q_H + Q_E), \tag{1}$$

where *Res* is the residual or missing energy, Q^{*} is the net radiation, Q_G is the ground heat flux, Q_H is the sensible heat flux, and Q_E is the latent heat flux. Each term in Eq. 1 is positive, as the energy is transported away from the ground.

In the past few years, despite improvements in measuring and data processing techniques, this closure problem still remains. It is believed that the residual is caused by large scale eddies or secondary circulations. These secondary circulations are generated by surface heterogeneity and normally move away from the ground (Kanda et al., 2004; Inagaki et al., 2006). Due to their large size and slow motion, their contributions to the low frequency part of the turbulent spectrum cannot be detected by the eddy-covariance (EC) measurement, which is typically averaged over a period of 30 minutes. This results in the underestimation of Q_H and Q_E, which are normally measured by the EC technique.

An extension of the averaging time was suggested and expected to result in a greater contribution from the low frequency parts. Two different approaches were introduced for this task: the ogive analysis (Desjardins et al., 1989; Oncley et al., 1990) and the block ensemble average (Finnigan et al., 2003). The ogive analysis uses the turbulent spectrum to estimate the turbulent fluxes at different frequency ranges, allowing assessment of the contribution of the low frequency parts to the turbulent fluxes measured by the EC method. In Foken et al. (2006), the ogive analysis was applied to the data measured over a maize field of the LITFASS-2003 experiment. It was focused mainly on data from three selected days, where the averaging time was extended up to 4 hours. It was found that the time extension would not significantly increase the turbulent fluxes overall.

For the block ensemble average, low frequency contributions were added to the turbulent fluxes from long term fluctuations over several hours to days. In Mauder and Foken (2006), this treatment was also applied to the dataset from the same maize field of the LITFASS-2003 experiment. The length of the selected dataset was 15 days, while the block ensemble averaging period varied from 5 minutes to 5 days. This study showed that the block ensemble average can close the energy balance at longer averaging time. Extensive discussion of the energy balance closure of the LITFASS-2003 experiment can be found in Foken et al. (2010).

In our study, to investigate whether the averaging time extension would have the same impact over different types of surface, we extended both ogive analysis and block ensemble average to cover more land use types of the LITFASS-2003 experiment. Since the LITFASS area is composed of many distinct agricultural fields, this surface heterogeneity could induce secondary circulations, some of which may still exist in the vicinity of the measuring stations. However, since the data obtained from different measuring stations do not always have the same sampling rate, some minor modifications in both ogive analysis and block ensemble average were made. These modifications were validated by repeating the ogive analysis in Foken et al. (2006) and the block ensemble average in Mauder and Foken (2006). Then we continued our investigations, which was more oriented toward the low frequency contributions. Finally, we came up with the appropriate method for correcting the energy balance of a near-surface eddy-covariance measurement.

2 Material and Method

2.1 LITFASS-2003 experiment and data processing

The LITFASS-2003 experiment was performed between 19 May 2003 and 18 June 2003 near the meteorological observatory of the German Meteorological Service in Lindenberg, Germany. The local time zone in this area is UTC+1. During the experiment, there were 14 ground-based micrometeorological measuring stations over 13 sites, and 2 elevated measuring stations on the tower at 50 and 90 metre heights. This experiment covered an area of 20x20 km^2 and made up of 5 major land use types: grass, maize, rape, cereals (include rye, barley and triticale), lake and forest. More information about the LITFASS-2003 experiment can be found in Beyrich and Mengelkamp (2006).

To cover the most important land use types of the LITFASS-2003 experiment, we selected the following measuring stations for our study: grass (NV2 and NV4), maize (A6), rape (A7), rye (A5), lake (FS) and forest (HV). Note that NV2 and NV4 were actually installed on the same field. They were oriented to different wind sectors to monitor turbulence at this field from all wind directions. We combined these two stations according to the wind direction and they were reported as the single station NV. Information of these selected stations can be found in Table 1.

All selected stations were equipped with EC systems as listed in Table 1. Four-component net radiometers and soil heat flux plates were also installed in each station. Each measuring station can measure all the energy balance components in Eq. 1. Details of these measurements were well described in Mauder et al. (2006) and Liebethal et al. (2005). These measurements allow estimation of the residual, which—on average—reached its maximum during 1000 -1200 UTC. For low vegetation, its average value during this time ranged from 75 to 145 W m^{-2} (or 20% - 30% of the available energy as shown in Table 1).

Over the forest, an additional term, for canopy heat storage, needs to be added to Eq. 1. For all plants, the canopy heat storage has two main contributions, the plant material (or biomass) and the air between plants. Over low vegetation, e.g. cotton

Table 1 Summary of selected measuring stations from the LITFASS-2003 experiment during 20 May 2003, 1200 UTC - 18 June 2003, 0000 UTC. Notations: h_c = canopy height; z_m = measurement height; θ = accepted wind direction; Δt = timestep of short term time series; *Res* = Mean residual between 1000-1200 UTC, this is when the residual is normally reach its maximum; %*Res* = $100 \cdot Res/(-Q^* - Q_G)$ between 1000-1200 UTC. Full details can be found in Beyrich and Mengelkamp (2006) and Mauder et al. (2006)

Station	Canopy	h_c (m)	z_m (m)	θ (degree)	Turbulence Sensors	Δt (minutes)	*Res* ($\mathrm{Wm^{-2}}$)	%*Res* (%)
HV	Pine forest	14	30.5	30 - 330	USA-1/LI-7500	10	133	24%
A5	Rye	0.75-1.50	2.80	60 - 30	USA-1/KH20	5	144	30%
A6	Maize	0.05-0.70	2.70	90 - 270	CSAT3/LI-7500	5	122	31%
A7	Rape	0.70-0.90	3.40	30 - 240	CSAT3/KH20	5	87	22%
NV2	Grass	0.05-0.25	2.40	60 - 180	USA-1/LI-7500	5	75	22%
NV4	Grass	0.05-0.25	2.40	150 - 330	USA-1/LI-7500	5	82	24%
FS	Lake	0	3.85	180 - 30	USA-1/LI-7500	10	247	63%
M50	Grass	0.05-0.25	50.7	90 -300	USA-1/LI-7500	5	-	-
M90	Grass	0.05-0.25	90.7	90 - 300	USA-1/LI-7500	5	-	-

fields, both contributions of canopy heat storage are relatively small and negligible (Oncley et al., 2007). The canopy heat storage becomes significant over forest and must be included in the energy budget equation (Lindroth et al., 2010). Unfortunately, we did not collect all required biomass properties of the forest during the LITFASS-2003 experiment, so the forest's canopy heat storage could not be precisely estimated. Hence, all analyses of this site were done without a canopy heat storage term. Over the lake, due to its large heat capacity, Q_G was calculated according to Nordbo et al. (2011).

During the LITFASS-2003 campaign, the raw data were processed and averaged over 30 minutes. For this task, all the participating groups agreed to use the software package TK2 (Mauder and Foken, 2004), which has been tested and compared internationally (Mauder et al., 2008). During flux calculation processes, several flux corrections were applied. Cross-correlation analysis was used for fixing the time delay between the sonic anemometer and hygrometer. Moore correction was used to correct the spectral loss in the high frequency range (Moore, 1986). The planar-fit rotation was used to align the sonic anemometer with a long term mean streamline (Wilczak et al., 2001). SND correction was used to convert the sonic temperature, as recorded by the sonic anemometer, to the actual temperature (Schotanus et al., 1983). WPL correction was used to correct the density fluctuation (Webb et al., 1980). Crosswind correction was used to account for a different type of sonic anemometer (Liu et al., 2001). Tanner correction was used to correct the cross sensitivity between H_2O and O_2 molecules (Tanner et al., 1993), which was only applied for the Krypton Hygrometer KH20 (deployed in A5 and A7). More details of these corrections can be found in Mauder et al. (2006) and Foken et al. (2012).

After all these flux corrections, quality flags were assigned to each 30 minute period. These quality flags are the steady state flag, the integral turbulence characteristic (ITC) flag (Foken and Wichura, 1996) and combined flag. The steady state flag is a result of the steady state test and represents the stationarity of the data. The ITC flag represents the development of turbulent conditions, which is the result of the flux variance similarity test. The combined flag is the combination of the steady state and ITC flags. All these flags range from 1-9 (from best to worst). High quality data, considered suitable for fundamental scientific research, have flag values of 1-3. More details of the data quality analysis can be found in Foken et al. (2012, 2004).

Besides flux calculations, flux corrections and assignment of data quality flags, TK2 can also generate short term averages and covariances at 5 or 10 minute intervals. Due to the limited storage capacity, these short term average data points were stored instead of the raw data in some measuring stations. However, the statistics for longer periods can be reconstructed from these short term information with the following relations (Foken, 2008b),

$$\overline{a'b'} = \frac{1}{M-1}\left[(U-1)\sum_{j=1}^{N}\left(\overline{a'b'}\right)_j + U\sum_{j=1}^{N}\overline{a}_j\,\overline{b}_j - \frac{U^2}{M-1}\sum_{j=1}^{N}\overline{a}_j\sum_{j=1}^{N}\overline{b}_j\right], \tag{2}$$

where $\overline{a'b'}$ is the long term covariance and M is the number of measurement points of the long term time series. This long term time series consists of N short term time series, whose number of measurement points is U. $\left(\overline{a'b'}\right)_j$ is the short term covariance, and $\overline{a}_j$ and $\overline{b}_j$ are the short term averages. These short term averages are derived from raw data, to which no flux corrections have been applied. Therefore, any necessary flux corrections must be included when using these short term averages for flux calculations. These short term average data points from selected stations were used for both ogive analysis and block ensemble average calculations. Short term averaging intervals of selected stations are shown in Table 1.

2.2 Data selection

In most selected measuring stations, ground heat flux and radiation data are only available since 20 May 2003, 1200 UTC, so the period during 20 May 2003, 1200 UTC - 18 June 2003, 0000 UTC was used in this study. To ensure high data quality as well as to minimize the irrelevant factors which might influence turbulent fluxes, we imposed sets of data selection criteria to the ogive analysis and block ensemble average separately. For the ogive analysis, we increased the averaging time to up to 4 hours. This 4 hour period consists of 8 consecutive subperiods (or blocks) of 30 minutes. We performed the ogive analysis over any 4 hour period only if all blocks satisfied the selection criteria.

The first selection criterion is identical to Mauder et al. (2006), which is that the sonic anemometers must not be disturbed by either the internal boundary layer resulting from the heterogeneity of the surface, or the flow distortion caused by obstacles. The internal boundary layer height was estimated from

$$z_m \leq \delta = 0.3\sqrt{x}, \tag{3}$$

(Raabe, 1983) where z_m is the measurement height, δ is the internal boundary layer height and x is the distance from the sensor to boundary of the next land use class.

To keep the measurement undisturbed, z_m must not exceed δ. Hence, we rejected any wind direction whose corresponding x did not satisfy Eq. 3. The undisturbed wind sectors (θ) of each measuring station, from both internal boundary layer and flow distortion, are listed in Table 1. Additionally, footprint analysis was used to confirm that the target land use type has a significant contribution to our measurement. This contribution varied over the stability range. We further rejected any wind sectors whose contribution from target land use type is less than 80%.

The next data selection criterion is a steady state condition of the time series, which is indicated by the steady state flag (section 2.1). We only accepted data with high quality flags (flag 1-3). In this study, we did the ogive analysis of the energy balance components (Q_H and Q_E) and CO_2 flux ($F_c = \overline{w'c'}_{CO_2}$) separately. For the energy balance components, we only considered the steady state flags of friction velocity (u_*), Q_H and Q_E. We only performed the ogive analysis on any periods during which these three steady state flags qualified simultaneously. For F_c, we considered only steady state flags of u_* and CO_2 flux, and performed the ogive analysis on any periods where these two steady state flags were accepted simultaneously.

We avoided the transition period by excluding from our analysis the time period covering one hour before to one hour after both sunrise and sunset. We also specified the threshold value of each turbulent flux as a minimum requirement in our analysis. For u_*, which indicates the level of turbulence (Massman and Lee, 2002), the threshold value is 0.1 m s^{-1}. This was set to rule out very small turbulent fluxes, which can result from instrumentation noise. This limit normally excludes periods with very weak wind as well. For Q_H, Q_E and F_c, threshold values were formulated to avoid complication with their measurement errors. According to Mauder et al. (2006), based on 30 minutes averaging time, the measurement errors of Q_H and Q_E are 10% - 20% of the turbulent flux at 30 minutes, or 10 - 20 W m^{-2}, whichever is larger. For u_* and F_c, the measurement errors are 0.02 - 0.04 m s^{-1} and 0.5 - 1 μmol $m^{-2}s^{-1}$, respectively (Meek et al., 2005). Therefore, we set the threshold values of Q_H and Q_E to be 20 W m^{-2}, and the threshold value of F_c to be 1 μmol m^{-2} s^{-1}. Unusually large uncertainty of F_c during the night time was taken into account by using only data periods with u_* greater than 0.25 m s^{-1} (Hollinger and Richardson, 2005).

Similar selection criteria cannot apply to the block ensemble average, as it involves averaging times of several hours to days. Therefore, the quality control of this part was done by discarding any periods with more than 10% of missing raw data. This missing data could result from various factors, e.g. electrical black out.

2.3 Modified ogive analysis

The ogive analysis was introduced by Desjardins et al. (1989) and Oncley et al. (1990) to investigate the flux contribution from each frequency range as well as to determine suitable averaging periods to capture most of the turbulent fluxes. The ogive function of the turbulent flux ($og_{w,c}$) is defined as the cumulative integral of the cospectrum of the turbulent flux ($Co_{w,c}$) starting with the highest frequency:

$$og_{w,c}(f_0) = \int_{\infty}^{f_0} Co_{w,c}(f)\,df, \tag{4}$$

where w is the vertical wind velocity, c is the horizontal wind velocity or a scalar quantity (i.e. temperature and humidity), and f is a frequency which corresponds to a time period (τ) as

$$\tau = \frac{1}{f}. \tag{5}$$

This analysis was applied to data measured over the maize field (A6) of the LITFASS-2003 in Foken et al. (2006), where the ogive function was calculated from raw 20 Hz data over a 4 hour period and mainly focused on 3 selected days (7-9 June 2003). It was shown that the ogive curves could be classified into three cases. Case 1, where the ogive curve exhibits an asymptotic behavior toward the low frequency within a 30 minute period. This indicates that the 30 minute averaging time is enough to capture most of the turbulent fluxes. Case 2, in which the ogive curve shows the extreme value (peak) within a 30 minute period, meaning that the total turbulent fluxes have been reached before 30 minutes. Hence a longer averaging time obviously reduces the flux and a period shorter than 30 minutes would be enough to capture most of the turbulent fluxes. Case 3, in which the ogive curve does not converge within a 30 minute period. This implies that there is a significant contribution from the low frequency part of the turbulent spectrum and a 30 minute averaging time is not enough to capture most of the fluxes.

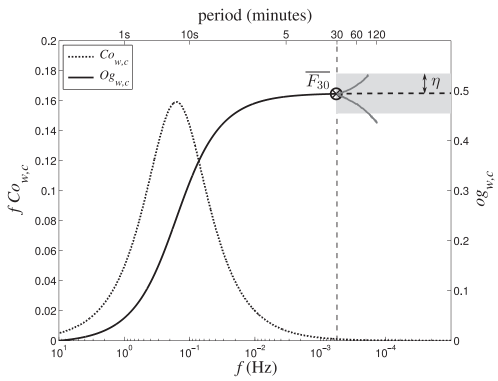

Fig. 1 The short term average time series can estimate the turbulent flux at a 30 minute period ($\overline{F_{30}}$) and its evolution after that (gray solid lines in a gray band). The error band of width 2η (gray band) was defined for identifying the ogive case. See Table 2 for ogive case definition.

As mentioned in section 2.1, raw data are not available for all selected sites. Since only the short term average data at every 5 or 10 minutes exist for all selected sites, we developed a modified ogive analysis (MOG) to deal with these data. According to the spectral analysis, the spectra calculated from high and low frequency data behave similarly in the low frequency region (Kaimal et al., 1972). This means that we can use the turbulent spectrum calculated from the short term average data to estimate

Table 2 Ogive case definition in analogy to Foken et al. (2006). Δ_{max} is a maximum flux difference after 30 minute averaging time. $\overline{F_{30}}$ is an average size of turbulent flux at 30 minute period. η is the width of an error band. See more details in section 2.3.

Case	Criterion
1	$\Delta_{max}/\overline{F_{30}} \leq \eta$
2	$\Delta_{max}/\overline{F_{30}} > \eta$ and $\Delta_{max} < 0$
3	$\Delta_{max}/\overline{F_{30}} > \eta$ and $\Delta_{max} > 0$

the change in turbulent fluxes after 30 minutes, without any information prior to 30 minutes (Fig. 1).

We calculated the turbulent cospectra of the short term average data with a standard Fast Fourier Transform (FFT) method. To avoid influences from the diurnal effect, we still keep the time extension up to 4 hours as in Foken et al. (2006). We then determined the change in turbulent fluxes after a 30 minute period from the cumulative integral of the cospectra starting from the frequency which corresponds to a period of 30 minutes, and set its maximum value to be the maximum flux difference (Δ_{max}), i.e.,

$$\Delta_{max} = \max\left(\int_{\tau=30}^{\tau} Co_{w,c}(f)df\right). \tag{6}$$

We compared Δ_{max} with the turbulent flux at 30 minutes ($\overline{F}_{30}$), which we can estimate in two different ways. Firstly, by averaging the fluxes from each 30 minute block, $(\overline{w'c'})_j$, together as

$$\overline{F}_{30} = \frac{1}{8}\sum_{j=1}^{8}(\overline{w'c'})_j\,. \tag{7}$$

Secondly, we calculated the total flux over a 4 hour period ($\overline{F}_{4hr}$) from short term average data with the help of Eq. 2 and the turbulent flux after a 30 minute period ($F_{\tau>30}$) from the cumulative integral of the cospectra from the lowest frequency (f_{min}) to the frequency corresponding to a 30 minute period,

$$F_{\tau>30} = \int_{f_{min}}^{\tau=30} Co_{w,c}(f)df. \tag{8}$$

The difference between $\overline{F}_{4hr}$ and $F_{\tau>30}$ can give us the estimation of $\overline{F}_{30}$ as

$$\overline{F}_{30} = \overline{F}_{4hr} - F_{\tau>30}\,. \tag{9}$$

Both estimations in Eq. 7 and 9 give compatible $\overline{F}_{30}$. We then set the error band of width 2η for the turbulent flux at a 30 minute period (Fig. 1). If Δ_{max} is still confined within this band, it indicates that the turbulent flux difference after 30 minutes is not significant, which conforms to case 1 in Foken et al. (2006). If the maximum flux difference after a 30 minute period exceeds this band, this means the turbulent flux difference is significant and could be classified into 2 cases, depending on the changes in turbulent fluxes after a 30 minute period. It is equivalent to case 2 in Foken et al. (2006), when the size of turbulent flux decreases and case 3, when the size of turbulent flux increases. In this study, we set η to be 10% (or 20%) of the turbulent flux at a 30 minute period, which must not be smaller than the measurement errors of each turbulent flux (section 2.2). The ogive case definition in analogy to Foken et al. (2006) is shown in Table 2.

To extend the investigation beyond 3 golden days and cover more land use types, the MOG was applied over a period of time and selected measuring stations of the LITFASS-2003 experiment as described in section 2.2 and Table 1. The MOG was applied to all selected sites for the energy balance component. However, for F_c, we only applied it to the land use types maize, grass and forest, because the F_c measurement was not available in rye (A5) and rape (A7) sites (both equipped with KH20), and F_c was very low over the lake. Note that in this study, we did not apply the flux correction as mentioned in section 2.1. Since each point of the cospectra corresponds to the turbulent flux at a different duration, the choice of suitable duration for the flux corrections would be ambiguous. According to Mauder and Foken (2006), these flux corrections would reduce the residual by 17%, we may therefore assume that this reduction would have reflected in an increase of the sensible and latent heat fluxes.

2.4 Block ensemble average

The averaging operator which we apply to the single tower EC measurement is the *time average*. Over a period P, the time average of any variable $a(t)$ is (see Fig. 2 in Finnigan et al., 2003)

$$\overline{a(t)} = \frac{1}{P}\int_0^P a(t)\,dt. \tag{10}$$

This averaging operator can apply to the mass balance equation as long as it satisfies the Reynolds averaging rules (de Feriet, 1951; Bernstein, 1966). A standard approach is to impose the steady state condition over a period P, which makes the time average constant in this period ($\overline{a(t)} = \overline{a}$). Then any variable $a(t)$ can be decomposed into mean ($\overline{a}$) and fluctuation parts ($a'(t)$) as

$$a(t) = \overline{a} + a'(t) \tag{11}$$

This is the Reynolds decomposition. When applied to the product of vertical velocity w and variable c, which can be horizontal wind velocity or a scalar quantity, it gives

$$\overline{w(t)c(t)} = \overline{w}\,\overline{c} + \overline{w'c'}, \tag{12}$$

which represents the mean vertical transport of a scalar or momentum over the period P. This period must be long enough to capture most of the atmospheric turbulence, yet it must not violate the steady state condition. The typical value of P in most EC measurements is 30 minutes. We can further simplify Eq. 12 by applying coordinate rotation, which sets $\overline{w}$ to zero, e.g., the double rotation (Kaimal and Finnigan, 1994).

When the averaging period P is extended to be much longer than 30 minutes, it is very difficult to maintain the steady state condition. Without a steady state condition, the Reynolds averaging rules no longer hold, in which case the time average is no longer a good representative statistic. Finnigan et al. (2003) and Bernstein (1966) proposed using the block ensemble average as it always obeys the Reynolds averaging rules, allowing the formulation to be carried out without a steady state condition.

Suppose we extend our period of interest to NP, which consists of N consecutive blocks (or subperiods, or runs) of period P. Let a subscript n represent the n^{th} block, whose time average of any variable $a_n(t)$ in this block is $\overline{a}_n(t)$. This time average becomes a function of time because it can vary from block to block. The block ensemble average of all N blocks (denoted by $\langle\ \rangle$) of $a_n(t)$ over period NP is

$$\langle \overline{a} \rangle = \frac{1}{N} \sum_{n=1}^{N} \overline{a}_n(t). \tag{13}$$

$\langle \overline{a} \rangle$ is always constant over the period NP and obeys Reynolds averaging rules. This allows us to use the block ensemble average operator with the mass balance equation. The time average of each block $\overline{a}_n(t)$ deviates from $\langle \overline{a} \rangle$ by $\tilde{a}_n(t)$,

$$\tilde{a}_n(t) = \overline{a}_n(t) - \langle \overline{a} \rangle . \tag{14}$$

Hence we replace the Reynold decomposition by the triple decomposition, in which any variable in the n^{th} block can be separated into three parts as (see Fig. 3 in Finnigan et al., 2003)

$$a_n(t) = \langle \overline{a} \rangle + \tilde{a}_n(t) + a'(t). \tag{15}$$

All the turbulence information rests in $\tilde{a}_n(t)$ and $a'(t)$. $a'(t)$ is an instantaneous fluctuation, while the $\tilde{a}_n$ is the block to block fluctuation. This triple decomposition leads to the block ensemble average of the vertical transport of momentum or scalar over N blocks of period P as (we drop the subscript n and omit t)

$$\left\langle \overline{w(t)c(t)} \right\rangle = \langle \overline{wc} \rangle = \langle \overline{w} \rangle \langle \overline{c} \rangle + \langle \tilde{w}\tilde{c} \rangle + \left\langle \overline{w'c'} \right\rangle \tag{16}$$

This shows that the mean vertical flux average over a period NP does not only depend on the usual turbulent flux $\overline{w'c'}$, it also depends on the flux caused by block to block variations $\tilde{w}\tilde{c}$. In Bernstein (1966), the moving average or overlapped block ensemble average was used instead of a non-overlapped one as in Finnigan et al. (2003).

To use the block ensemble average, every single block in period NP must be in the same coordinate system: the long term coordinate. It has been shown in Finnigan et al. (2003) that a period to period rotation, e.g. the double rotation, is not a long term coordinate. It sets $\overline{w}$ of each n^{th} period to zero and acts as a high-pass filter. In our analysis, we obtained the long term coordinate through the planar fit rotation (Wilczak et al., 2001; Paw U et al., 2000), which determines the rotation angle from multiple periods. This rotation set the block ensemble average of vertical velocity of the period NP to zero ($\langle \overline{w} \rangle = 0$), while the mean vertical velocity in each period P is not necessary zero. Thus the block ensemble average of the vertical flux becomes

$$\langle \overline{wc} \rangle = \langle \tilde{w}\tilde{c} \rangle + \left\langle \overline{w'c'} \right\rangle \tag{17}$$

According to Finnigan et al. (2003), $\tilde{w}\tilde{c}$ has two roles, which are

1. To balance the unsteady horizontal flux divergence and transient changes in source and storage terms.
2. To carry the low frequency contribution to the long-term vertical flux.

The first role can cause $\tilde{w}\tilde{c}$ to become very large in any arbitrary period, which can be much larger than the mean vertical flux itself. It was suggested that the period NP must be long enough to suppress and minimize the effect of the first role. Then only the second role would contribute to the vertical flux. In our case, in addition to suppressing the transient effect, we would like to suppress the diurnal effect as well, so an observation period over a few days would help to balance the strong daytime fluxes with the weak nighttime fluxes as well as suppress any extreme days in between. Therefore, only the low frequency part of the diurnal effects would be left at the end, which would lead to a weak inflection at this scale. However, an observation period over a few days would also intensify any errors in $\tilde{w}\tilde{c}$. These errors may be from instrumentation drift, gaps and some synoptic scale events. Since our measurement lasted only about a month and was well installed, instrumentation drift can be neglected. Hence, we need to select an observation period not influenced by any synoptic events, and with minimum gaps, to minimize the errors.

This approach was applied with the dataset from the Amazonian rain forest in Finnigan et al. (2003). It was shown that the residual goes to zero at around 4 hours. A similar strategy was applied to the 15 day dataset from the maize field (A6) of the LITFASS-2003 experiment during the period 2 June 2003, 1800 UTC - 18 June 2003, 0000 UTC (Mauder and Foken, 2006), which we also used in our study as a period NP. Overlapping blocks ensemble averages were used, with the starting point of each consecutive block being shifted by 5 minutes. The period P of the block ensemble average was varied from 5 minutes to 5 days. Flux corrections were applied as described in section 2.1 in each individual block. It was shown that the energy balance was closed within a day and mainly caused by the increase of $\langle Q_H \rangle$.

In this study, to investigate whether this approach could generally close the energy balance, we applied the block ensemble average to selected ground-based stations of the LITFASS-2003 experiment as listed in Table 1 and used an identical period as in Mauder and Foken (2006). We made slight changes compared to Mauder and Foken (2006), because the turbulent data from lake and forest as well as the ground heat fluxes and net radiations from most selected stations are only available every 10 minutes. Our block ensemble period P was varied from 10 minutes to 5 days, with the starting points of each consecutive block being shifted by 10 minutes. We also used the same flux corrections as in Mauder and Foken (2006).

2.5 Scale analysis

Since we are interested in how the secondary circulations contribute to the low frequency part of the turbulent spectra, we used the wavelet analysis to resolve the underlying scale of motion. The wavelet analysis routine employed in this study is similar to Mauder et al. (2007), which is based on the algorithm provided by Torrence and Compo (1998). The Morlet wavelet was used in this routine as it was proved to fit with the atmospheric turbulence analysis. In this study, we can only apply the wavelet analysis to the data from rye, maize and grassland, whose high frequency data are available. The CO_2 flux is not discussed in this part, as it is not related to the energy balance.

Other than the high frequency data requirement, the wavelet analysis also consumes a lot of computing resources, so it is almost impossible to apply it over a large dataset at once. Therefore, a specific period when large scale structures exist needs to be identified before the wavelet analysis is performed over this specific period.

3 Results and discussion

3.1 Modified ogive analysis

As mentioned in section 2.3, we investigated the impact of averaging time extension with the MOG on energy balance components and F_c separately. Our data selection criteria (section 2.2) ruled out most nighttime periods in both analyses, because their turbulent fluxes were below thresholds. We expected measuring stations with broader undisturbed wind sectors, which are rye (A5), grass (NV) and forest (HV), to have more qualified periods. This was confirmed by the highest number of qualified periods from grass and rye stations, however, the number of qualified periods of the forest station for the MOG of energy balance component was less than for the other two measuring stations. This is because steady state flags of Q_E of the forest were randomly bad throughout the day. This is in contrast to data from the lake (FS), whose steady state flags of Q_H were randomly bad. Because of this unsteadiness in Q_H and Q_E, many data periods were removed from forest and lake stations. Over low vegetation, steady state flags of Q_H and Q_E were normally good during 0600 - 1600 UTC. Some random unsteady periods mostly appeared in the afternoon. For all selected measuring stations, steady state flags of F_c (if measurements were available) were randomly bad throughout the day, while steady state flags of u_* were mostly good. Hence, passing the steady state criterion is mainly dependent on the stationarity of Q_H, Q_E and F_c. In the end, in each measuring station, only 5% -20% of available periods were left for the MOG. These MOG qualified periods were mainly during 0600 - 1600 UTC. For the energy balance components, they all had unstable stratification, while for F_c, there were a few periods with stable stratification.

The results of the MOG of energy balance components and F_c are shown in Table 3 and 4 respectively. Both different analyses gave very similar results in u_*. Hence, only the results of u_* from the MOG of F_c (Table 4) are shown. In these two tables, we report the average size of turbulent fluxes at 30 minute periods ($\overline{F_{30}}$) and the number of runs in each ogive case at two different sizes of error bands (η), 10% and 20%, which must be larger than the threshold fluxes (section 2.2). For case 2 and 3, the average of maximum flux difference ($\overline{\Delta_{max}}$) is also shown.

$\overline{F_{30}}$ of Q_H and Q_E were closely grouped together over low vegetation. $\overline{F_{30}}$ of Q_H was the largest over the forest and smallest over the lake, and vice versa for Q_E. Over lake and low vegetation, the MOG classified most qualified periods of both Q_H and Q_E as Case 1. This suggests that a 30 minute averaging time is generally enough to capture most turbulent fluxes. However, there were significant numbers of Case 2

Table 3 Results from the modified ogive analysis of the energy balance components (Q_H and Q_E) from selected stations of the LITFASS-2003 experiment between 20 May 2003, 1200 UTC - 18 June 2003, 0000 UTC. Notations: η is the width of error band, which is set to be 10% and 20% of the turbulent flux at 30 minute period and has a minimum value equals to the measurement error of each turbulent flux; $\overline{F_{30}}$ is the average size of turbulent flux at 30 minute period; $\overline{\Delta_{max}}$ is the average of maximum flux difference; Runs(%) is number of runs in each ogive case, which is also available in percentage in the parenthesis.

Station	**Flux**	η	**Case 1**		**Case 2**			**Case 3**		
			$\overline{F_{30}}$	Runs(%)	$\overline{F_{30}}$	$\overline{\Delta_{max}}$	Runs(%)	$\overline{F_{30}}$	$\overline{\Delta_{max}}$	Runs(%)
Forest	Q_H	10%	261	92(74.8%)	205	-33	4(3.3%)	224	33	27(22.0%)
	(Wm^{-2})	20%	252	119(96.7%)	237	-56	1(0.8%)	217	70	3(2.4%)
(HV)	Q_E	10%	107	53(43.1%)	128	-33	12(9.8%)	119	27	58(47.2%)
	(Wm^{-2})	20%	112	93(75.6%)	126	-45	6(4.9%)	125	40	24(19.5%)
Rye	Q_H	10%	148	192(88.1%)	99	-15	6(2.8%)	85	19	20(9.2%)
	(Wm^{-2})	20%	143	213(97.7%)	-	-	0(0.0%)	61	36	5(2.3%)
(A5)	Q_E	10%	145	196(89.9%)	118	-20	10(4.6%)	131	23	12(5.5%)
	(Wm^{-2})	20%	143	212(97.2%)	116	-26	2(0.9%)	132	30	4(1.8%)
Maize	Q_H	10%	106	99(84.6%)	98	-12	3(2.6%)	116	28	15(12.8%)
	(Wm^{-2})	20%	108	111(94.9%)	-	-	0(0.0%)	92	39	6(5.1%)
(A6)	Q_E	10%	134	97(82.9%)	77	-20	14(12.0%)	80	18	6(5.1%)
	(Wm^{-2})	20%	127	112(95.7%)	91	-37	3(2.6%)	57	22	2(1.7%)
Rape	Q_H	10%	127	85(90.4%)	83	-13	8(8.5%)	94	12	1(1.1%)
	(Wm^{-2})	20%	123	94(100.0%)	-	-	0(0.0%)	-	-	0(0.0%)
(A7)	Q_E	10%	181	93(98.9%)	-	-	0(0.0%)	141	16	1(1.1%)
	(Wm^{-2})	20%	181	94(100.0%)	-	-	0(0.0%)	-	-	0(0.0%)
Grass	Q_H	10%	117	187(93.0%)	101	-15	12(6.0%)	132	23	2(1.0%)
	(Wm^{-2})	20%	116	200(99.5%)	99	-27	1(0.5%)	-	-	0(0.0%)
(NV)	Q_E	10%	131	173(86.1%)	95	-19	4(2.0%)	118	19	24(11.9%)
	(Wm^{-2})	20%	140	196(97.5%)	94	-31	1(0.5%)	114	27	4(2.0%)
Lake	Q_H	10%	40	69(95.8%)	-	-	0(0.0%)	31	14	3(4.2%)
	(Wm^{-2})	20%	40	72(100.0%)	-	-	0(0.0%)	-	-	0(0.0%)
(FS)	Q_E	10%	197	69(95.8%)	93	-15	1(1.4%)	121	14	2(2.8%)
	(Wm^{-2})	20%	193	72(100.0%)	-	-	0(0.0%)	-	-	0(0.0%)

and 3 of both Q_H and Q_E from rye, grass, maize and—remarkably—forest stations. These periods of Case 2 and 3 of rye, grass and maize sites were closely related to the stationarity of Q_H and Q_E over a 4 hour period. For these three sites, periods of Case 1 usually had a four hour steady state flag of 1 for Q_H and Q_E, while Case 2 and 3 usually had steady state flags of 2 or more. This relation was not readily apparent in the forest site, implying that the averaging time extension has imposed unsteadiness on the turbulence over low vegetation. If we restrict our consideration to rye, grass, maize and forest sites, we found that the number of Case 3s was normally greater than the number of Case 2s in both Q_H and Q_E. This would tell us that the averaging time extension most likely increases Q_H and Q_E. The average maximum flux difference ($\overline{\Delta_{max}}$) for Q_H was mostly higher than for Q_E. $\overline{\Delta_{max}}$ is increased with larger size of

Table 4 Results from the modified ogive analysis of friction velocity (u_*) and CO_2 flux (F_c). The description is similar to Table 3

Station	Flux	η	Case 1		Case 2			Case 3		
			$\overline{F_{30}}$	Runs(%)	$\overline{F_{30}}$	$\overline{\Delta_{max}}$	Runs(%)	$\overline{F_{30}}$	$\overline{\Delta_{max}}$	Runs(%)
Forest	u_*	10%	0.64	191(99.5%)	-	-	0(0.0%)	0.38	0.06	1(0.5%)
	(ms^{-1})	20%	0.64	192(100.0%)	-	-2.48	0(0.0%)	-	-	0(0.0%)
(HV)	F_c	10%	8.68	112(58.3%)	8.25	-1.57	24(12.5%)	7.43	1.54	56(29.2%)
	$\mu mol\ m^{-2}s^{-1}$	20%	8.29	171(89.1%)	7.73	-2.48	8(4.2%)	8.21	3.23	13(6.8%)
Maize	u_*	10%	0.31	111(97.4%)	0.26	-0.03	1(0.9%)	0.15	0.03	2(1.8%)
	(ms^{-1})	20%	0.31	114(100.0%)	-	-1.70	0(0.0%)	-	-	0(0.0%)
(A6)	F_c	10%	9.09	71(62.3%)	7.13	-1.56	16(14.0%)	7.34	2.40	27(23.7%)
	$\mu mol\ m^{-2}s^{-1}$	20%	8.69	90(78.9%)	7.10	-1.70	12(10.5%)	7.52	4.09	12(10.5%)
Grass	u_*	10%	0.33	183(88.8%)	-	-	0(0.0%)	0.27	0.04	23(11.2%)
	(ms^{-1})	20%	0.33	199(96.6%)	-	-	0(0.0%)	0.22	0.05	7(3.4%)
(NV)	F_c	10%	9.95	153(74.3%)	8.80	-1.67	29(14.1%)	7.65	1.27	24(11.7%)
	$\mu mol\ m^{-2}s^{-1}$	20%	9.57	195(94.7%)	8.47	-2.74	8(3.9%)	9.41	2.82	3(1.5%)

an error band (η), while lower numbers of Case 2 and 3 were observed. This would indicate that the fewer periods left had larger $\overline{\Delta_{max}}$. However, even with the greatest $\overline{\Delta_{max}}$ added on top of flux corrections, the energy increase is still not enough to close the energy balance. Furthermore, from scalar similarity of Q_H and Q_E, we expected these fluxes to increase or decrease together. This means we should see Case 2 or Case 3 in both Q_H and Q_E simultaneously, which was rarely observed.

$\overline{F_{30}}$ of u_* had the highest value over the forest and the smallest value over the lake, and they were closely grouped together over low vegetation. Our MOG classified most periods from all sites as Case 1. This suggests that the time extension has almost no impact on u_* regardless of canopy types.

For F_c, all sites gave compatible values of $\overline{F_{30}}$. Case 1 was still in the majority, with a larger fraction of Case 2 and 3 than the energy balance components. Forest also had larger fraction of Case 2 and 3 than did low vegetation. Overall, the number of Case 3s was greater than number of Case 2s, and $\overline{\Delta_{max}}$ was also increased with η. The four hour steady state flags were normally 1 for Case 1 and higher for Case 2 and Case 3. However, Case 2s generally had higher steady state flags than Case 3. This suggests that if the averaging time extension does not impose much unsteadiness, it tends to increase F_c, and decrease it when more unsteadiness has been imposed.

3.2 Block ensemble average

The block ensemble average (Eq. 17) of all selected sites during 2 June 2003, 1800 UTC - 18 June 2003, 0000 UTC, are shown in Fig. 2. We chose this period as our observation period *NP* to repeat Mauder and Foken (2006) with some minor modifications (section 2.4). We found that our result from the maize station (Fig. 2 d) differed from the original by less than the measurement errors of Q_H and Q_E. Therefore, these modifications still give the same results and we can confidently apply them with other selected measuring stations.

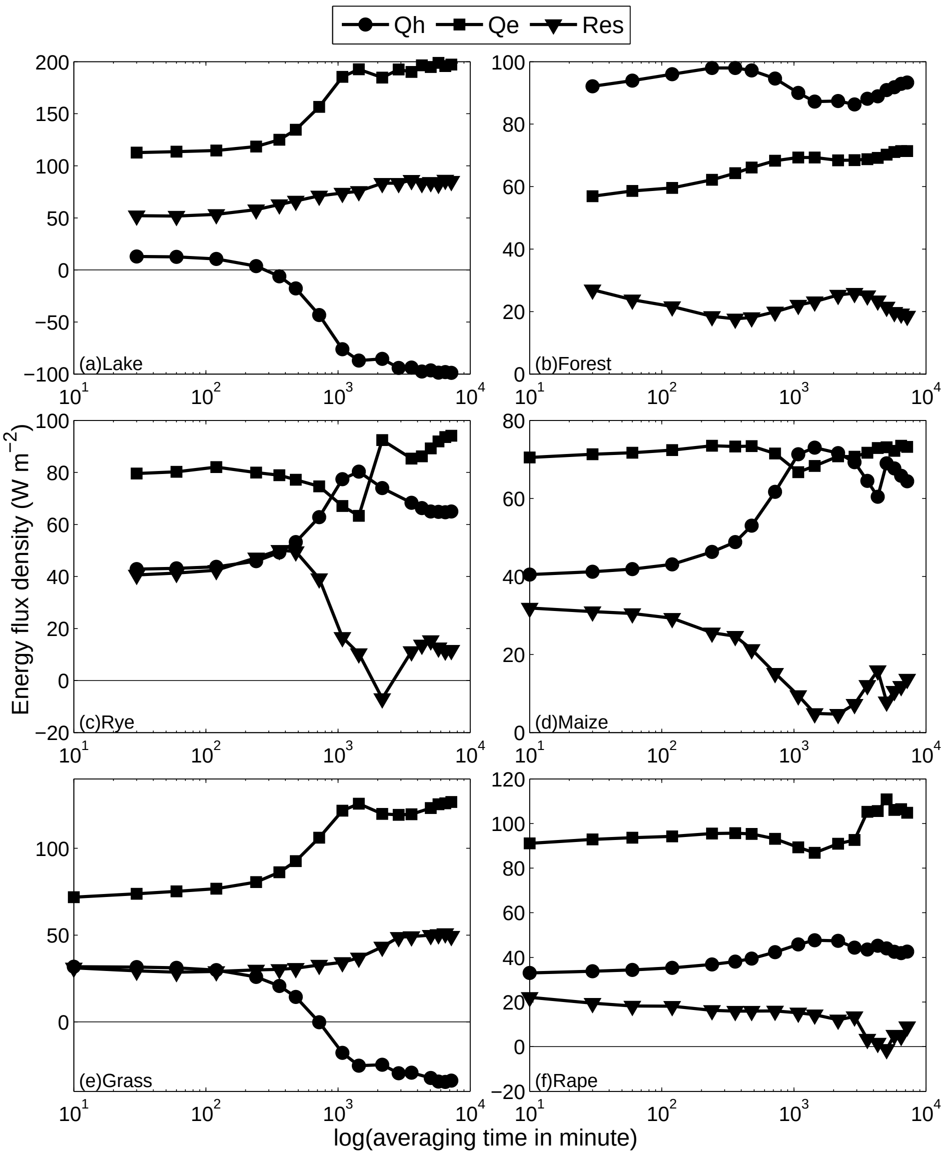

Fig. 2 Block ensemble averages of sensible heat flux and latent heat flux (Eq. 17 with *c* is temperature and absolute humidity), and their corresponding residuals, during 2 June 2003, 1800 UTC - 18 June 2003, 0000 UTC of selected sites in the LITFASS-2003 experiment: (a) lake, (b) forest, (c)rye, (d) maize (reproduction of Mauder and Foken (2006)), (e) grass and (f) barley.

The outcome of the block ensemble average was quite unexpected to us. It could close the energy balance only over maize, rye and rape sites. For maize and rye sites, the closures were at around 15 - 30 hours, which is close to the results obtained in Mauder and Foken (2006). These closures were mainly caused by the increasing of

$\langle Q_H \rangle$ with longer block ensemble averaging period P. For the rape site, both $\langle Q_H \rangle$ and $\langle Q_E \rangle$ were approximately constant at all P. During the observation period, this site was also influenced by rain events in the southern part of the LITFASS area. Therefore, its closure at very long P was not enhanced by the block ensemble average. For grassland and lake, $\langle Q_H \rangle$ was decreased with longer P, which was compensated by the increase in $\langle Q_E \rangle$, and caused the residual to be approximately constant at all P. For lake and forest sites, we must interpret the results carefully, because the lake has different characteristics from other terrain sites and we cannot precisely estimate the canopy heat storage (section 2.1) of the forest from our data.

At all sites, both $\langle Q_H \rangle$ and $\langle Q_E \rangle$ were approximately constant within the first few hours. Over longer P, $\langle Q_E \rangle$ was more steady than $\langle Q_H \rangle$. The inflection at the diurnal scale was found at all sites of both $\langle Q_H \rangle$ and $\langle Q_E \rangle$. As all these selected sites are practically in the same 20x20 km^2 area, the diurnal effects should not be much different and the degree of inflection should be compatible. Therefore, the stronger inflection over some sites and fluxes may not be entirely caused by the diurnal effects.

As the block ensemble average could not close the energy balance for all selected sites from 2 June 2003, 1800 UTC to 18 June 2003, 0000 UTC, we need to determine the reason behind this and whether it would be the same in a different observation period NP. We know that the $\tilde{w}\tilde{c}$ term of the block ensemble average is related to the low frequency flux contribution. In principle, $\tilde{w}\tilde{c}$ represents the flux contributions beyond the averaging period P. If we set P to be 30 minutes, $\tilde{w}\tilde{c}$ would represent additional flux after the 30 minute averaging time. Hence, long term observation of $\tilde{w}\tilde{c}$ would show variation of additional fluxes from low frequency contributions, which may be related to observed block ensemble average fluxes. These variations can be observed more clearly when the observation period NP is long enough to suppress any transient effects in the block ensemble average fluxes.

Our observation period NP, which covered an entire period of the LITFASS-2003 experiment, was 20 May 2003, 1200 UTC - 18 June 2003, 0000 UTC. We used $\tilde{w}\tilde{c}$ from all 30 minute non-overlapping blocks ($P = 30$ minutes) within this period NP to construct the Hovmøller diagrams of $\tilde{Q}_H$ ($\tilde{w}\tilde{T}$ in energetic units, T is temperature) and $\tilde{Q}_E$ ($\tilde{w}\tilde{a}$ in energetic units, a is absolute humidity). These diagrams would show the variation of additional fluxes beyond 30 minute averaging time. According to section 2.4, $\tilde{w}\tilde{c}$ can be very large in any arbitrary blocks. Therefore, we expected to observe some random large $\tilde{Q}_H$ and $\tilde{Q}_E$ in these diagrams.

The Hovmøller diagrams of $\tilde{Q}_H$ for rye and grassland are shown in Fig. 3. Throughout the entire experiment, we found large $\tilde{Q}_H$ more often than large $\tilde{Q}_E$. We firstly started with the period during 2 June 2003, 1800 UTC - 18 June 2003, 0000 UTC. Within this period, large $\tilde{Q}_H$ were mainly positive for the rye (Fig. 3 a) and maize (not shown) sites, and mainly negative over the grassland (Fig. 3 b). These observations are consistent with the observed block ensemble average fluxes, in which $\langle Q_H \rangle$ was increasing at longer P for the rye and maize sites, and vice versa for the grassland (Fig. 2). The lake site is more dominated by large negative $\tilde{Q}_H$ (not shown), which is consistent with the decreasing of $\langle Q_H \rangle$ at longer P. There were only few large $\tilde{Q}_E$ at all sites, which are consistent with approximately constant $\langle Q_E \rangle$ at all P over rye, maize, rape and forest sites. However, over lake and grassland, these few large

$\tilde{Q}_E$ were extremely large when compared to their own block ensemble averages, and caused their $\langle Q_E \rangle$ to increase at longer P.

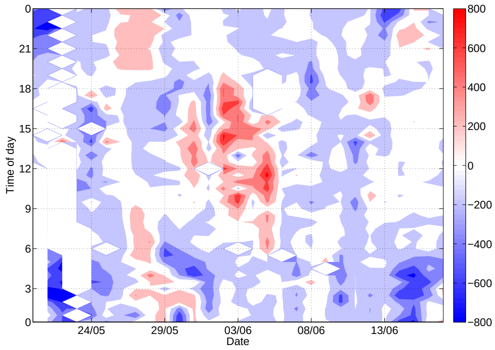

(a) Rye

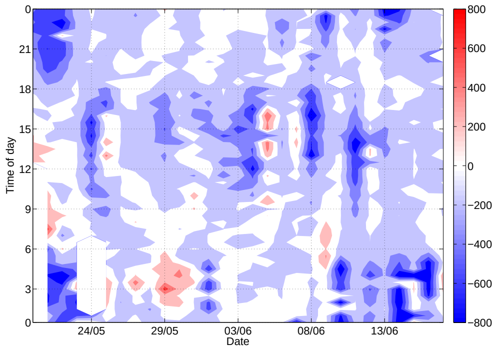

(b) Grass

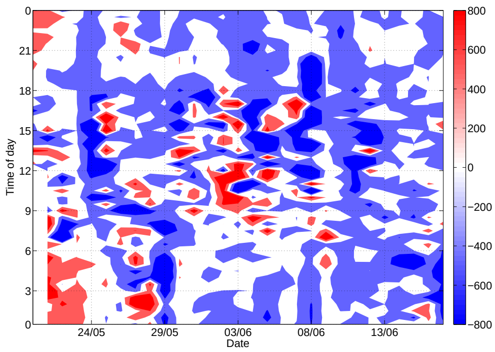

(c) 90 m tower

Fig. 3 The Hovmøller diagrams of $\tilde{Q}_H$ from (a) Rye, (b) Grass and (c) 90 m tower, they represent $\tilde{w}\tilde{T}$ of each 30 minute block in the energetic units. Series of large $\tilde{Q}_H$ were observed in rye (positive) and grass (mainly negative) during 1 June 2003 - 5 June 2003. These patterns are related to secondary circulations, which is consistent with frequent observations of large $\tilde{Q}_H$ at 90 m height. Each colour depicts the flux in W m^{-2}.

More interestingly, large $\tilde{Q}_H$ were observed consecutively for a few days during 1 June 2003 - 5 June 2003, over rye, maize, grass and lake. This period was the dry period between the rain events and was not influenced by any significant synoptic events. These large $\tilde{Q}_H$ were positive for rye and maize, and mainly negative for grass and lake. Large $\tilde{Q}_E$ was not found in this same period. As decribed in section 2.4, large $\tilde{Q}_H$ (or large $\tilde{w}\tilde{T}$) could compensate a strong horizontal divergence in an individual block. However, consecutive occurrences indicate that they were certainly not transient effects. A strong horizontal divergence would imply to a strong horizontal advection, which is related to secondary circulations. Hence, we believe that these patterns of large $\tilde{Q}_H$ were caused by near-surface secondary circulations. To support this statement, we inspected the Hovmøller diagram of $\tilde{Q}_H$ obtained from the measurement at 90 metre height (M90). At this height, there always exist secondary circulations, which means we should observe series of large $\tilde{Q}_H$ more often than in ground measurements. We did actually observe series of large positive and negative $\tilde{Q}_H$ throughout the entire period of the LITFASS-2003 experiment (Fig. 3 c).

To observe the effect of near-surface secondary circulations more clearly, we chose 1 June 2003, 1500 UTC - 5 June 2003, 1500 UTC as the new observation period *NP*. We used the beginning and ending time of 1500 UTC to avoid gaps in the data from the maize field on the morning of 1 June 2003 and the rain event on the evening of 5 June 2003. Additionally, we wanted to complete a daily cycle as well. Since this long period only lasted for 4 days, the block ensemble averaging period *P* was varied from 10 minutes to 3 days. The block ensemble averages of this new observation period are shown in Fig. 4. As expected, we found that during this period, the energy balance is closed using averaging times of half a day for rye and maize sites. Over grassland and lake, $\langle Q_H \rangle$ was decreased at longer *P*, which corresponds to the large negative $\tilde{Q}_H$. $\langle Q_E \rangle$ were approximately constant at all *P* at all sites, which were consistent with the absence of large $\tilde{Q}_E$.

Accepted models state that secondary circulations can only reach down to levels near the earth's surface under the free convection condition, which occurs when the buoyancy term dominates the shear production term as $z/L \leq -1$. This situation is also accompanied by low friction velocity (Eigenmann et al., 2009). As we did not observe any free convection during 1 June 2003, 1500 UTC - 5 June 2003, 1500 UTC, we believe that these near-surface secondary circulations were caused by the thermal heterogeneity between different land use types (Stoy et al., 2013).

3.3 Scale analysis

We used the wavelet analysis to resolve the scales of motion during 1 June 2003, 1500 UTC - 5 June, 2003 1500 UTC with data from rye, maize and grassland stations. The wavelet analysis of rye and grassland stations are shown in Fig. 5 and Fig. 6 respectively. Results for the maize field and the rye field are very similar. From these wavelet cross-scalograms, we found small and large scales of motion. The size of the small one is around a few minutes, which should be captured by the eddy-covariance measurement over 30 minute averaging time. It appears during the daytime at all sites and transports both Q_H and Q_E. The size of the larger scale is approximately a day, and mainly transports Q_H. It tends to increase Q_H in the maize and rye sites, while decreasing Q_H over grass. This conforms to the patterns of $\tilde{Q}_H$ and the block

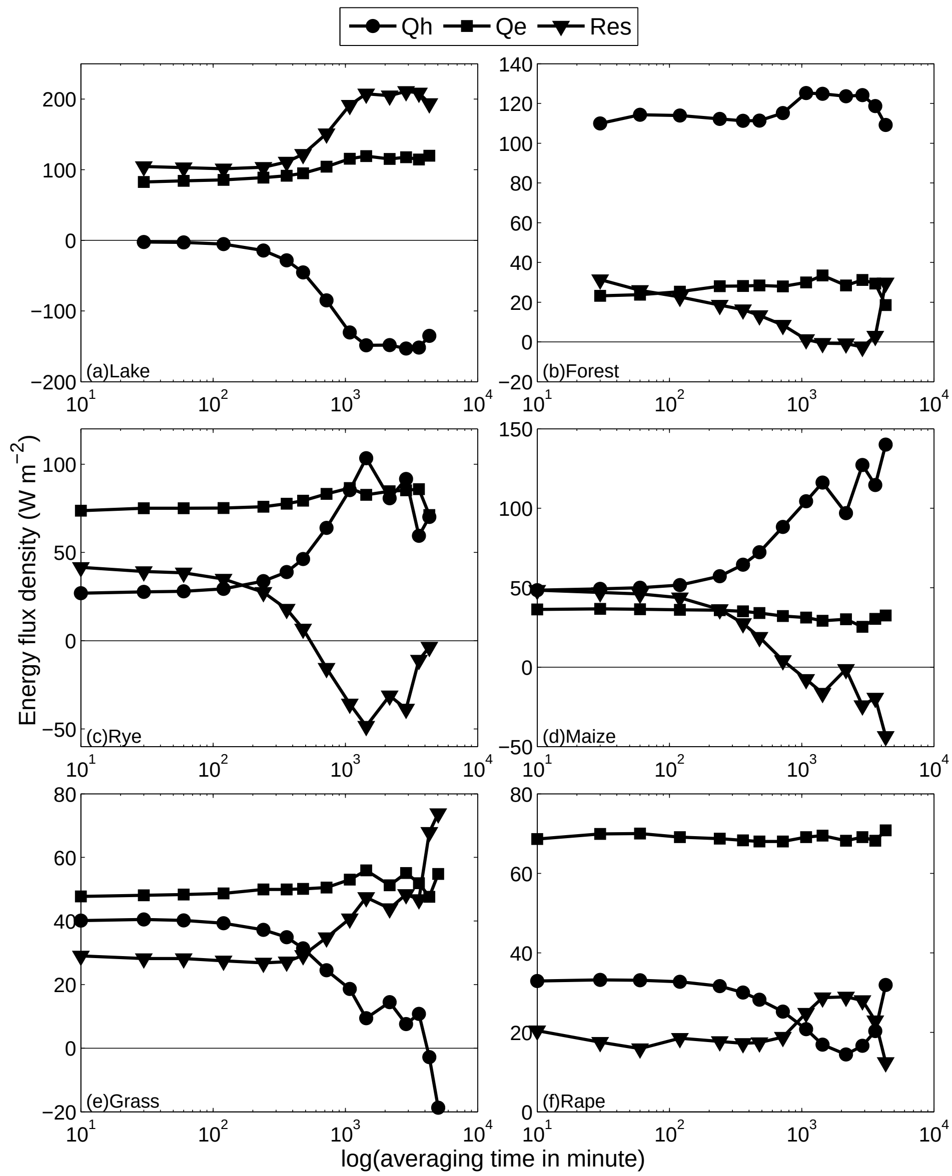

Fig. 4 Block ensemble averages of sensible heat flux and latent heat flux (Eq. 17 with *c* is temperature and absolute humidity), and their corresponding residuals, during 1 June 2003, 1500 UTC - 5 June 2003, 1500 UTC of selected sites in the LITFASS-2003 experiment: (a) lake, (b) forest, (c) rye, (d) maize, (e) grass and (f) barley.

ensemble average fluxes. This scale of motion would not be captured by the eddy-covariance measurement averaging over the 30 minute period.

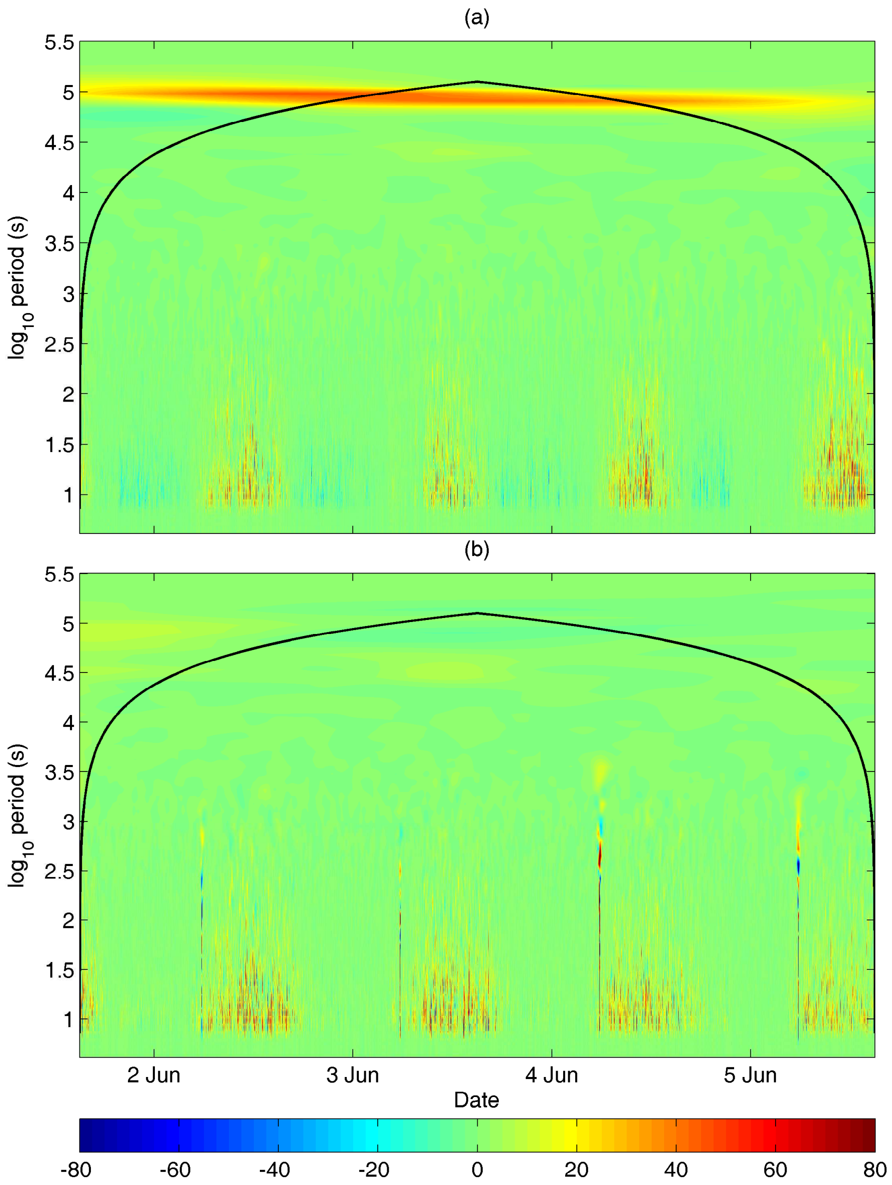

Fig. 5 Wavelet cross-scalograms over the rye field during 1 June 2003, 1500 UTC - 5 June 2003, 1500 UTC of (a) sensible heat flux and (b) latent heat flux. The colour represents the value in W m^{-2}. The black solid line represents the cone of influence.

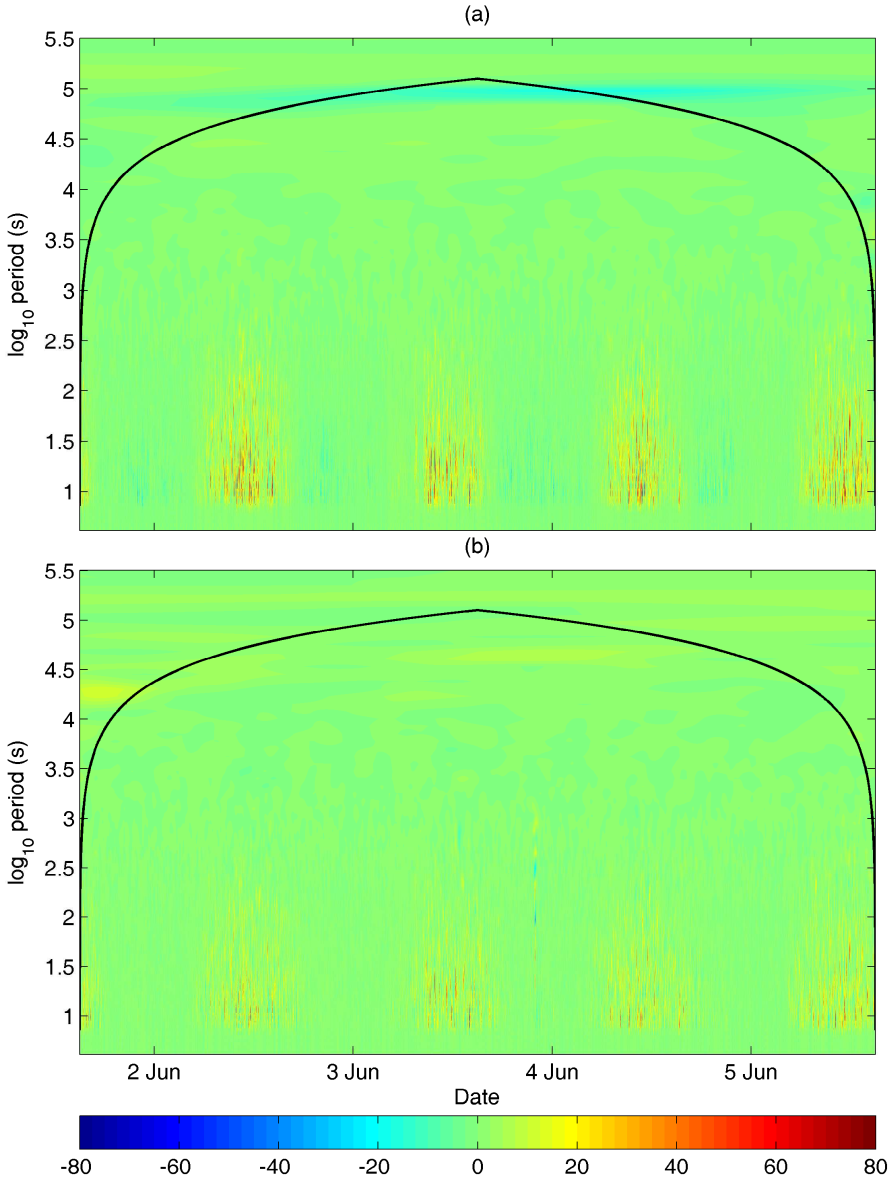

Fig. 6 Wavelet cross-scalograms over the grassland during 1 June 2003, 1500 UTC - 5 June 2003, 1500 UTC of (a) sensible heat flux and (b) latent heat flux. The colour represents the value in W m^{-2}. The black solid line represents the cone of influence.

Both patterns from the Hovmøller diagram and wavelet analysis show the increase or decrease of $\tilde{Q}_H$. However, they do not actually show what contributes to these changes. For the turbulent fluxes ($\overline{w'c'}$), which are caused by instantaneous fluctuations, we can carry out a quadrant analysis by dividing instantaneous contributions of $\overline{w'c'}$ into four quadrants of w' and c' (Shaw, 1985). Our findings suggest that the main contribution for closing the energy balance is $\tilde{Q}_H$, which is caused by block to block fluctuations ($\tilde{w}$ and $\tilde{c}$). We therefore divided block to block contributions of $\tilde{w}\tilde{c}$ into four quadrants of $\tilde{w}$ and $\tilde{c}$. We used $\tilde{T}$ (temperature) and $\tilde{a}$ (absolute humidity) as horizontal axes and $\tilde{w}$ (vertical velocity) as a vertical axis, which gave our four quadrants ($Q_i, i = 1, \ldots, 4$) as

Q_1: $\tilde{w} > 0$ and $\tilde{T} > 0$ or $\tilde{a} > 0$ warm air rising or moist air rising,
Q_2: $\tilde{w} > 0$ and $\tilde{T} < 0$ or $\tilde{a} < 0$ cold air rising or dry air rising,
Q_3: $\tilde{w} < 0$ and $\tilde{T} < 0$ or $\tilde{a} < 0$ cold air sinking or dry air sinking,
Q_4: $\tilde{w} < 0$ and $\tilde{T} > 0$ or $\tilde{a} > 0$ warm air sinking or moist air rising.

Q_1 and Q_3 contribute to the positive flux, while Q_2 and Q_4 contribute to the negative flux. We then normalized each axis by its standard deviation and set the hyperbolic hole size to 0.5 ($H = 0.5$). We can neglect the weak contribution by excluding the contribution inside the hole and only considering any points which satisfy

$$\left| \frac{\tilde{w}\tilde{T}}{\sigma_{\tilde{w}}\sigma_{\tilde{T}}} \right| \text{ or } \left| \frac{\tilde{w}\tilde{a}}{\sigma_{\tilde{w}}\sigma_{\tilde{a}}} \right| > H. \tag{18}$$

With the quadrant analysis, we expect to see which types of turbulence actually contribute to the increasing or decreasing of $\tilde{w}\tilde{c}$. To make it consistent with our Hovmøller diagrams, we used the same observation period NP, which is 20 May 2003, 1200 UTC - 18 June 2003, 0000 UTC, and set P to 30 minutes (non-overlapped). Therefore, any points on the quadrant analysis diagram represent the normalized $\tilde{w}\tilde{c}$ from each non-overlapped 30 minute period.

The results of the quadrant analysis of rye and grassland stations are shown in Fig. 7. In this figure, we distinguished all points during 1 June 2003, 1500 UTC - 5 June 2003, 1500 UTC from the rest by the use of red colour dots. By considering only strong contribution outside a hyperbolic hole (blue line), we found that during this period, $\tilde{Q}_H$ (via $\tilde{w}\tilde{T}$) has more contribution from Q_1 (warm air rising) for the rye sites (Fig. 7 a), while there are more contributions from Q_4 (warm air sinking) for the grassland (Fig. 7 b). There was no significant contribution outside the hyperbolic hole for $\tilde{Q}_E$ (via $\tilde{w}\tilde{a}$) in both rye and grass stations. Over the maize field, the quadrant analysis is similar to that of the rye field, while the lake is similar to the grassland. For both rape and forest (not shown), Q_1 and Q_4 equally contributed to $\tilde{Q}_H$, with no significant contribution outside the hole for $\tilde{Q}_E$. These results tell us that the increase of $\langle Q_H \rangle$ at longer P of rye and maize fields were caused by warm air near the surface rising, while the decreasing of $\langle Q_H \rangle$ of grassland and lake were caused by warm air aloft sinking. For forest and rape stations, both contributions from Q_1 and Q_4 canceled each other and keep $\langle Q_H \rangle$ approximately constant at all P. The absence of significant contributions outside the hyperbolic hole keeps $\langle Q_E \rangle$ approximately constant at all sites.

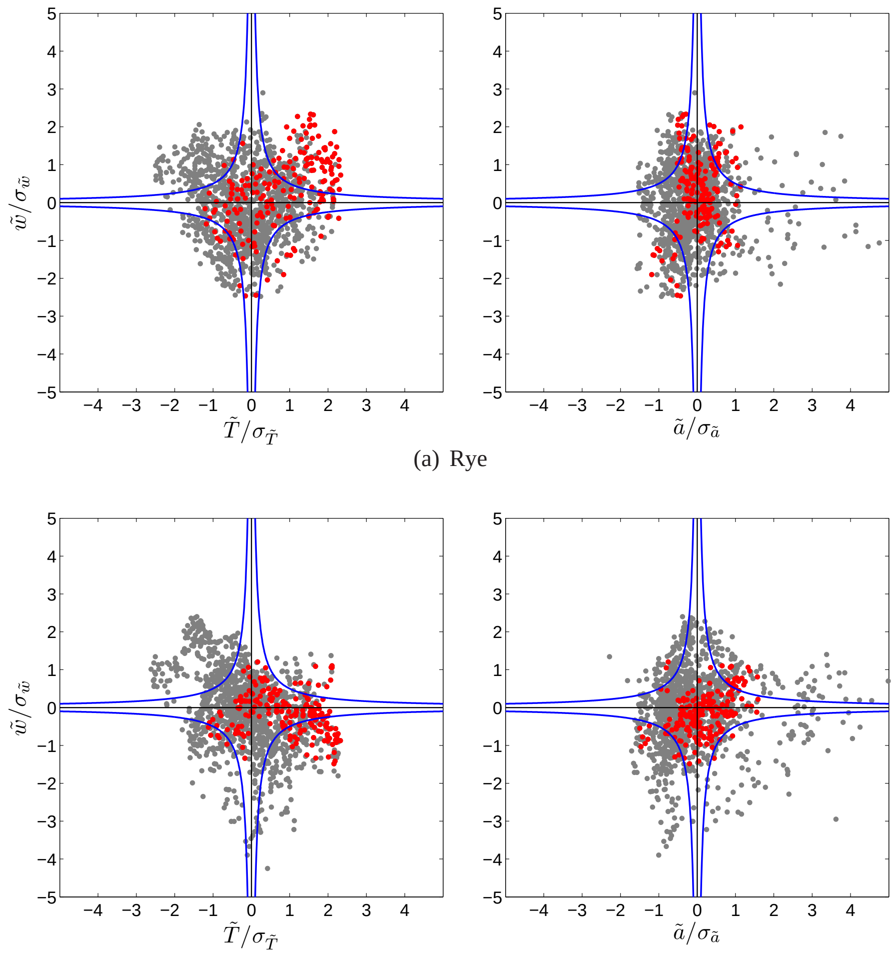

(a) Rye

(b) Grassland

Fig. 7 Quadrant analysis of $\tilde{w}\tilde{T}$ (left panels, represent the sensible heat flux) and $\tilde{w}\tilde{a}$ (right panels, represent the latent heat flux) of (a) rye and (b) grass during 20 May 2003, 1200 UTC - 18 June 2003, 0000 UTC. The period from 1 June 2003, 1500 UTC to 5 June 2003, 1500 UTC has been highlighted using red dots. The blue solid lines represent the hyperbolic hole ($H = 0.5$).

4 Conclusions

The modified ogive analysis, which requires steady state conditions, reveals that by extending the averaging time by a few hours would not much improve the energy balance. Therefore, the 30 minute averaging time is still enough for the eddy-covariance calculation in general. The time extension has more impact over tall vegetation. Sensible heat flux, latent heat flux and CO_2 flux are more sensitive to the time extension than is friction velocity. Over low vegetation, these three turbulent fluxes tend to increase with the time extension, which is related to the imposed unsteadiness of longer periods. When unsteadiness increases, it tends to decrease the CO_2 flux. The increase of a sensible heat flux is generally greater than occurs with a latent heat flux. Over a longer period, the increases or decreases of sensible and latent heat fluxes do not always behave according to the scalar similarity as expected. And lastly, the sizes of the energy increases in both sensible and latent heat fluxes are not enough to close the energy balance at all sites.

Without assuming steady state conditions, the block ensemble average can extend the averaging time to several days by including the period to period fluctuations ($\tilde{w}\tilde{c}$, c is temperature or humidity) into the mean vertical flux. However, it does not usually help us to close the energy balance. The Hovmøller diagram, which shows variation of $\tilde{w}\tilde{c}$ over a long period, can help us to locate when secondary circulations exist in the vicinity of the sensor by exhibiting consecutive large $\tilde{w}\tilde{T}$. From our findings, when secondary circulations exist near the earth's surface, they mainly transport sensible heat. This finding also supports the poor scalar similarity between the sensible and latent heat fluxes in the low frequency region (Ruppert et al., 2006; Foken et al., 2011).

Since secondary circulations move very slowly and are very large in size, a single tower EC measurement averaging over 30 minutes is unable to detect them. If the sensor is coincidentally at the right time and location, when secondary circulations transport near-ground warm air upward, the block ensemble average at a longer period would yield higher sensible heat flux that improve the energy balance closure. However, when these near-surface secondary circulations transport warm air aloft downward, the block ensemble average would yield the lower sensible heat flux at a longer averaging time. This suggests that near-surface secondary circulations do transport significant amounts of energy, which are responsible for the energy balance closure problem rather than the sensor efficiency.

To account for low frequency turbulent fluxes caused by near-surface secondary circulations, we must accept that the scalar similarity between the sensible and latent heat fluxes is no longer valid throughout all scales. Therefore, the widely used energy balance correction in Twine et al. (2000), EBC-Bo, which assumes the scalar similarity between sensible and latent heat fluxes by preserving the Bowen ratio, would not generally hold.

As we found that near-surface secondary circulations transport more sensible heat, we expect a larger fraction of the residual to be attributed to the sensible heat flux. Hence, we would like to propose an alternative energy balance correction for a near-surface EC measurement through the buoyancy flux ratio (EBC-HB), in which the convection plays a key role. The buoyancy flux, Q_B, is defined as

$$Q_B = \rho c_p \overline{w'T_v'}, \tag{19}$$

where ρ is the air density, c_p is the specific heat capacity of air at constant pressure, and T_v is the virtual temperature, which can be replaced by the sonic temperature (T_S) with negligible loss of accuracy (Kaimal and Gaynor, 1991). This means that sonic anemometers can be used to directly measure Q_B with a good accuracy. The virtual temperature is related to the actual temperature (T) and specific humidity (q) in the same way as the sonic temperature (Schotanus et al., 1983), which leads to

$$\begin{aligned} Q_B = \rho c_p \overline{w'T_v'} &= \rho c_p \left(\overline{w'T'} + 0.61\,\overline{T}\,\overline{w'q'}\right) \\ &= Q_H \left(1 + 0.61\,\overline{T}\,\frac{c_p}{\lambda\,Bo}\right) \end{aligned} \tag{20}$$

We next partition the residual via the buoyancy flux ratio, which contains both sensible and latent heat fluxes. A fraction of the residual, which would attribute to the sensible heat flux, is dependent on the relative contribution of the sensible heat flux to the buoyancy flux. The remaining would then go to the latent heat flux. Therefore the corrected sensible and latent heat fluxes obtained with the buoyancy flux ratio approach ($Q_H^{\mathrm{EBC-HB}}$ and $Q_E^{\mathrm{EBC-HB}}$ respectively) are,

$$Q_H^{\mathrm{EBC-HB}} = Q_H + f_{HB} \cdot Res, \tag{21}$$

$$Q_E^{\mathrm{EBC-HB}} = Q_E + (1 - f_{HB}) \cdot Res, \tag{22}$$

with

$$f_{HB} = \frac{Q_H}{Q_B} = \left(1 + 0.61\,\overline{T}\,\frac{c_p}{\lambda\, Bo}\right)^{-1}. \tag{23}$$

Since this method does not preserve the Bowen ratio, Eq. 21-23 must be calculated iteratively until the Bowen ratio in Eq. 23 converges. The comparison between the Bowen ratio approach and the buoyancy flux ratio approach is shown in Fig. 8. Both approaches are identical at very high Bowen ratio, i.e. all the residual is shifted to the sensible heat flux. For the typical range of Bowen ratio, however, the buoyancy flux ratio approach would attribute more residual to the sensible heat flux than the Bowen ratio approach, which is more consistent with our findings.

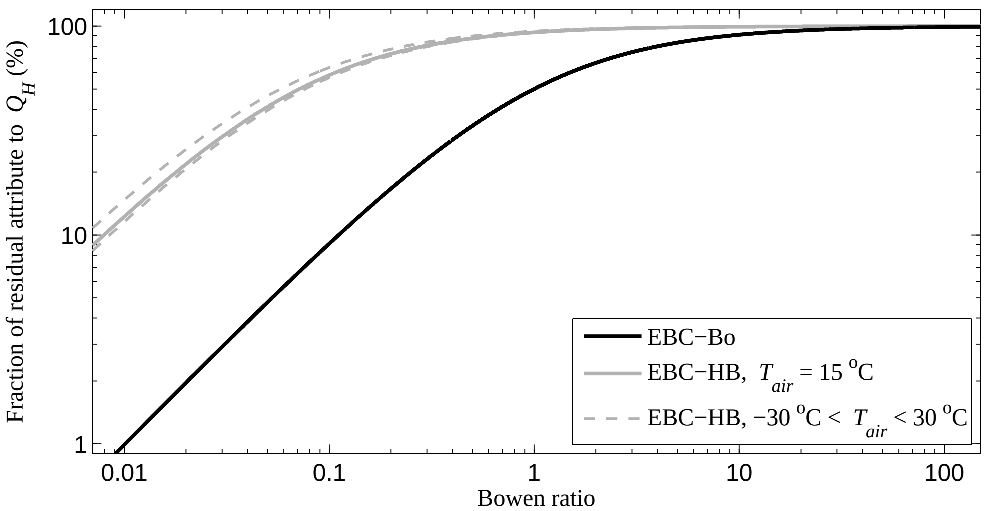

Fig. 8 Fraction of the residual attributed to the sensible heat flux at different Bowen ratios from two different approaches. The Bowen ratio approach (EBC-Bo, black line) assumes the scalar similarity between the sensible and latent heat fluxes by preserving the Bowen ratio (Twine et al., 2000). The buoyancy flux ratio approach (EBC-HB, gray lines) partitions the residual according to the ratio between the sensible heat flux and the buoyancy flux, and is shown at different temperatures from -30°C to 30°C. Even both approaches are identical at very large Bowen ratio, in most cases the larger fraction of the residual would attribute to the sensible heat flux with the buoyancy flux ratio approach.

Acknowledgements This research was funded by the German Research Foundation (DFG) within the projects FO 226/20-1 and BE 2044/4-1. The authors wish to thank all participants of the LITFASS-2003 experiment who produced data used in this analysis. All participants of the LITFASS-2003 experiment are listed in Beyrich and Mengelkamp (2006).

References

Bernstein AB (1966) Examination of certain terms appearing in Reynolds' equations under unsteady conditions and their implications for micrometeorology. Q J R Meteorol Soc 92:533–542

Beyrich F, Mengelkamp HT (2006) Evaporation over a heterogeneous land surface: EVA_GRIPS and the LITFASS-2003 experiment-an overview. Boundary-Layer Meteorol 121:5–32

Desjardins RL, MacPherson JI, Schuepp PH, Karanja F (1989) An evaluation of aircraft flux measurements of co2, water vapor and sensible heat. Boundary-Layer Meteorol 47:55–69

Eigenmann R, Metzger S, Foken T (2009) Generation of free convection due to changes of the local circulation system. Atmos Chem Phys 9:8587–8600

de Feriet JK (1951) Average processes and Reynolds equations in atmospheric turbulence. J Meteorol 8:358–361

Finnigan JJ, Clement R, Malhi Y, Leuning R, Cleugh H (2003) A re-evaluation of long-term flux measurement techniques part i: Averaging and coordinate rotation. Boundary-Layer Meteorol 107:1–48

Foken T (2008a) The energy balance closure problem: an overview. Ecol Appl 18:1351–1367

Foken T (2008b) Micrometeorology. Springer-Verlag, Berlin-Heidelberg

Foken T, Wichura B (1996) Tools for quality assessment of surface-based flux measurements. Agric For Meteorol 78:83–105

Foken T, Göckede M, Mauder M, Mahrt L, Amiro B, Munger W (2004) Post-field data quality control. In: Lee X, Massman W, Law B (eds) Handbook of Micrometeorology, Atmospheric and Oceanographic Sciences Library, vol 29, Springer Netherlands, pp 181–208

Foken T, Wimmer F, Mauder M, Thomas C, Liebethal C (2006) Some aspects of the energy balance closure problem. Atmos Chem Phys 6:4395–4402

Foken T, Mauder M, Liebethal C, Wimmer F, Beyrich F, Leps JP, Raasch S, DeBruin H, Meijninger W, Bange J (2010) Energy balance closure for the LITFASS-2003 experiment. Theor Appl Climatol 101:149–160

Foken T, Aubinet M, Finnigan JJ, Leclerc MY, Mauder M, Paw U KT (2011) Results of a panel discussion about the energy balance closure correction for trace gases. Bull Am Meteorol Soc 92:ES13–ES18

Foken T, Leuning R, Oncley SR, Mauder M, Aubinet M (2012) Corrections and data quality control. In: Aubinet M, Vesala T, Papale D (eds) Eddy Covariance, Springer Atmospheric Sciences, Springer Netherlands, pp 85–131

Hollinger DY, Richardson AD (2005) Uncertainty in eddy covariance measurements and its application to physiological models. Tree Physiol 25:873–885

Inagaki A, Letzel MO, Raasch S, Kanda M (2006) Impact of surface heterogeneity on energy imbalance: A study using LES. J Meteorol Soc Jpn 84:187–198

Kaimal JC, Finnigan JJ (1994) Atmospheric boundary layer flows: their structure and measurement. Oxford University Press

Kaimal JC, Gaynor JE (1991) Another look at sonic thermometry. Boundary-Layer Meteorol 56:401–410

Kaimal JC, Wyngaard JC, Izumi Y, Cote OR (1972) Spectral characteristics of surface-layer turbulence. Q J R Meteorol Soc 98:563–589

Kanda M, Inagaki A, Letzel MO, Raasch S, Watanabe T (2004) LES study of the energy imbalance problem with eddy covariance fluxes. Boundary-Layer Meteorol 110:381–404

Leuning R, van Gorsel E, Massman WJ, Isaac PR (2012) Reflections on the surface energy imbalance problem. Agric For Meteorol 156:65 –74

Liebethal C, Huwe B, Foken T (2005) Sensitivity analysis for two ground heat flux calculation approaches. Agric For Meteorol 132:253–262

Lindroth A, Mölder M, Lagergren F (2010) Heat storage in forest biomass improves energy balance closure. Biogeosciences 7:301–313

Liu H, Peters G, Foken T (2001) New equations for sonic temperature variance and buoyancy heat flux with an omnidirectional sonic anemometer. Boundary-Layer Meteorol 100:459–468

Massman WJ, Lee X (2002) Eddy covariance flux corrections and uncertainties in long-term studies of carbon and energy exchanges. Agric For Meteorol 113:121–144

Mauder M, Foken T (2004) Documentation and instruction manual of the eddy covariance software package TK2. No. 26 in Arbeitsergebnisse, University of Bayreuth, Department of Micrometeorology, URL http://opus.ub.uni-bayreuth.de/opus4-ubbayreuth/frontdoor/index/index/docId/639

Mauder M, Foken T (2006) Impact of post-field data processing on eddy covariance flux estimates and energy balance closure. Meteorol Z 15:597–609

Mauder M, Liebethal C, Göckede M, Leps JP, Beyrich F, Foken T (2006) Processing and quality control of flux data during LITFASS-2003. Boundary-Layer Meteorol 121:67–88

Mauder M, Desjardins RL, Oncley SP, MacPherson I (2007) Atmospheric response to a partial solar eclipse over a cotton field in central california. J Appl Meteorol Climatol 46:1792–1803

Mauder M, Foken T, Clement R, Elbers JA, Eugster W, Grünwald T, Heusinkveld B, Kolle O (2008) Quality control of carboeurope flux data – part 2: Inter-comparison of eddy-covariance software. Biogeosciences 5:451–462

Meek DW, Prueger JH, Kustas WP, Hatfield JL (2005) Determining meaningful differences for SMACEX eddy covariance measurements. J Hydrometeorol 6:805–811

Moore CJ (1986) Frequency response corrections for eddy correlation systems. Boundary-Layer Meteorol 37:17–35

Nordbo A, Launiainen S, Mammarella I, Leppranta M, Huotari J, Ojala A, Vesala T (2011) Long-term energy flux measurements and energy balance over a small boreal lake using eddy covariance technique. J Geophys Res 116:D02,119

Oncley SP, Businger JA, Itsweire EC, Friehe CA, C LJ, Chang SS (1990) Surface layer profiles and turbulence measurements over uniform land under near-neutral conditions. In: 9th Symposium on Boundary Layer and Turbulence, American Meteorological Society, Roskilde, Denmark, pp 237–240

Oncley SP, Foken T, Vogt R, Kohsiek W, DeBruin HAR, Bernhofer C, Christen A, van Gorsel E, Grantz D, Feigenwinter C, Lehner I, Liebethal C, Liu H, Mauder M, Pitacco A, Ribeiro L, Weidinger T (2007) The energy balance experiment EBEX-2000. part I: overview and energy balance. Boundary-Layer Meteorol 123:1–28

Paw U KT, Baldocchi DD, Meyers TP, Wilson KB (2000) Correction of eddy-covariance measurements incorporating both advective effects and density fluxes. Boundary-Layer Meteorol 97:487–511

Raabe A (1983) On the relation between the drag coefficient and fetch above the sea in the case of off-shore wind in the near-shore zone. Z Meteorol 33:363–367

Ruppert J, Thomas C, Foken T (2006) Scalar similarity for relaxed eddy accumulation methods. Boundary-Layer Meteorol 120:39–63

Schotanus P, Nieuwstadt F, De Bruin H (1983) Temperature measurement with a sonic anemometer and its application to heat and moisture fluxes. Boundary-Layer Meteorol 26:81–93

Shaw RH (1985) On diffusive and dispersive fluxes in forest canopies. In: Hutchinson BA, Hicks BB (eds) The Forest-Atmosphere interaction, Reidel Publishing Company, Dordrecht, pp 407–419

Stoy PC, Mauder M, Foken T, Marcolla B, Boegh E, Ibrom A, Arain MA, Arneth A, Aurela M, Bernhofer C, Cescatti A, Dellwik E, Duce P, Gianelle D, van Gorsel E, Kiely G, Knohl A, Margolis H, McCaughey H, Merbold L, Montagnani L, Papale D, Reichstein M, Saunders M, Serrano-Ortiz P, Sottocornola M, Spano D, Vaccari F, Varlagin A (2013) A data-driven analysis of energy balance closure across fluxnet research sites: The role of landscape scale heterogeneity. Agric For Meteorol 171172:137–152

Tanner BD, Swiatek E, Greene JP (1993) Density fluctuations and use of the krypton hygrometer in surface flux measurements. In: Allen RG (ed) Management of Irrigation and Drainage Systems: Integrated Perspectives, American Society of Civil Engineers, New York, pp 945–952

Torrence C, Compo GP (1998) A practical guide to wavelet analysis. Bull Am Meteorol Soc 79:61–78

Twine TE, Kustas WP, Norman JM, Cook DR, Houser PR, Meyers TP, Prueger JH, Starks PJ, Wesely ML (2000) Correcting eddy-covariance flux underestimates over a grassland. Agric For Meteorol 103:279–300

Webb EK, Pearman GI, Leuning R (1980) Correction of flux measurements for density effects due to heat and water vapour transfer. Q J R Meteorol Soc 106:85–100

Wilczak J, Oncley S, Stage S (2001) Boundary-layer meteorol. Boundary-Layer Meteorol 99:127–150

F. Li et al. (2013)

Li, M., Babel, W., Tanaka, K., and Foken, T.: Note on the application of planar-fit rotation for non-omnidirectional sonic anemometers, Atmos. Meas. Tech., 6, 221–229, doi:10.5194/amt-6-221-2013, 2013.

Atmos. Meas. Tech., 6, 221–229, 2013
www.atmos-meas-tech.net/6/221/2013/
doi:10.5194/amt-6-221-2013

Atmospheric Measurement Techniques
Open Access

Note on the application of planar-fit rotation for non-omnidirectional sonic anemometers

M. Li[1], W. Babel[2], K. Tanaka[3], and T. Foken[2,4]

[1]Cold and Arid Regions Environmental and Engineering Research Institute, Chinese Academy of Sciences, Lanzhou, China
[2]Department of Micrometeorology, University of Bayreuth, Bayreuth, Germany
[3]Hiroshima Institute of Technology, Hiroshima, Japan
[4]Member of Bayreuth Centre of Ecology and Environmental Research (BayCEER) of the University of Bayreuth, Bayreuth, Germany

Correspondence to: W. Babel (wolfgang.babel@uni-bayreuth.de)

Received: 12 April 2012 – Published in Atmos. Meas. Tech. Discuss.: 1 October 2012
Revised: 17 January 2013 – Accepted: 20 January 2013 – Published: 5 February 2013

Abstract. For non-omnidirectional sonic anemometers like the Kaijo-Denki DAT 600 TR61A probe, it is shown that separate planar-fit rotations must be used for the undisturbed (open part of the sonic anemometer) and the disturbed sector. This increases the friction velocity while no effect on the scalar fluxes was found. In the disturbed sector, irregular values of $-\overline{u'w'} < 0$ were detected for low wind velocities. Up to a certain extent these results can be transferred to the CSAT3 sonic anemometer (Campbell Scientific Ltd). This study was done for data sets from the Naqu-BJ site on the Tibetan Plateau.

1 Introduction

The planar-fit method (Wilczak et al., 2001) was developed to allow for the use of the eddy-covariance technique in a heterogeneous landscape with a non-uniform wind field and to align the sonic anemometer with the streamlines of this wind field (Finnigan, 2004; Foken et al., 2012a; Rebmann et al., 2012). The rotation angles must be calculated for a long-term data set of some weeks or months duration. This time period must be carefully determined depending on the structure of the underlying surface and the time of the year, including typical wind speeds and stratifications (Siebicke et al., 2012). Before the planar-fit method (PF) had come to the community's attention, the double rotation, described e.g. by Kaimal and Finnigan (1994), was predominantly used to remove mean vertical wind components in eddy-covariance data processing. It forces the mean vertical wind velocity to zero, independently for each single averaging period. Therefore, the double rotation is a very efficient method and it can be used for real time flux calculations (Rebmann et al., 2012). The planar-fit method is preferred now in the community, as it overcame the deficiencies related to the double rotation method. Basically, these are potential overrotation, information loss, deterioration of data quality and a non-consistent reference surface on timescales beyond the averaging period, which is required for seasonal of annual budget estimations (Wilczak et al., 2001; Lee et al., 2004; Foken et al., 2004; Rebmann et al., 2012). Especially in complex landscapes and over tall vegetation, the vertical wind velocity may not always be zero for 30-min averages, which has to be taken into account (Lee, 1998; Paw U et al., 2000; Finnigan et al., 2003). In many cases, however, the terrain structure is too complex to be levelled on a plane by a single planar-fit rotation. Finnigan et al. (2003) mention a dependence of the rotation angle on wind direction for such cases, which can be realized, e.g. by a sector-wise planar-fit. This has been proposed by Foken et al. (2004) and already adopted, e.g. by Ono et al. (2008), Yuan et al. (2011), and Siebicke et al. (2012).

The planar-fit method is ideally suited for omnidirectional sonic anemometers like USA-1 (Metek GmbH), R3 (Gill Instruments Ltd.) and others. For this type of sensors, no wind sector is significantly influenced by flow distortion. Therefore, the rotation follows the wind field and should not be affected by sonic anemometer structures. Nevertheless, an

Published by Copernicus Publications on behalf of the European Geosciences Union.

influence of such structures can also be found for omnidirectional sonic anemometers (Göckede et al., 2008), but often these are symmetric in three or four directions. This is not the case for sonic anemometers with an open measuring sector and a disturbed sector due to the anemometer mounting structure (Dyer, 1981). A classical representative of this anemometer type is the DAT 600 with the so-called TR61A-probe, produced by Kaijo-Denki, Japan (Fig. 1a, Hanafusa et al., 1982), which is still in use. The most commonly currently used example is the CSAT3, produced by Campbell Scientific Ltd., USA (Fig. 1b).

The non-omnidirectional sonic anemometer has two sectors: the disturbed sector and the undisturbed measuring sector with nearly no flow distortion. The undisturbed (open) sector extends from its centre $\pm 60°$ for the Kaijo-Denki TR61A-probe (Fig. 1a), and $\pm 170°$ in the case of the CSAT3 (Fig. 1b, any direction except flow from the back side). The disturbed sector for CSAT3 was confirmed to be approximately $\pm 20°$ in wind tunnel measurements (Friebel et al., 2009). Field measurements typically show a standard deviation for wind direction of $\pm 20°$, which is also found in the data sets used for this study. It is usually recognised in flux processing to exclude the disturbed sector in the back of the CSAT3 measuring paths (Foken et al., 2004). The opposite sector, when the wind passes the measuring paths before encountering the CSAT3 mounting structure (front sector), is usually not considered as disturbed in flux processing. Siebicke and Serafimovich (2007) can confirm a strong effect on wind velocities in the back sector of a CSAT3, but also a weak effect of the front sector on low wind velocities in a wind tunnel study.

To account for these instrument-specific characteristics combined with the standard deviation of wind direction, the undisturbed sector is assumed to be $\pm 40°$ for DAT 600 and $\pm 150°$ for CSAT3 in the following analyses, and the CSAT3 front sector will be handled separately. When using the planar-fit method for the whole wind sector, the determination of the regression coefficients (and therefore rotation angles) is influenced by the disturbed flow due to sensor structure. Hence the flux calculation is based on a wrong coordinate system. As this problem is often not considered in flux processing, we will discuss the effect when correctly applying the planar-fit method for the undisturbed sector only.

The Kaijo-Denki sonic anemometer must normally be used together with a rotator and moved into the mean wind direction for each measuring series (Foken et al., 1988). If this is not done, the results are significantly influenced in the 240° disturbed sector. A typical error is the occurrence of negative frictions, $-\overline{u'w'} < 0$ (Gerstmann and Foken, 1984), where w' and u' are the fluctuations of the vertical wind component and the horizontal wind component, respectively; the latter is aligned into the mean wind direction. The anemometer is typically rotated into the mean wind direction and $-\overline{v'w'} \approx 0$ (v' wind component perpendicular to the mean wind direction). It follows for continuity reasons that $-\overline{u'w'} > 0$. A self-correlation, however, occurs between u' and w' due to flow distortion mainly in the case of low wind speeds, creating irregular friction values. Similar errors were also found in the data set of the CAMP/Tibet (Coordinated Enhanced Observing Period (CEOP), Asia-Australia Monsoon Project (CAMP) on the Tibetan Plateau) experiment (Li et al., 2006). Furthermore, for earlier experiments at this site in 1998 and 2002, Hong et al. (2004) reported unexplained differences of the wind measurements with the Kaijo-Denki TR61A-probe and the CSAT3.

2 Material and methods

For this study, two well-analysed and quality-checked data sets from 6 February to 30 September 2008 (data set A) and from 14 May to 25 June 2010 (data set B), with half hour values of the calculated fluxes, were used. These data sets have been examined in preference to an earlier data set of CAMP/Tibet from 12 April 2004 to 3 September 2007 at the Naqu-BJ site (91° 48′ 59″ E, 31° 18′ 42″ N, 4502 m a.s.l.), where we already found negative friction for about 50 % of the data. Like during CAMP/Tibet, the Kaijo-Denki DAT 600 TR61A probe sonic anemometer was installed at 20 m height on a tower orientated to a westerly direction (270°, Fig. 1c) for data set A. Data set B also stems from the Naqu-BJ site, but was a direct comparison of the Kaijo-Denki DAT 600 TR61A probe (orientation 263°) and the Campbell CSAT3 (orientation 213°) at a measuring height of 3.02 m (Fig. 1d). The Naqu-BJ site is located on a flat grassland (5 cm high during the monsoon season) near Nagqu city. The Nagqu area lies in the sub-frigid climatic zones, and annual mean temperature ranges from -0.9 °C to -3.3 °C. The landscape is very flat (incline $< 2°$), and gentle hills occur in NNW–NE of the measurement location; the shortest distance to the hill slope is 900 m in NNE (Fig. 1c). Other hills and mountains in sectors E, S, and W are at least 10 km away from the eddy-covariance setup (south-west sector is shown in Fig. 1d). Thus a possible terrain influence on the wind field can be neglected, and the deviations from its ideal behaviour can be attributed to sensor structures and the influence of the tower.

The data were analysed with the software package TK2/TK3 (Mauder and Foken, 2004, 2011; Mauder et al., 2008), which offers the possibility of applying the planar-fit method sector-wise within a given data set. The applied corrections were done in the software package according to Foken et al. (2012b).

The planar-fit method was applied for (i) the whole data set, and (ii) separately for the undisturbed and the disturbed sector. The undisturbed sector of the DAT 600 sonic anemometer was defined as $\pm 40°$ from the centre of the undisturbed sector. For CSAT3 we used $\pm 150°$, but separated the front sector, selected as $\pm 30°$. This sector is positively rated by the community in general but shows weak influence of sensor structure. Hence the front sector is rotated

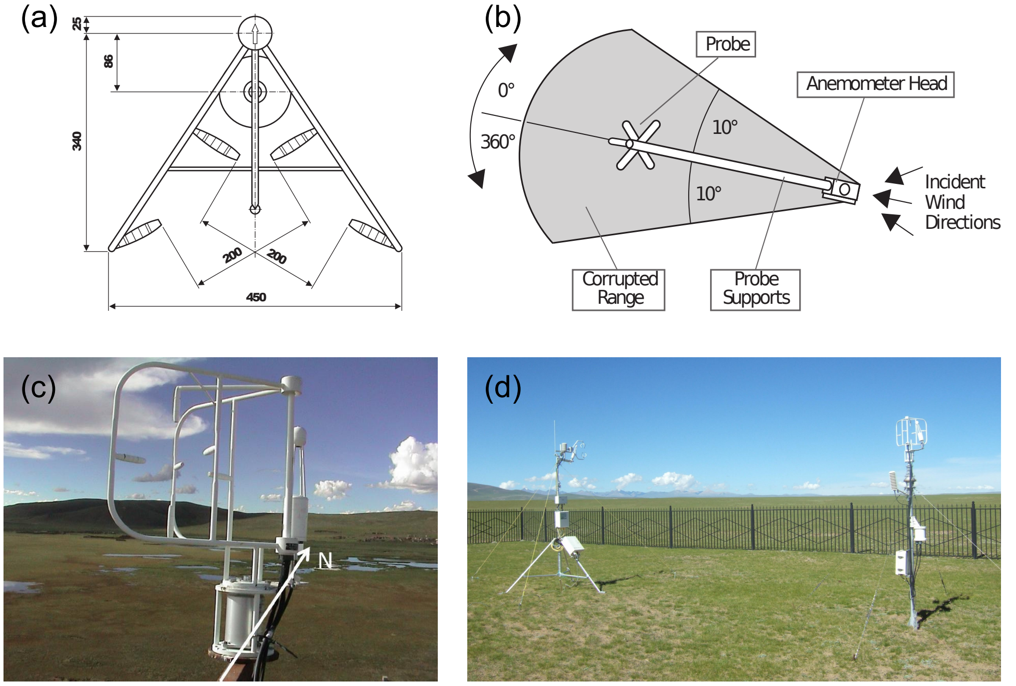

Fig. 1. (a) Kaijo-Denki, DAT 600, TR61A-probe, view from top (redrawn from Hanafusa et al., 1982). **(b)** Campbell CSAT3, view from top and orientation to north (Campbell Scientific Ltd., redrawn from Friebel et al., 2009); for the given orientation the disturbed sector is 170°–190° in accordance with wind tunnel measurements and is therefore assumed to be smaller than in this study. **(c)** Kaijo-Denki, DAT 600, TR61A-probe installed at Naqu-BJ site at 20.8 m height on a 22-m tall tower with the open sector to west, data set A. The picture is taken from the perspective of the tower; the sonic measuring paths appear at an angle of roughly 320° (photograph: Kenji Tanaka). **(d)** Campbell CSAT3 (left) and Kaijo-Denki, DAT 600 TR61A probe (right) installed in 2010 at Naqu-BJ site at 3.02 m height with the open sector to west, data set B (photograph: Tobias Gerken).

separately and associated with the undisturbed sector, but occasionally excluded in order to yield comparisons for open sectors in the strict sense. An overview of the sensor orientation and wind sector definitions is given in Table 1. Based on these values, the DAT 600 and the CSAT3 have an overlap of their undisturbed sectors from 223° to 303° when including the CSAT3 front sector and from 243° to 303° when solely using the open sectors. The planar-fit angles calculated for all sectors described in Table 1 show generally low values, which is to be expected. The largest angles are approx. 4° (data set A), which can be explained by misalignment of the sensor. They are consistent; i.e. angles for a certain sector may deviate from the respective value of the whole planar-fit, but face a compensative deviation in the opposing sector. These deviations are larger for smaller sectors and vice versa. The determination of the coefficients of the planar-fit method was only done for such data classified as data with high or moderate quality (classes 1–6 according to Foken et al., 2004). Furthermore, the flat topography and the low vegetation allow for the usage of the double rotation as well. Therefore, the double rotation is applied for comparison in this study.

3 Results

Because the mean vertical wind velocity is mainly affected by flow distortion, these data are investigated in detail for both instruments and data sets. Figure 2 shows that the vertical velocity without any rotation for data set A is larger in the sector from 150° to 260° due to the higher wind speeds (Fig. 2a). After normalization with the mean horizontal wind velocity, the finding agrees with a tilt error and a sinuous-like w-value distribution (Fig. 2d). Singular and negative w-values were found for a wind direction of 130°–135°, which is nearly identical to the tower position (Fig. 1c). For this analysis only data with high quality (classes 1–3 according to Foken et al., 2004) were used. When including data with moderate and low quality, the sinuous-like distribution can hardly be seen (not shown). The scatter around this distribution can be mainly attributed to data points where irregular friction occurs (red points in Fig. 2d). For data set

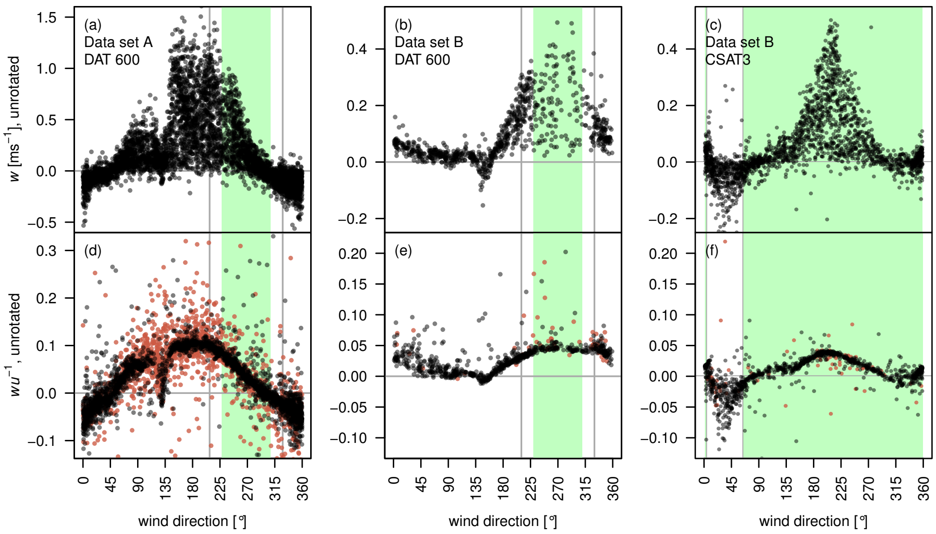

Fig. 2. Vertical wind velocity and its dependency on the wind direction for unrotated data and high data quality (flag 1–3 according to Foken et al., 2004); the upper row displays mean vertical velocity **(a–c)**, the lower row mean vertical wind velocity normalised by the horizontal wind velocity **(d–f)**; $wu^{-1} = 0.1$ equals a tilt angle of 5.7°; columns represent DAT 600, data set A on the left **(a, d)**, DAT 600, data set B in the middle **(b, e)** and CSAT3, data set B on the right **(c, f)**. The green sector is the undisturbed sector, and the red points indicate data with $-\overline{u'w'} < 0$.

Table 1. Definition of the specific wind sectors as related to sensor orientation. The open sector marks the undisturbed sector; the CSAT3 front sector is occasionally associated with the undisturbed sector.

Data set	Device	Sensor-specific sectors Label	Orientation [°]	Size [°]
A	DAT 600	whole	0–360	360
		open	230–310	80
		disturbed	0–230 ∪ 310–360	280
B	DAT 600	whole	0–360	360
		open	223–303	80
		disturbed	0–223 ∪ 303–360	280
B	CSAT3	whole	0–360	360
		open	0–3 ∪ 63–183 ∪ 243–360	240
		front	183–243	60
		disturbed	3– 63	60

B, smaller values occur due to the changed measurement height (Fig. 2b, c, e, f). After applying the planar-fit method for all wind directions, the vertical wind velocity is much smaller but still with a high scatter (Fig. 3a, b, c). After sector-wise planar-fit, the undisturbed sector shows considerably lower vertical wind speeds of approx. $\pm 0.1\,\mathrm{m\,s^{-1}}$ for data set A, DAT 600 (Fig. 3d). Only a small number of outliers are left with a higher-than-average occurrence of irregular friction. Significant scatter in the data can be found at 210° and 330°, corresponding to the anemometer construction (Fig. 1a), while the range from 120° up to 140° also includes the effects of the tower (Fig. 1c). Around 90° the data are affected due to the flow through the probe from behind. For data set B the results for DAT 600 are similar. For CSAT3 the vertical wind velocity after rotation is reduced by the sector-wise planar-fit only in the front sector (Fig. 3e, f). In the open sector, the sector-wise planar-fit reduces vertical wind velocity mainly near the disturbed sector, but at the expense of the fit near the front sector, creating strong discontinuities there. The reason could be that flow from the CSAT3 back side might be disturbed beyond the defined sector limits and therefore still influences the open sector.

Secondly, the data set was analysed regarding the condition $-\overline{u'w'} < 0$ for the planar-fit rotated data. The result is illustrated in Fig. 4 for high data quality, and Table 2 summarises the number of occurrences for different data quality ranges. In data set A irregular friction values are reduced by the sector-wise rotation in the optimal measuring sector (Fig. 4a, d). In the sector with flow distortion, these values were only found for wind velocities below $6\,\mathrm{m\,s^{-1}}$ and in the non-neutral stability range. This is similar to the findings of Gerstmann and Foken (1984) and is obviously related to flow distortion, which is more significant for low wind velocities. The double rotation decreases irregular friction velocities in the undisturbed sector even more (Fig. 4g). For data set B, similar results for the DAT 600 were obtained (Fig. 4b, e,

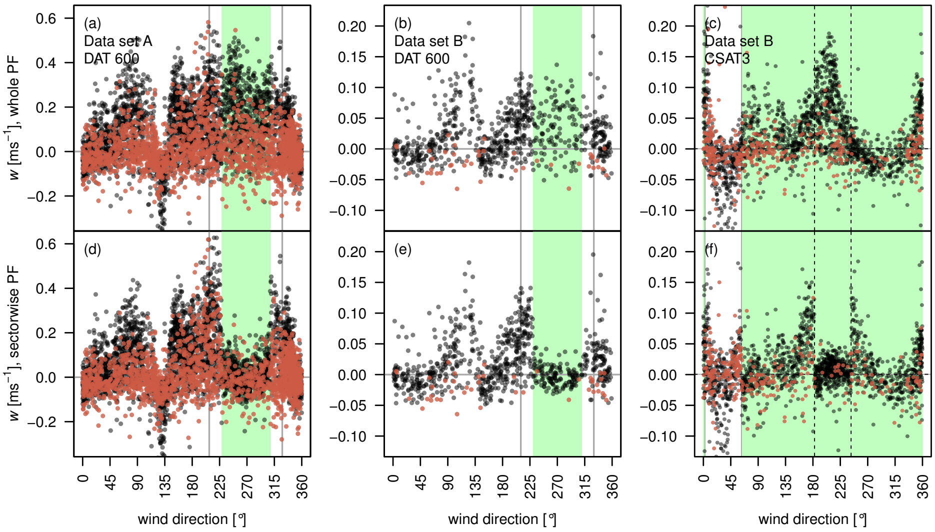

Fig. 3. Mean vertical wind velocity and its dependency on the wind direction for rotated data and high data quality (flag 1–3 according to Foken et al., 2004); the upper row displays mean vertical velocity rotated for the whole period **(a–c)**, the lower row mean vertical wind velocity rotated sector-wise **(d–f)**; columns represent DAT 600, data set A on the left **(a, d)**, DAT 600, data set B in the middle **(b, e)** and CSAT3, data set B on the right **(c, f)**. The green sector is the undisturbed sector and the red points indicate data with $-\overline{u'w'} < 0$; dashed lines for CSAT3 indicate the front sector, which is rotated separately.

h), but many fewer occurrences of irregular friction velocity were found due to the low measuring height. For high data quality the rare incidences prohibit an interpretation of the differences, but both the sector-wise planar-fit and the double rotation yield substantial reduction compared to the whole planar-fit when including moderate and low data quality (Table 2). Also, for CSAT3, data with $-\overline{u'w'} < 0$ occur mainly in the disturbed sector (Fig. 4c, f, i) and for low data quality (Table 2), although the relative frequency in the open sector is in general larger than for DAT 600, data set B. The sector-wise planar-fit yields substantial reduction of irregular friction velocities especially in the front sector (between the dashed lines). In the open sector, however, the improvement is small and the double rotation fails to reduce such incidents for high and moderate data quality. The reduction of irregular friction velocities by the sector-wise planar-fit increases when including the CSAT3 front sector. When no separate rotation for the front sector of the CSAT3 is made, however, there is nearly no difference visible between whole and sector-wise rotation (not shown). This suggests that the disturbed sector should be excluded but that the front and side sectors should be rotated separately.

The friction velocity and the sensible heat flux were compared when using only one rotation for the whole data set versus sector-wise rotation (Fig. 5a, b). Slope and offset were obtained using a geometric mean regression (e.g. Helsel and Hirsch, 2002). The data of the disturbed sector were discarded, and only data with high data quality (classes 1–3) are shown for data set A and DAT 600. When including moderate data quality (classes 4–6), the scatter is larger but the tendency of the regressions does not change (not shown). The friction velocity is enhanced by 10 % through the sector-wise planar-fit rotation (Fig. 5, a), while the sensible heat flux was obviously not different for both planar-fit rotations (Fig. 5, b). The double rotation yields much larger

Table 2. Percentage of irregular data with $-\overline{u'w'} < 0$ for only the undisturbed sector (for sector definitions see Table 1) and different data qualities (QC flag) according to Foken et al. (2004).

Data set	Device	QC flag	Sector-wise planar-fit N	Sector-wise planar-fit irr.*	Whole planar-fit N	Whole planar-fit irr.*	Double rotation N	Double rotation irr.*
A	DAT 600	1–3	964	20	920	34	1035	14
		1–6	1795	25	1766	43	1960	17
		1–8	2056	26	2056	46	2056	18
B	DAT 600	1–3	140	2.1	121	3.3	146	1.4
		1–6	209	2.4	182	8.8	245	1.6
		1–8	302	3.0	302	17.2	302	1.3
B	CSAT3 nF [a]	1–3	617	3.9	609	4.3	698	5.7
		1–6	836	9.2	814	10.8	913	10.4
		1–8	1137	15.6	1138	17.5	1138	12.3
B	CSAT3 sF [b]	1–3	832	3.4	795	4.4	916	5.0
		1–6	1154	7.4	1110	9.6	1256	9.1
		1–8	1608	12.0	1609	15.9	1609	10.5

* irr: irregular occurrences of friction $-\overline{u'w'} < 0$ in %
[a] nF: no front sector, front sector excluded from undisturbed sector
[b] sF: front sector included but rotated separately in the sector-wise planar-fit.

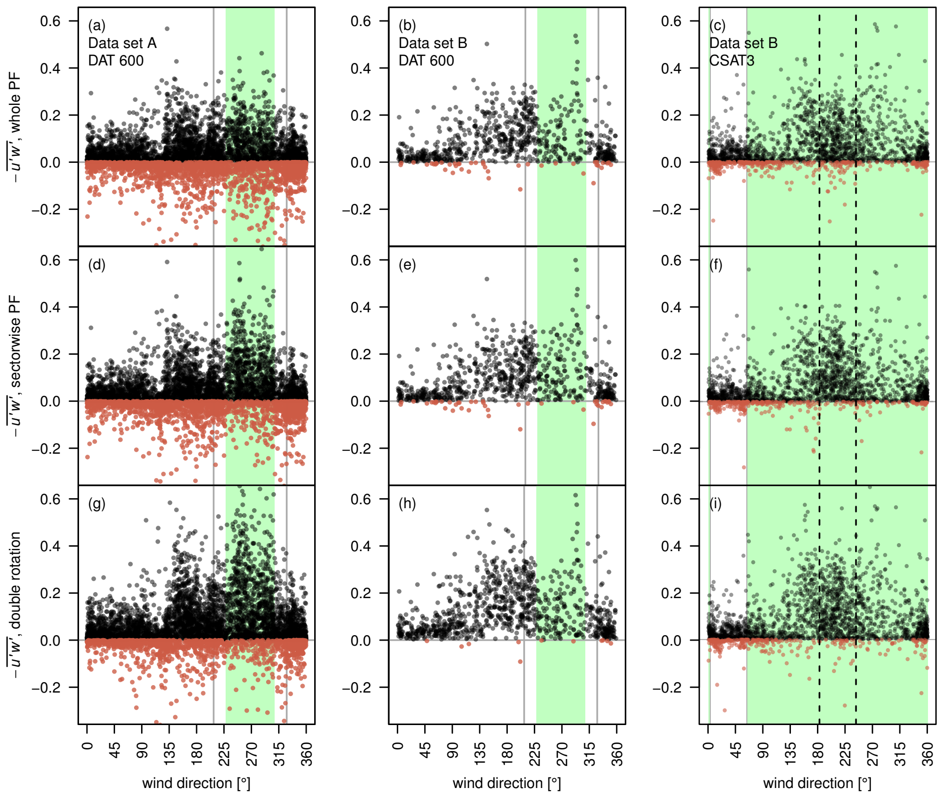

Fig. 4. Covariance $-\overline{u'w'}$ and its dependency on the wind direction for rotated data and high data quality (flag 1–3 according to Foken et al., 2004); The upper row displays $-\overline{u'w'}$, data rotated for the whole period **(a–c)**, the middle row $-\overline{u'w'}$, data rotated sector-wise **(d–f)**, the lower row $-\overline{u'w'}$, using double rotation **(g–i)**; columns represent DAT 600, data set A on the left **(a, d, g)**, DAT 600, data set B in the middle **(b, e, h)** and CSAT3, data set B on the right **(c, f, i)**. The green sector is the undisturbed sector and the red points indicate data with $-\overline{u'w'} < 0$; dashed lines for CSAT3 indicate the front sector, which is rotated separately.

friction velocities than the sector-wise planar-fit (Fig. 5, c). For moderate and low data quality, even unrealistic values of $u_* > 2\,\mathrm{m\,s^{-1}}$ occur due to double rotation. The sensible heat flux is not affected for high data quality, but the number of outliers again increases with data quality, complicating accurate slope estimation. The results for both data sets and instruments are shown in Table 3. In data set B the DAT 600 behaves similarly as in data set A, but the friction velocity is increased by only 4–5 %. The friction velocity from CSAT3 is not markedly affected, even if the front sector is included. Compared to the double rotation, the sector-wise planar-fit slightly increases the friction velocity for data set B, DAT 600, and decreases the friction velocity for CSAT3. The sensible heat flux is again not affected. Few outliers occurred for double rotation, which could be easily removed by applying consistency limits to fluxes with $u_* > 2\,\mathrm{m\,s^{-1}}$ and $Q_\mathrm{H} > 1000\,\mathrm{W\,m^{-2}}$.

The results confirm the findings by Hong et al. (2004) for the Naqu-BJ site: "*There was little difference in kinematic sensible heat fluxes (not shown) [. . .] However, $\overline{u'w'}$ from KD was 5 % smaller than that from CS*" (KD: Kaijo-Denki, CS: Campbell Scientific CSAT3). Hong et al. (2004) could not give an explanation for these differences and corrected the KD data with the CS measurements. Contrary to Hong et al. (2004), our findings for σ_u and σ_v showed no considerable effect of the rotation method.

4 Conclusions

If non-omnidirectional sonic anemometers are not moved into the mean wind direction for each measuring series or the data are not selected only for the open sector of the anemometer, the coordinate rotation or planar-fit method must be applied with care. For the open sector of the anemometer, a separate planar-fit should be used. All data from the other sector must be flagged as low data quality, especially because, for low wind velocities, irregular friction

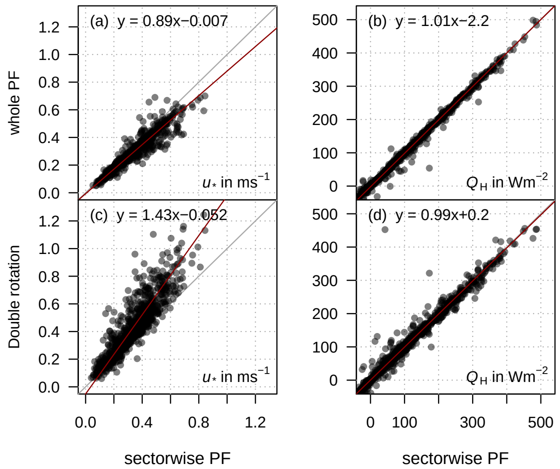

Fig. 5. Comparison of the sector-wise planar-fit rotation vs. planar-fit rotation for all wind directions **(a, b)** and vs. double rotation **(c, d)** for the friction velocity **(a, c)** and the sensible heat flux **(b, d)**; data set A, DAT 600, was used, only from the undisturbed sector and with high quality (flag 1–3 according to Foken et al., 2004).

Table 3. Regression analysis of the friction velocity and sensible heat flux using geometric mean regression for different data qualities (QC flag) according to Foken et al. (2004). Only data from the undisturbed sector are used. For sector definitions, see Table 1.

Data set	Device	QC flag	Friction velocity $[\mathrm{m\,s^{-1}}]$			Sensible heat flux $[\mathrm{W\,m^{-2}}]$		
			a	b	R^2	a	b	R^2
Regression $y = ax + b$ with x: sector-wise planar-fit, y: planar-fit for the whole sector								
A	DAT 600	1–3	0.89	−0.007	0.87	1.01	−2.2	0.98
		1–6	0.85	−0.003	0.84	1.01	−3.5	0.95
B	DAT 600	1–3	0.96	−0.011	0.99	0.99	0.3	0.99
		1–6	0.95	−0.015	0.97	0.99	0.3	0.99
B	CSAT3 nF [a]	1–3	1.02	−0.005	0.99	1.01	−0.4	0.99
		1–6	1.01	−0.004	0.99	1.00	−0.1	0.99
B	CSAT3 sF [b]	1–3	1.00	−0.006	0.98	1.00	0.0	0.99
		1–6	0.99	−0.003	0.97	1.00	0.1	0.97
Regression $y = ax + b$ with x: sector-wise planar-fit, y: double rotation								
A	DAT 600	1–3	1.43	−0.052	0.80	0.99	0.2	0.96
		1–6	1.66[c]	−0.078	0.70	1.17[c]	−6.9	0.74
B	DAT 600	1–3	0.97	0.039	0.89	1.01	−0.3	0.99
		1–6	0.98	0.039	0.87	1.02	−0.4	0.99
B	CSAT3 nF [a]	1–3	1.05	0.005	0.98	1.02	−0.4	0.98
		1–6	1.06	0.008	0.96	1.02	−0.9	0.95
B	CSAT3 sF [b]	1–3	1.04	0.005	0.98	1.01	−0.1	0.98
		1–6	1.05	0.006	0.95	1.02	−1.1	0.96

[a] nF: no front sector, front sector excluded from undisturbed sector
[b] sF: front sector included but rotated separately in the sector-wise planar-fit
[c] slope sensitive to several outliers occurring in data from double rotation.

Table 4. Regression analysis of the friction velocity and sensible heat flux using geometric mean regression for different data qualities (QC flag) according to Foken et al. (2004). Only data from the undisturbed sector are used. For sector definitions, see Table 1.

Rotation method	QC flag	Friction velocity $[\mathrm{m\,s^{-1}}]$			Sensible heat flux $[\mathrm{W\,m^{-2}}]$		
		a	b	R^2	a	b	R^2
Regression $y = ax + b$ with y: DAT 600, data set B, x: CSAT3, data set B, front sector excluded							
Sector-wise planar-fit	1–3	1.00	0.004	0.97	1.03	−4.3	0.95
	1–6	1.00	0.000	0.96	0.92	2.9	0.81
Whole planar-fit	1–3	0.94	−0.006	0.97	1.01	−5.7	0.93
	1–6	0.95	−0.019	0.95	0.93	1.0	0.87
Double rotation	1–3	0.97	0.016	0.93	1.01	−3.4	0.95
	1–6	1.02	0.000	0.86	0.91	4.0	0.82
Regression $y = ax + b$ with y: DAT 600, data set B, x: CSAT3, data set B, front sector included							
Sector-wise planar-fit	1–3	1.01	−0.002	0.95	0.99	−0.7	0.95
	1–6	1.01	−0.007	0.94	0.95	1.5	0.89
Whole planar-fit	1–3	0.94	−0.007	0.95	0.97	−1.1	0.92
	1–6	0.93	−0.016	0.91	0.95	0.1	0.89
Double rotation	1–3	0.97	0.009	0.89	0.97	0.9	0.90
	1–6	0.95	0.013	0.81	0.94	2.6	0.85

data are possible. The problem is not limited to the Kaijo-Denki DAT 600 TR61A probe but is similar in the case of other sonic anemometer types, such as CSAT3 (Campbell Scientific Ltd.), with a much larger open sector of 340°. By applying the data quality scheme according to Foken et al. (2004, Table 9.5, but not included in TK3 software), the data from the remaining disturbed sector of 20° (CSAT3) are flagged as containing errors (flag 9). But this selection must be applied before the planar fit rotation. However, a substantial fraction of irregular friction data cannot be eliminated by a sector-wise planar-fit. Furthermore, the vertical wind velocity is also influenced by the CSAT3 probe supporting structures for wind directions from the front sector. A separate planar-fit rotation for this sector substantially reduces mean vertical wind velocity in this sector and also has an effect on the friction velocity.

Published data of the Naqu-BJ site (Hong et al., 2004; Li et al., 2006) or other sites with Kaijo-Denki, TR61A-probe sonic anemometers, should be used with care. Fortunately, only the friction velocity and standard deviations of the wind components are affected, with no substantial influence being found for scalar fluxes. Nevertheless, the separate planar-fit rotation should be used for all data. If the coefficients of the planar-fit rotation for both instruments were only determined for the undisturbed sector, differences in friction velocity between DAT 600 and CSAT3 can be substantially reduced (Table 4). Therefore, a correction of DAT 600 data according to a comparison with a CSAT3, as done by Hong et al. (2004), does not seem to be necessary for high quality flux data from the undisturbed sector. The double rotation yields reasonable results for high data quality, but the occurrence of outliers and larger scatter (lower coefficients of determination in Table 4) confirms the mentioned problem of potential overrotation.

The CSAT3 is one of the best rated sonic anemometers available (Mauder et al., 2007). This study does not call these findings into question, but rather it demonstrates some problems related to the CSAT3 probe structures, which could not be conclusively clarified. Therefore, more thorough experiments should be conducted regarding influence of the CSAT3 geometry on the flow field, including information about internal sensor-specific corrections as pointed out by Burns et al. (2012).

Acknowledgements. This work is financed by the German Research Foundation (DFG) Priority Programme 1372 TiP and the Chinese National Key Programme for Developing Basic Sciences (2010CB951703). It is further financed by CEOP-AEGIS, a Collaborative Project/Small or medium-scale focused research project – Specific International Co-operation Action financed by the European Commission under FP7 topic ENV.2007.4.1.4.2 “Improving observing systems for water resource management” and coordinated by the University of Strasbourg, France. The authors acknowledge support from the National Natural Science Foundation of China (Grant No. 41175008). Furthermore, this publication is funded by the DFG and the University of Bayreuth in the funding programme Open Access Publishing.

Edited by: A. Stoffelen

References

Burns, S. P., Horst, T. W., Jacobsen, L., Blanken, P. D., and Monson, R. K.: Using sonic anemometer temperature to measure sensible heat flux in strong winds, Atmos. Meas. Tech., 5, 2095–2111, doi:10.5194/amt-5-2095-2012, 2012.

Dyer, A. J.: Flow distortion by supporting structures, Bound.-Lay. Meteorol., 20, 243–251, doi:10.1007/BF00119905, 1981.

Finnigan, J. J.: A re-evaluation of long-term flux measurement techniques, Part II: Coordinate systems, Bound.-Lay. Meteorol., 113, 1–41, doi:10.1023/B:BOUN.0000037348.64252.45, 2004.

Finnigan, J., Clement, R., Malhi, Y., Leuning, R., and Cleugh, H.: A re-evaluation of long-term flux measurement techniques, Part I: Averaging and Coordinate Rotation, Bound.-Lay. Meteorol., 107, 1–48, doi:10.1023/A:1021554900225, 2003.

Foken, T., Zelený, J., Zubkovskij, S. L., and Fedorov, M. M.: Comparison of turbulence measuring instruments, in: Structure of the Boundary Layer over Non-Homogeneous Terrain, Proceedings of the Field Experiment KOPEX-86, Prague, 25–35, 1988.

Foken, T., Göckede, M., Mauder, M., Mahrt, L., Amiro, B., and Munger, J.: Post-field data quality control, in: Handbook of Micrometeorology: a Guide for Surface Flux Measurement and Analysis, edited by: Lee, X., Massman, W., and Law, B., Kluwer, Dordrecht, 181–208, 2004.

Foken, T., Aubinet, M., and Leuning, R.: The eddy covariance method, in: Eddy Covariance: a Practical Guide to Measurement and Data Analysis, edited by: Aubinet, M., Vesala, T., and Papale, D., Springer Atmospheric Sciences, Springer, The Netherlands, doi:10.1007/978-94-007-2351-1_1, 1–19, 2012a.

Foken, T., Leuning, R., Oncley, S. R., Mauder, M., and Aubinet, M.: Corrections and data quality control, in: Eddy Covariance: a Practical Guide to Measurement and Data Analysis, edited by: Aubinet, M., Vesala, T., and Papale, D., Springer Atmospheric Sciences, Springer, The Netherlands, doi:10.1007/978-94-007-2351-1_4, 85–131, 2012b.

Friebel, H. C., Herrington, T. O., and Benilov, A. Y.: Evaluation of the flow distortion around the Campbell scientific CSAT3 sonic anemometer relative to incident wind direction, J. Atmos. Ocean. Tech., 26, 582–592, doi:10.1175/2008JTECHO550.1, 2009.

Gerstmann, W. and Foken, T.: Eigenschaften des Ultraschallanemometers der Firma Kaijo-Denki auf Grund der Ergebnisse von MESP-81 (Properties of the sonic anemometer of the Kaijo-Denki company on the basis of the results of the experiment ITCE-81), Geod. Geophys. Veröff., R. II, 26, 30–35, 1984.

Göckede, M., Foken, T., Aubinet, M., Aurela, M., Banza, J., Bernhofer, C., Bonnefond, J. M., Brunet, Y., Carrara, A., Clement, R., Dellwik, E., Elbers, J., Eugster, W., Fuhrer, J., Granier, A., Grünwald, T., Heinesch, B., Janssens, I. A., Knohl, A., Koeble, R., Laurila, T., Longdoz, B., Manca, G., Marek, M., Markkanen, T., Mateus, J., Matteucci, G., Mauder, M., Migliavacca, M., Minerbi, S., Moncrieff, J., Montagnani, L., Moors, E., Ourcival, J.-M., Papale, D., Pereira, J., Pilegaard, K., Pita, G., Rambal, S., Rebmann, C., Rodrigues, A., Rotenberg, E., Sanz, M. J., Sedlak, P., Seufert, G., Siebicke, L., Soussana, J. F., Valentini, R., Vesala, T., Verbeeck, H., and Yakir, D.: Quality control of CarboEurope flux data – Part 1: Coupling footprint analyses with flux data quality assessment to evaluate sites in forest ecosystems, Biogeosciences, 5, 433–450, doi:10.5194/bg-5-433-2008, 2008.

Hanafusa, T., Fujitani, T., Kobori, Y., and Mitsuta, Y.: A new type sonic anemometer-thermometer for field operation, Pap. Meteorol. Geophys., 33, 1–19, 1982.

Helsel, D. and Hirsch, R. M.: Statistical Methods in Water Resources, Techniques of Water Resources Investigations, Book 4, chapter A3, US Geological Survey, 522 pp., available at: http://water.usgs.gov/pubs/twri/twri4a3/, 2002.

Hong, J., Choi, T., Ishikawa, H., and Kim, J.: Turbulence structures in the near-neutral surface layer on the Tibetan Plateau, Geophys. Res. Lett., 31, L15106, doi:10.1029/2004GL019935, 2004.

Kaimal, J. C. and Finnigan, J. J.: Atmospheric Boundary Layer Flows: their Structure and Measurement, Oxford University Press, New York, NY, 289 pp., 1994.

Lee, X.: On micrometeorological observations of surface-air exchange over tall vegetation, Agr. Forest Meteorol., 91, 39–49, doi:10.1016/S0168-1923(98)00071-9, 1998.

Lee, X., Finnigan, J., and Paw U, K.: Coordinate systems and flux bias error, in: Handbook of micrometeorology: A guide for surface flux measurement and analysis, edited by: Lee, X., Massman, W., and Law, B., 33–66, Kluwer, Dordrecht, 2004.

Li, M., Ma, Y., Ma, W., Hu, Z., Ishikawa, H., Su, Z., and Sun, F.: Analysis of turbulence characteristics over the Northern Tibetan Plateau area, Adv. Atmos. Sci., 23, 579–585, doi:10.1007/s00376-006-0579-z, 2006.

Mauder, M. and Foken, T.: Documentation and Instruction Manual of the Eddy Covariance Software Package TK2, Work Report University of Bayreuth, Dept. of Micrometeorology, ISSN

1614-8916, 26, 42 pp., available at: http://opus.ub.uni-bayreuth.de/opus4-ubbayreuth/frontdoor/index/index/docId/639, 2004.

Mauder, M. and Foken, T.: Documentation and Instruction Manual of the Eddy-Covariance Software Package TK3, Work Report University of Bayreuth, Dept. of Micrometeorology, ISSN 1614-8916, 46, 58 pp., available at: http://opus.ub.uni-bayreuth.de/opus4-ubbayreuth/frontdoor/index/index/docId/681, 2011.

Mauder, M., Oncley, S., Vogt, R., Weidinger, T., Ribeiro, L., Bernhofer, C., Foken, T., Kohsiek, W., De Bruin, H., and Liu, H.: The energy balance experiment EBEX-2000. Part II: Intercomparison of eddy-covariance sensors and post-field data processing methods, Bound.-Lay. Meteorol., 123, 29–54, doi:10.1007/s10546-006-9139-4, 2007.

Mauder, M., Foken, T., Clement, R., Elbers, J. A., Eugster, W., Grünwald, T., Heusinkveld, B., and Kolle, O.: Quality control of CarboEurope flux data – Part 2: Inter-comparison of eddy-covariance software, Biogeosciences, 5, 451–462, doi:10.5194/bg-5-451-2008, 2008.

Ono, K., Mano, M., Miyata, A., and Inoue, Y.: Applicability of the Planar Fit Technique in Estimating Surface Fluxes over Flat Terrain using Eddy Covariance, J. Agric. Meteorol., 64, 121–130, doi:10.2480/agrmet.64.3.5, 2008.

Paw U, K., Baldocchi, D., Meyers, T., and Wilson, K.: Correction Of Eddy-Covariance Measurements Incorporating Both Advective Effects And Density Fluxes, Bound.-Lay. Meteorol., 97, 487–511, doi:10.1023/A:1002786702909, 2000.

Rebmann, C., Kolle, O., Heinesch, B., Queck, R., Ibrom, A., and Aubinet, M.: Data acquisition and flux calculations, in: Eddy Covariance: a Practical Guide to Measurement and Data Analysis, edited by: Aubinet, M., Vesala, T., and Papale, D., Springer Atmospheric Sciences, Springer, The Netherlands, doi:10.1007/978-94-007-2351-1_3, 59–83, 2012.

Siebicke, L. and Serafimovich, A.: Ultraschallanemometer-Überprüfung im Windkanal der TU Dresden, Work Report University of Bayreuth, Dept. of Micrometeorology, ISSN 1614-8916, 30, 42 pp., available at: http://opus.ub.uni-bayreuth.de/opus4-ubbayreuth/frontdoor/index/index/docId/628, 2007.

Siebicke, L., Hunner, M., and Foken, T.: Aspects of CO_2 advection measurements, Theor. Appl. Climatol., 109, 109–131, doi:10.1007/s00704-011-0552-3, 2012.

Wilczak, J., Oncley, S., and Stage, S.: Sonic Anemometer Tilt Correction Algorithms, Bound.-Lay. Meteorol., 99, 127–150, doi:10.1023/A:1018966204465, 2001.

Yuan, R., Kang, M., Park, S.-B., Hong, J., Lee, D., and Kim, J.: Expansion of the planar-fit method to estimate flux over complex terrain, Meteorol. Atmos. Phys., 110, 123–133, doi:10.1007/s00703-010-0113-9, 2011.

Erklärung

Hiermit erkläre ich, dass ich die Arbeit selbständig verfasst und keine anderen als die von mir angegebenen Quellen und Hilfsmittel benutzt habe.

Ferner erkläre ich, dass ich anderweitig mit oder ohne Erfolg nicht versucht habe, diese Dissertation einzureichen. Ich habe keine gleichartige Doktorprüfung an einer anderen Hochschule endgültig nicht bestanden.

Bayreuth, den ____________________ ____________________________

Wolfgang Babel